Textile Science and Clothing Technology

N. Gokarneshan
D. Anitha Rachel
V. Rajendran
B. Lavanya
Arundhathi Ghoshal

Emerging Research Trends in Medical Textiles

Springer

Textile Science and Clothing Technology

Series editor

Subramanian Senthilkannan Muthu, Hong Kong, Hong Kong SAR

More information about this series at http://www.springer.com/series/13111

N. Gokarneshan · D. Anitha Rachel
V. Rajendran · B. Lavanya
Arundhathi Ghoshal

Emerging Research Trends in Medical Textiles

Springer

Dr. N. Gokarneshan
Department of Textile Technology
Park College of Engineering
and Technology
Coimbatore
Tamil Nadu
India

D. Anitha Rachel
NIFT TEA College of Knitwear Fashion
Tirupur
Tamil Nadu
India

V. Rajendran
NIFT TEA College of Knitwear Fashion
Tirupur
Tamil Nadu
India

B. Lavanya
NIFT TEA College of Knitwear Fashion
Tirupur
Tamil Nadu
India

Arundhathi Ghoshal
NIFT TEA College of Knitwear Fashion
Tirupur
Tamil Nadu
India

ISSN 2197-9863 ISSN 2197-9871 (electronic)
Textile Science and Clothing Technology
ISBN 978-981-287-507-5 ISBN 978-981-287-508-2 (eBook)
DOI 10.1007/978-981-287-508-2

Library of Congress Control Number: 2015939234

Springer Singapore Heidelberg New York Dordrecht London

Printed on acid-free paper

Springer Science+Business Media Singapore Pte Ltd. is part of Springer Science+Business Media (www.springer.com)

This book is dedicated to
my beloved mother
my beloved late father
my reverred master
my beloved wife and son
and my dear readers

Preface

This book provides a comprehensive review of the recent significant research advances in the area of medical textiles during the past five years. It would be useful for students, scholars, teachers, and researchers. The book contains a number of illustrations for enabling easier reading. Chapters have been well organized so as to provide readers with a good insight into the significant researches in the field. The different areas of medical fields covered include gynecology, urology, cardiology, neurology. I wish to duly acknowledge the researchers whose noteworthy contributions have been included in this book, and I am confident that it would motivate researchers to carry out extensive research in the area. The role of knits in the areas of medical textile applications has been highlighted in some chapters. The recent researches in the area of medical textiles hold promises in the treatment of ailments related to vital organs of the human body. They also indicate scope for further research in the respective areas of applications. The newly developed implants from PET have been evaluated. The role of nonwovens and viscose fibers has been discussed in separate chapters. A number of chapters cover the developments in wound dressings. Thus, the book provides interesting reading and would prove useful to researchers in textile and medical areas as well. Suggestions are welcome for upgrading the quality of the book.

N. Gokarneshan

Contents

Introduction

A good deal of developments is happening in the field of medical textiles. This book highlights the significant researches during the past five years. One interesting and major area is wound dressings. Wound dressing containing calcium alginate and polyvinyl alcohol in varying proportions has been evaluated for wound healing capacity. Wound dressing from cyanoethyl chitosan-electrospun fibers have been assessed for healing performance. The chitosan nano fiber component of the wound dressing has been found to exhibit excellent antimicrobial behavior. Membranes containing blend of chitosan and polyethylene glycol with different molecular weights have been coated on cotton fabric to obtain wound dressing, which resulted in a porous structure and good permeability. Textile-based smart wound dressings have been developed. These are artificial wound coverings that are expected to meet the requirements necessary for the treatment of major skin wounds. Antimicrobial silver–sodium-carboxymethylated cotton print cloth has been developed from the sodium salt of carboxymethylated cotton and silver–calcium–sodium alginates from four commercially available alginate moist wound dressings. The proven swell ability of these silver dressings, taken together with the known absorptive and antimicrobial properties of the dressings, should make them suitable for the treatment of exudative wounds that are at risk of infection. A phosphorylated form of cotton gauze for the treatment of chronic wounds was designed to improve the wound dressing capacity to remove harmful proteases from the wound and facilitate healing. Moist wound healing dressing based on cotton gauze fabrics have been developed. The cotton gauze fabrics have been carboxymethylated to varied concentrations and treated with tetracycline hydrate and gentamicin sulfate. Properties of the tetracycline hydrate or gentamicin sulfate containing Ca/Na carboxymethylated samples make them suitable candidates as antibacterial moist wound healing dressings. Knitted scaffolds of polylactic acid filament have been developed for urinary bladder reconstruction. An intelligent wearable garment with transcutaneous electrical nerve stimulation function has been designed from a knitwear design perspective. The knitwear technique, garment design skill, Chinese acupuncture therapeutic method, and transcutaneous electrical nerve stimulation technology have been integrated interactively in

the garment. Nonwoven scaffolds have been developed using multilobal fibers that contain several grooves and have greater surface area than round fibers. The ability of the multilobal fibers to accommodate large quantities of cells presents an excellent alternative to round fibers as scaffolds for tissue engineering. A novel double-layered weft-knitted fabric has been developed to be used in protective applications, and antimicrobial properties have been evaluated. Antimicrobial formulation has been applied onto the fabric at different concentrations. Also, the durability of the wash fastness of the applied antimicrobial agents has been measured. The need for protective surgical gowns has arisen due to the increasing awareness of highly communicable bacteria and viruses. The various aspects related to the development, application, and quality evaluation of surgical gowns have been highlighted. The types of gowns available, their classification, technology behind them, technical aspects, testing means, their limitations, and future course of action to satisfy the growing needs of healthcare professionals are also discussed. The development of flared textile cuffs represents a considerable advancement in endovascular therapy by allowing a fenestrated solution to be readily available off the shelf and providing an adequate seal of the ancillary stent–graft to the main body of the stent–graft. Diclofenac sodium microparticles have been applied onto the orthopedic support materials. In vitro drug release studies of microparticles and textiles impregnated with microparticles have been carried out. This study suggested that textile systems containing diclofenac sodium microparticles could have a potential for long-term therapy for rheumatic disorders.

Chapter 1
Wound Dressings from Nanofiber Matrix of Calcium Alginate/PVA Blend

1.1 Introduction

Nanofibers, which are produced from electrospinning technique, are finding diverse applications in nanocomposites such as scaffolding, biomedical, and drug-delivery system [1, 2]. Polyvinyl alcohol (PVA) has the advantages of being water soluble, good mechanical properties, chemical resistance, and biological resistance. It is a water soluble polyhydroxy polymer and can be cross-linked with biopolymers for enhancement of mechanical properties and reduce solubility in water [3, 4]. PVA has been electrospun into nanofibers ranging in diameter between 100 and 1000 nm [5]. Calcium alginate is an anionic polysaccharide, in which the alginates form firmer structure with calcium ions, producing calcium alginates which form stronger gels on wound surface compared to that of sodium alginate [6]. Ordinary wounds heal easily. But chronic wounds do not heal due to the excessive production of exudates, which causes maceration of healthy skin tissue around the wound and prevents wound healing [7, 8]. A variety of wound dressings are available and their effectiveness is being evaluated. Hydrogel creates a moist wound surface which reduces the buildup of necrotic tissue and thereby enables quick wound healing. Experiments on rats have proved that sodium alginate- and polyvinyl-alcohol-based hydrogel exhibited an improved healing rate of artificial wounds. Alginates are gel-forming agents that are highly absorbent and have hemostatic properties. The wound exudates convert the calcium into sodium salt and form gel, which gets absorbed by body, upon contacting the wound surface, and enables removal of alginate dressing by dissolution [9]. Pure alginate solution could not be electrospun [10]. PVA and sodium alginate solutions have been mixed in the ratios of 100:0, 70:30, 50:50, and 30:70. The results revealed that increase in PVA proportion in the blend caused uniform generation of nanofibers [11]. The maximum concentration of sodium alginate electrospun was ~4 wt%. This chapter investigates the calcium alginate/PVA-blended

N. Gokarneshan et al., *Emerging Research Trends in Medical Textiles*,
Textile Science and Clothing Technology, DOI 10.1007/978-981-287-508-2_1

nanofiber matrix as wound dressing, in two phases. The first phase focuses on the examination of PVA and calcium alginate blend, while the second phase involves investigation on the rate of wound healing on the surface of the wound.

1.2 Electrospinning of Solution Mixture

In order to achieve better spinnability of blended solution and mechanical properties of the fiber, PVA has been blended with calcium alginate solution. The nanofiber web produced from the blended solution is shown in Fig. 1.1. The figures clearly establish that the diameter of the fiber is influenced by the proportion of calcium

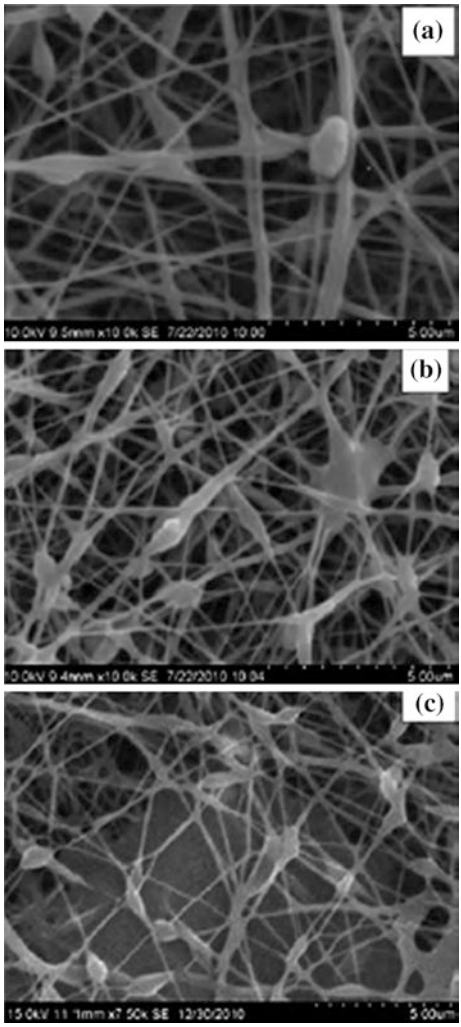

Fig. 1.1 SEM photographs of electrospun nanofibers prepared from mixture of 4 % calcium alginate and 7 % PVA at different volume ratios PVA and calcium alginate **a** 90:10 **b** 80:20 and **c** 70:30. [12]

alginate in the blend solution [12]. Also the viscosity of the solution mixture is one of the critical factors that influence the structure and diameter of the fiber. At a blend ratio of 70:30(PVA/Calcium alginate), fibers appear along with beads (Fig. 1.1c) and the average fiber diameter is 98 nm. At a ratio of 80:20, even though the beads are seen in the fiber, they are comparatively reduced, and the average fiber diameter is about 114 nm (Fig. 1.1b). At a ratio of 90:10, uniform fibers appear, even though with a few beads and the average diameter is about 191 nm (Fig. 1.1a).

1.3 FTIR Investigations

FTIR has been used to observe peak shift caused due to the interactions between two blended polymers such as hydrogen bonding or any complex structure formation [12]. The observed spectra of PVA and calcium alginate are shown in Fig. 1.2. The spectra of calcium alginate and PVA-blended fibers in the wavelength range between 4000 and 5000 cm^{-1} are shown in Fig. 1.3. The figure exhibits the characteristic bands of PVA and calcium alginate at 3418 cm^{-1} and 3347 cm^{-1} belong to all types of hydrogen bond. It is observed from Fig. 1.3a–c that OH stretching has shifted to lower frequencies compared to pure calcium alginate Fig. 1.2a. Hydroxyl stretching frequency becomes lower with the increase in calcium alginate content. It is evident that OH stretching has a favorable extent in changing the molecular spectra.

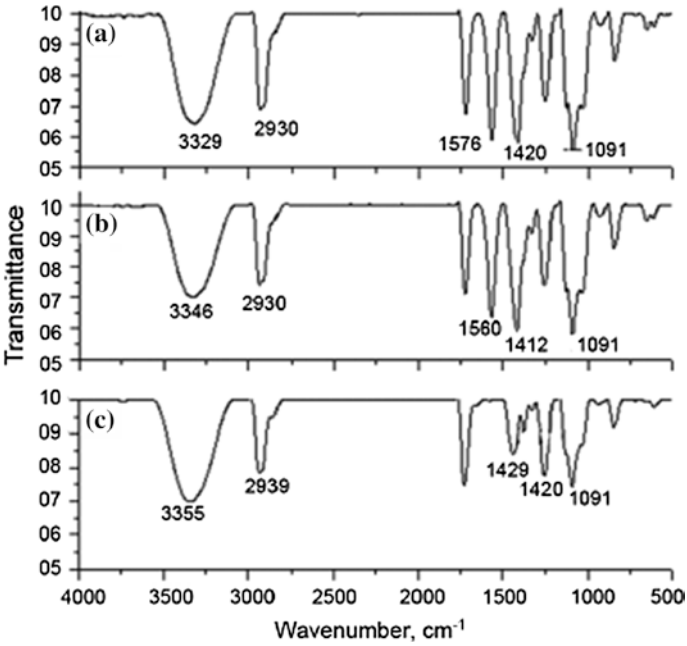

Fig. 1.2 FTIR spectra of calcium alginate PVA-blended nanofibers **a** 90:10 **b** 80:20, **c** 70:30 PVA/calcium alginate [12]

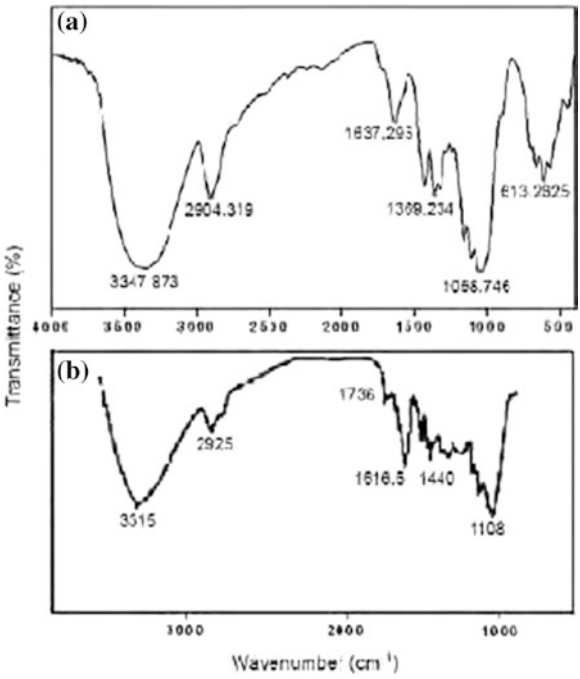

Fig. 1.3 FTIR spectra of (**a**) calcium alginate and (**b**) polyvinyl alcohol [12]

1.4 Moisture Transmission and Porosity Measurement

It is expected that a good wound dressing should be able to control the loss of water from wound at an optimal rate. The water loss from the wound is found to increase proportionately with time. The moisture vapor transmission characteristics (MVTR) of the nanofiber web that is produced from the three different blend proportions is calculated as the gradient of the weight loss versus the time plot [12]. The studies indicate that the MVTR decreases as the calcium content in the nanofiber increases. The SEM image of the blended nanofiber matrix dipped in water is shown in Fig. 1.4.

It is found that while calcium alginate is not degraded due to its insoluble nature in water, PVA does get degraded due to its soluble nature. The results of porosity measurements are shown in Table 1.1. The results indicate that the decrease in pore diameter is insignificant, with the decrease in average fiber diameter.

1.5 Antibacterial Evaluation

After appropriate sample preparation and incubation for a period of 24 h, zone of inhibition appears around the tested material. Nanofiber matrix prepared from specified percentage of solution mixtures and proportions of calcium alginate and PVA have been used to determine the antibacterial activity in Staphylococcus

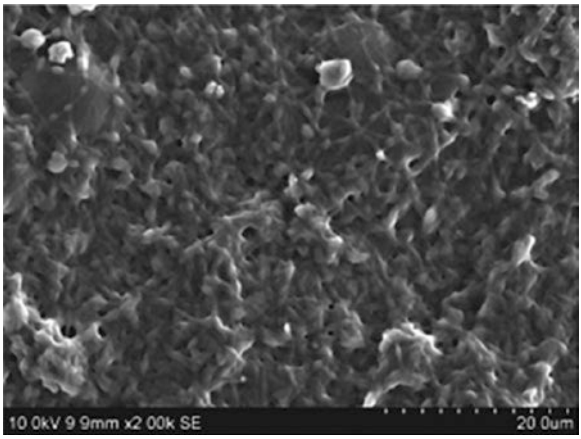

Fig. 1.4 SEM image of blended nanofiber matrix after treatment in water [12]

Table 1.1 Pore size of blended electrospun nanofiber matrix [12]

Solution ratio	Average fiber Diameter nm	Areal density g/m	Mean pore Diameter um
90:10	191.5	10	10.41
80:10	113.6	20	10.39
70:30	98.1	30	10.38

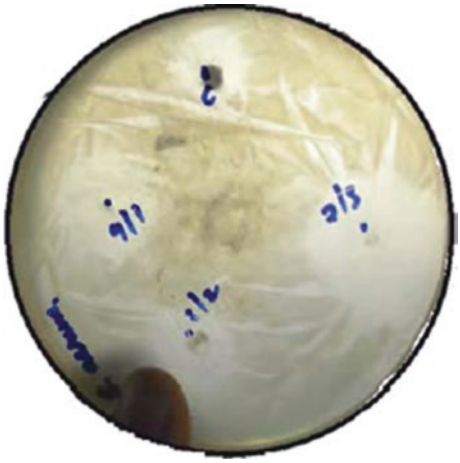

Fig. 1.5 Assessment of antibacterial activity in nanofiber matrix prepared from blended solution of 4 % calcium alginate and 7 % polyvinyl alcohol [12]

Aureus. [12] The area of inhibition zone formed in control wound is 10 mm (Fig. 1.5). At blend proportion of 90:10, the area of zone formed is 10 mm. In the case of blend proportion of 80:20, the area of zone formed is 12 mm, and in the case of blend proportion of 70:30, the area of the zone formed is 20 mm. The increase of calcium alginate in the blend exhibits higher zone of inhibition value and that the zone of inhibition value for 70:30 and 80:20 is higher as compared to the control wound.

1.6 Gross Examination

Test has been conducted on female Wistar rats with a wound incision length of 1 cm. The observation period ranged between 5 and 8 days [12]. The incised wound has been covered with the blended nanofiber matrix of 70:30 proportions and the web dimension was 1 cm × 2 cm. After a period of observation of 5 days, epithelial cells appeared on both control and test wounds. The healing rate showed significant difference. Figure 1.6c shows that the control wound remains open and

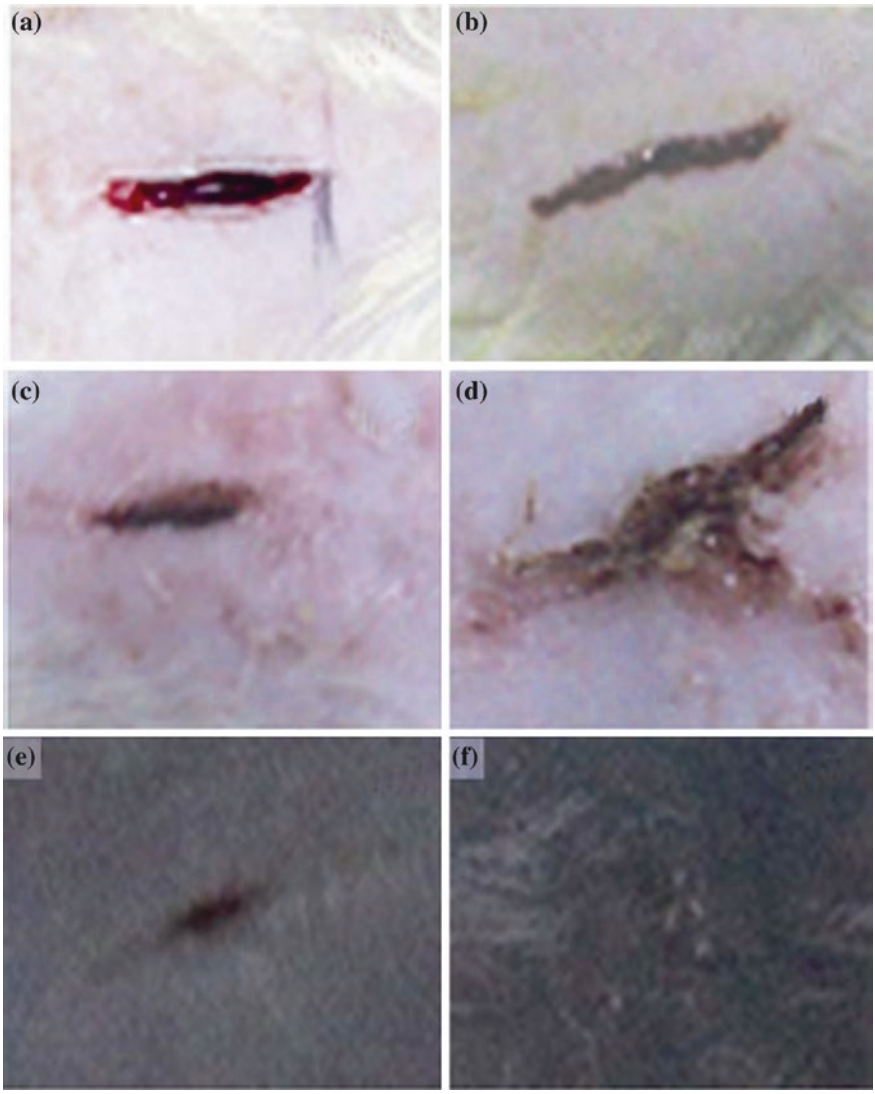

Fig. 1.6 Examination of nanofiber matrix on wound healing control wounds and (**b**), (**d**) and (**f**) test wounds [12]

the wound length is reduced to 0.7 cm. The test wound has been partially covered with the gel and the length of the wound is 0.5 cm, as shown in Fig. 1.6d. After 8 days of observation, the control and test wound appears as shown in Fig. 1.6e, d. Figure 1.6e shows that control wound is found to be open and epithelial cells are grown well in comparison with observation of 5 days. However, the test wound (Fig. 1.6f) shows that the epithelial cells have grown well and it has covered the wound, and also growth of hairs has been noticed in both control and test rats.

References

1. Pharm QP, Sharma U, Mikos AG (2006) Electrospinning of polymeric nanofibres for tissue engineering applications : A review. Tissue Eng 12:1197–1211
2. Huang ZM, Zhang YK, Kotaki M, Ramakrishna S (2003) A review on polymer nano fibres by electrospinning and their applications in nanocomposites. Compos Sci Technol 63:2223
3. Ding B, Kim HY, Lee SC, Lee DR, Choi KJ (2002) Preparation and characterization of a nano scale poly(vinyl alcohol) fiber aggregate produced by an electrospinning method. Fibres Polym 3(2):73–79
4. Zhang C, Yuan X, Wu L, Han Y, Sheng J (2005) Study on morphology of electrospun(polyvinyl alcohol) mats. Euro Polym J 41:423–432
5. Ying Y, Jia ZD, Liu J, Li Q, Qiang LL, Hou L, Wang L, Guan Z (2008) J Appl Phys 103:104307
6. Kriegel C, Arrechi A, Kit K, McClementsa DJ, Weiss J (2010) Crit Rev Food Sci Nutr 48(8):775
7. Pascal M, Anthony CD (2008) Mechanisms involved in wound healing. Biomed Sci 609
8. Boateng JS, Matthewes KH, Stevens HNE, Eccleston GM (2008) Wound healing dressings and drug delivery systems: A review. J Pharmaceut Sci 97(8):2892
9. Barnett SE, Varley SJ (1987) The effects of calcium alginate on wound healing. Ann Roy Coll Surg Engl 69:153
10. Nie H, Hi A, Zheng J, Xu S, Li J, Han CC (2008) High performance ultrafiltration membrane based modified chitosan coating. Biomacromolecules 9:1362
11. Safi S, Morshed H, Ravandi SA, Ghiaci M (2007) Study of electrospinning of sodium alginate, blended solutions of sodium alginate/poly(vinyl alcohol) and sodium alginate/poly(ethylene oxide). J Appl Polym Sci 104:3245
12. Tarun K, Gobi N (2012) Calcium alginate/PVA blended nano fibre matrix for wound dressing. Indian J Fibres Text Res 37:127

Chapter 2
Evaluation of the Healing Performance of Cyanoethyl Chitosan Wound Dressing

2.1 Introduction

Owing to their large surface area, nanofibers are able to find applications in medical textile products such as surgical facemasks, wound dressings, and drug-delivery systems [1]. Chitosan, which is a biopolymer, is suited for such applications [2–5]. However, due to its polyelectrolyte nature and intrinsically high viscosity, it is not easily electrospun. Though it can be used in film form for burns and wound healing, it is quite expensive and also the film properties are quite delicate [6–8]. Blend of films or fibers of chitosan–cellulose can inhibit the antimicrobial behavior of the chitosan based on polymer dominating the surface [9]. Chitosan nanofibers can be obtained by dissolving chitosan in acetic acid [10]. But, recent research has shown that electrospinning from a solution of chitosan in acetic acid failed to produce fibers [11]. Chitosan nanofibers have been electrospun using core/sheath geometry with polyethylene oxide (PEO) as sheath and chitosan in the core [12]. But the PEO has to be dissolved in order to obtain the chitosan nanofiber web. Chitosan had to be mixed with other polymers to form solutions sustainable for electrospinning, owing to its difficulty in electrospinning [13]. Cyanoethyl chitosan, which is a derivative of chitosan, has been developed and then electrospun using different spinning parameters to produce fiber for their application in wound dressings. Contact kill performance of the electrospun structures against a range of microbes has been investigated. The findings reveal that the developed nanofiber webs from cyanoethyl chitosan show an excellent antimicrobial behavior.

N. Gokarneshan et al., *Emerging Research Trends in Medical Textiles*,
Textile Science and Clothing Technology, DOI 10.1007/978-981-287-508-2_2

2.1.1 Synthesis of Cyanoethyl Chitosan

The cyanoethyl chitosan has been prepared by initially dissolving chitosan in acetic acid to give 1 % of aqueous acetic acid solution. The solution has been stirred for 4 h at room temperature and filtered. The filtered solution has been added to the aqueous solution of sodium hydroxide of 6 % concentration with vigorous stirring to obtain regenerated activated chitosan in a form of fine powder with high surface area. The activated chitosan was exposed to acrylonitrile vapor for 3 h, and the resultant cyanoethyl chitosan has been washed with methanol and dried. This method of preparation produced cyanoethyl chitosan with substitution of 1.2° which permitted the product to be soluble in solvents such as Dimethylformamide (DMF), Dimethyl Sulfoxide (DMSO), Trifluroacetic acid (TFA), and Acetone [14].

2.1.2 Preparation of Electrospinning Solutions

Trifluoroacetic acid has been used as the solvent to form the electrospinning solution. A bath has been prepared by the addition of acetone to dry ice at a temperature of −70 °C. Cyanoethyl chitosan in the desired amount has been added to a bottle and the required quantity of solvent has been added depending on the concentration needed. Then, the solution was stirred and the bottle was closed using an airtight lid and then placed in the bath; the solution was cooled instantly and then the bottle was removed out of the bath so as to allow the solution to thaw. Due to sudden cooling and thawing, the cyanoethyl chitosan was dissolved into Trifluoroacetic acid very quickly. The solution was then subsequently used for electrospinning after being left overnight.

2.1.3 Electrospinning

The electrospinning device comprises of an extrusion system, fiber collection system, and high-voltage power supply. The extrusion system enables a regulated rate of feed of the spinning solution. A high-voltage power supply has been used to give a positive field to the polymer solution. The terminal wire (positive electrode) from the high-voltage power supply was fixed to the extrusion needle (1 mm inner diameter).

A drum made of polyvinyl chloride having a diameter of 22 cm and length of 35.6 cm comprises of fiber collection system [21]. It is fixed to an electrically isolated wooden frame and connected to a motor, and speed controller. A brass ring is attached to one side of the drum. The ring is connected with a brass brush which in turn is connected to the negative electrode of high-voltage power supply.

A brass is placed on a groove in the drum throughout its length and fixed at one end by the brass ring. The electric field is carried by a rod given by the brass ring. An aluminum (or any conductive material) foil is wound over the drum and passes under the brass rod. This is done to maintain the same electric field over the area covered by conductive foil. The negative end for the system is derived from the high-voltage power supply to the brass rod with the help of the connection wire and the brass bush which is attached to the brass ring. A strip of 10-cm-wide aluminum foil was mounted securely around the fiber collecting drum. Gauze of the same width was mounted over the aluminum foil part of the aluminum foil not covered by gauze by rotating the drum with low speed (1–3) m/min, and a nanofiber layer was spun over the gauze and the aluminum, since the gauze structure is very open and allowed the electrical field to form nanofibers. Nanofiber web samples with aluminum foil have been taken from SEM imaging and taken for antimicrobial evaluation. The details of the equipments design are shown elsewhere [15]. The equipment has been accommodated inside a ventilation hood owing to the use of trifluoroacetic acid.

2.2 Results of Findings

Electrospinning solutions with low cyanoethyl chitosan concentration (4–6 %) produce beads with low or no fiber formation as indicated in Fig. 2.1 [21]. At higher concentration of 8–10 %, the fiber formation has been good with low or no bead formation as shown in Fig. 2.2. This agrees with the earlier research findings [16], wherein it has been reported that higher viscosity favors formation of fibers with little or no beads. Besides, lower solution surface tension helps in fiber formation without beads.

At low concentrations of the electrospun solution, the viscosity is inadequate to produce solid continuous fibers. The viscosity of the solution increases with the increase in the polymer concentration and is accompanied with the increase in the number of interchain associations of the polymer molecules in the solution. This leads to continuous fiber formation. The surface tension is reduced at concentration level of 8–10 %. The viscosity increase coupled with surface tension reduction creates excellent conditions for electrospinning of polymer solution, with little or no beads as can be seen in Fig. 2.2. This has also been observed in earlier research investigations.

The inhibition zone has been investigated along with the electrospinning process and solution parameters. A sample during the disk diffusion test is shown in Fig. 2.3. The sample can be seen at the center of the figure and the clear ring around the sample is the area where the microorganisms are dead, and the remaining area is the zone where the microorganisms are growing. The zero inhibition zone indicates killing of the microorganisms existed on the sample, but it does not affect those outside the sample [21]. The antimicrobial property of the cyanoethyl chitosan improves when more fibers are formed. Cyanoethyl chitosan structures

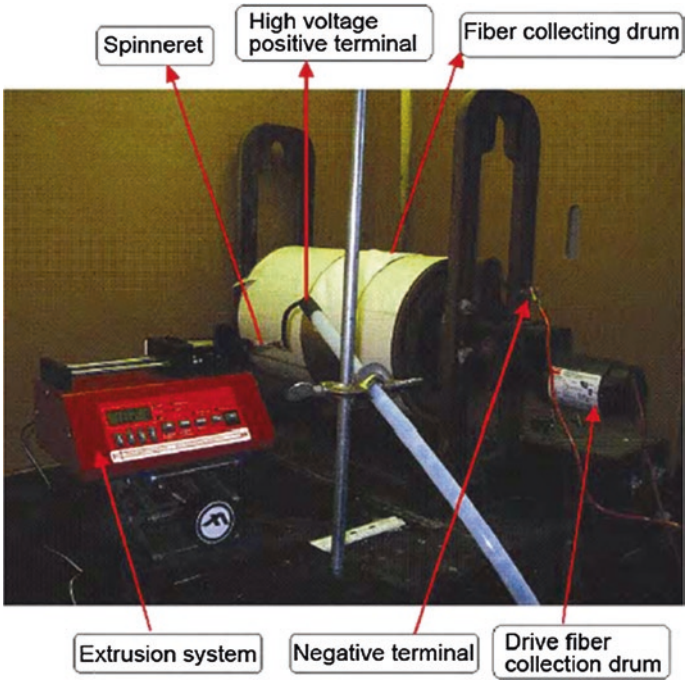

Fig. 2.1 Electrospinning device [21]

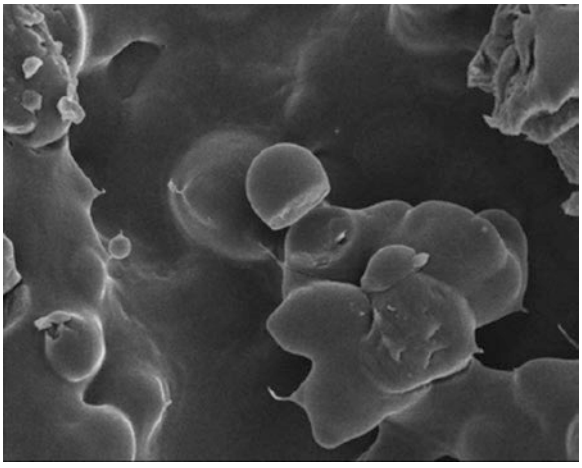

Fig. 2.2 Formation of SEM structure at 2 % solution concentration [21]

without fiber formation and with beads show the least inhibition zones, whereas the structures with fibers and least or no beads formation show the highest antimicrobial activity. Experimental trials have shown that inhibition zone gets higher

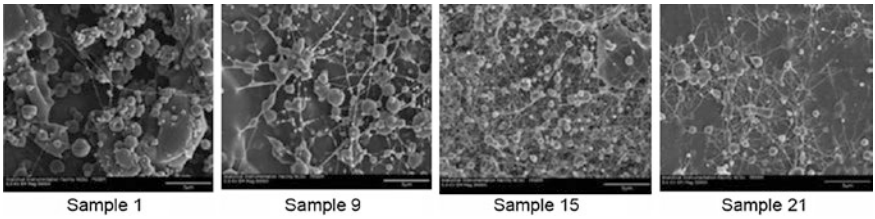

Fig. 2.3 SEM images of electrospun cyanoethyl structure (low concentration) [21]

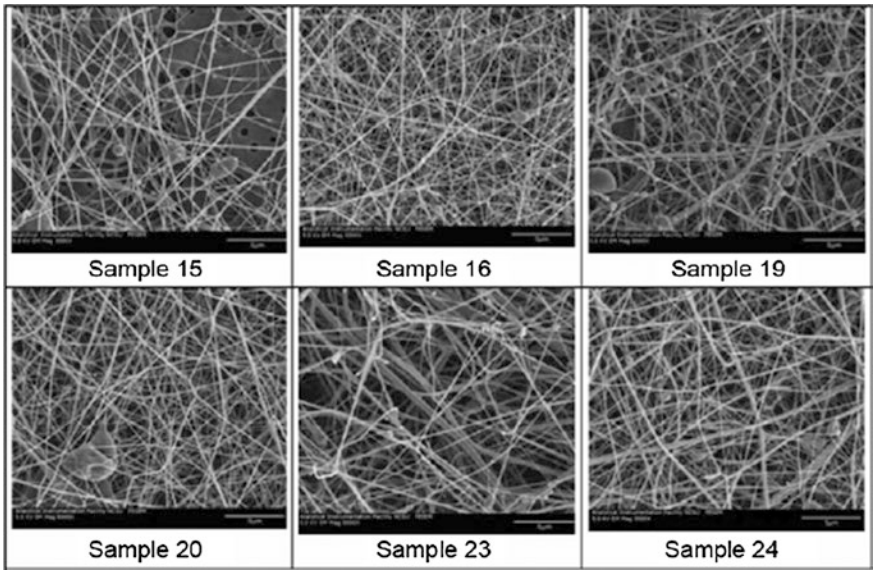

Fig. 2.4 SEM images of electrospun cyanoethyl structure (high concentration) [21]

with the increase in the polymer concentration in the solution. This is directly related to the following:

(a) More fibers formed with increase in concentration and
(b) The fiber diameter reduced with increase in concentration

The above two factors increase the area covered by the fibers and provide high surface area for better antimicrobial performance (Fig. 2.4).

2.3 Mechanism of Microbial Inhibition

Though a number of mechanisms for microbial inhibition have been suggested for chitosan and its derivatives, none have been able to clearly establish the exact mechanism. The interaction of the positively charged cyanoethyl chitosan with

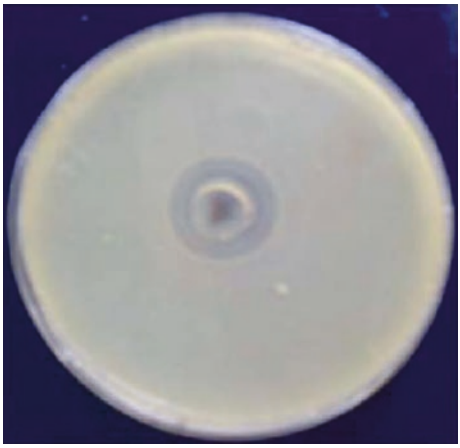

Fig. 2.5 Sample during disk diffusion test [21]

the negatively charged residues at the cell surface of many fungi and bacteria appears to be the most accepted theory and is responsible for extensive cell surface changes and also changes the permeability of the cell [17–23]. This causes the leakage of intracellular substances, such as electrolytes, UV absorbing proteins, amino acids, glucose, and lactate dehydrogenase. As a result, cyanoethyl chitosan inhibits the normal metabolism of microorganisms and finally leads to the death of these cells. Structures with high beads create low inhibition zone due to their low surface area, which tend to create a low field between the polymer and the cell surface of the microorganism. On the contrary, the structures with low or no beads increase the inhibition zone and thereby cause more effective killing of the microorganisms, as they provide a high surface area and thus create a strong field between the polymer and the cell surface of the microorganism (Fig. 2.5).

References

1. Jayaraman K, Kotaki M, Zhang Y, Mo X, Xiu M, Ramakrishna S (2004) Recent advances in nano fibres. J Nanosci Technol 4(1–2):52–65
2. Hudson SM, Jenkins DW (2001) Chitin and chitosan. Encyclopedia of polymer science and technology. Wiley Interscience, New York
3. Hudson SM, Lim S (2003) Review of chitosan and its derivatives as antimicrobial agents and their uses as textile chemicals. J Macromol Sci Rev 43(2):223–269
4. Hudson MV, Kumar MNVR (2004) Chitosan, in Encyclopedia of biomaterials and biomedical engineering. Dekker publication, New York
5. Whang HS, Kirsch W, Zhu YH, Yang, Cheng Z, Hudson SM (2005) Hemostatic agents derived from chitin and chitosan. J Macromol Sci Polym Rev 45(4):309–323
6. Qin Y (1994) Chitin and chitosan and wound dressing materials. Text Horiz 14(6):19–21
7. Ueno H, Mori T, Fujinaga T (2001) Topical formulations and wound healing applications of chitosan. Adv Drug Delivery Rev 52:105–115
8. Raymond L, Morin FG, Marchessault RH (1993) Degree of deacetylation of chitosan using conductometric titration and solid state NMR. Corbohyd Res 246:331–336

9. Hasegawa M, Isogai A, Kuga S, Onabe F (1994) Preparation of cellulose chitosan blend film using chloral/dimethylformamide. Polymer 35(5):983–987
10. Geng X, Kwon O (2005) Electrospinning of chitosan dissolved in concentrated acetic acid solution. Jang J Biomater 26:5427–5432
11. Nawalakhel RG (2009) Improving healing performance of wound dressing: electrospinning of chisaton based, cellulose based, fibres and their blends, MS thesis, North Carolina state university, Raleigh, North Carolina, USA
12. Ojha S, Gorga R (2008) Fabrication and characterization of electrospun chitosan nano fibres formed via templating with polyethylene oxide. Biomacromolecules 9:2523–2529
13. Bhattirai N, Edmondson D, Veishe O, Masten FA, Zhang M (2005) Biomaterials 26(31):6176–6184
14. Fong H, Chun I, Renekar DH (1999) Beaded nanofibers formed during electrospinning. Polymer (40):4585–4592
15. Abdel Fatteh MS, Sam MH, Hassan MI, Ahmed IW, Nabil YZ (2012) Healing performance of wound dressing from cyanoethyl chitosan electrospun fibres. Indian J Fibre Text Res 37:205–210
16. Sudarshan NR, Hoover DG, Knorr D (1992) Antibacterial action of chitosan. Food Biotechnol 6(3):257–272
17. Fang SW, Li CF, Shih DYC (1994) Antifungal activity of chitosan and its preservative effect on low sugar candied kumquat. J Food Prot 56(2):136–140
18. Hwang JK, Kim HJ, Yoon SJ, Pyun YR (1998) Advances in chitin science. In: Chen RH, Chen HC (eds) Vol III. Rita Advertising Co, ltd, Taiwan, pp 340–344
19. Tsai G-J, Su, W-H (1999) Antibacterial activity of shrimp chitosan against Escherichia coli. J Food Prot 62(3):239–243
20. Helander IM, Nurmiaho-Lassila EL, Ahveinain R, Rhoades J, Roller S (2001) Chitosan disrupts the barrier properties of the outer membrane of Gram-negative bacteria. J Food Microbiol 71:235–244
21. Young DH, Kohle H, Kauss (1982) Effect of chitosan on membrane permeability of suspension-cultured glycine max and phaseolus vulgaris cells. Plant physiology 70:1449–1454
22. Young DH, Kauss H (1983) Release of calcium from suspension-cultured glycine max cells by chitosan, other polycations, and polyamines in relation to effects on membrane permeability. Plant Physiol 73:698–702
23. Seyam AFM, Hudson SM, Ibrahim HM, Waly AI, Abou Zeid NY (2012) Healing performance of wound dressing from cyanoethyl chitosan electrospun fibres. Indian J Fibre Text Res 37:205–210

Chapter 3
Membrane-Coated Cotton Wound Dressings

3.1 Introduction

Biopolymers have gained popularity during recent times, being prompted by increasing environmental awareness, growing public health and environmental regulations, and are therefore being considered as alternatives to synthetic polymers [1]. They are well applicable in the areas of wound dressings, sutures, tissue engineering, and drug delivery [2–6]. Chitosan, chitin, polysaccharides, cellulose, and starch are popular biopolymers. Chitosan is positively charged and is water soluble and is readily reacts with many negatively charged materials [7]. In order to overcome the low water sorption characteristic of chitin, polyacrylic acid has been grafted on it to obtain a hydrogel characteristic for wound dressing application [8]. Chitosan holds a great promise in therapeutic applications due to its antimicrobial nature, scar prevention, and biocompatibility [9–14]. Wound dressing is one such application wherein all these properties are found [15]. Asymmetric chitosan membrane has been prepared, which is tissue compatible and impermeable to exogenous microorganism due to its top layer and inherent antimicrobial property, and also exhibits excellent oxygen permeability, controlled evaporative water loss, and enhanced fluid drainage ability [16]. Similarly, silver sulfadiazine incorporated asymmetric membrane has been prepared, and it acts as a rate-controlling release of the sulfadiazine and silver ion in a sustained way [17]. It also exhibited prolonged antibacterial activity and decreased potential silver toxicity. Nanoparticles have penetrated into the biomedical field [18]. Silver nanocrystalline chitosan wound dressing composed of nanosilver and chitosan has been used for treating deep partial thickness wounds. They improve wound healing and resist infection, accompanied by reduction in risk of silver absorption [19]. Membranes have been prepared using chitosan blended with polyethylene glycol [20–23]. Polyethylene glycol exhibits outstanding characteristics such as protein resistance, low toxicity, immunogenicity, and biocompatibility. Thus, chitosan–polyethylene glycol blends improve the biological characteristics of blend membranes. Wound dressings from electrospun

N. Gokarneshan et al., *Emerging Research Trends in Medical Textiles*,
Textile Science and Clothing Technology, DOI 10.1007/978-981-287-508-2_3

materials potentially offer many advantages over conventional process with its huge surface area and microporous structure. These membranes have been found to promote wound healing and induce cell migration and proliferation [24]. Chitosan has been blended with polyethylene glycol (molecular weight 20,000) in different ratios, and the mixture was coated on cotton fabric followed by the freeze-drying to develop porous membranes [25]. The proportion of polyethylene glycol in the blend significantly influences the morphology and the physical structure. The physical structure and surface morphology as a function of the polyethylene glycol molecular weight have been investigated.

3.2 Membrane Morphology

An investigation has shown that chitosan–polyethylene glycol-coated cotton membranes are porous in nature and the porosity ranges between 50 and 70 % [25]. The molecular weight of polyethylene glycol strongly influences the porosity development in these membranes. The effects of these are shown in Figs. 3.1, 3.2,

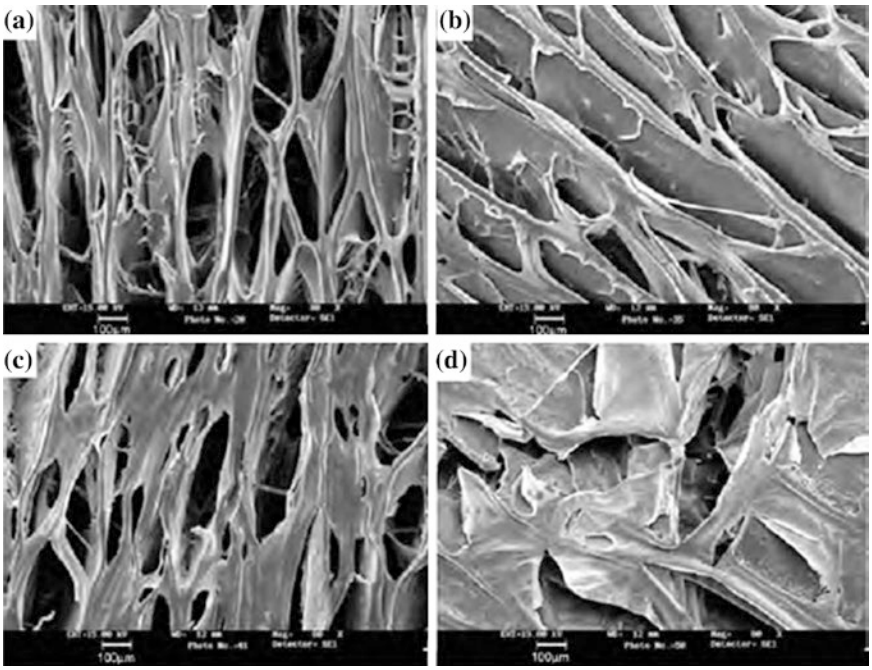

Fig. 3.1 SEM photographs of coating on padded fabrics [26]. **a** Chitosan-coated cotton membrane and chitosan–polyethylene glycol-coated membranes with molecular weight of 4000. **b** 10 % polyethylene glycol with molecular weight of 4000. **c** 30 % polyethylene glycol with molecular weight of 4000. **d** 50 % polyethylene glycol with molecular weight of 4000

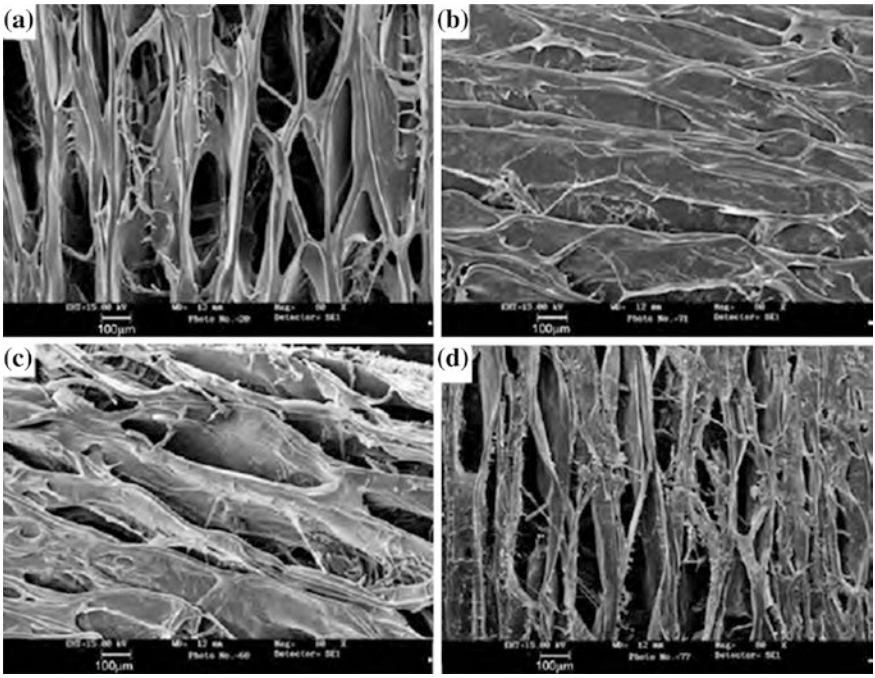

Fig. 3.2 SEM photographs of coating on padded cotton fabric [26]. **a** Chitosan-coated cotton membrane and chitosan–polyethylene glycol-coated membranes with molecular weight of 1000. **b** 10 % polyethylene glycol with molecular weight of 10,000. **c** 30 % polyethylene glycol with molecular weight of 10,000. **d** 50 % polyethylene glycol with molecular weight of 10,000

and 3.3. A systematic evaluation of the porous structure proceeds with the polyethylene glycol molecular weight and their amount. Similar observations have been made wherein a regular porous structure with a top dense layer has been observed [17]. Polyethylene of different molecular weights has been investigated for the structure–property correlation. The molecular weight of the polyethylene glycol strongly influences the porosity and density of the membranes. There is a distinct trend in the partial loss of elongated porous structure and in the formation of the collapsed structure due to the increase in the polyethylene glycol content. With the increase in the molecular weight of polyethylene glycol, the porous structure becomes more opened, and the pore size ranges between 75 and 120 μm. As can be visualized from Figs. 3.2 and 3.3, the pores become more elongated and larger in size with the addition of polyethylene glycol having molecular weights of 10,000 and 20,000, respectively, into the chitosan matrix [26]. The porous structure of polyethylene glycol with 20,000, molecular weight, at 50 % content becomes wide open with the appearance of large pits. When the compatibility between chitosan and polyethylene glycol is better, the phase separation diminishes. The molecular interaction between chitosan and polyethylene glycol with molecular weight of 4000 is much better as compared to that with of polyethylene

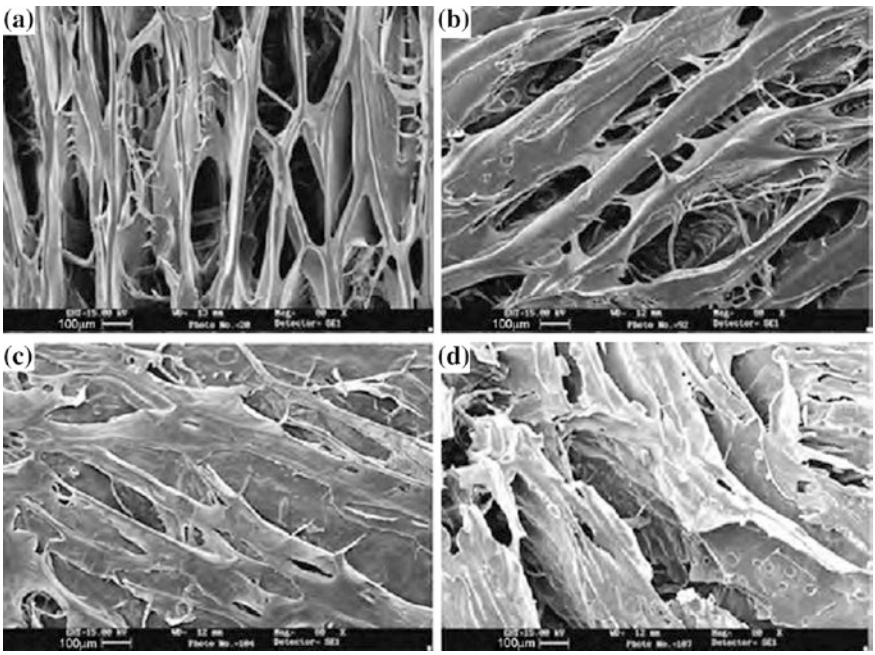

Fig. 3.3 SEM photographs of coating on padded cotton fabric [26]. **a** Chitosan-coated cotton membrane and chitosan–polyethylene glycol-coated membranes with molecular weight of 20,000. **b** 10 % polyethylene glycol with molecular weight of 20,000. **c** 30 % polyethylene glycol with molecular weight of 20,000. **d** 50 % polyethylene glycol with molecular weight of 20,000

glycol having higher molecular weight of 10,000 and 20,000. This could be attributed to the fact that polyethylene glycol with molecular weight of 4000 has higher number of terminal hydroxyl groups per unit mass and is expected to act more intensely due to higher extent of hydrogen bonding with chitosan molecules. Hence, polyethylene glycol with molecular weight of 4000 gives better compatibility with chitosan and low level of phase separation and thus does not affect pore such significantly.

In the case of polyethylene glycol with molecular weight of 20,000, the hydrogen bonding interaction is weak and therefore leads to more isolation of polyethylene glycol molecules from the chitosan matrix. This is reflected by collapsing of pores in a regular fashion. With the increase in the polyethylene glycol content in the chitosan, larger pore size and higher porous structure can be seen in the membranes [22]. This results from the weak interaction of polyethylene glycol with the chitosan chains. The observed diminishing porous morphology in polyethylene glycol-added membranes is the reflection of the limited interactions of these two components in the blended matrix [26]. Based on the interaction of the polyethylene glycol with chitosan matrix and the generated morphology as well as the porosity, it could be proposed that polyethylene glycol with molecular weight of 20,000 is the most appropriate additive for the dressing development.

3.3 Membrane Characterization

Figure 3.4 shows the differential scanning calorimetry thermograms of membranes in temperature range between 40 and 80 °C. The melting of the polyethylene glycols of different molecular weights is suppressed as the blended component increases in the chitosan matrix as compared with virgin polyethylene glycol [26]. The decrease in melting point is higher in the case of polyethylene glycol with molecular weight of 4000 as compared to that of polyethylene glycol with molecular weight of 20,000. The results indicate that strong hydrogen bonding between polyethylene glycol with molecular weight of 4000 and chitosan molecules interferes with the crystallization process of polyethylene glycol during the membrane fabrication step and is reflected in the diminishing melting temperature.

With the increase in the molecular weight of polyethylene glycol, the interaction is less effective due to relatively lower content of hydroxyl groups and polyether chain is not much affected during the crystallization process. Hence, the melting temperature is not significantly affected. Studies have shown that the corrected heat of fusion value for polyethylene glycol with molecular weight of 4000 in membrane is much lower than that for pure polyethylene glycol. But, in the case of polyethylene glycol with molecular weight of 10,000, the difference between corrected and inherent values is less pronounced. This difference is even much less for polyethylene with molecular weight of 20,000. This could be attributed to the fact that chitosan–polyethylene glycol association is stronger in polyethylene

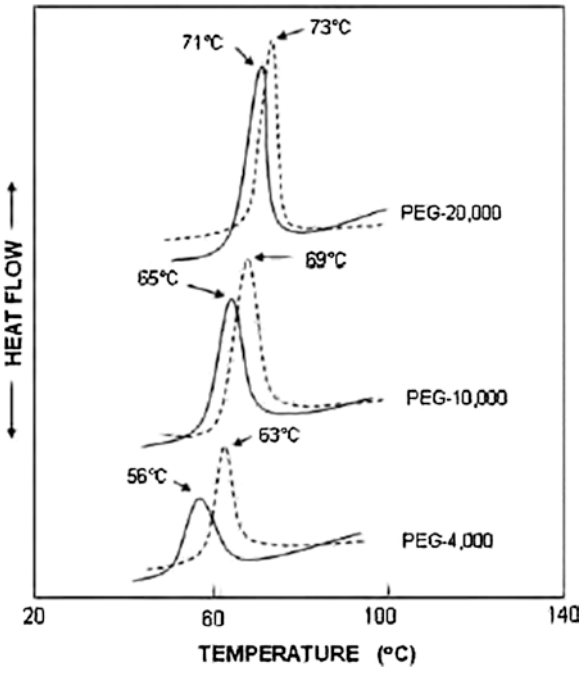

Fig. 3.4 Thermograms from differential scanning calorimetry at different molecular weights of polyethylene glycol (*dotted line* virgin; *dashed line* blended) [26]

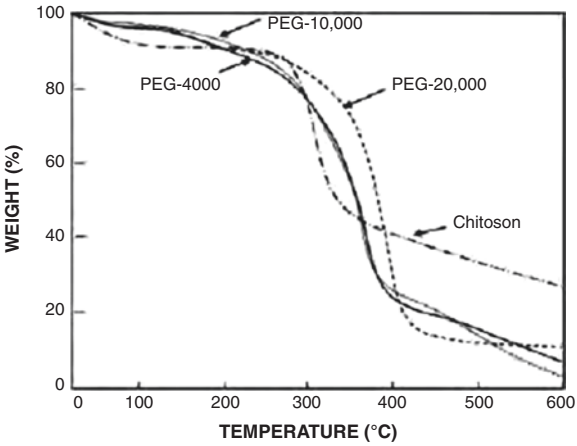

Fig. 3.5 Thermogravimetric analysis of chitosan-coated membrane and chitosan–polyethylene glycol-coated membranes with polyethylene glycol having molecular weights of 4000, 1000, and 20,000 [26]

glycol with molecular weight of 4000 as compared to polyethylene glycol with molecular weight of 20,000, and does not permit the polyethylene component with molecular weight of 4000. This supports the strong interaction of polyethylene glycol (4000 MW) with chitosan molecules, which interferes with its crystalline structure. Similar findings have been reported in earlier research [22].

Figure 3.5 shows the thermogravimetric analysis thermograms of pure chitosan and composite membranes. Chitosan shows a typical multistep degradation pattern. However, the polyethylene glycol containing composite membranes shows better thermal stability as compared to the chitosan-coated membranes [26]. Moreover, polyethylene glycol (20,000 MW) shows the most stable matrix as compared to the other blended membranes. This could be attributed to the better thermal stability of polyethylene glycol (2000 MW) which is also reflected by the enhanced thermal stability of membranes.

3.4 Membrane Properties

Figure 3.6 shows the variation of air and water permeability of membranes with the changes in the molecular weight of polyethylene glycol. This is indicted as the pressure required to force water to pass through the membrane. The air permeability decreases in chitosan–polyethylene glycol composite membrane (molecular weight of 4000) as compared to the virgin chitosan-coated membrane. But the permeability of the membranes increases with the increase in molecular weight of polyethylene glycol. The decrease in the permeability of the polyethylene (4000 MW) membrane is caused due to the changes in porosity with the addition of polyethylene glycol. The SEM micrographs shown in the previous figures indicate that the porosity changes significantly in the blended membranes and may lead to lowering in the permeability [26]. The compatibility of the polyethylene

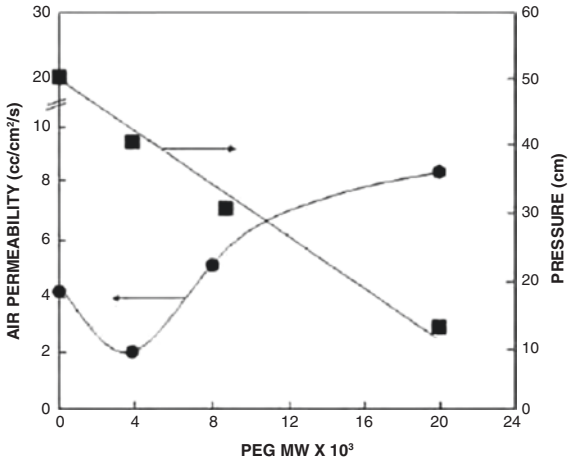

Fig. 3.6 Variation in air permeability and water permeability of membranes with polyethylene glycol molecular weight in chitosan–polyethylene glycol-coated membranes [26]

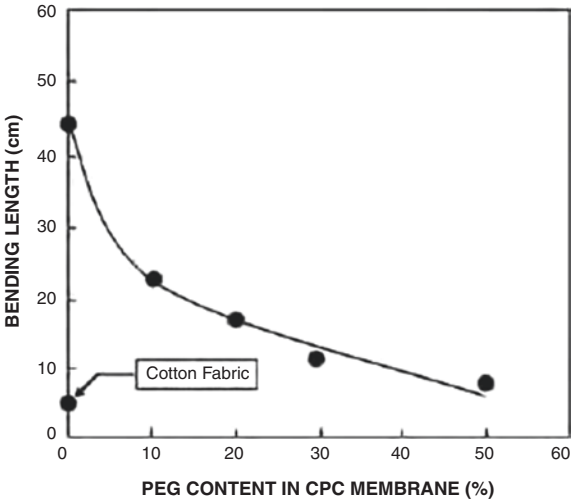

Fig. 3.7 Bending length of fabrics having different polyethylene glycol (20,000 molecular weight) contents in chitosan–polyethylene glycol-coated membrane [26]

component with chitosan decreases with the increase in molecular weight and in turn results in more open and larger porous structure. This results in increase in air permeability. The water permeability also increases significantly as seen from the lower pressure needed for water to pass through. The importance of large pore size in enhancing the permeability has been shown in earlier research [21].

Studies have indicated that polyethylene glycol with molecular weight of 20,000 has been evaluated as the appropriate component for the blended wound dressing. Its bending length has been measured as the flexibility in the membranes. An interesting finding is that the bending length of chitosan-coated fabric is 11 times greater than that of uncoated cotton fabric (Fig. 3.7).

The addition of polyethylene glycol to chitosan reduces the bending length based on its content. The bending length is found to decrease with increase in the polyethylene glycol content in the blend. These findings could be comprehended from the plasticizing effect of polyethylene glycol component in the membrane. Chitosan has a glass transition temperature of 170 °C and has a rigid molecular structure, and hence, its coating onto cotton fabric imparts a very good rigidity. The addition of polyethylene glycol to the chitosan results in a flexible structure. With the increase in polyethylene glycol, the flexibility improves and results in lower bending length. The glycols are known for imparting the plasticization effect in the hydrogels. This is where, glycerin has been observed to plasticization in chitosan-based hydrogels [26]. Other researches have supported the investigations on chitosan–gelatin complex in combination with glycerol and sorbitol. The films casted from this combination exhibit plasticizing effect of the glycol.

References

1. Krajewska B (2005) Membrane based processes performed with use of chitin/chitosan materials. Sep Purif Technol 41:305
2. Czaja W, Krystynowicz A, Bielicki S, Brown RM (2006) Microbial cellulose—The natural power to heal wounds. Biomaterials 27:145
3. Liu XD, Nishi N, Tokura S, Sakairi N (2001) Chitosan coated cotton fiber: preparation and physical properties. Carbohydr Polym 44:233
4. Martino AD, Sittinger M, Risbud MV (2005) Chitosan: a versatile biopolymer for orthopaedic tissue engineering. Biomaterials 26:5983
5. Dang JM, Leong KW (2006) Natural polymers for gene delivery and tissue engineering. Advan Drug Deliv Rev 58:487
6. Ishihara M, Nakanishi K, Ono K, Sato M, Kikuchi M, Saito Y, Yura H, Matsui T, Hattori H, Uenoyama M, Kurita A (2002) Photocrosslinkable chitosan as a dressing for wound occlusion and accelerator in healing process. Biomaterials 23:833
7. Dutta PK, Dutta J, Tripati VS (2004) Chitin and chitosan: chemistry, propreties and applications. J Sci Indian Res 63:20
8. Tanodekaew S, Prasitsilp M, Swasdison S, Thavorniyutikarn B, Pothsree T, Pateepason R (2004) Biomaterials 25:453
9. Paul W, Sharma CP (2004) Chitosan and alginate wound dressings: a short review. Trends Biomater Artif Organs 18:18
10. Saxena S, Ray AR, Kapil A, Pavon-Djavid G, Letourneur D, Gupta B, Meddahi-Pelle A (2011) Development of a new polypropylene based suture: plasma grafting, surface treatment, characterization, and biocompatibility studies. Macromol Biosci 11:373
11. Shelma R, Paul W, Sharma CP (2008) Chitin nano fibre reinforced thin chitosan films for wound healing application. Trends Biomater Artif Organs 22:111
12. Ueno H, Yamada H, Tanaka I, Kaba N, Matsuura M, Okumura M, Kadosawa T, Fujinaga T (1999) Accelerating effects of chitosan for healing at early phase of experimental open wound in dogs. Biomaterials 20:1407
13. Muzzarelli R, Tarsi R, Tarsi R, Fillipini O, Giovanetti E, Biagini G, Varaldo PE (1990) Antimicrobial properties of N-Carboxybutyl chitosan. Antimicrobial Agents Chemotherm 34:2019
14. Williams GM, Herbert JQ (1985) US Patent 4532134
15. Kojima K, Okamoto Y, Miyatake K, Kitamura Y, Minami S (1998) Collagen typing of granulation-tissue induced by chitin and chitosan. Carbohydr Polym 37:109

16. Mi FL, Shyu SS, Wu Y, Lee ST, Shyong JY, Huang RN (2001) Fabrication and characterization of a sponge like asymmetric chitosan membrane as a wound dressing. Biomaterials 22:165
17. Mi FL, Wu YB, Shyu SS, Chao AC, Lai JY, Su CC (2003) Chitosan modified membranes for wound dressing applications: Preparations, characterization, and bio evaluation. J Membr Sci 212:237
18. Brun F, Travan A, Accardo A, Paoletti S (2010) An improved method for ring artifacts removing in reconstructed tomograhpic images. Biomed Sci Instrum 46
19. Lu S, Gao W, Gu HY (2008) Construction, application, and biosafety of silver nanocrystalline chitosan wound dressing Burns 34:623
20. Zhang M, Li XH, Gong YD, Zhao NM, Zhang XF (2002) Properties and biocompatibility of chitosan films modified by blending with PEG. Biomaterials 23:2641
21. Zeng M, Fang Z (2004) Preparation of sub-micrometer porous membrane from chitosan/polyethylene glycol semi IPN. J Membr Sci 245:95
22. Zeng M, Fang Z, Xu C (2004) Effect of compatibility on the structure of the microporous membrane prepared by selective dissolution of chitosan/synthetic polymer blend membrane. J Membr Sci 230:175
23. Kim J, Cai Z, Chen Y (2010) Biocompatible bacterial cellulose composites for biomedical applications. J Nano Technol Eng Med 1:1
24. Chen JP, Chang GY, Chen JK (2008) Electrospun collagen/chitosan nanofibrous membrane as wound dressing. Colloids Surf A: Physiochem Eng Aspects 313–314:183
25. Gupta B, Arora A, Saxena S, Alam MS (2009) Preparation of chitosan–polyethylene coated cotton membranes for wound dressings: preparation and characterization. Polym Advan Technol 20:58
26. Bhuvanesh G, Shalini S, Abha A, Mohammed SA (2011) Chitosan–polyethylene glycol coated cotton membranes for wound dressings. Indian J Fibre Text Res 36:272

Chapter 4
Smart Textile Wound Dressings

4.1 Introduction

During the recent times, wound management has become increasingly challenging task, owing to the new insights on wound healing and the rising demand to manage complicated wounds outside hospital. Wound management requires instant wound healing so as to achieve both functional and cosmetic effects [1]. Modern wound dressings are tailored to enable functional healing of wound more than covering it [2]. The wound healing involves four processes, namely homeostasis, inflammation, granulation tissue formation, and remodeling, which overlap in time [3–5]. It is a highly complex process affected by factors that are specific to the individual such as nutritional status, age, systemic disease, medication, and behavior, along with the size, depth, causation, and etiology of the wounds [6]. Textile-based composite structures are good material to be incorporated as wound dressings because of their large porosity, surface area, and air as well as moisture permeability [7]. These textile materials provide strength, extensibility, and flexible support for the reinforcement with the healing materials.

4.2 Smart Textile Wound Dressings

A dressing is used as application for wound so as to enhance healing and/or prevent further harm. It is different from a bandage in the sense that it comes in direct contact with the wound. A bandage is used to hold a dressing in place. It can serve many functions based on the type, severity, and position of the wound. However, all purposes are focused toward promoting recovery and preventing further harm from the wound. The fibers used in wound care could be of natural or synthetic origin [7]. Sometimes, nonfibrous materials such as carbon and metals such as silver are also used.

N. Gokarneshan et al., *Emerging Research Trends in Medical Textiles*,
Textile Science and Clothing Technology, DOI 10.1007/978-981-287-508-2_4

4.2.1 Coating Materials

These include hydrocolloids, alginates, and hydrogels along with supporting textile materials. Such coated materials have been designed to achieve specific functions such as air and moisture vapor permeability, good strength, and flexibility for their use as smart wound dressings.

Hydrocolloids are dressings, which heal wound by providing occlusion. It is a multilayered structure comprising an outer layer that protects and a supporting material that could be a film, fiber, or foam. The supporting material is laminated with a composite containing an adhesive through which hydrophilic particles are distributed. Nonwoven polyester fibers and semipermeable polyurethane films are generally used as the supporting materials [8]. The hydrophilic component of the adhesive contains synthetic polymers including polyurethane gels, protein, and polysaccharides. The hydrocolloid forms hydrated gel over the wound surface through physical interaction with the wound surface. When the dressing is removed from the wound, the gel is separated and thereby prevents damage to the newly formed skin [9]. The hydrocolloids absorb exudates and help debride the wound. The dressing has to be changed when the gel leaks out. The dressing should have a diameter at least 2 cm greater than the wound in order to avoid frequent changes. They can be used with necrotic material, but tend to have problems with overwhelming exudates that build up in large wounds and those having anaerobic colonization.

Alginates are block copolymers of two hexuronic acid residues, and the wound dressing made from them has attracted attention as wound management aids. They are useful for lightly contaminated wounds and cavities, but are unsuitable for dry, necrotic tissue, since there are no exudates to activate them. As the alginates lack adhesive power, they have to be held in place by another dressing. Alginate dressings can be changed twice a week, based on the amount of exudates. Moreover, alginate dressings in combination with hydrocolloids prove more effective.

Hydrogels are hydrophilic in nature, have good biocompatibility, and also have gained scientific interest over the years [10–12]. They are basically two-component systems, in which one of the components is a hydrophilic polymer insoluble in water due to its three-dimensional network, and the other component is water. These systems may swell in water up to an equilibrium state and retain their original shape, thus providing a moist environment needed for an ideal dressing [13]. They are either chemically stable or degrade, gradually disintegrate, and dissolve. They are known as ‘reversible’ or ‘physical’ gels where the networks are held together by molecular entanglements and/or by secondary forces including ionic and secondary forces including ionic and H bonding, and also called ‘permanent’ or ‘chemical’ gels when they have covalently cross-linked networks as shown in Fig. 4.1 [14].

Hydrogel dressings are prepared by the following methods:

(a) Physical means involving repeated freezing and thawing,
(b) Chemical method using borax, boric acid, formaldehyde, and glutaraldehyde, and
(c) Irradiation [15]

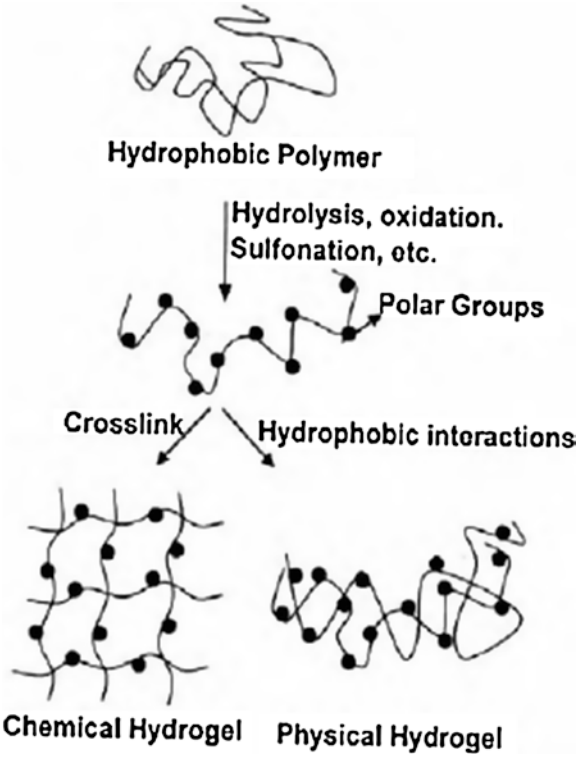

Fig. 4.1 Formation of physical and chemical hydrogels [14]

The major setback with hydrogels is their low mechanical strength. Their general areas of application include scaffolds in tissue engineering, environmentally sensitive (pH and temperature) hydrogels, sustained delivery release system, biosensors, disposable diapers, sanitary towels, contact lenses, and medical electrodes. Other areas of application include breast implants, granules for holding soil moisture in arid areas, dressings for burn patients, and reservoirs in topical drug delivery. The polymers generally used as hydrogels are shown in Fig. 4.2.

The use of hydrogels as temporary skin covers or as wound dressing is gaining good commercial importance [16–20]. A popular wound dressing is produced by chemical polymerization and cross-linking of acrylamide and methylene-bis-acrylamide in aqueous solution containing some additives such as polysaccharides and proteins [21]. Hydrogels are suitable for treating burn injuries, since they reduce the loss of body liquid and maintain the high humidity in the wound area. They also have outstanding tissue compatibility. Hydrogels outscore other coating materials, namely hydrocolloids and alginates, since they possess all the characteristics necessary for an ideal wound dressing. One major demerit is the poor mechanical properties after swelling. In order to overcome this problem, recent developments have emerged in the shape of composite membranes, in which a textile material is coated with the polymer solution. The fabric reinforcement provides strength to the dressing, and the drug-loaded dressings offer precise control of the release behavior [22].

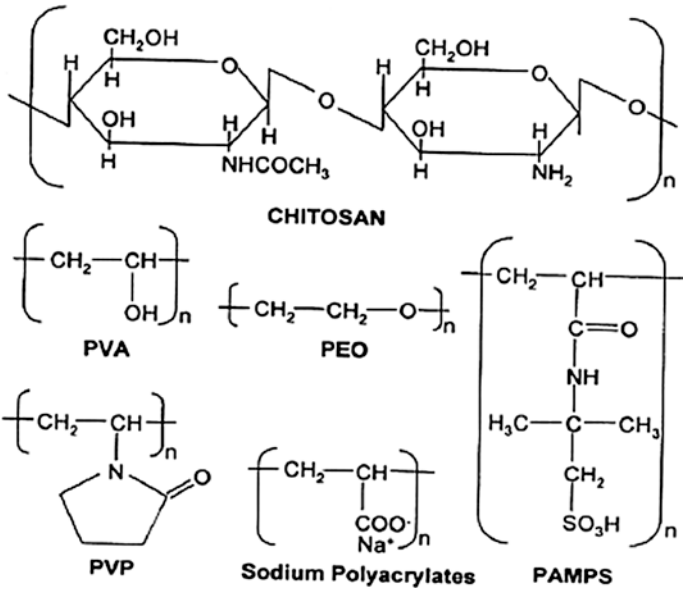

Fig. 4.2 Chemical structure of polymers used as hydrogel

Hydrogel wound dressings have been made from natural and synthetic polymers. The natural polymers include dextran dialdehyde, bovine serum albumin, glycosaminoglycan, chitosan, and collagen, and these have been explored for their suitability as hydrogel wound dressings. Among these, chitosan and collagen have been mostly used as the wound dressing with textile materials. In one of the research works, collagen containing dressing was generally produced in the form of pad, which contained supporting material in the form of pad which contained supporting material (nonwoven fabric) and collagen layer [23]. The antibiotic molecules are absorbed from aqueous solution by the cotton fabric coated with chitosan. It paves the way for therapeutic new generation dressings for combating infections resulting from surgical wounds [24]. Chitosan has also been coated on polypropylene nonwoven fabrics for dressing wounds in order to impart good water vapor transmission rates, antibacterial activities, and cell adhesiveness [25]. Recently, chitosan and collagen hydrogel derivatives have gained acceptance in wound healing [26].

4.2.2 Wound Dressings Coated with Chitosan

Chitin is a natural polymer endowed with bioactive properties. These include antibacterial, antiviral, antifungal, nontoxic, and nonallergic. The products made from chitin are well suited for wound dressings with wound healing properties owing to their soft handle, breathability, absorbency, smoothness, and nonchemical

additives [7]. Both chitin and chitosan required properties for a wound dressing, such as biocompatibility, biodegradability, hemostatic activity, antiinfectional activity, and property to accelerate wound healing [27]. Chitosan, which is a bioactive component, offers itself as a scar prevention wound dressing, thereby exhibits its uniqueness, and is the most desirable aesthetic criterion in today's world of wound dressing technology.

An innovative type of asymmetric chitosan membrane has been developed and has a skin surface on the top layer supported by a macroporous sponge-like sublayer [28]. This asymmetric membrane shows controlled evaporative water loss, excellent oxygen permeability, and promoted fluid drainage ability, but could inhibit exogenous microorganisms' invasion due to the dense skin layer and inherent antimicrobial property of chitosan. The epithelialization rate is enhanced, and the deposition of collagen in the dermis is well organized, and thus, serves well as a wound dressing [28]. When the chitosan membrane is used with a supporting material such as cotton and polypropylene, it would be well suited as wound dressing that is biocompatible, exudates absorptive, antimicrobial, and scar preventive. Cotton fabric has been used as the support layer for the chitosan–polyethylene glycol layer and leads to very thin and lightweight structures. The structure of the dressing has been designed in such a way that it leads to the high porosity. The thickness of the chitosan coating also plays an important role in developing porosity on the surface.

The hydrogels containing polyvinyl alcohol, polyvinylpyrrolidone, and chitosan are developed containing both antibiotic agent and chitosan oligomer. It has been found that both undergo quick release at the beginning and then become slower and slower with time. Hence, these dressings prove to be excellent materials for wound care management as they exhibit comprehensive properties suitable for wound dressings, such as high gel content, a reasonable ESR, and an acceptable tensile strength and elongation at break [29].

A semi-interpenetrating polymer network system has been developed [30], in which chitosan cross-linking acts as matrix and linear polymer polyethylene glycol acts as domain. The pores are formed due to extraction with hot water, in which the dispersion-phase polyethylene glycol is effectively extracted in water. Chitosan-coated gauge fabric has been developed and investigated for its chemical, thermal, and antimicrobial properties [31]. It has been evaluated against *E. Coli* and *Lactobacillus*, found to be effective, and considered to be a potential wound dressing.

The graft copolymerization of polymeric materials has been enabled to achieve desired properties through specific choice of the molecular characteristics of the side chain to be grafted. Chitosan has reactive groups that can be modified by grafting. Membranes for wound treatment have been obtained that would serve two purposes, viz. speeding up of the wound healing time and also serve as a delivery system for various drugs to prevent or treat bacterial infections. Based on this objective, new material has been synthesized by grafting vinyl monomers onto chitosan (Fig. 4.3) [32].

New textile wound dressings comprising of regenerated chitin or dibutyrylchitin have been developed by coating a polypropylene nonwoven material

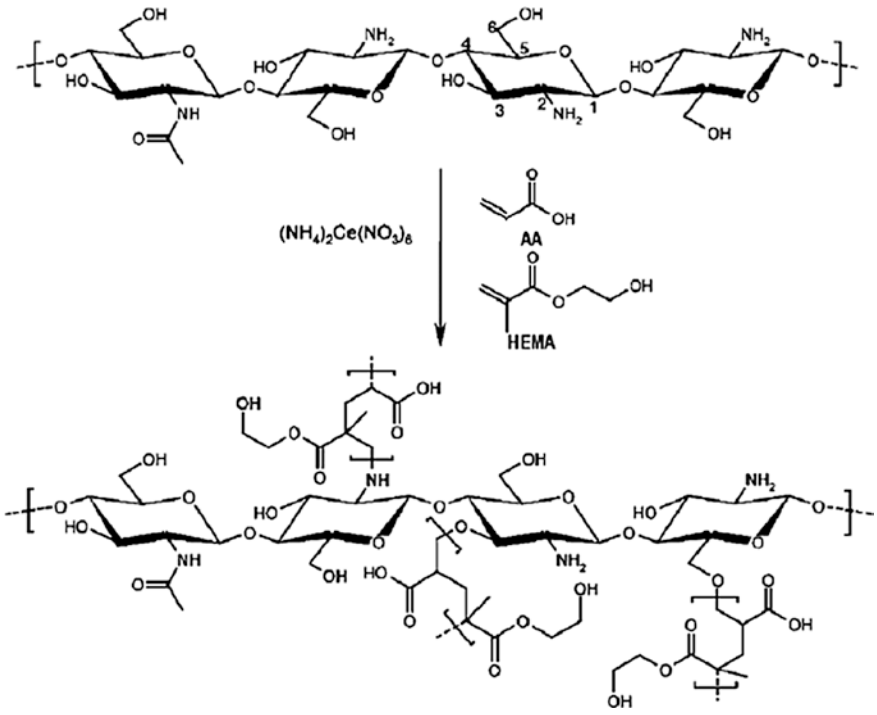

Fig. 4.3 Graft copolymerization of HEMA and AA into chitosan [32]

with either of these films [25]. The sterilized dressings have been biologically assessed. Both the materials had no cytotoxic effect or primary irritation either in vitro or in vivo and both have a positive influence on the wound healing process. Microscopic evaluation revealed that the wounds covered with the dressing containing dibutyryl chitin healed fastest.

Bacterial cellulose/chitosan wound dressings possess good antibacterial, barrier, and mechanical properties in wet state and moisture retention properties, and are therefore unique [33]. These characteristics render them an excellent dressing material for treating various kinds of wounds, burns, and ulcers. The chitosan has a favorable impact on the mechanical properties of modified cellulose. High elongation at break indicates good elasticity, so such dressing fits the wound site well and therefore provides good protection against external infection. Bioactive material made from chitosan-modified bacterial cellulose provides optimal moisture conditions for rapid wound healing without irritation or allergization. Such composite structures have applications in management of burns, bedsores, skin ulcers, hard-to-heal wounds as well as wounds requiring frequent dressing change [34]. Bacterial cellulose modified with chitosan combines different properties such as bioactivity, biocompatibility, and biodegradability of the two biopolymers, thereby creating an excellent dressing material [35].

4.2.3 Wound Dressings from Nonwovens

Nonwoven fabric serves as an excellent dressing material with its high porosity and larger surface area, which provides an open structure for drainage of exudates and reduces the risk of secondary infection. Acticoat™, a commercial textile dressing with silver nanocrystal, is good for wound dressing of burn patients [36].

NUCRYST Pharmaceuticals and the Advanced Wound Management Division of Smith and Nephew Plc announced that Health Canada granted marketing approval of Acticoat™ Flex barrier dressings for wounds that require up to seven days of sustained antimicrobial activity. The reviewed literature shows certain limitations related to study methodology, small sample sizes, and heterogeneity of the products to which Acticoat is compared among others. Despite these limitations, studies show that Acticoat possesses effective antimicrobial activity in vitro and in vivo, capable of reducing colonization and preventing contamination by microorganisms. Its release mechanism ensures a continuous distribution of 70–100 mg/L of ionized silver over more than 48 h and rapid start of action (within 30 min of application) in optimal moisture conditions. It reduces pain, and this benefit can be intensified if dressings are changed only after every three days, as recommended by the manufacturer [28]. Based on these results and the lack of clinical studies comparing Acticoat with similar silver-based dressings, AETIMS concludes the following:

(i) Acticoat is a therapeutic option for the treatment of severe burns,
(ii) The rationale for its use is based more on empirical results observed in the clinical setting than on published scientific evidence, and
(iii) Burn care is an emerging field of research, and its development paves the way for additional, better designed clinical studies, especially cost-benefit analysis, capable of demonstrating the potential benefits of Acticoat in the care of burns.

Grafting is known to be useful for the introduction of various functional groups into various polymers by selecting the type of monomer. It is conceivable that the function of the groups introduced is influenced by the monomer sequence distribution in the grafted chains and its location in the polymer substrate depending on the method of introduction [37]. Polypropylene nonwoven fabric (NWF) has been extensively used due to its porosity, allowing ventilation, high surface area, and excellent mechanical properties. However, the hydrophobic surface of PP nonwoven limits its applications, and to overcome these limitations grafting is done. Yang and Lin [38] developed PP-g-AA NWF by modifying PP NWF with AA using UV radiation. Furthermore, NIPAAm N ISOPROPYL acrylamide was graft copolymerized onto this PP-g-AANWF using ultraviolet photografting. CS was impregnated onto the PP-g-AA-g-NIPAAm biograft NWF with freeze-drying to form PP-g-AA-g-NIPAAm-CS. This modified fabric was found to be suitable for wound dressing application. In this work, wound dressings of AA-grafted CS/collagen-immobilized PP fabric were produced by using two types of CS obtained from the nourishment of Mucore (m-chitosan) and from commerce (c-chitosan). The antibacterial properties

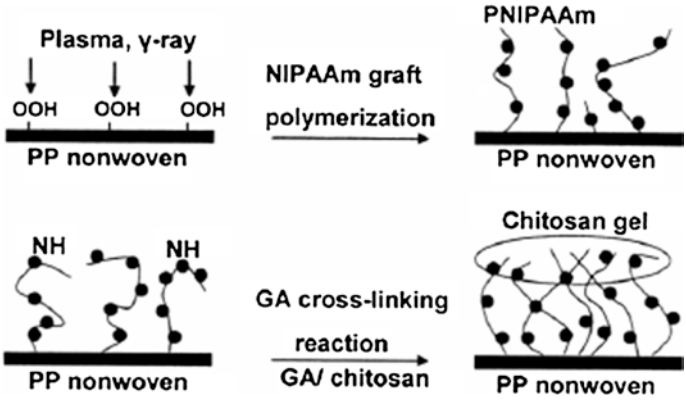

Fig. 4.4 Photoinduced grafting polymerization [39]

of the PP-AAgCmCi PP-AAgCcCi samples were found to be excellent. The zone around the sample is caused by the bacterial inhibition by CS [1].

Grafting of AA onto PP NWF modified by direct-current pulsed plasma and with PNIPAAm shows good potential as wound dressing. From animal studies, modified NWFs were found to promote wound healing. The wound areas decreased gradually and reached 9 and 5 % after 17 days of PP-g collagen and PP-g collagen-g-PNIPAAm NWFs, respectively. In contrast to wound covered with gauze, the wound area only reduced to 26 % during the same period. In one of the studies [39], CS was immobilized on PNIPAAm gel/PPNWF by using cross-linking agent, glutaraldehyde (GA) for its use as wound dressing (Fig. 4.4). The plasma activation treatment and subsequently UV light graft polymerization were done. The result showed that the CS hydrogels displayed antibacterial ability to *E. coli* and *S aurous*.

In the above study, the complex structure was also characterized by SEM. It is found that the PNIPAAm grafted layer is attached well to plasma-penetrated nonwoven as compared to untreated nonwoven, due to the increase in the wettability between hydrogel and substrate. It is also found that the freeze-dried composite develops porous structure while no porous is observed when CS is dried at room temperature.

However, due complicated entangled structure between NWF and CS, the nonwoven was difficult to strip. Consequently, an easy stripped interlayer fabric is really required for preparing an ideal wound dressing. Therefore, a PINPAAM hydrogel interface was chosen to solve the entanglement due to its temperature and sensitivity and hydrophilic property. This trilayer wound dressing can be a promising approach for tissue engineering applications (Fig. 4.5).

The controlled release of tetracycline hydrochloride (T-HCL) drug from polyester (PET) fabric from temperature is shown in Fig. (4.5). Because the hydrogels having NIPPAAm shrink at 37.5 °C, the T-HCL gels will be released due to the driving force of the volume change and concentration gradient of the drug. Hence, the amount released initial 10 min, which is highest at 37.5 °C. Those drugs

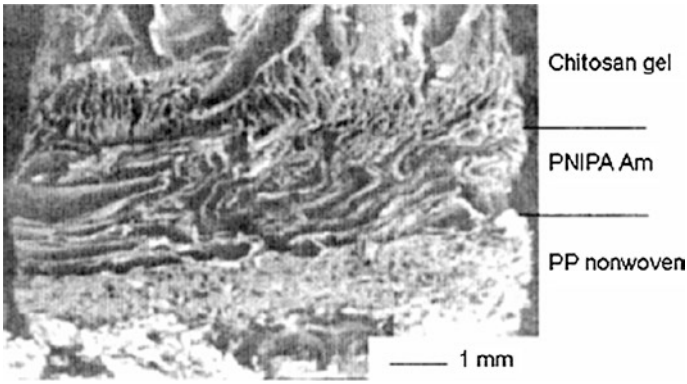

Fig. 4.5 SEM of trilayer wound dressing structure freeze-dried at −80 °C [39]

located near and at the surface released immediately from graft copolymer to the surrounding medium [40].

In one of the reports, a nonantigenic membrane closely resembling dermis in its anatomic structure and chemical composition, in which wound acts as a biodegradable scaffolding inducing the synthesis of a 'neodermis', is prepared as a trilayer membrane system for artificial skin. In this process, the NIPPAAm monomer is successfully grafted on the NWF by copolymerization and then initiated by plasma. Then, the layer of bovine gelation with glycosaminoglycans (chondroitin-6-sulfate) is grafted by ultraviolet light, which serves as a matrix for the infiltration of fibroblast, macrophages, lymphocytes, and capillaries derived from the wound bed. Six weeks after the operation, both the controlled group with no dressing and group with NWF stayed in the proliferative phase, where no epidermis or dermis structure could not be traced at the section; however, the third group having NWF grafted with NIPPAAm healed completely in the maturation phase. In the group where NWF grafted with NIPPAAm, gelatin, and glycosaminoglycans, the wound recovered to the final stage of maturation phase. The wound site had totally recovered at the 4th week post-operation. The dressing material of the group fell off automatically from wound site without any damage to the skin after recovery. It is believed that the dressing material has a great potential in the medical application in the near future [41].

4.3 Nanofibers Containing Sliver Nanoparticles for Wound Dressings

Nanotechniques have acquired tremendous impulse in the last decade. Coated products such as smart clothing as well as nanocoated materials are the present innovations. Nanofibers are preferred due to their unique properties, such as high

surface-area-to-volume ratio, film thinness, nanoscale fiber diameter porosity of structure, and lighter weight [42].

In one of the studies, PVA nanofibers containing silver nanoparticles were prepared by electrospinning PVA/silver nitrate aqueous solutions followed by short heat treatment. Their antimicrobial activity is found to be suitable for wound dressing. Electrospinning is simple, low cost, and effective technology to produce polymer nanofibers. The electrospinning technique provides nonwovens to the order of a few nanometers with large surface area, ease of functionalization for various purposes, and superior mechanical properties. Also, the possibility of large-scale productions combined with the simplicity of the process makes this technique very attractive for many different applications. Biomedical field is one of the important application areas among others utilizing the technique of electrospinning for various applications such as filtration and protection material, electrical and optical applications, sensors, and nanofiber-reinforced composites. In the electrospinning process, a polymer solution or melt is placed into a syringe with a millimeter-size nozzle and is subjected to electric fields of several kilovolts. Under the applied electrostatic force, the polymer is ejected from the nozzle and deposited on a collector. These nanofiber webs have unique properties such as a high surface-area-to-volume ratio, small pore size, high porosity. [43, 44]. These drug-impregnated nanofibers are very effective for topical drug administration because of their high surface-area-to-volume ratio [45, 46]. In particular, incorporation of therapeutic compounds into the electrospun nanofibers has attracted a great deal of attention, because the resultant nanofiber webs have very strong efficacy of the drug due to their high surface-area-to-volume ratio and the composite electrospun nanofiber webs afforded the prospect of preparing useful polymer system for controlled release of the activity the release behavior of the Ag ions from the PVA/AgNO. Nano fiber is dionized in water and examined at 37 °C. A fast and constant release of Ag ions from the heat-treated PVA/AgNO nanofibers would allow them to have fast and constant antimicrobial activity [8]. Also, it is found that Ag ions in the PVA/AgNO nanofibers subjected only to the heat treatment move more rapidly than those in the PVA/AgNO nanofibers subjected to the heat treatment and subsequent UV radiation. This is because of the fact that the residual Ag ions in the heat-treated PVA/AgNO nanofibers were reduced by UV irradiation [46]. Among the antimicrobial agents, silver has long been known to have strong antimicrobial activities, and hence, antibacterial disinfection and finishing techniques are developed for many types of textiles using treatment with nanosized silver [47].

The release of tetracycline from electrospun mats of polyethylene-co.vinyl acetate, polylactic acid (PEVA), and their 50/50 blend has also been studied, and it is found that the electrospun PEVA and 50/50 PLA/PEVA mats give relatively smooth release of drug over about 5 days. The simplicity of the electrospinning process and the wide selection of the polymers that can be processed by this means suggest that electrospun polymers' matrices may have broad applicability in controlled release technology. Wound dressings composed of electrospun polyurethane nanofibrous membrane and silk fibroin nanofibers were developed. Such materials were characterized by range of pore size distribution, high

surface-area-to-volume ratio, and high porosity, which are proper qualities for cell growth and proliferation [48, 49].

4.3.1 Alginate Fiber Wound Dressings

The first modern alginate wound dressing was brand-named as sorbsan, which was launched in 1983 [50]. This was followed by other products that differed in both their chemical composition and textile structure. For example, Kaltostat, a fibrous high G calcium alginate, was introduced into the market in 1986. Kaltostat consists of a mixture of calcium and sodium alginate. The sodium alginate was introduced to improve gel-forming ability of the fibers. It was found that the alginate dressings absorb a large quantity of liquid in addition to those held between the fibers in the textile structure because of the ion exchange between the calcium ions in the fiber and sodium ions in the wound exudates. Alginate fibers can form gel when applied to exuding wounds. The gelling process is accompanied by the absorption of wound exudates into the fiber structure, and as the fiber swelling, the capillary structure in the nonwoven dressing is closed, thereby blocking the lateral spreading of liquid. This gives rise to the unique gel-blocking properties of alginate wound dressings. These also have hemostatic and antimicrobial properties as well as ability to promote wound healing since 1980s, and alginate fibers have been widely used in the manufacture of hightech wound dressings [8, 51, 52].

References

1. Kokabi M, Sirousazar M, Hassan ZM (2007) Eur Polym J 43:773
2. Hayward PG, Morrison WA (1996) Current concepts in wound dressing. Aust Presscr 19:11–6
3. Martin P (1997) Science 276:75
4. Singer AJ, Clark RA (1999) New Engl J Med 341:738
5. Clark RA (1995) J Am Acad Dermatol 13:701
6. Purnasai K, Babu M (2000) Burns 26:54
7. Petrulyte S (2008) Dan Med Bull 55(1):72
8. Quin Y, Gilding DK (1996) Med Device Technol 7:32
9. Lloyx LL, Kennedy JF, Methacanon P, Paterson M, Knill CJ (1998) Carbohydr Polym 373:315
10. Wichterle O, Lim D (1960) Nature 185:117
11. Ulbrich K, Subr V, Podperova P, Buresova M (1995) J Controlled Release 34:155
12. Hoffman AS, Schmer G, Harris C, Kraft WG (1972) Trans Am Soc Artif Intern Orgens 18:10
13. Park KR, Nho YC (2003) Rad Phys Chem 67:361
14. Hoffman AS (2002) Advanced Drug Deliv Rev 43
15. Varshney L (2007) Nucl Instrum Methods Phys Res B 255:343
16. Bruin P, Jonkman MF, Meijer HJ, Pennings AJ (1990) J Biomed Mater Res 24:217
17. Wise DL (ed) (1984) Burn wound coverings. CRC Press, Boca Raton
18. Aiba S, Minoura N, Pujiwara Y, Yamada S, Nakagawa T (1985) Biometerials 6:290
19. Peppas NA (1987) Hydrogels in medicine and pharmacy II and III. CRC Press, Boca Raton

20. Rosiak JM (1991) Radiation effects on polymers. In: Clough RL, Shalaby SW (ed) (ACS Book Series, Washington DC 475)
21. Eloy R, Brack A, Drome N, Cornillac AM (1992) J Biomed Mater Res 695
22. Yoshii F, Zhanshan Y, Isobe K, Shinozaki K, Makuuchi K (1999) Radiat Phys Chem 55:133
23. Wang CC, Su CH, Chen JP, Chen CC (2009) Mater Sci Eng C29
24. Rybicki E, Filipiwoska B, Kozicki M, Jezoriski A, Jackubie J (2005). In: Proceedings 5th international scientific conference medtex 2005, vol 118
25. Pielka S, Paluch D, Staniszwesla-Kus J, Zywicka B, Solski L, Szosland L, Czarny A, Zaczynska E (2003) Fibres Text East Eur 11:79
26. Wang CC, Su CH, Chen CC (2008) J Biomed Mater Res Part A 84A:1006
27. Ishihara M, Nakanishi K, Ono K, Sato M, Kikuchi M, Saito Y, Yura H, Matsui T, Hattori H, Ueonoyama M, Kurita A (2002) Biomaterials 23:833
28. Gupta B, Agarwal R, Alam MS (2010) Indian J Fibers Text Res 35:174–187
29. Mi FL, Shyu S-S, Wu Y-B, Lee ST, Shyong J-Y, Huang R-N (2001) Biomaterials 22:165
30. Yu H, Xu X, Chen X, Hao J, Jing X (2006) J Appl Polym Sci 101:2453
31. Zeng M, Fang Z (2004) J Membr Sci 245:95
32. Samah NA, Zakaria MA, Yarmo, Ayub MK (2001) Preparation of chitosan coated gauze and its morphological and physical properties. In: Paper presented at the NSF workshop, Kuala Lumpur
33. dos Santos KSCR, Coelho JFJ, Ferreira P, Pinto I, Lorenzetti SG, Ferreira EI, Higa OZ, Gil MH (2006) Int J Pharm 310:37
34. Ciechanaska D (2004) Fibres Text East Eur 12 N4(48):69
35. Ciechanaska D, Kazimeirczak J, Gusta M (2005). In: Proceedings of 5th international scientific conference medtex, vol 44
36. Ciechanaska D, Struszczyk H, Guzinska K (1998) Fibres Text East Eur 64(23):61
37. Gupta B, Aggarwal R, Alam MS (2010) Indian J Fibres Text Res 35:174
38. Kondo T, Koyama M, Kubota H, Katakai R (1998) J Appl Polym Sci 67:2057
39. Yang JM, Lin HT (2004) J Membr Sci 243:1
40. Chen KS, Ku Y-A, Li C-H, Lin HR, Lin FH, Chen TM (2005) Mater Sci Eng C25:472
41. Gupta B, Mishra S, Saxena S (2008) Radiat Phys Chem 77:553
42. Lin FH, Chen TM, Chen KS, Wu TH, Chen CC (2000) Mater Chem Phys 64:189
43. Graham K, Schreuder GH, Gogins M (2003) Intcorporation of electrospun nano fibers into functional structures. Proceedings of the international non woven technical conference, Baltimore, 15–18 Sept 2003
44. Jin WJ, Jeon HJ, Kim JH, Youk JH (2007) Snythetic Metals 157:454
45. Hong KH, Kang TJ (2000) J Appl Polym Sci 100:167
46. Kenawy ER, Bowlin GL, Mansfield K, Layman J, Simpson DG, Sanders EH, Wenk GE (2002) J Control Release 81:57
47. Hong KH, Park JL, Sul IH, Youk JH, Kang TJ (2006) J Polym Sci Part B 44:2468
48. Lee HJ, Yeo SY, Jeong SH (2003) J Mater Sci 38:2199
49. Khil MS, Cha DI, Kim HY, Kim IS, Bhattarai N (2003) J Biomed Mater Res Part B Appl Biomater 67:675
50. Min BM, Lee G, Kim SH, Nam YS, Lee TS, Park WH (2004) Biomaterials 25:1289
51. Quin Y (2008) Polym Advan Technol 19:6
52. Gupta B, Agarwal R, Alam MS (2010) Textile based smart wound dressings. Indian J Fibers Text Res 35:174–187

Chapter 5
PLA Knitted Scaffold

5.1 Introduction

Tissue engineering is an outcome of the dramatic advances in the area of material science coupled with the latest knowledge of molecular cell biology. It enables the development of biological substitutes that restore, maintain, or improve tissue function [1]. The three important techniques used in tissue engineering are cell substitutes, tissue-inducing substances, and cell placed on/within matrices. The last one has become popular in tissue engineering research. It involves the development of biological substrates to treat the loss or dysfunction of an organ, indicating certain combination of cells and scaffold materials. A scaffold is a material system upon which a cell is implanted and permitted to grow and proliferate three dimensionally. The scaffolds not only permit formation of new tissues with appropriate structures, but also allow growth of new tissues with specific functions [2]. Scaffolds are generally made of polymeric materials so as to immobilize biologically active molecules and living cells. Polymers such as hydroxyapatite and polyhydroxyesters, and natural polymers such as collagen and chitin have been used in tissue engineering [3]. The tailoring of scaffold is not usually generic but is always application specific [4]. Each scaffolding material or combination of materials possesses different processing requirements and varying degree of processability to form scaffolds. The main parameters influencing the fabrication technique for scaffold production are process conditions, accuracy of the process, repeatability, and consistency of the process [5]. The most common scaffold fabrication techniques for tissue engineering are phase separation, particulate leaching, freeze-drying, composite foams preparation, polymeric films modification, solid free-form development, and textile processing techniques [6–22]. Each technique has its own merits and demerits. Hence, the designing and fabrication of scaffolds are done according to its application. The minimum requirements for the scaffold material to be used for human urinary bladder are elasticity, porosity, drapeability,

N. Gokarneshan et al., *Emerging Research Trends in Medical Textiles*,
Textile Science and Clothing Technology, DOI 10.1007/978-981-287-508-2_5

and good mechanical properties. Bioreceptive PET films have been developed earlier, wherein urothelial cells and smooth muscle cells have been seeded for their subsequent growth into a tissue [17, 23, 24]. The modified PET films were observed to be an excellent surface for urinary cell bladder culture, but had some drawbacks such as porosity and elasticity. In later attempt, bioreceptive PET knittings were developed for the same application [25]. The knitted surface has various advantages such as high porosity and elasticity besides good mechanical properties and drapeability. However, the drawback of this bioreceptive PET knitted scaffold is its nonbiodegradability. It can be overcome by replacing the biostable PET by any biodegradable polymer such as lactides and polysaccharides.

5.2 Spinning and Drawing of PLA Fiber

The PLA filament, which is produced by dry–jet–wet spinning technique, comprises of the process of phase inversion where the polymer solution gets precipitated in the nonsolvent. The process of phase inversion results in the development of porous structure. The PLA solution has been prepared in chloroform, and coagulation has been done in methanol which acts as a nonsolvent. The process details and resultant filament properties have already been discussed in the earlier publications [26, 27]. The filaments produced from this process are trilobal in cross section having tenacity between 0.14 and 0.60 GPa. The mechanical properties were observed to be dependent on the draw ratio, drawing temperature, and heat-setting temperature; the cumulative effect of these process parameters on molecular orientation and development of crystallinity in resultant filament result into filaments with different mechanical properties. The speed of take up at the spinning stage determines the development of the fiber properties. The stretch in spinning increases with the take-up speed and results in better molecular chain orientation.

The use of the PLA as spun fibers for the drug delivery prepared by dry–wet spinning process has been reported [28]. The use of wet spinning technique in the production of PLA fiber has also been reported for biomedical application [29]. However, both the reports have been restricted to fiber formation. In the present discussion, the post-spinning operations have been further carried out to develop the PLA filament with desired properties. The as-spun PLA filament has been drawn at various draw ratios on two-stage drawing machine at drawing temperature 90 °C and heat-setting temperature of 120 °C [31]. The filament having draw ratio of 6 and tenacity of 0.49 GPa and elongation of 25 % has been chosen for the knitting. The knittings have been fabricated separately with 2, 4, and 8 ply yarns, respectively.

5.3 Flexural Rigidity

The filament flexural rigidity reflects directly on the bending properties of the filament which is most important property to be considered in knitting. It is the

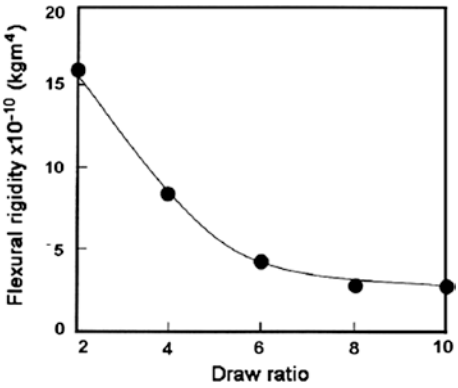

Fig. 5.1 Influence of draw ratio on flexural rigidity of polylactic acid monofilament [31]

force couple to bend monofilament to a unit of curvature. The formation of the loop, the size of the loop, and fabric behavior are depended on the rigidity of a filament [31]. The ring-loop test is the simplest method of measuring the flexural rigidity. The flexural rigidity of the PLA monofilament drawn at different ratios was found out by the above-described process as shown in the Fig. 5.1.

The flexural rigidity is seen to reduce with the increase in draw ratio. The bending property of the filament is considered to be important in the knitting process. Flexural rigidity is a direct measurement of bending property. All the filament drawn at different draw ratios have been tested for flexural rigidity. The reduction in the flexural rigidity on increases in draw ratio is well predicted since as the draw ratio increases, thinning of the filament takes place, which means mass per unit length decreases. It influences the filament rigidity directly.

5.4 Mechanical Properties

The PLA has been knitted on single-end weft-knitting machine with 2, 4, and 8 ply PLA yarns, and the knitted structures are shown in the Fig. 5.2.

Uniformed size of the loops is formed. All the three structures have been studied for mechanical properties and in vitro degradation as well. The behavior of the knitted

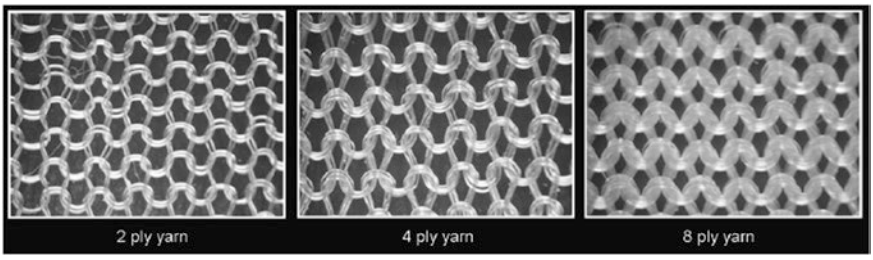

Fig. 5.2 Structures of knitted fabrics as viewed by optical microscope [31]

fabric under pressure has been studied by use of the ball bursting technique. It more or less simulates the behavior of urinary bladder in the urine filling process. The maximum intra vesical pressure on human urinary bladder wall is 40 mmHg which is equivalent to 5.3×10^{-3} MPa. The stress value obtained by bursting test for knitted fabric of 8 ply yarn is 0.33 MPa which is considerably higher than the required value. Also, the extension of the knitted fabric is found to be high. The maximum bursting load of the fabric is dependent on the number of plies in the yarn. For the knitting of 8 ply yarn, the maximum load required to burst is 53.7 kg which is quite high as compared to 20.3 and 11.6 kg for 4 ply and 2 ply yarn, respectively. Similar trend can be seen in the case of extension though the difference is small (Fig. 5.3). The crack in the fabric is due to the bursting that happens in 'I' shape (Fig. 5.4).

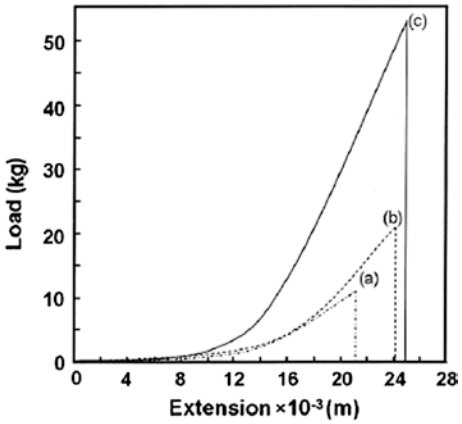

Fig. 5.3 Load extension curves of polylactic acid knitted fabrics in ball bursting test [31]. **a** 2 ply yarn, **b** 4 ply yarn, and **c** 8 ply yarn

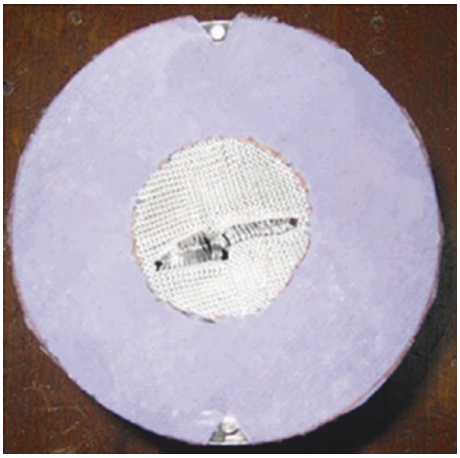

Fig. 5.4 Burst knitted fabric [31]

The cyclic loading at 50 % of bursting load has been carried out to study the performance of the knitted structure. The intended application of knitted structure is as a scaffold material for human bladder reconstruction, that is, why this test was performed to determine the deformation property of the knitting. After 4–5 cycles of loading, the material gets stabilized and the load extension curve starts repeating for further loading cycles. The residual extension in the fabric becomes almost constant after that. Figure 5.5 depicts the cyclic load extension curves for every type of knitting. In case of cyclic loading, initially fabric shows higher extension. During initial cycles of loading, individual loops contribute toward the extension in addition to the elasticity of the yarn. The contribution from the loop reduces after few cycles of loading, because of their deformation and the residual extension is the result of the inherent extension of yarn. It can be seen that the fabric gets deformed in all the three cases, after 4–5 cycles of loading.

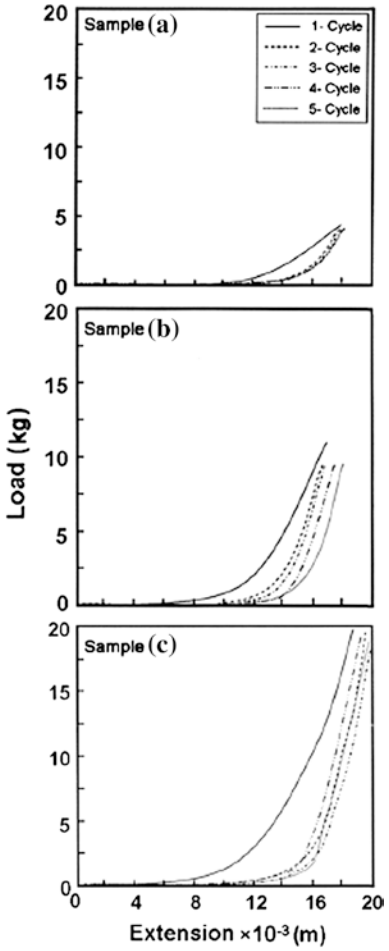

Fig. 5.5 Load extension curves of fabrics cyclically loaded [31]. **a** 2 ply yarn, **b** 4 ply yarn, and **c** 8 ply yarn

5.5 Porosity of Knitted Fabrics

The data of knitted fabrics thickness weight are given in the Table 5.1.

The porosity of a knitted fabric is the ratio of void volume to total volume. The porosity value obtained for knitted fabric of 8 ply yarns is 80 %, which is well within required range [31]. Each pore area has been calculated to visualize the openness of the knitted structure. A knitted fabric has two kinds of pores—one is within the loop and the other between the loops. These pores differ in their area. The areas of pores for knitted fabric are given in Table 5.1. Porosity of the scaffold plays a crucial role in the cell culture. It is necessary for the easy passage

Table 5.1 Porosity and pore area of knitted fabrics [31]

Fabric made with	Thickness (cm)	Weight (cm)	Porosity (%)	Area of pore (μm^2)	
				Between the loops	Inside the loops
2 ply yarn	0.056	270.0	93	688,215	579,985
4 ply yarn	0.057	83.75	89	641,715	422,183
8 ply yarn	0.104	52.50	80	260,502	122,672

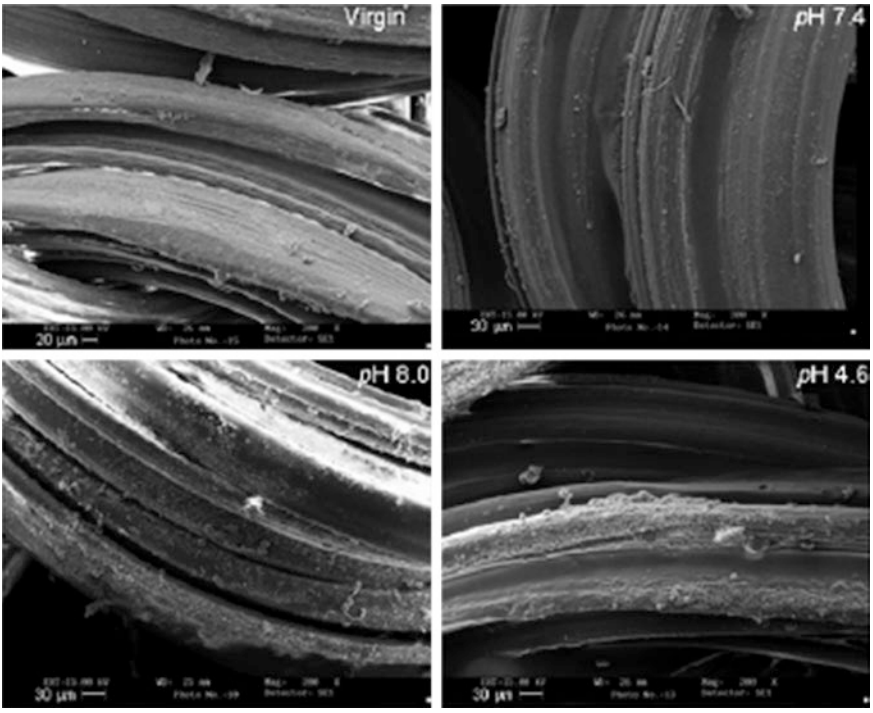

Fig. 5.6 SEM images showing degradation of knitted fabrics at different pH over duration of 20 weeks [31]

of nutrients and also for the tissue culture growth in all dimensions. The knitted fabric structure is highly porous. The values of porosity obtained for knitted fabric are given in Table 5.1. The porosity reduces with increase in the number of plies in yarn. The size of the pore size depends on number of plies in the yarn. With the increase in the number of yarn plies, the fabric openness reduces.

5.6 Scanning Electron Microscopy

The knitted PLA scaffold has been considered as the scaffolding material in the reconstruction of the urinary bladder. The pH of urine ranges between 4.6 and 8.6. The investigation of in vitro degradation has therefore been conducted on three different pH values in order to simulate the body fluid. The detailed investigation is reported in a work [30]. The surface morphology of the knitted fabric degraded for 20 weeks has been reported in the study. The severity of degradation increases as the pH deviates from 7.2. The SEM images confirm this aspect (Fig. 5.6) [31].

At lower PH, the degradation becomes higher which conforms catalytic effect of hydronium ions on hydrolysis process.

References

1. Langer R, Vacanti JP (1993) Tissue engineering. Science 260:920
2. Nikolosvski J, Mooney DJ (2000) Smooth muscle cell adhesion to tissue engineering scaffolds. Biomaterials 21:2025
3. Hutmacher DW (2000) Scaffolds in tissue engineering bone and cartilage. Biomaterials 21:2529
4. Thomson RC, Yaszemski MJ, Mikos AG (1997) In: Lanza R, Langer R, Chik W (eds) Principles of tissue engineering. R.G Landes Company, USA, p 263
5. Leong KF, Cheah CM, Chua CK (2003) Solid free form fabrication of three dimensional scaffolds for replacement of tissues and organs. Biomaterials 24:2363
6. Nam YS, Park TG (1999) Porous biodegradable polymeric scaffolds prepared by thermally induced phase seperation. J Biomed Mater Res 47:8
7. Zhang R, Ma PX (1999) Poly(α-hydroxyl acids)/hydroxyapatite porous composites for bone tissue engineering—Preparation and morphology. J Biomed Mater Res 44:446
8. Yang F, Murugan R, Ramakrishna S, Wang X, Ma Y-X, Wang S (2004) Neo cartilage formation in vitro and in vivo using cells cultured on synthetic biodegradable polymers. Biomaterials 25:1891
9. Freed LE, Marquis JC, Noharia A, Emmanual J, Mikos AG, Langer R (1993) Development of a mechano-active scaffold for tissue engineering. J Biomed Mater Res 27:11
10. Yang Y, Magnay JL, Cooling L, Haj AJE (2002) Optimizing the sterilization of PLGA scaffolds for use in tissue engineering. Biomaterials 23:2119
11. Holy CE, Cheng C, Davies JE, Shoichet MS (2001) Effect of basic fibroblast growth factor on cartilage regeneration in chondrocyte-seeded collagen sponge scaffold. Biomaterials 22:25
12. Fujisato T, Sajiki T, Liu Q, Ikada Y (1996) Human preadipocytes seeded on freeze dried collagen scaffolds investigated in vitro and in vivo. Biomaterials 17:155

13. Heimburg DV, Zachariah S, Heschel I, Kuhling H, Schoof H, Hasemann B, Pallua N (2001) Rat costochondral cell characteristics on poly (L-lactide-co-epsilon-caprolactone) scaffolds. Biomaterials 22:429
14. Honda M, Moktikawa N, Hata K, Yada T, Morita S, Ueda M, Kimata K (2003) Preparation of poly(glycolic acid) bonded fibre structures for cell attachment and transplantation. Biomaterials 24:3511
15. Mikos AG, Bao Y, Cima LG, Ingber DE, Vacanti JP, Langer R (1993) Plasma sprayed calcium phosphate particles with high bioactivity and their use in bioactive scaffolds. J Biomed Mater Res 27:183
16. Wenga J, Wang M, Chen J (2002) Thermal cross linking of collagen immobilized on PAA grafted (polyethylene terephthalate) films. Biomaterials 23:2623
17. Gupta B, Plummer C, Bisson I, Frey P, Hilborn J (2003) Biomemetic surface modification of poly(L-lactic) acid with chitisan and its effects on articular chondrocytes in vitro. Biomaterials 23:3859
18. Cui YL, Qi AD, Liu WG, Wang XH, Wang H, Ma DM, Yao KD (2003) Biodegradable polymer scaffolds for tissue engineering. Biomaterials 24:3859
19. Freed LE, V-Novakovic G, Biron RJ, Eagles DB, Lesnoy DC, Barlow SK, Langer R (1994) Thermal compression and characterization of three dimensional non woven PET matrices as tissue engineering scaffolds. Biotechnology 12:689
20. Li Y, Ma T, Yang S-T, Kniss DA (2001) Novel biodegradable electrospun membrane: scaffold for tissue engineering. Biomaterials 22:609
21. Bhattarai SR, Bhattarai N, Yi HK, Hwang PH, Cha DI, Kima HY (2004) Tissue engineering scaffolds using superstructures. Biomaterials 25:2595
22. Wintermantel E, Mayer J, Blum J, Eckert KL, Luscher P, Mathey M (1996) Plasma induced graft polymerization of acrylic acid onto poly(ethylene terephthalate) films. Biomaterials 17:83
23. Gupta B, Hilborn J, Bisson I, Frey P, Plummer C (2001) Acrylic acid grafting and collagen immobilization on poly(ethylene terephthalate) surfaces for adherence and growth of human bladder smooth muscle cells. J Appl Polym Sci 81:2993
24. Bisson I, Kosinski M, Ruault S, Gupta B, Hilborn J, Florian W, Frey P (2002) Acrylic acid grafting and collagen immobilization on poly(ethylene terephthalate) surfaces for adherence and growth of human bladder smooth muscle cells. Biomaterials 23:3149
25. Revagade N (2001) Development of bioreceptive poly(ethylene terephthalate) for medical application, M.Tech thesis, Department of Textile Technology, Indian Institute of Technology, Delhi, India
26. Gupta B, Revagade N, Anjum N, Atthoff B, Hilborn J (2006) Preparation of poly(lactic acid) by dry jet wet spinning—I—Influence of draw ratio on fiber properties. J Appl Polym Sci 100:1239
27. Gupta B, Revagade N, Anjum N, Atthoff B, Hilborn J (2006) Preparation of poly(lactic acid) by dry jet wet spinning—II—Effect of process parameters on fiber properties. J Appl Polym Sci 101:3774
28. Eenink MJD, Feijen J, Olisglager J, Albers JHM, Reiki JC, Greidanus PJ (1987) J Contr Rel 6:225
29. Nelson KD, Romero A, Waggoner P, Crow B, Borneman A, Smith GM (2003) Technique paper for wet spinning poly(L-lactic) acid and poly(DL - lactide and co glycolide) mono filament fibers. Tissue Eng 9:1323
30. Gupta B, Revagade N, Hilborn J (2007) In vitro degradation of dry jet wet spun poly(lactic acid) monofilament and knitted scaffold. J Appl Polym Sci 103:2006
31. Gupta B, Revagade N (2009) Development and structural evaluation of polylactic based knitted scaffold for human urinary bladder reconstruction. Indian J Fibre Text Res 34:115–121

Chapter 6
Silver-Containing Wound Dressings

6.1 Introduction

Alginate dressings possess special gel-forming properties and a high degree of absorption and are therefore considered to be one of the most versatile wound dressings [1]. They are able to form occlusive dressings that are applied on wounds ranging between moderate and high degree of exudation. An interesting work has focused on the effects of occlusion on the rate of epithelialization in surgically induced wounds, which are left to heal in open air or occluded under a transparent film, and has provided the base for development of occlusive dressings [2, 3]. Occlusive wound dressings help to maintain a moist environment on the wound surface by restricting the transmission of water vapor and gases to the external environment [4]. A moist environment enables better wound healing, and thereby prevents desiccation and death of epithelial cells, facilitates epidermal migration, angiogenesis, and connective tissue regeneration [5]. All occlusive dressings provide the benefits of insulation and mechanical protection, and act as a barrier against bacteria [6]. The scar caused by an occlusive dressing is more acceptable than that caused by an exposed wound [7, 8]. Occlusive dressings limit the pain in partial-thickness wounds to a greater degree than nonocclusive dressings [9]. Occlusion can decrease the incidence of infection in the case of simple wounds. Calcium alginate fiber is used in the production of dressings that interact with wound exudate to form a gel. The fibers are generally carded or needle-punched. The dressings could be categorized as low absorbency or high absorbency [10]. Dressings that absorb less than 6 g of liquid per g of fiber (or less than 12 g/100 cm^2) are classified as dressings of low absorbency, and dressings that absorb 6 g or more (or 12 g or more/100 cm^2) are classified as dressings of high absorbency. Ten commercially available alginate dressings are generally a blend of calcium and sodium alginates. Different commercially available alginate dressings vary in their proportions of calcium and sodium alginates. Alginates are

N. Gokarneshan et al., *Emerging Research Trends in Medical Textiles*,
Textile Science and Clothing Technology, DOI 10.1007/978-981-287-508-2_6

highly absorbent, hydrophilic, and gel-forming materials. When a calcium alginate fibrous dressing absorbs sodium ions from a wound exudate, a gel is formed in situ, a moist environment is created at the wound site, and proportionate calcium ions are released from the dressing. Calcium ions, when released into wounds, stimulate both platelet activation and whole blood coagulation. This explains the hemostatic performance of alginate dressings.

6.2 Silver-Based Dressings

Silver has been used as an antimicrobial agent for a very long period of time and hence a good historical significance [11]. Silver nitrate has been used in the treatment of burns [12]. It has a broad antibacterial spectrum and is effective against most bacterial strains especially *Staphylococcus aureus, Staphylococcus epidermidis,* and *Klebsiella pneumonia.* It turns to brown-black on things that it comes into contact, without its antibacterial property getting affected. Wound dressings with high absorbency and good antibacterial properties can be obtained by introducing silver ions into alginate fibers. A research reports that wound dressings with silver content when used in clean wounds enhance the epithelialization rate by about 30 % [13]. This indicates a beneficial effect of the silver ions in wounds, besides the antimicrobial activity. The sustained slow release of low concentration of silver ions appears to stimulate healing. Apart from being used for wound dressings, antimicrobial silver coatings are also being used in medical health care, hygiene, bedding products, sports protective clothing, and personal care [14]. Silver at the nanoscale or silver-based nanoparticles provide high availability of bactericidal (and bacteriostatic) silver ions for improved antimicrobial effect. The antimicrobial activity of the silver-alginate wound dressing (silver/sodium/calcium alginate) is improved by the sustained release of silver ions present in the dressing.

6.3 Silver-Alginate and CM Print Cloth Dressings

The antimicrobial properties of silver have been incorporated into commercially available alginates that produce dressings, which are more effective in the treatment of exudative wounds. When alginate dressings are used on exudative wounds in the clinical setting, the recommended frequency of dressing changes is determined by the volume of the exudate. Product labels of the commercially available alginates recommend that the dressing can be left in place for up to one week, but may need to be changed more than once a day on highly exudative wounds. For clinical use, the silver dressings should retain the high absorptive ability of their alginate counterparts. Hence, an investigation on the absorption and swelling characteristics of the alginate/silver alginates and of cotton-CM print cloth/silver-CM print cloth in distilled water and 0.9 % saline solution at 8 h and

at one week (range of time commercially dressings are kept on wounds) have been discussed herein. The research work on silver antimicrobials has resulted in the measurement of the diameters of swollen silver antimicrobial dressings [12, 15].

6.4 Earlier Research Findings

A cat ion exchange method has been adopted so as to enable impregnation of commercially available alginate moist wound dressings and CM cotton print cloth with silver [12, 15, 16]. Silver–calcium–sodium alginates have been evolved from sterile calcium alginate dressings currently on the market, for example, Kaltostat (ConvaTec), Curasorb (Kendall), Sorbsan (Maersk Medical), and Algisite M (Smith & Nephew), and involved a two-step process. In the first step, each of these alginate dressings was treated with acetic acid in 80/20–90/10 ethanol/water for 45 min with fiber-to-liquor ratio of 1:10 to partially exchange the calcium ions with hydrogen ions. The dressings have then been treated with silver nitrate wet-to-wet to replace hydrogen ions with silver cat ions in 80/20–90/10 ethanol/water for 45 min to 12 h at room temperature. A prolonged reaction of 12 h with silver nitrate has been chosen in the laboratory to permit (red-brown, brown-black) staining of the antimicrobial dressing visually confirming the presence of the silver cat ion (qualitative test). The exact quantity of silver cat ion on silver alginates has been measured [17]. Silver–sodium-CM print cloth has been prepared from a low DS (degree of substitution = 0.15) hygroscopic carboxymethylated cotton print cloth (CM print cloth) involving a two-step aqueous process: the first step consisted of acidulation to partially replace sodium with hydrogen ions, and subsequently in the second step, the hydrogen ions have been replaced with silver ions by the treatment with silver nitrate. Low DS CM cotton print cloth does not swell in water to the extent to get it dispersed in water as does the highly swelling high DS cotton (DS = 0.31–4.0). Hence, it does consider nonaqueous media for cat ion exchange, as in the case in alginates [16]. But, only low DS CM cotton print cloth has been used in the investigation. The saline absorbency data of the four silver-alginate products (with their needle-punched alginate controls), along with that of silver-CM print cloth as an assessment of the dressings ability to function in a heavily exudating wound, have been obtained. The absorption determinations have been carried out as per certain standards [18, 19]. The alginate dressings exhibited various absorption capabilities. The saline absorbency assesses how well the presently developed silver antimicrobials would function on exudating wounds; the silver antimicrobials have the potential to function well when used on heavily exudating wounds where alginates are typically applied. The antimicrobial activity of the silver-CM print cloth has been evaluated [20]. It has been effective against both Gram-positive (Staphylococcus aureus) and Gram-negative (Klebsiella pneumoniae) organisms. The fabric exhibited a high degree of lethality resulting in a viable organism count of <10 CFU/mL as compared to the exponential growth in the control fabrics. Viability controls had an average organism

count of 1.8×10^6 CFU/mL for *Staphylococcus Aureus* and 7.8×10^6 CFU/mL for *Klebsiella Pneumoniae*. The antimicrobial activity of silver antimicrobials has been confirmed through specific tests. This test method has been updated as ASTM E 2149 by ASTM. The test challenges the antimicrobial product with one organism, and effectiveness is determined after 24 h of incubation. The plate counts obtained before and after shaking have been used to determine percent reduction in bacteria and thus effectiveness of the antimicrobial product. All three silver-alginate dressings evaluated for antimicrobial activity have been found to be effective against Gram-positive (*Staphylococcus Aureus*) and Gram-negative (*Klebsiella Pneumoniae*) organisms. The activities have been compared. The fabrics practically destroyed the bacterium resulting in an organism count of <10 CFU/mL as compared to exponential growth in the control fabrics with organism count of 4.5×10^4 CFU/mL for *Staphylococcus Aureus* and 6.8×10^5 CFU/mL for *Klebsiella Pneumoniae.* The Ag-CM cotton print cloth may be suitable for potential use against nosocomial acquired infections [17]. The antimicrobial silver-CM cotton print cloth could prove effective against both Gram-positive and Gram-negative bacteria after four laundering cycles. It signifies that the antimicrobial print cloth is durable to washing and favors future study for its potential application in the prevention of nosocomial infection (hospital-acquired infection). It has been acquired 2–3 days after admitting patient and is considered to be secondary reason.

6.5 Results of Findings

Figure 6.1a–d show the photomicrographs of four silver-alginate dressings (Sorbsan, Kaltostat, Curasorb, and Algisite—with their controls) before and after immersion in saline. The increase in the diameter of the fiber can be easily observed from the figure. Figure 6.1e shows the photomicrographs of silver-CM print cloth and its control for 8 h and one week of immersion in saline solution. A perceivable swelling can be noticed after 8 h of immersion and also a slight further increase is noticeable at one week. It is easy to observe the swelling: 1 week > 8 h > dry with the decrease in fabric interstices (open area). Significant swelling is observed in saline immersion compared to those in water in each of the dressings (photomicrographs in water not shown). The data obtained for swelling data correlate with those of the absorbency. The absorbency of the silver alginates and silver-CM print cloth was excellent, albeit less than that of the control samples. The silver print cloth absorbed 3.61 g of saline per g of print cloth compared with 3.93 g/g for the control CM print cloth sample. The four silver-alginate dressings absorbed 12.82–20.23 g of saline per g of alginate dressing compared to 12.50–24.99 g/g for the controls. The lower absorbency of the silver–sodium–calcium alginates is due to fewer sodium ions as compared to their controls, sodium–calcium alginates. The results of the microscopic measurements of the fiber diameters of silver-alginate dressings and their alginate controls in

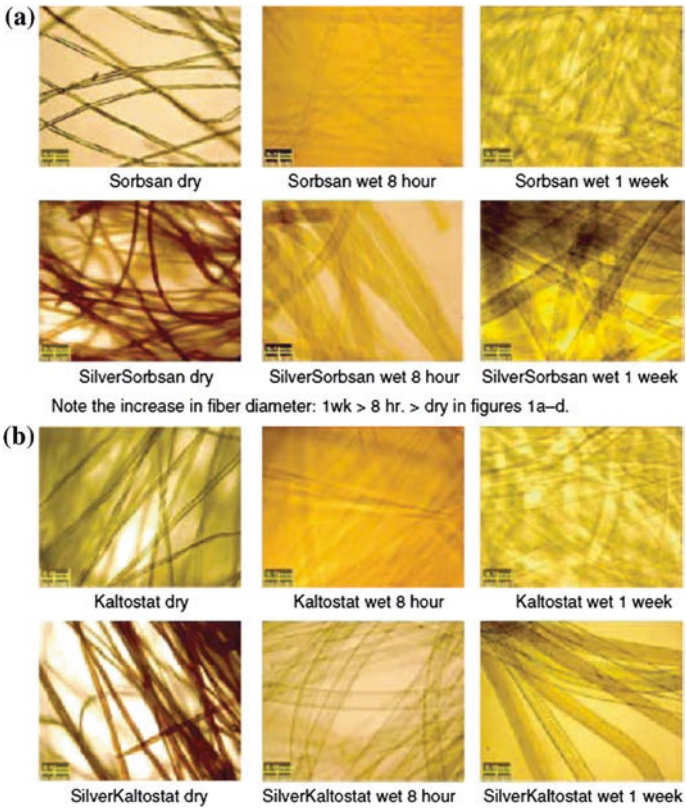

Fig. 6.1 **a** Data from December 2003 to January 2004 (in 0.9 % NaCl)—Increase in fiber [18] diameter can be seen: 1 week > 8 h > dry in Fig. 6.1**a**–**d**; **b** data from December 2003 to January 2004 (in 0.9 % NaCl); **c** data from December 2003 to January 2004 (in 0.9 % NaCl); **d** data from December 2003 to January 2004 (in 0.9 % NaCl); **e** Data from December 2003 to January 2004 (in 0.9 % NaCl). *Note* the swelling: 1 week > 8 h > dry with decrease in fabric interstices (open area)

water and in saline at 8 h and at one week have been observed. All measurements are averages of the results from the four experimental runs and are reported as a change in diameter in micrometers (mm). The absorption and swelling capabilities of the four alginate dressings have caused increase in diameter. The change in diameter of the silver-alginate fibers at 8 h of saline immersion has been found to be 166, 108, 59, and 162 % for the silver-Sorbsan, silver-Kaltostat, silver-Curasorb, and silver-Algisite, respectively.

The studies on alginate dressings and CM print cloth show a percent change in diameter after 1 week of immersion in saline for silver dressings and found to be 153, 124, 54, and 176, respectively. The control alginate fibers and silver-alginate fibers show same extent of swelling. The relative fiber absorbency of Algisite, Kaltostat, and Sorbsan is similar, whereas that of Curasorb is lower. The absorbency and swellability of the various dressings are different. The following

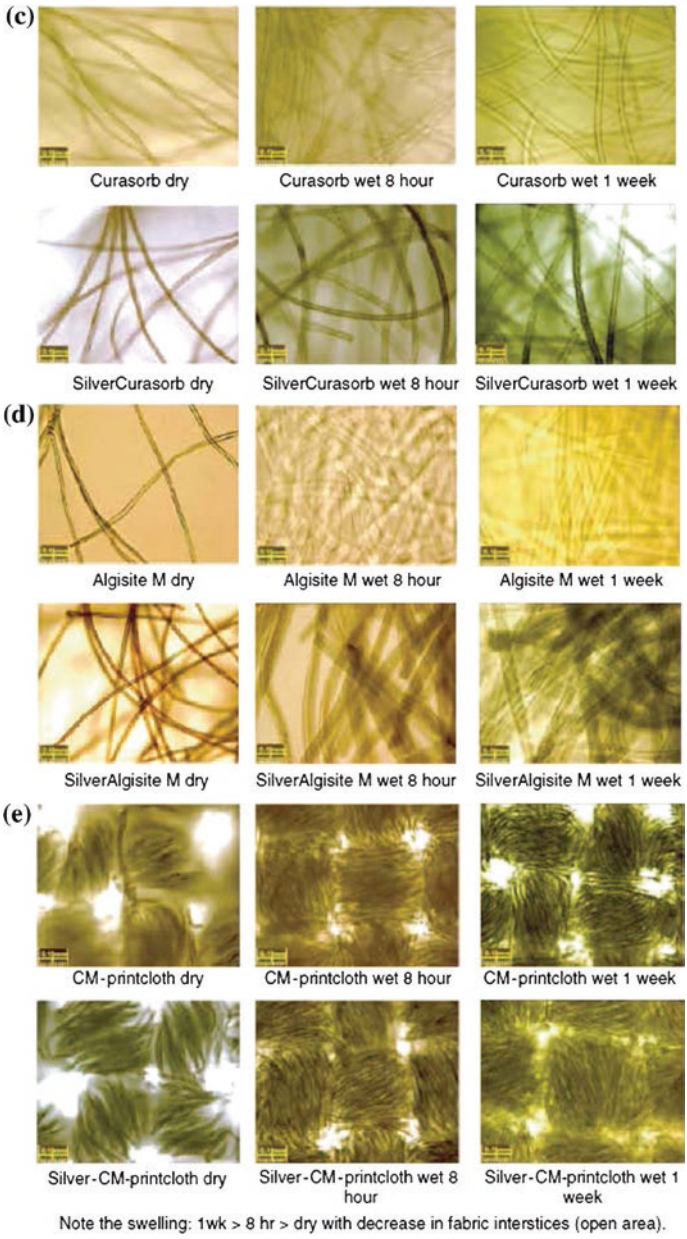

Fig. 6.1 (continued)

inferences are made from the results. In the case of control and silver alginates, a very significant increase in diameter of fibers has been observed in both saline and water, at 8 h and at one week. The major diametrical happens within

the initial 8 h of immersion and continued immersion for a week results in only a slight further increase. On the whole, silver alginates exhibit lesser swelling than their controls in both solutions at 8 h and at one week. As an instance, the Sorbsan control after 1 week of saline immersion had a 193 % increase in diameter, while the silver-Sorbsan swelled by only 153 %. The swelling in saline has been noticed to be greater than that in water for each of the dressings and points to potential for clinical use. The data show that Sorbsan could be well suited for highly exudation wounds, while Curasorb could suit well on moderately/less exudating wounds. Nevertheless, the final result of wound healing that occurs during epithelialization may be very similar between the two silver-treated dressings. The percent diameter change due to swelling in print cloth for 8 h and one week in saline has been recorded. As can be visualized, the swelling of print cloth is much lower than the swelling of alginates. And as with the alginates, print cloth swelled more in saline than in water and the majority of the swelling occurred during the first 8 h of immersion. The silver print cloth swelled less than its control. Single fiber swelling of alginate dressings is illustrated in Fig. 6.2, for the swelling of silver-Sorbsan alginate fiber in 0.9 % NaCl solution. It could be generally inferred

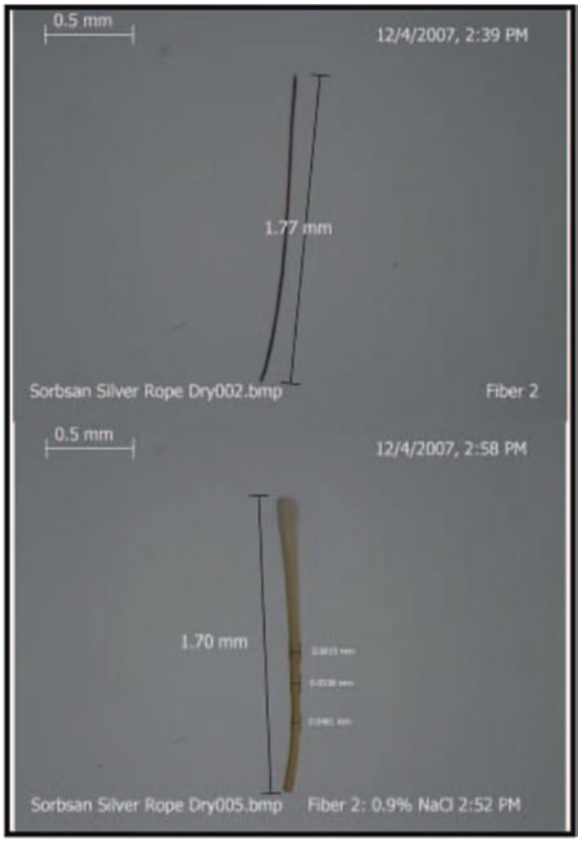

Fig. 6.2 Sorbsan silver rope—upper part shows dry fiber and lower part shows same fiber after 6 min in 0.9 % NaCl at room temperature [18]

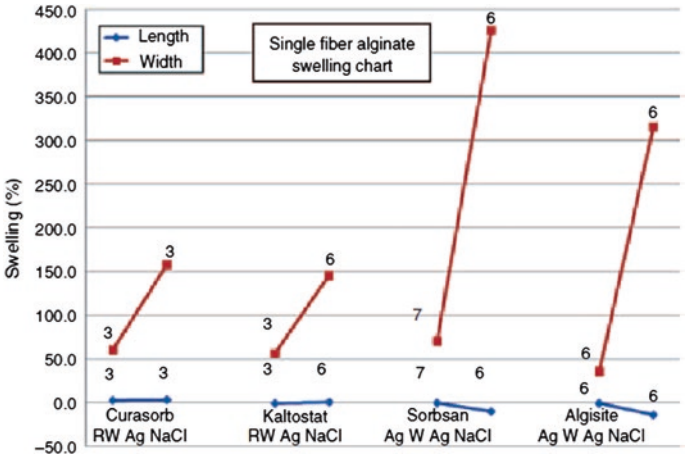

Fig. 6.3 Type of alginate fiber and treatment (Numbers represent sample size) [18]. *RW* Regular alginate fiber (control) soaked in water; *Ag NaCl* silver-alginate fiber soaked in 0.9 % NaCl; *AgW* silver-alginate fiber soaked in water. *Lower blue lines* represent length of the fiber, and *upper red lines* represent diameter

that the fluid absorption resulted in diameter increase in the fiber but not in length (Fig. 6.3). Six of the eight single fiber measurements showed a statistically significant expansion (swelling) in diameter, whereas length measurements showed no significant increase. The swelling percentage of a small sample size of 1–2 mm with variability, (shown in Fig. 6.3) can improve since more fluid can easily enter the cut fibers. Also the cut ends of the single fibers probably resulted in some fiber damage and may be responsible for differential swelling at fiber tips as shown in Fig. 6.3. On the one hand, the degree of swelling in individual fibers does not represent intact fibers and on the other hand, the measurements of the cut single fiber clearly exhibit that fibers swell in diameter, whereas the increase in the length is insignificant.

6.6 Discussion of the Findings

Acute and chronic wounds such as those caused by burns or pressure ulcers generally produce a large amount of exudate, which impairs wound healing and provides a medium for bacterial growth. Such wounds are at high risk for getting infected. Efficient absorption of the wound exudate, and the maintenance of a sterile (or near sterile) environment at the wound site is preferred. Alginate dressings have become the standard of care for treatment of these open, exudating wounds. These dressings have the ability to absorb significant amounts of the exudating fluid without desiccating the wound. The silver-alginate dressings have additional antimicrobial properties imparted into them to improve their efficacy in wound

healing by reducing the bacterial burden in the wound. Although this study reported effectiveness on Staphylococcus aureus and Klebsiella pneumoniae, it is possible that silver (I)-alginate dressings may be effective on other bacterial or fungal strains. By demonstrating fiber swelling after immersion in water and saline, it was shown (in this study) that these antimicrobial dressings retain their absorptive qualities. Similar findings were reported for silver-CM print cloth. However, the Ag-CM cotton print cloth (less expensive) may be suitable for potential use against nosocomial acquired infections. It was also shown that the absorption of fluid leads to fiber swelling in diameter without increase in the length of the fibers. If used in vivo, when the exudates are absorbed in the fiber structure of the needle-punched alginate dressings, the fibers may expand circumferentially upon swelling. As a result, the space between the fibers in the dressing is greatly reduced and the wound fluid is trapped not only in the fibers, but also between the swollen fibers. It is hypothesized that any bacteria from or around the wound are trapped, both within the fibers and in the space between the swollen fibers. With the change of dressings, these bacteria are removed from the wound site. Simultaneously, bacteria are killed at the wound site as the silver cations from the antimicrobial dressings are exchanged for sodium ions on the wound surface. Thus, infection is either prevented or eliminated. These properties may expand the clinical utility of the antimicrobial silver alginates beyond that of commercially available dressings. The fibrous swelling of silver alginates measured in this work was correlated with the absorption of saline fluid (g of saline fluid per g of the dressing), as well as with the antimicrobial properties (against Gram-positive and Gram-negative microbes) of silver alginates of our earlier work. This study summarized that alginate dressings treated with ion-paired silver had robust antimicrobial activity while retaining the high absorption properties needed for medium to heavily exudating wounds.

References

1. Qin Y (2004) Absorption characteristics of alginate wound dressings. J Appl Polym Sci 91(2):953–957
2. Winter GD (1962) Formation of the scab and the rate of epithelization of superficial wounds in the skin of the young domestic pig. Nature 193(4812):293–294
3. Winter GD, Scales JT (1963) Effect of air drying and dressings on the surface of a wound. Nature 197(4862):91–92
4. Bolton LL, Pirone L, Chen J, Lydon M (1990) Dressings' effects on wound healing. Wounds 2(4):126–134
5. Alvarez OM, Rozint J, Wiseman D (1989) Moist environment for healing: matching the dressing to the wound. Wounds 1:35–51
6. Lionelli GT, Lawrence WT (2003) Wound dressings. Surg Clin North Am 83(3):617–638
7. Linsky CB, Rovee DT, Dow T (1981) Effects of dressings on wound inflammation and scar tissue. In: Dineen P, Hildick-Smith G (eds) The surgical wound. Lea & Febiger, Philadelphia, pp 191–205
8. Wiseman DM, Rovee DT, Alvarez O (1990) Wound dressings: design and use. In: Cohen IK, Diegelmann RF, Lindblad WJ (eds) Wound healing: biochemical and clinical aspect. W.B. Saunders Co., Philadelphia, pp 562–580

9. Barnett A, Berkowitz RL, Mills R, Vistnes LM (1983) Comparison of synthetic adhesive moisture vapor permeable and fine mesh gauze dressings for split-thickness skin graft donor sites. Am J Surg 145(3):379–381
10. Surgical Materials. British Pharmacopeia, 1993, Addendum 1995
11. Holme I (2004) Durable freshness through antimicrobial finishes. Text Mag 30(4):14–16
12. Parikh DV, Fink T, Rajasekharan K, Sachinvala ND, Sawhney APS, Calamari TA, Parikh AD (2005) Antimicrobial silver/sodium carboxymethyl cotton dressings for burn wounds. Text Res J 75(2):134–138
13. Qin Y (2004) Silver streak. Textile Horizons, pp 16–17
14. Tessier D (2008) SilverClear® an outstanding silver technology. Text J 125:15–18
15. Parikh DV, Sachinvala ND, Calamari TA, Negulescu I (2003) Carboxymethylated cotton for moist wound healing. AATCC Rev 3(6):15–19
16. Daul GC, Reinhardt RM, Reid JD (1952) Studies on the partial carboxymethylation of cotton. Text Res J 22(12):787–792
17. Parikh DV, Edwards JV, Condon BD, Parikh AD (2008) Silver-carboxylate ion-paired alginate and carboxymethylated cotton with antimicrobial activity. AATCC Rev 8(8):38–43
18. Chakravathy D, Fleck C, Falconio-West M (2006) An evaluation of two polysaccharide-silver based high absorbency wound dressings. Presentation at the Symposium on Advanced Wound Care, San Antonio, TX
19. British Pharmacopeia Monograph for Alginate Dressings and Packings (1993) Addendum 1995 (Published on the recommendation of the Medicines Commission Pursuant to the Medicines Act 1968)
20. Joiner BG (2001) Determining antimicrobial efficacy and biocompatibility of treated articles using standard test methods. In: Edwards JV, Vigo TL (eds) Bioactive Fibers and Polymers, ACS Symposium Series 792. Oxford University Press, Washington, DC, pp 201–217

Chapter 7
Intelligent Garment for Nerve Stimulation

7.1 Introduction

During the treatment of different diseases relating to pains and disorders of the body, electrical stimulation on the afflicted area is beneficial, and even the more for stimulation of the nervous system. This transcutaneous electrical nerve stimulation (TENS) therapy has been applied through conductive silica gel hydropads in the affected area where front end of body nerves is stimulated by the electrical current [1]. The present TENS products consisting conductive silica gel hydromaterial help to decrease the skin resistance, but are normally supplied in two to four pieces and do not readily target the back of the body. Their stickiness can create discomfort. They are unlaunderable, and repeated use is unhygienic. With the fast advancement of technology, intelligent garments are becoming one of the important innovations in the textile industry, particularly in the areas of intelligent medical and athletic textiles [2–5]. TENS is frequently being used in the treatment of different painful conditions. Many investigations have shown the effectiveness of TENS on different pain conditions, provided patients use them continuously in the correct way. It stimulates the large afferent fibers that can decrease the transmission of pain signals through the small nonreceptive afferent fibers, consequently inhibiting pain discrimination and perception [6]. Moreover, studies have shown that patients given TENS therapy with acupuncture point stimulation yield better results [6–8]. Figure 7.1 shows the commercial products of available electrodes. They are commonly used, but their property is not suitable for use in intelligent garment. In the medical treatment products used at present, electrodes are mostly made of silica gel hydropads that can be absorbed to skin, which can be repeatedly used for several tens of times. This type of electrode performs very well. But, their demerits are apparent: They are susceptible to fragmentation, nonwashable, and uncomfortable because of their stickiness. Placing conductive ointment between the conductor and skin to reduce the resistance is a

N. Gokarneshan et al., *Emerging Research Trends in Medical Textiles*,
Textile Science and Clothing Technology, DOI 10.1007/978-981-287-508-2_7

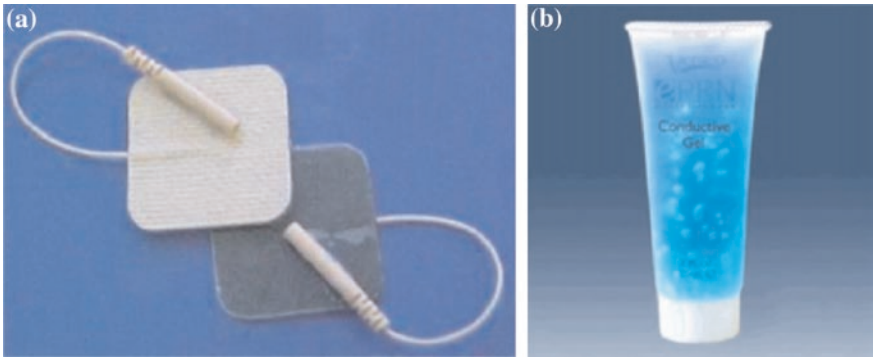

Fig. 7.1 Common products for electrode and conducting material [12]. **a** Conductive silica gel hydropads. **b** Conductive ointment

possible solution to the problem. But this is rarely practiced because of its uncomfortable feeling and spreading to neighboring places. Fabric electrodes are being used often in smart clothing needing a good contact to skin, such as acquiring breath, temperature, and electrocardiogram signal. A simple way to achieve good contact is to increase the contact area and pressure. But, the bulky electrode is less flexible and high contact pressure would cause discomfort. Hence, a water filler is commonly used to increase the moisture and conductivity of skin, compromising convenience. Attempt has been made to develop a wearable TENS garment with incorporated Chinese acupuncture therapy for long-term continuous treatment and establish a novel therapeutic technique for health care. The design of TENS garment is discussed, followed designs of textile electrode and TENS signal generator, using two experimental setups to evaluate the newly proposed intelligent clothing prototype incorporating textile electrodes and conductive yarns.

7.2 Design of TENS Intelligent Knitwear

The yarns for knitting consists of 100 % pearl fiber of 40 S/2 Nm, and the conductive yarn has been made of silver-coated yarn of 40 S/2 Nm having electrical resistance of 1.58 Ω/cm. The fabric has been knitted on a flat knitting machine having intarsia stitches, and the number of wales and courses is 9.3 and 6.9 unit loop per 10 mm, respectively, and neither washing nor ironing has been done before the testing.

7.3 Acupuncture Points for Pain Relief

Figure 7.2 shows the various acupuncture points in the body. These acupuncture points can reduce shoulder and neck pain based on the theory of traditional Chinese medicine [9]. The selected group of acupuncture points has been used in

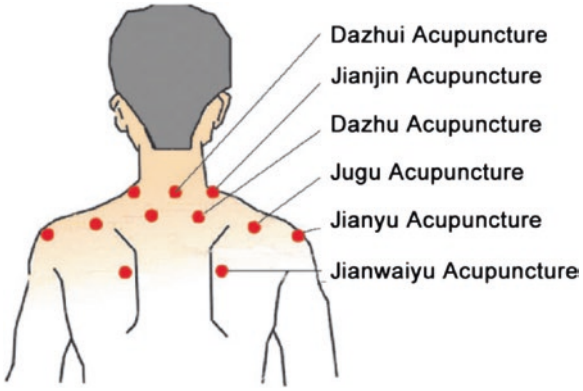

Fig. 7.2 Points of acupuncture for pain relief (Chinese system) [12]

TENS knitwear design for the treatment of shoulder and neck pain. The points of acupuncture are situated with reference to the 'Human Acupuncture Point Model' and matched with the clothing prototype. Every acupuncture point is shown as a small area on the body surface, instead of a tiny point, for all practical purposes. Hence, they can easily be matched in the clothing in a precise manner.

7.4 Design of Knitwear

Figure 7.3 depicts the measurement settings and design details of the TENS knitwear. The distribution of pressure in clothing is crucial for the intelligent clothing, particularly in the case of intelligent medical clothing, as most of the product is made of elastic fabric which needs tight contact with skin for effective treatment [10]. Hence, the present investigation focuses on garment that is smaller

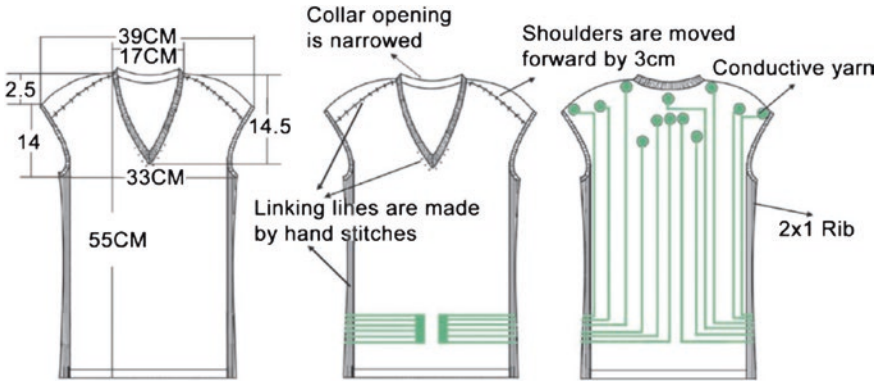

Fig. 7.3 Measurement settings and design details [12]

in dimension than normal clothing, and 2 × 1 rib knitting stitch at two sides have been used for elastic as the stitches are more elastic than others [11]. The sewing lines at two shoulders have been moved forward by 3 cm, and the width of collar opening has been narrowed so as to accommodate the electrodes to be situated at the acupuncture points. The linking lines have all been stitched by hand to ensure contact between clothing and skin. The confining pressure has been maintained within the comfortable clothing pressure range (1.96–3.92 kPa). Silver conductive yarn has been knitted to act as electrodes and conducting wires. The circles representing the terminals of the electrodes have been situated at acupuncture points for pain treatment.

7.5 Design of Washable Textile Electrode

Four types of washable textile electrodes have been designed as compared to original electrodes. A metal button has been installed at the electrode of this textile material, which could be buttoned with knitwear (Fig. 7.4).

The textile electrodes consisted of one piece of absorbent fabric (amethyst color), conductive fabric (resistance: 0.1 Ω/cm), conductive mesh fabric (resistance: 0.2 Ω/cm), absorbent sponge, and metallic dual-lock button (diameter 10 mm) (Fig. 7.5).

7.6 Design of TENS Signal Generator

The positive and negative terminals of the TENS device have been connected to two metal buttons (labeled E) on the face side of the clothes. The TENS signals have been produced by the electronic device (labeled D) (Fig. 7.6), and the block

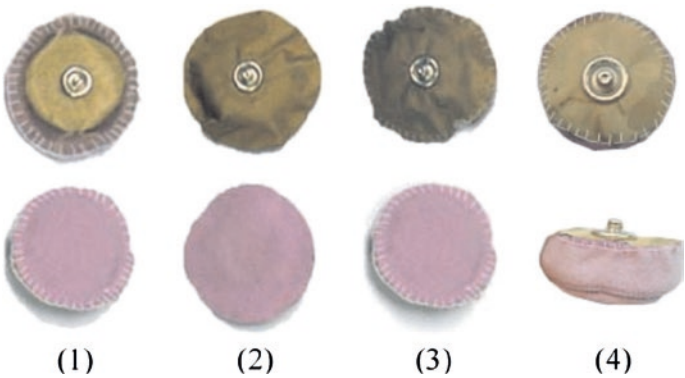

Fig. 7.4 Textile electrodes (front and back views) [12]

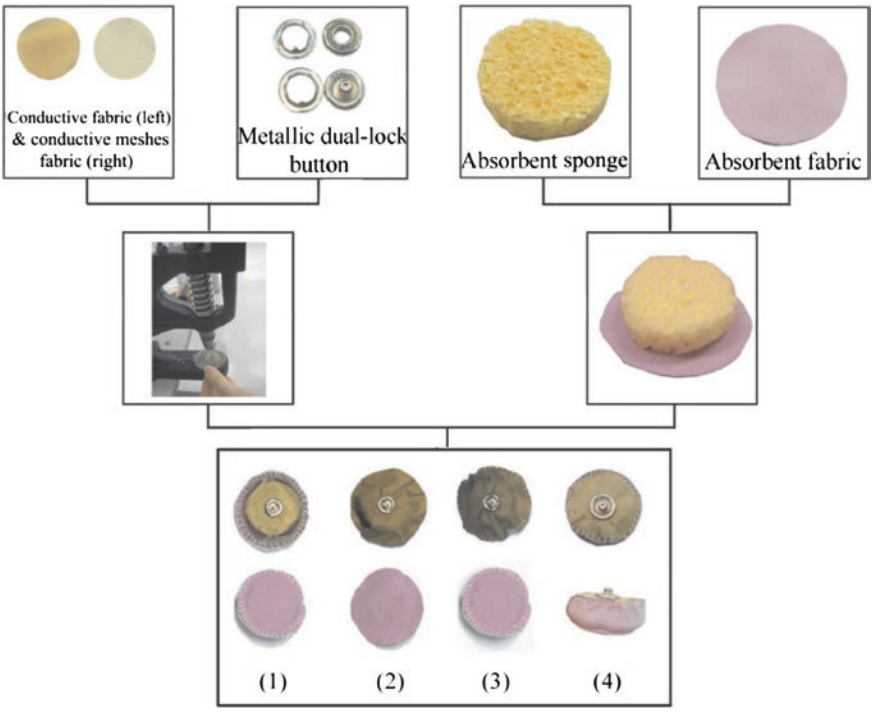

Fig. 7.5 Materials for textile electrodes [12]

Fig. 7.6 Prototype of TENS signal generator [12]

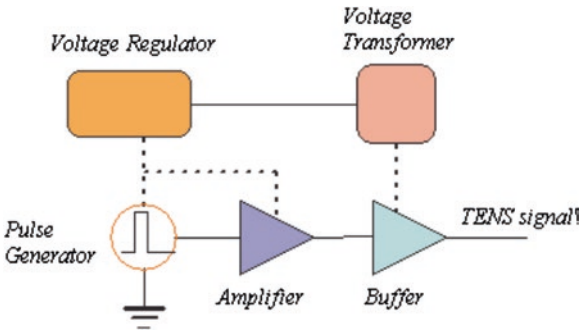

Fig. 7.7 Circuit diagram of TENS signal generator [12]

diagram is shown in Fig. 7.7. This battery-powered electronic device was made to be compact in size and light in weight so that it could be mounted on the clothes.

7.7 Discussion of the Findings

The objective of the investigation is to evaluate the TENS knitwear for repeated use, washability, and conductivity. The four newly designed electrodes have been tested and found that the electrodes are made of conductive fabric generally that exhibited satisfactory performances as compared to the metallic ones. The electrodes made with adhesives became hardened and would create skin irritation [12]. The second electrodes wrapped in conductive mesh fabric could not retain water well, as water could easily evaporate through the conductive mesh. The third and fourth electrodes with higher water sustainability have been considered to be suitable for use as textile electrodes. Since the fourth ones had better skin contact, they were chosen as the prototype for the experiments.

7.8 Washability

The chosen textile electrode normally exhibited lower effective resistance (221 kΩ) as compared with the original electrode (465 kΩ) for fabric. The conductive fabric of the electrode and the conductive stitch exhibited slight changes in effective resistance between 0.1–0.55 Ω and 1.58–1.83 Ω/cm, respectively, after 10 washing cycles. These subtle changes have been insignificant to the overall resistance of the textile electrode. The proposed electrode has high laundering ability and also easy to clean [12]. It is capable of retaining medicine inside for ease of medical treatment and can be used in smart clothing for a long duration in clinical use. It was convenient to use and readily targeted the predefined location of the body without expert knowledge. Practically, the electrode can be made thinner without alteration of its properties.

7.9 Conductivity

Comparisons have been done on the waveforms produced by a pair of the original electrodes and proposed electrodes (Fig. 7.8). Both the proposed and original electrodes gave almost the same output signal, without the introduction of phase distortion, except for a small voltage drop due to the finite resistance of the conductive stitch (45.6 Ω) where the TENS signal passed through before appearing at the textile electrode. Most of the applied TENS signal has been passed through the electrode instead of the conductive yarn, through the potential divider rule. Hence, majority of the power supply has been effectively delivered to the focussed areas of the body. As the electrical properties of the proposed and original electrodes are found to be the same, the former can be suitable as textile electrode in future TENS intelligent knitwear.

7.10 Influence of Increasing the Number of Textile Electrode Pairs

In the case of the clothing prototype that has been fabricated, the number of textile electrode pairs is not restricted to six, but is based on the size of electrodes and wiring routing in the fabric. The equivalent resistance, R_{eq}, of N electrode pairs of a parallel resistive system is given by the equation below:

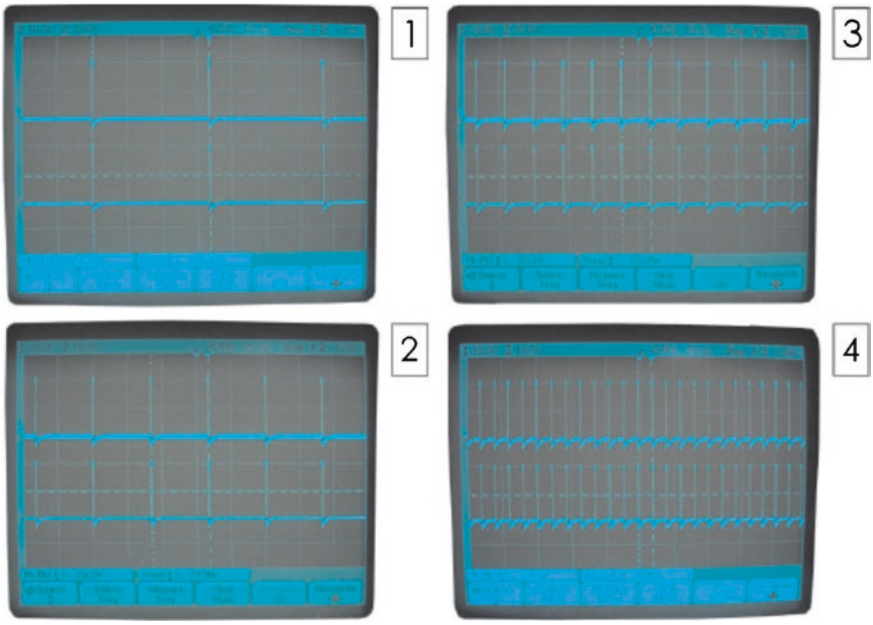

Fig. 7.8 Comparison of proposed and original electrodes [12]

$$\frac{1}{R_{\text{eq}}} = \sum_{i=1}^{N} \frac{1}{R_i} \tag{7.1}$$

where R_i is the total equivalent resistance including human skin of each electrode pair $i = 1, 2, \ldots, N$. Assuming for the same skin, electrode, and wiring resistance for each pair, i.e., $R = R_1 = R_2 = \ldots RN$, Eq. (7.1) becomes:

$$R_{\text{eq}} = \frac{R}{N} \tag{7.2}$$

The total equivalent resistance gets reduced with the increase in the number of electrode pairs. Greater current is drawn for the same supply voltage, V_{a}. The total power consumption, P_{T}, is given by the equation below:

$$P_{\text{T}} = \frac{V_{\text{a}}^2}{R_{\text{eq}}} \tag{7.3}$$

For the same applied voltage, the power dissipation is proportional to the number of electrodes used, given by Eqs. (7.2) and (7.3). The total available power, P_{a}, and power efficiency, η, to the treatment region of the human body are given as follows:

$$P_{\text{a}} = \frac{N\left[V_{\text{a}}\left(\frac{R_{\text{s}}}{R}\right)\right]^2}{R_{\text{s}}} = \frac{NV_{\text{a}}^2 R_{\text{s}}}{\left(R_l + R_{\text{p}} + R_{\text{s}}\right)^2} \tag{7.4}$$

$$\eta = \frac{P_{\text{a}}}{R_{\text{T}}} \tag{7.5}$$

where $R = R_{\text{l}} + R_{\text{p}} + R_{\text{s}}$, and R_{l}, R_{p}, and R_{s} are the effective resistance of the conductive stitch, textile electrode, and skin, respectively. At lesser resistance of the conductive yarn and textile electrode, more available power has been delivered to the treatment area by an electrode pair. The power efficiency of the proposed electrodes has been higher than that of the original electrodes, for the same skin resistance.

7.11 Corner Effect of Conductive Wire (Conductive Knitted Stitches Versus Conductive Threads Sewn on the Fabric)

The routing conductive yarn in the fabric has unavoidable turnings. Due to the sewing of conductive threads on fabric, there is a sharp corner turning that causes significant resistance change. But, this resistance change did not occur in the

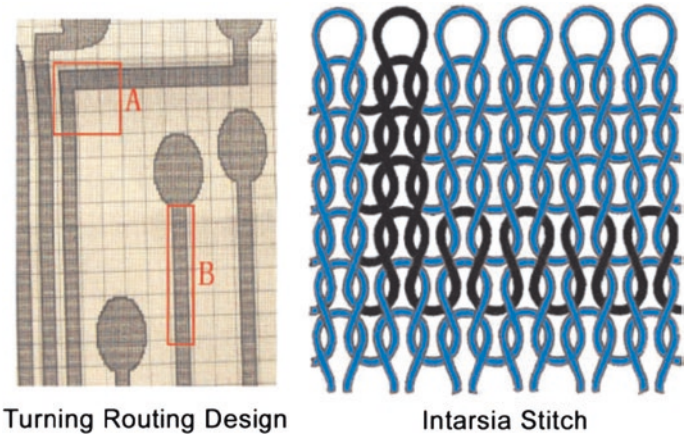

Fig. 7.9 Design of turning routing with intarsia knitting method [12]

designed knitting fabric. For the same distance A and B, as shown in Fig. 7.9, resistances of 4.21 and 4.60 Ω were obtained, respectively. This increased resistance has been because of the corner effect which retarded the flow of the electron, thereby increasing its effective resistance.

7.12 Further Improvement to Garment Design and Functionality

In relation to the Worth Global Style Network, a prominent global service Web site found that one of the reasons for this retail market's slow growth is because of consumption factors like acceptance of wearable technology and consumers viewing of products as 'technical' instead of 'fashion' interest [13]. Hence, from the experimental results, knitwear can satisfy the basic functions, as shown in Fig. 7.10. The use of garment design skills has enabled the previously mentioned problems to be readily solved, and the aesthetics are further improved by hiding the conductive yarn using the knitting method of the intarsia pattern. The routing of the connecting wires can be hidden beneath the fabric, as shown in Fig. 7.11. The dark green color is the conductive yarn knitted into knitwear as conductive wire. After the pattern redesign, the wires were totally dissolved into the pattern of the clothes. The white circle dot is the metallic dual lock for connecting the conductive yarn and the electrodes and TENS device. A knitted pocket can replace the black mesh pocket for the battery holder and is knitted by the same yarn of the knitwear. The TENS generator could be sealed by silicon and hid inside the pocket so that the batteries could be removed during washing. One of the possible future developments of this TENS knitwear is to focus on the selectable treatment

Fig. 7.10 Prototype garment having TENS function

Fig. 7.11 Innovative design pattern of intarsia for routing hiding based on garment prototype [12]

of group points including neck pain, shoulder pain, and low back pain. The points of treatment controlled individually or in groups by textile switches according to the acupuncture point theory to treat pains in various positions.

References

1. Imboden JB, Hellmann DB, Stone JH (2007) Current rheumatology diagnosis and treatment. Lange Medical Books McGraw-Hill, NY
2. Tsang HY (2006) PhD thesis, design and development of electrically conducting textile sensors for smart textiles and apparel. The Hong Kong Polytechnic University, Hong Kong
3. Langenhove LV (2007) Smart textiles for medicine and healthcare:materials, systems and applications. Woodhead Pub Ltd, Cambridge

4. Bradley Q (2002) Techno fashion. Oxford, NY
5. Lee S (2005) Fashioning the future: tomorrow's wardrobe. Thames & Hudson, London
6. Chiu TW, Hui-Chan WY, Chein G (2005) A randomized clinical trial of TENS and exercise for patients with chronic neck pain. Clin Rehabil 19:850–860
7. Wang LS, Lin HY, Hu GC (2006) The hypoalgesic effect of TENS during needle EMG study. Taiwan J Phy Med Rehabil 34(4):235–240
8. Wang NH, Xu YY (2003) Effects of acupoints TENS on heat pain threshold in normal subjects. Chin Med J 116(12):1864–1868
9. Li GH Licence to practice medicine No. 19981414114010452060827l
10. Talk2myshirt (2009) Health-care. Retrieved 2009, from Talk2myshirt: http://www.talk2myshirt.com/blog/archives/category/products/ health-care
11. Li L, Au WM, Li Y, Wan KM, Chung WY, Wong KS (2009) A novel design method for intelligent clothing embedded sensor system based on knitting technology and garment design. Textile Res J, First Published on July 1 doi:10.1177/0040517508096219
12. Li L, Au WM, Yi L, Wan KM, Wan SH, Wong KS (2009) Design of intelligent garment with transcutaneous electrical nerve stimulation function based on the intarsia technique. Textile Res J 80(3):279–286
13. Watkins P, Avantex Symposium: Electronics + Textiles. Retrieved 2008, from WGSN: http://www.GMSN%20report/Avantex%20symposium%20Electronics%20+%20Textile

Chapter 8
Nonwoven Scaffolds for Improved Cell Growth

8.1 Introduction

Three-dimensional (3D) scaffolds offer the required architectural support for cell growth and tissue regeneration [1, 2]. Synthetic polymers such as polyglycolic acid, polycaprolactone, polylactic acid, and polytetrafluoroethylene are normally used in making 3D scaffolds. 3D scaffolds are produced by different methods such as gas foaming, nonwoven, electrospinning, and 3D printing [3, 4]. They can also be produced by adopting nonwoven technique, resulting in structures that are highly porous with interconnected networks. These advantageous characteristics have been shown to assist with cellular distribution and tissue integration within the scaffolds [5, 6]. Also, high porosity and interconnectivity help to effectively transport the nutrients and oxygen to cells throughout the scaffolds [7–9]. An earlier investigation has revealed that fluid permeability correlated to tissue formation in cancerous bone grafts whereby low fluid permeability prevented tissue regrowth [8]. Scaffolds with a pore size greater than 100 mm and high interconnectivity (>90 %) were demonstrated to be favorable for cellular migration and tissue integration. Nonwoven scaffolds produced from a variety of both natural and synthetic polymers have proven to effectively support growth of endothelial cells, smooth muscle cells, and arachnoid cells [10–12]. But, scaffolds used in tissue engineering, besides assisting cell growth, also should accommodate a large number of cells as the number of cells present in tissues is 10^7–10^8 cells/cm^3 [13]. For example, in order to engineer 50 g of cardiac tissue to compensate for muscle damaged by heart failure, 1–2 $\times$ 10^9 myocytes are required [14, 15]. It has been shown that a minimum of 1.3 $\times$ 10^9 b-cells are required for patients to be insulin independent after islet transplantation [16]. The extruded filaments for producing nonwoven scaffolds have circular cross section. During the past few years, innovative multilobal fibers, ranging from bilobal to a specialized eight-channeled fiber known as capillary channel fibers, have been developed. These fibers have been utilized in the industries only

N. Gokarneshan et al., *Emerging Research Trends in Medical Textiles*,
Textile Science and Clothing Technology, DOI 10.1007/978-981-287-508-2_8

because of their filtration and wicking characteristics [17]. The use of the multilobal fibers has since extended to applications for thermal insulation in space suits and as stationary phases in liquid chromatography [18–20]. But, not much research has been carried out regarding the potential of multilobal fibers as scaffolds in tissue engineering. It is assumed that multilobal fibers are irregularly shaped and would well improve the cell density by providing a greater surface area than circular fibers. The objective of the research discussed in this chapter has been to investigate the potential of two types of commercially available multilobal fibers as 3D scaffolds for applications in tissue regeneration. Nylon 6,6 and polyethylene terephthalate (PET) were chosen as these polymers have been used in various biomedical applications such as cardiovascular and bone tissue engineering [21–25]. Scaffolds of multilobal fibers have been evaluated for the capacity to promote cell growth in comparison with circular fiber, given their increased surface-area-to-volume ratio. The fibroblast and osteoblast types of cells have been used to investigate the cellular interactions on the different types of scaffolds.

8.2 Fiber and Scaffold Characterization

The SEM and optical microscopic techniques have been used to study the cross sections of the different types of fibers [26]. The fibers of both the nylon 6,6 and PET groups showed the standard morphology of circular fibers (Fig. 8.1a, c). The mean diameters of the nylon 6,6 and PET round fibers were 40.5 ± 2.7 and 43.7 ± 5.4 μm, respectively.

The trilobal nylon 6,6 fiber cross section appears like the letter Y (Fig. 8.1b). The fibers have two major grooves of 95.0 ± 6.6 mm in width and 8.9 ± 1.0 mm in depth, and one minor groove of 42.7 ± 1.8 mm wide and 33.9 ± 6.4 mm deep. The multilobal PET fiber was an eight-channeled fiber comprising a mixture of major grooves with a mean width of 20.9 ± 9.0 mm and depth of 10.0 ± 4.9 mm, and minor grooves of 12.7 ± 3.1 mm wide and 11.6 ± 4.4 mm (Fig. 8.1d). Properties of the various nonwoven scaffolds such as surface area and porosity have been tested. Both the multilobal fiber groups have higher surface areas, wherein the trilobal nylon 6,6 and multilobal PET scaffolds were 1.7 and 3 times larger than the circular cross-sectional fibers, respectively. Also, scaffolds produced from multilobal fibers exhibited a 20 % increase in porosity in comparison with the circular cross-sectional fiber scaffolds.

8.3 Cytotoxicity and Cell Proliferation Study

During the duration of three days, the cells cultured in media extracted from the various groups of scaffold did not exhibit toxicity. There was no significant difference in cell viabilities between the scaffold groups and the standard tissue culture

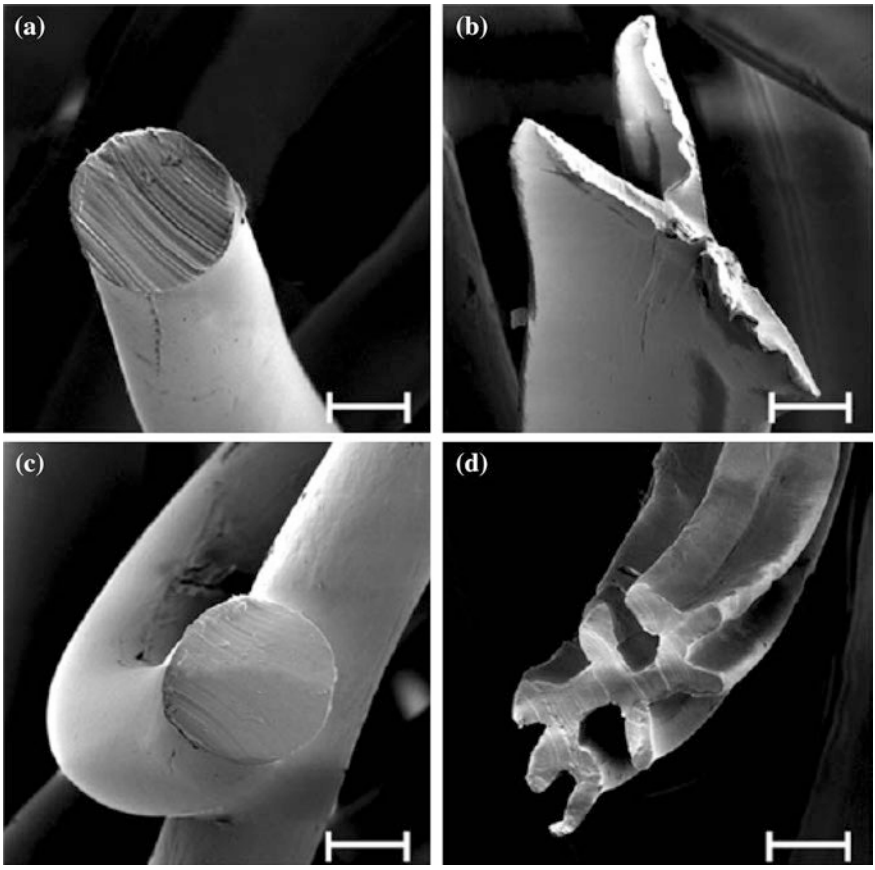

Fig. 8.1 Cross-sectional SEM images of **a** Round nylon 6.6 fiber. **b** Trilobal nylon 6.6 fiber. **c** Round pet fiber. **d** Multilobal pet fiber (600×). The *scale bar* denotes a measurement of 20 μm [26]

wells which served as negative controls. The cell viabilities of the four scaffold groups ranged between 95.5 ± 1.6 and 98.2 ± 0.9 % (Fig. 8.2).

They are comparable to the control scaffold (98.0 ± 1.7 %). The cell growth on nylon 6,6 and PET scaffolds have been studied for a duration of 14 days [26]. The data for cell proliferation were presented in the form of total cell number and as a rate of increase (Fig. 8.3). The number of fibroblasts and osteoblast-like cells has been the highest when cultured on multilobal PET scaffolds after a period of 14 days.

But, as the initial number of cells attached onto the scaffolds differed across experimental groups, the cell proliferation data for each group have been normalized against their respective baseline on the third day. Hence, the number of cells at each point of time has been compared to the number of cells on the third day of the same scaffold group and expressed as a fold increase as compared to the third day. The technique helps to make proper comparisons of cell proliferation among the

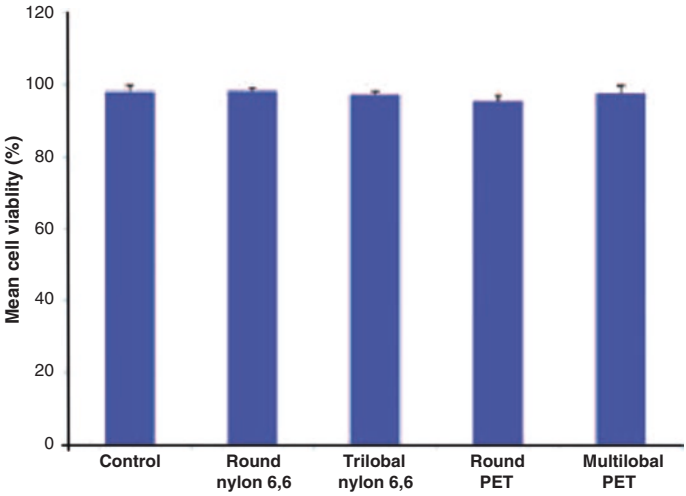

Fig. 8.2 Nontoxicity across the four scaffolds groups as indicated by the high cell viability [26]

experimental groups tested. An improved growth of fibroblast has been observed on both trilobal nylon 6,6 and PET multilobal fibers over a period of two weeks. A significant increase has been noticed in both multilobal groups after a week of culture. The trilobal nylon 6,6 showed a 37 % increase to $6.3 \pm 105 \pm 5.4 - 104$ cells in fibroblast growth when compared to its round-fibered counterpart at Day 14 (Fig. 8.3a). The multilobal PET scaffold exhibits a same trend in that the number of fibroblasts increased 12.0 ± 1.1 fold after 14 days, whereas on the round-fibered PET scaffold, an increase of 8.2 ± 0.5 fold has been noticed. As expected, fibroblasts cultured on the standard tissue culture wells (2D) exhibited minimal increase in cell growth after 7 days due to limited surface area. In general, the fibroblasts exhibited greater tendency to be cultured on nylon 6,6 in comparison with PET scaffolds. Cell proliferation was significantly enhanced in the trilobal nylon 6,6 group when compared to the other experimental groups, producing an increase of 21.8 ± 1.9 fold after 14 days of culture. The osteoblast-like cells show a different trend in that no difference has been noticed in cell growth between the circular cross-sectional fibers and trilobal nylon 6,6 scaffolds (Fig. 8.4b). After a duration of two weeks of culture, both nylon 6,6 groups increased the number of cells by about 12 times (12.0 ± 0.6 times for circular cross-sectional nylon 6,6 and 12.8 ± 0.4 times for trilobal cross-sectional nylon 6,6). But, the multilobal PET shows an enhancement of cell proliferation on the fourteenth day when compared to the PET scaffold with circular cross-sectional fibers, on being cultured on PET scaffolds. An increase of 16.7 ± 2.8 times in cell growth on the multilobal PET group as against the circular cross-sectional PET group of 9.2 ± 1.5 times has been noticed. The difference in cell proliferation among the experimental groups studied has been noticed after culture duration of two weeks.

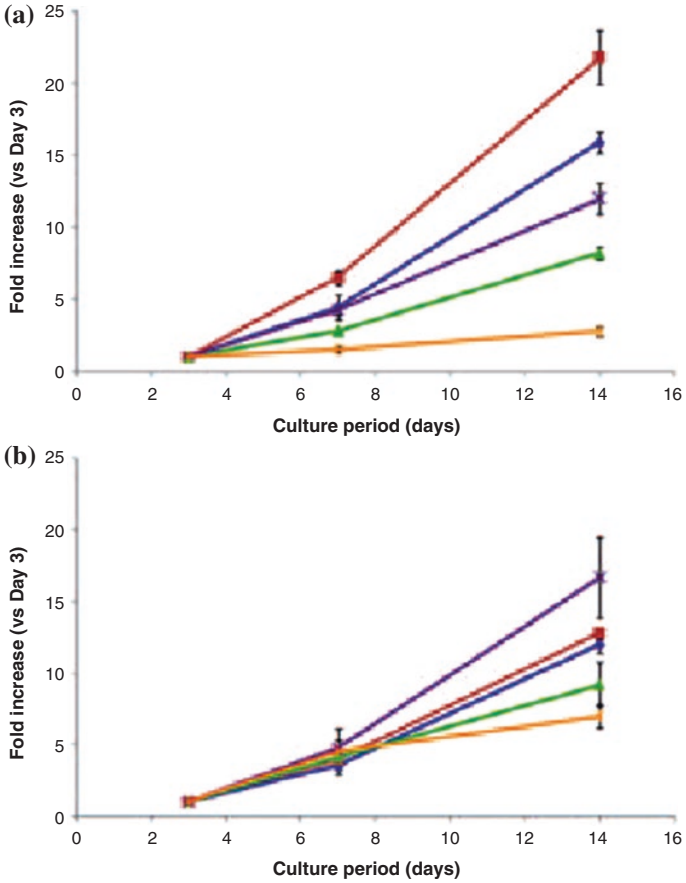

Fig. 8.3 **a** Fibro blasts and **b** osteoblast-like cells cultured on round Nylon 6.6, trilobal nylon 6.6, round PET Multilobal PET fiber(*x*) and tissue cultured walls (*) for 14 days [26]

8.4 Microscopy

Confocal microscopy and SEM have been utilized for viewing the cell morphology on the different kinds of scaffolds and observed for fibroblasts and osteoblast like cells [26]. The microscopic studies revealed an elongated and flattened morphology on all the scaffold groups after culture duration of a week (Figs. 8.4 and 8.5). The cells have been wrapped around the circular cross-sectional nylon 6,6 and PET fibers, proliferating randomly along the fiber length(Figs. 8.4a, c and 8.5a, c). Fibroblasts that were cultured on multilobal-fibered scaffolds attached and proliferated within the depths of the grooves and along the channels of the multilobal PET and trilobal nylon 6,6 fibers, as shown in Fig. 8.4b, d. The osteoblast-like cells show the profile of growth as can be seen in Fig. 8.5b, d. Both

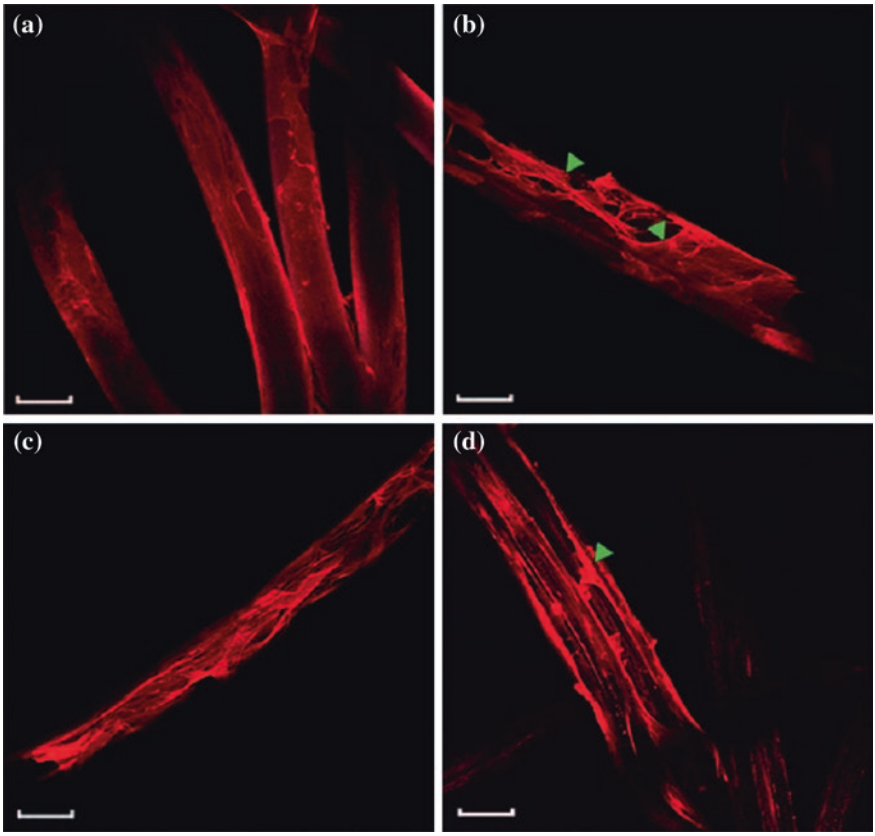

Fig. 8.4 Fibroblasts wrapped around **a** Circular cross-sectional nylon 6,6. **b** Trilobal nylon 6,6. **c** Circular cross-sectional PET fibers. **d** Multilobal cross-sectional PET fibers, after a duration of one week (as viewed through confocal microscope). The *scale bar* indicates 50 mm [26]

fibroblasts and osteoblast-like cells demonstrated an alignment parallel to the longitudinal axis of the fibers when cultured on the multilobal PET scaffolds (Figs. 8.4d and 8.5d). Also, the fibroblasts have been seen to cover the grooves of multilobal fibers, thereby creating a cellular sheath (Fig. 8.6). In the case of fibroblasts cultured on multilobal PET scaffolds, a greater prominence in the behavior has been observed.

8.5 Discussion of Findings

The potential of multilobal fibers in the area of tissue regeneration has not yet been fully exploited, as very limited research work has been done in this area [27–30]. In the available literature, particularly, the capillary channel fibers have

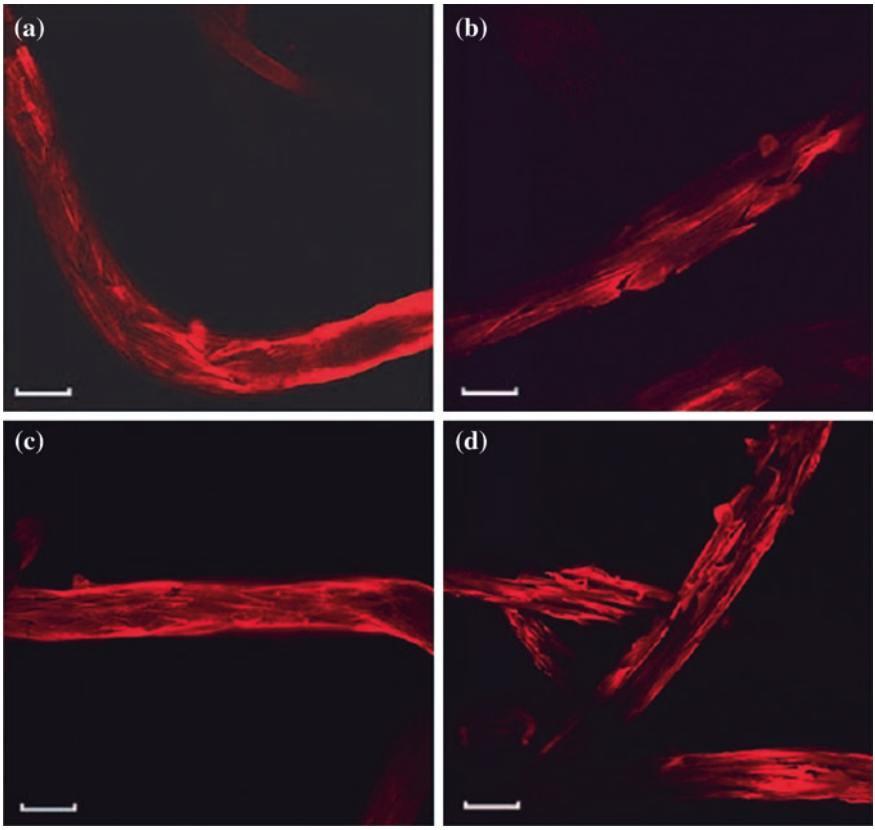

Fig. 8.5 Osteoblast-like cells following the contours of **a** Circular cross-sectional fibers of nylon 6,6. **b** Cultured trilobal cross-sectional nylon 6.6. **c** Circular cross-sectional PET fibers. **d** Multilobal cross-sectional PET fibers, after culture duration of a week (as viewed through confocal microscope). The *scale bar* indicates 50 mm [26]

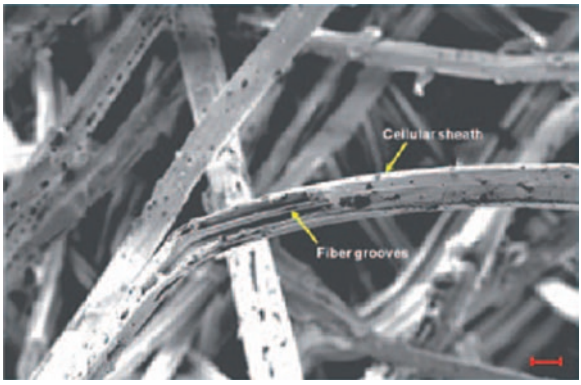

Fig. 8.6 Culturing of fibroblasts over the grooves of the multilobal cross-sectional PET fibers, having cellular sheath around the fibers, after a culture duration of two weeks (as viewed through SEM) [26]

been used to produce fiber meshes or scaffolds having parallel orientation through alignment of the fibers on wire frames to promote cell guidance. Hence, till now, the cellular interactions on nonwoven 3D scaffolds comprising of nonaligned multilobal fibers have not been studied. The 3D multilobal-fibered scaffolds, besides aiding in cell alignment, offer the advantage of supporting improved cell growth owing to their increased surface area. This has been highlighted in the foregoing discussion, in which cell growth of trilobal nylon 6,6 and multilobal PET fibers improved by 37 and 81 % in comparison with the circular cross-sectional fiber scaffolds of the same polymer. Both fibroblasts and osteoblast-like cells show an increase in cell numbers when cultured on multilobal cross-sectional fiber scaffolds that have larger surface areas than the circular cross-sectional scaffolds (Fig. 8.3). However, the two cell types demonstrated a preference for different polymers. Fibroblasts cultured on trilobal nylon 6,6 scaffolds exhibited the greatest increase in cell number after 14 days, whereas a similar effect was observed with $SaOS_2$ cultured on multilobal PET scaffolds. These results highlight the vital role of surface topography in cell attachment and proliferation. Surface topography and roughness have been shown to influence cell adhesion and proliferation of a variety of cells such as smooth muscle cells, osteoblasts, and hepatocytes [31–33]. Yang and Lee [34] demonstrated that osteoblasts cultured on a microgrooved titanium-coated surface exhibited higher cell adhesion strength and subsequently higher cell number than the smooth surface. Enhanced smooth muscle cell number was observed on nanostructured polyurethane surfaces when compared to the smooth surface [35]. In contrast, premyoblast cells preferred nonpatterned polymeric surfaces to micropatterned surfaces having 5–14-mm-high pillars [36]. Micro-islands (4 mm in diameter) have been used to improve fibroblast attachment on PDMS sheets [37]. Also, good fibroblast alignment has been noticed on 2D collagen membranes that are micropatterned [38] and multilobal fibers which are 30 mm wide and 25 mm deep [28]. The results of the present study showed that fibroblasts favoured the trilobal nylon 6,6 over the multilobal PET scaffolds. This was most likely attributed to the dimensions of the major and minor grooves of multilobal PET fibers, measuring at a mean width between 12.7 and 20.9 mm. The dimensions of some of the multilobal PET grooves have been shown to be too narrow for fibroblasts, preventing cell attachment and proliferation within these channels [28]. The fibroblasts tended to flatten and cover the grooves of the fiber, as they are capable of extending to the extent of 100 mm and thereby creating a sheath along the longitudinal axis of the fibers (Fig. 8.6). The channels of the trilobal nylon 6,6 fibers, on the other hand, were much wider with a mean width of 95.0 and 42.7 mm for the major and minor grooves, respectively. It aided the fibroblasts to attach and grow within all three grooves of the trilobal nylon 6,6 fibers. Osteoblast-like cells were able to attach and proliferate within both the major and minor grooves of the multilobal PET scaffolds. Typically, the osteoblast-like cells do not flatten and spread out as much as fibroblasts. Hence, the cellular sheaths, unlike fibroblasts, have not been formed by the osteoblast-like cells when cultured on multilobal PET fibers. The preference of the osteoblast-like cells for multilobal PET scaffolds could be due

to the fiber's surface topography. The osteoblast-like cells have shown enhanced attachment and spreading on nano- and microtextured polystyrene and poly-L-lactide surface compared to a smooth surface [39]. In this discussion, the surface topography provided by the multilobal PET scaffolds appeared to be conducive to the osteoblast-like cell attachment and growth compared to the circular cross-sectional PET fiber and both nylon 6,6 scaffold groups. Also, addition to surface topography, the hydrophilicity of polymers influences cell attachment [40, 41]. Fibroblasts have been shown to attach optimally on the hydrophilic surface with a water contact angle between 50° and 60° [42, 43]. The fibroblasts tend to be cultured on nylon 6,6 scaffolds in comparison with PET scaffolds, irrespective of whether the fibers are circular or multilobal cross section (Fig. 8.3a). This result correlates to nylon 6,6 being a hydrophilic polymer with a contact angle of 53°–58° [44]. In contrast to the fibroblasts, the osteoblast-like cells prefer a more hydrophobic surface. Earlier research shows that optimal cell attachment of osteoblast-like cells was achieved on polymers with a contact angle of 90° (hydrophobic polymers) such as polystyrene and poly(vinylacetate) [45]. Improved osteoblast-like cell density has been noticed on multilobal scaffolds which have been produced from PET, a known hydrophobic polymer (Fig. 8.3b) [46, 47]. The mass transfer is another parameter that determines the cell survival and growth on 3D scaffolds, and it relates to the flow of nutrients and oxygen throughout the scaffolds. Excellent fluid flow is one of the merits in using multilobal 3D scaffolds made of these fibers, particularly multilobal PET fibers [17]. The major and minor grooves enabled fluid to be transported rapidly and had been shown to distribute fluid to 80 % of a surface within 15 s [27]. The multilobal fiber scaffolds, immaterial of the type of polymer, supported higher cell growth compared to their round-fibered counterparts (Fig. 8.3). The linear growth suggested that the scaffolds can accommodate more than 105 cells for a longer culture period (Fig. 8.3). Confocal microscopy shows that cells cultured within the scaffolds have flatten and well-spread-out morphology similar to those observed on the surface of the scaffold, indicative of healthy cells. It could be partly due to the high porosity (>90 %) and effective mass transport of multilobal fibers, which enabled nutrients and oxygen to be distributed even within the depths of the cell-seeded scaffolds. This investigation shows that the preferred type of fiber and polymer utilized is cell dependent. The trilobal nylon 6,6 scaffolds were shown to be more suitable for fibroblast growth, while the multilobal PET scaffolds improved the culture of cells. Hence, different types of polymeric scaffolds have to be screened with cells of interest as the needs for optimal cell growth such as surface topography and hydrophilicity are different [26]. The investigation has utilized two commercially available multilobal fibers, multilobal cross-sectional PET, and trilobal cross-sectional fibers. But, the polymers are nonbiodegradable, a physicochemical property suitable in tissue engineering applications. The investigation has shown the merit of using scaffolds made from multilobal fibers. The manufacture of biodegradable multilobal fibers will increase the potential of these fibers in tissue regeneration, in the times to come.

References

1. Hutmacher DW (2001) Scaffold design and fabrication technologies for engineering tissues–state of the art and future perspectives. J Biomater Sci Polym Ed 12(1):107–124
2. Lee J, Cuddihy MJ, Kotov NA (2008) Three-dimensional cell culture matrices: state of the art. Tissue Eng Part B Rev 14(1):61–86
3. Yang S, Leong KF, Du Z et al (2001) The design of scaffolds for use in tissue engineering. Part I. Traditional factors. Tissue Eng 7(6):679–689
4. Yang S, Leong KF, Du Z et al (2002) The design of scaffolds for use in tissue engineering. Part II. Rapid prototyping techniques. Tissue Eng 8(1):1–11
5. Holy CE, Fialkov JA, Davies JE et al (2003) Use of a biomimetic strategy to engineer bone. J Biomed Mater Res A 65(4):447–453
6. Wong DY, Krebsbach PH, Hollister SJ (2008) Brain cortex regeneration affected by scaffold architectures. J Neurosurg 109(4):715–722
7. Aydin HM, El Haj AJ, Piskin E et al (2009) Improving pore interconnectivity in polymeric scaffolds for tissue engineering. J Tissue Eng Regen Med 3(6):470–476
8. Hui PW, Leung PC, Sher A (1996) Fluid conductance of cancellous bone graft as a predictor for graft-host interface healing. J Biomech 29(1):123–132
9. Agrawal CM, Ray RB (2001) Biodegradable polymeric scaffolds for musculoskeletal tissue engineering. J Biomed Mater Res 55(2):141–150
10. Pasquinelli G, Vinci MC, Gamberini C et al (2009) Architectural organization and functional features of early endothelial progenitor cells cultured in a hyaluronan-based polymer scaffold. Tissue Eng Part A 15(9):2751–2762
11. Shen G, Tsung HC, Wu CF et al (2003) Tissue engineering of blood vessels with endothelial cells differentiated from mouse embryonic stem cells. Cell Res 13(5):335–341
12. Mehta BC, Holman DW, Grzybowski DM et al (2007) Characterization of arachnoidal cells cultured on three dimensional nonwoven PET matrix. Tissue Eng 13(6):1269–1279
13. Muschler GF, Nakamoto C, Griffith LG (2004) Engineering principles of clinical cell-based tissue engineering. J Bone Joint Surg Am 86-A(7):1541–1558
14. Beltrami CA, Finato N, Rocco M et al (1994) Structural basis of end-stage failure in ischemic cardiomyopathy in humans. Circulation 89(1):151–163
15. Jing D, Parikh A, Canty JM Jr et al (2008) Stem cells for heart cell therapies. Tissue Eng Part B Rev 14(4):393–406
16. Ryan EA, Lakey JR, Paty BW et al (2002) Successful islet transplantation: continued insulin reserve provides long term glycemic control. Diabetes 51(7):2148–2157
17. Clemens C (2010) Extremely high surface areas from oval shaped multi-lobal fibres. Adv Textile Tech. 1 Oct 2010. Available from http://findarticles.com/p/articles/mi_hb6547/is_2010_Oct/ai_n55498054/?tag¼content;col1
18. Paul HL, Diller KR (2003) Comparison of thermal insulation performance of fibrous materials for the advanced space suit. J Biomech Eng 125:639–647
19. Marcus RK, Davis WC, Knippel BC et al (2003) Capillary channeled polymer fibers as stationary phases in liquid chromatography separations. J Chrom A 986(1):17–31
20. Stanelle R, Mignanelli M, Brown P et al (2006) Capillary channeled polymer (C-CP) fibers as a stationary phase in microbore high-performance liquid chromatography columns. Anal Bioanal Chem 384(1):250–258
21. Andrews KD, Feugier P, Black RA et al (2008) Vascular prostheses: performance related to cell-shear responses. J Surg Res 149(1):39–46
22. Bhattacharya V, McSweeney PA, Shi Q et al (2000) Enhanced endothelialization and microvessel formation in polyester grafts seeded with CD34(+) bone marrow cells. Blood 95(2):581–585
23. Bonani W, Maniglio D, Motta A et al (2011) Biohybrid nanofiber constructs with anisotropic biomechanical properties. J Biomed Mater Res B Appl Biomater 96(2):276–286

24. Nasr-Esfahani M, Mehrabanian M (2011) Production of bone-like 40 % nylon 6,6-nano hydroxyapatite scaffold via salt-leaching/solvent casting technique. In: 2nd international conference on chemistry and chemical engineering. IACSIT Press, Chengdu, China, pp. 40–44
25. Shen J, Li Y, Zuo Y, Zou Q et al (2010) Characterization and cytocompatibility of biphasic calcium phosphate/polyamide 6 scaffolds for bone regeneration. J Biomed Mater Res B Appl Biomater 95(2):330–338
26. Wong CS, Nuhiji E, Sutti A, Keating G, Liu X, Kirkland M, Wang X (2012) Enhanced cell growth using non-woven scaffolds of multilobal fibres. Text Res J 82:1371
27. Lu Q, Simionescu A, Vyavahare N (2005) Novel capillary channel fiber scaffolds for guided tissue engineering. Acta Biomater 1(6):607–614
28. Sinclair KD, Webb K, Brown PJ (2010) The effect of various denier capillary channel polymer fibers on the alignment of NHDF cells and type I collagen. J Biomed Mater Res Part A 95A(4):1194–1202
29. Sinclair KD, Webb K, Brown PJ (2008) Capillary channel polymer fibers as structural templates for ligament regeneration. In: The American association of textile chemists and colorists conference, pp. 36–40
30. Sinclair KD, Webb K, Brown PJ (2008) Options for anterior cruciate ligament (ACL) reconstruction. In: The American association of textile chemists and colorists conference, pp. 32–34
31. Tong HW, Wang M, Lu WW (2011) Electrospinning and evaluation of PHBV-based tissue engineering scaffolds with different fibre diameters, surface topography and compositions. J Biomater Sci Polym Ed. Epub ahead of print 18 Mar 2011. doi:10.1163/092050611X560708
32. Parizek M, Novotna K, Bacakova L (2011) The role of smooth muscle cells in vessel wall pathophysiology and reconstruction using bioactive synthetic polymers: a review. Physiol Res 60(3):419–437
33. Yim EK, Leong KW (2005) Significance of synthetic nanostructures in dictating cellular response. Nanomedicine 1(1):10–21
34. Yang SP, Lee TM (2011) The effect of substrate topography on FOB cell behavior and initial cell adhesion evaluated by a cytodetacher. J Mater Sci Mater Med 22(4):1027–1036
35. Thapa A, Miller DC, Webster TJ et al (2003) Nano-structured polymers enhance bladder smooth muscle cell function. Biomaterials 24(17):2915–2926
36. Papenburg BJ, Rodrigues ED, Wessling M et al (2010) Insights into the role of material surface topography and wettability on cell-material interactions. Soft Matter 6(18):4377–4388
37. Kidambi S, Udpa N, Schroeder SA et al (2007) Cell adhesion on polyelectrolyte multilayer coated polydimethylsiloxane surfaces with varying topographies. Tissue Eng 13(8):2105–2117
38. Vernon RB, Gooden MD, Lara SL et al (2005) Microgroovedfibrillar collagen membranes as scaffolds for cell support and alignment. Biomaterials 26(16):3131–3140
39. Wan Y, Wang Y, Liu Z et al (2005) Adhesion and proliferation of OCT-1 osteoblast-like cells on micro- and nano-scale topography structured poly(L-lactide). Biomaterials 26(21):4453–4459
40. Kato S, Akagi T, Sugimura K et al (2000) Evaluation of biological responses to polymeric biomaterials by RT-PCR analysis IV: study of c-myc, c-fos and p53 mRNA expression. Biomaterials 21(5):521–527
41. Schlicht H, Haugen HJ, Sabetrasekh R et al (2010) Fibroblastic response and surface characterization of O(2)-plasma-treated thermoplastic polyetherurethane. Biomed Mater 5(2):25002
42. Choee J-H, Lee SJ, Lee YM et al (2004) Proliferation rate of fibroblast cells on polyethylene surfaces with wettability gradient. J Appl Polym Sci 92(1):599–606
43. Kim SH, Ha HJ, Ko YK et al (2007) Correlation of proliferation, morphology and biological responses of fibroblasts on LDPE with different surface wettability. J Biomater Sci Polym Ed 18(5):609–622
44. Huang X, Shi B, Li B et al (2006) Surface characterization of nylon 66 by inverse gas chromatography and contact angle. Polym Testing 25(7):970–974

45. Geckeler KE, Wacker R, Aicher WK (2000) Biocompatibility correlation of polymeric materials using human osteosarcoma cells. Naturwissenschaften 87(8):351–354
46. Donelli I, Taddei P, Smet PF et al (2009) Enzymatic surface modification and functionalization of PET: a water contact angle, FTIR, and fluorescence spectroscopy study. Biotech Bioeng 103(5):845–856
47. Wei Q, Liu Y, Hou D et al (2007) Dynamic wetting behavior of plasma treated PET fibers. J Mater Proc Technol 194(1–3):89–92

Chapter 9
Advanced Personal Protective Equipment Fabrics

9.1 Introduction

Knives are being used commonly in committing criminal offenses these days. Hence, it becomes necessary for law and medical professionals to get a good deal of protection from threats of physical harm. As crime rates have increased twofold in some European countries, the public need high-level protection [1]. The demand for protective garments is ever increasing and is more focused on ballistic protection and antistab protection. Ballistic protection provides protection against projectile penetration including the new kind of bullets and antistab and offers protection from sharp-pointed objects with or without sharp cutting edges such as knives and needles. The necessity for protection against slash and stab, requirements for such protection, and the test standards presently adopted to characterize such products are discussed in this chapter. The design, development, and characterization of novel slash-proof materials for army, police, children, and public that are light in weight, comfortable, and efficient are also elaborately discussed herein.

9.2 Slash-Resistant Garments

9.2.1 Importance of Personal Protective Garments

9.2.1.1 Resistance Against Knife

In some countries, police officials are physically attacked by individuals who use wielding knives, ice picks, and other such weapons [2]. The 'Protective Service Occupations' is a culmination of 14 different submajor occupation groups as defined by the Standard Occupational Classifications 2000 (SOC2000) [3]. The risk factors

N. Gokarneshan et al., *Emerging Research Trends in Medical Textiles*,
Textile Science and Clothing Technology, DOI 10.1007/978-981-287-508-2_9

relating to serious physical assaults at workplace are high in the case of protective service, health, and social welfare professionals. The highest risk is faced by the police, followed by social workers, probation officers, bar staff, security guards, etc. During any violent incident, knife is commonly used [4], and alarmingly enough, school children have been found to carry them. This poses a threat to the officers working in the community, especially the youth and community workers and officers in the protective service occupations. Available evidence indicates that a significant minority of school children and young people carry knives and this problem may be growing. Official statistics suggests that the use of knives in the commission of violent crimes and homicide has remained steady [2]. During the first half of 2008, in London alone, 25 fatal knife attacks on young people have been reported [5].

9.2.2 Slash Resistance

Most of the wounds caused by violent assaults are by the use of knives and have been of the slash type. Such kinds of knife attacks can cause disfiguring and could even prove fatal when it damages the blood vessels. Nearly 25 % of fatal wounds resulting from stab injury are centered in the chest region. The slash attacks are the most prominent among knife assaults, and the distribution of wounds include the arms, neck, shoulder, and thigh regions. Even though stab-resistant armor defeats slash attempts, it is impractical to provide stab protection to the arms, neck, shoulder, and thigh regions due to the thickness and stiffness required for the armor materials to withstand the force of a stab attack. Slash-resistant armors, in contrast, need not be bulky or stiff [6]. They can be more flexible and lighter as the maximum load exerted by a slash is approximately 25 % of the loads measured in stab attacks [7]. Investigations reveal that the maximum energy produced could reach up to 115 J for an overarm stabbing action and 64 J for an underarm stabbing action [8, 9]. The areas in which custodial and corrections officers perform their duties differ greatly from their street counterparts. Cells and hallways are sometimes small or narrow, and the ability to move or fight off an attacker becomes crucial. Handmade and sharp-edge weapons pose serious threat in such regions. Stab-resistant vests which utilize metal or plastic plates could restrict the wearer's ability to protect themselves, bend quickly, or rise up when knocked down. Such disability to protect oneself can cause serious injury during attack [10].

9.3 Objectives of Investigation

Research has been carried out to achieve the following objectives:

(a) Design, development, and characterization of innovative cut-resistant, slash, and stab-proof fabrics to be used in police and army.

(b) Engineering, testing, and analyzing lightweight, comfortable, and efficient system that could have durability in use.
(c) Testing of such materials through adoption of standard test practices.
(d) Introduction of suitable antimicrobial and other chemicals in the developed materials for protection against a range of viruses known as prokaryotes.
(e) Fully characterize the barrier properties of these chemicals/finishes, etc.

The intended application is to design special cut-resistant and slash-proof materials for the police, armed forces, children, and the public, which can have lightweight, comfort, efficient and be durable in use.

9.4 Development of Knitted Structures

The knitting process is considered to be cost-effective and flexible and can produce a range of structures suitable for contoured armor. However, it has not been effectively possible due to the high level of yarn interlocks that occurs during the process [11]. This produces a fabric with a very low initial modulus. When considering slash resistance, the low initial modulus guides the relative slippage of yarns and aids the stress distribution over a greater area and thereby prevents the blade from striking through the fabric. Therefore, weft knitting technique was utilized to design the slash-resistant fabric. The weft knitting process is also attractive when factors such as cost, design potential, and versatility are considered [12]. A series of fabric samples were knitted by using different combinations of various yarns and innovative two-layer weft-knitted structures. The knitted structures developed and used during this work have not been discussed in this chapter intentionally, because they are a vital part of the patent applications pending to protect the intellectual property rights (IPR) of this invention.

The yarns used in the fabric were:

- Spectra WF 408,
- Spectra WF 528,
- Wykes E669,
- Tilsa, 100 % spun aramid fiber, and
- Kevlar.

The above yarns have been used with Kevlar TW (2 ply).The fabrics have been knitted with Kevlar TW (2 ply) on one face and one of the other yarns in the other face and vice versa. An electronic flat knitting machine has been used for the purpose. The gray or unfinished fabrics were tested against the HOSDB slash-resistant standard for the UK police.

9.5 Discussion of the Findings

The fabrics designed and knitted for determination of their slash resistance have a novel double-layered structure. One face appears as a single jersey structure, while the other face has a racked structure. The fabrics have been tested on both sides [13]. The directions in which the test has been carried out are as follows: (i) walewise (lengthwise), (ii) coursewise (widthwise), and (iii) diagonal (30° to walewise). The force at which the blade strikes through the fabric is given in Newton (N). Tests indicate that the fabric has passed the slash test in that particular direction. During the analysis of the results, comparisons have been made between different yarns and structures to optimize the best combination for a lightweight slash-resistant personal protective equipment garment [11].

9.6 Comparison of Different Yarns

Figure 9.1 shows the resistance to slash for various yarns with different knitted structures. WF 408 yarn is the closest to passing the test with just 1 N short in the diagonal direction for the jersey structure tested with Kevlar as test face [13]. It passed with a value of 84.49 N in walewise direction, 61.24 N in coursewise direction, and 59.08 N in diagonal direction [11]. The fabrics knitted with WF 528 on the racked test face passed in both coursewise and diagonal direction with values of 86.52 and 91.84 N, respectively, but failed badly in walewise direction with a value of 23.99 N.

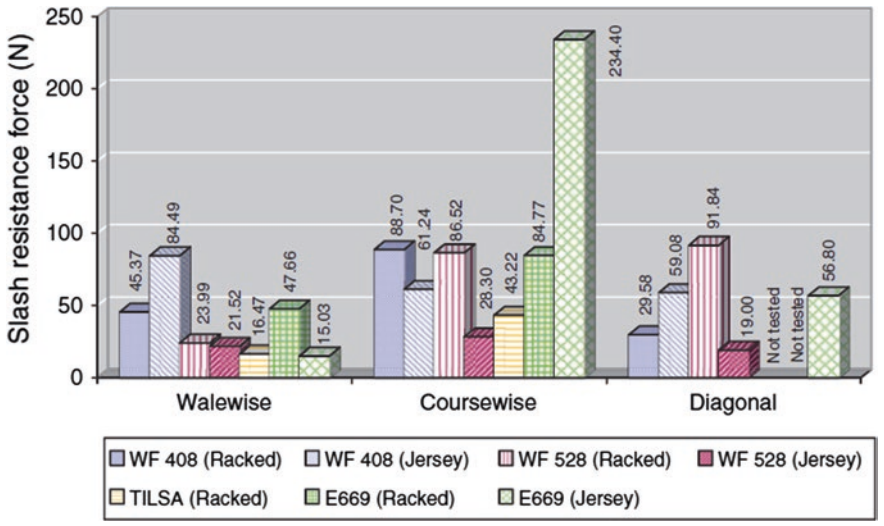

Fig. 9.1 Slash resistance force for different yarns in all three directions [11]

9.7 Comparison of Different Structures

Figure 9.2 shows the slash resistance force of different structures tested with Kevlar used as the test face. The test results indicate that even though the jersey structure showed the highest resistance of 234.4 N to the slash in the coursewise direction, it performed poorly in the walewise direction with a value of 15.4 N and failed marginally in the diagonal direction at 56.8 N. The racked structures exhibited consistency of results in all three directions, with 'Racked 2' structure performing well in comparison with the other two racked structures [13]. Racked 1, 2, and 3 (Fig. 9.2) represent the various racking sequences that have been used to compare the influence of different racking sequences on slash resistance. The 'Racked 2' structure withstood the slash resistance force of 84.77 N in coursewise direction and 101.73 N in diagonal direction, and failed at 48.69 N in walewise direction. The high value of 234.4 N in the coursewise direction achieved with jersey structure used as the test face has been confirmed by retesting the fabric [11].

9.8 Slash-Resistant Personal Protective Equipment

9.8.1 Garment

Besides Kevlar, Spectra WF 408 yarn gave the best resistance to slash (Fig. 9.2). However, this was replaced by three ends of WF 528, which reduced the linear density by 30 % but maintaining the same breaking force. This in turn reduced the area density of the knitted fabric by 250 g/m^2, and thereby rendering it lighter

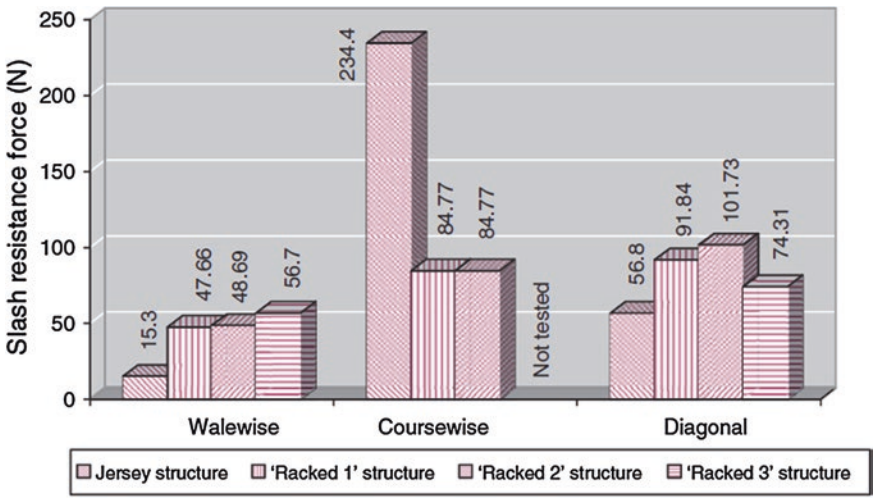

Fig. 9.2 Slash resistance force for various structures using Kevlar on face side [11]

and more comfortable to wear. The innovative two-layer structure, called SARK-1, has been able to go through the HOSDB slash-resistant standard for the UK police on both the faces and has been knitted with two ends of Kevlar as the racked face and three ends of WF 528 as the other face [13]. The results of the slash tests reveal that a minimum failure force of 71.64 N and average failure force of 158.38 N have been attained [11]. The average force of 158.38 N was almost double the minimum average necessary to pass the test. A second set of walewise and coursewise slash tests has been performed to substantiate the results obtained. This has not been done with Spectra WF5 28 used as the test face as there was not adequate sample remaining to conduct the slash test. The above fabric also passed the slash resistance standard with the WF 528 as the test face. It passed with a force of 65.81 N in walewise direction, 122.17 N in coursewise direction, and 61.61 N in diagonal direction. The high resistance of 122.17 N to slash in the coursewise direction enabled the fabric to obtain the required average of 80 N. Modifications have been done in the straight jersey structure to achieve a special racked structure in one of the faces. The innovative two-layer racked structure, called SARK-2, passed the standard on both faces of the fabric with an average value of 91.47 N on the Kevlar face and 108.36 N on the WF 528 face. SARK-2 achieved similar slash performance in all three directions. This indicates that the structure is more or less isotropic with regard to this property.

9.9 Antimicrobial Hygiene Garments

During the event of physical threats, law enforcement and medical personnel require a high level of protection. As the use of knives is more common in these days, the general public needs special protection from crimes arising due their use. The previous part of the discussion focused on the need for protection against slash and stab, the objectives of the design, development, and characterization of innovative slash-proof materials for the police, armed forces, children, and the public. This part discusses the application, testing, and evaluation of antimicrobial agents to the novel slash-proof materials described in the previous sections [11].

It is well known that microorganisms transmit diseases and infections through clothing, bedding, etc., and even aggravate the conditions. They are abundantly present on textile materials and help in transmitting diseases and infections [14]. Microorganisms cause damage to fibers under normal usage and storage conditions, thereby reducing the wear life of the materials [15]. The moisture transport characteristics of fabrics made wholly of synthetic fibers tend to cause a greater degree of ‘perspiration wetness’ which causes discomfort to the wearer, and they retain more odor causing bacteria than natural fibers, especially polyamide fibers [16, 17]. Hence, protective fabrics should have some kind of antibacterial protection imbued in them, particularly when they are designed to be worn over a long durations. One of the main objectives of this study discussed herein is to incorporate suitable antimicrobial agents into novel materials to provide protection against

a range of pathogenic bacteria and to fully characterize the barrier properties of the treated materials. The application of antibacterial agents into the innovative slash-resistant fabric highlighted in the previous section poses a problem as the fabric has only 13.6 % of its fibers by weight (polyamide), effectively available for incorporation of antibacterial agents [18]. The balance of about 85 % of the fabric is made of para-aramid fibers, ultrahigh molecular weight polyethylene, and glass fibers, which pose problems in applying antimicrobial agents into fiber matrix. The slash-resistant fabric has been designed as a double-layered structure, with one face comprising entirely of Kevlar aramid fibers and the other face having the engineered composite yarn that is double-covered using a polyamide continuous filament yarn. The development of antimicrobial textiles for healthcare workers has received good attention as they are highly exposed to many biological hazards at the work environments, and the applications and advancements in antibacterial finishes on textile products have been discussed by many researchers [19–22]. The fibers that are available for incorporating antibacterial agents are made up of polyamide (Nylon 6,6), and considerable research has been carried out to successfully incorporate antibacterial agents into the textile structures [23, 24]. The evaluation methods of antimicrobial finishes have been discussed elsewhere [25–29], and hence, this part focuses on the up-to-date results from the study of application of antimicrobial properties on this innovative double-layered weft-knitted slash-resistant fabric that has only 13.6 wt% of fibers available for incorporation of antimicrobial agents.

9.10 Pickup of Chemical Formulation

The antibacterial formulation has been applied at concentrations of 5, 10, 15, 20, and 25 %.The pickup percentage of the fabrics has been investigated at various concentrations so as to evaluate the efficiency of fabric to take up the chemical agents. Ten fabrics have been tested for each concentration. Figure 9.3 shows that the pickup percentage changes with the concentration of the recipe and is found

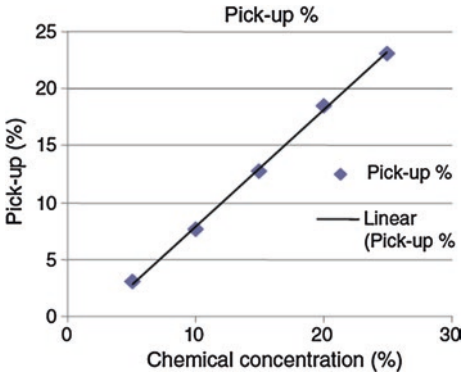

Fig. 9.3 Percentage pickup of chemical agents at various concentrations [18]

to be linear [18]. The relationship between the pickup percentage for the novel slash-resistant material and the recipe concentration is calculated by using a linear regression equation with a coefficient of determination (R2) value of 0.9985.

9.11 Antimicrobial Activity Against Gram-Positive Bacteria

The bacteria *S. Aureus* has been investigated at varied dilutions of 10^{-4}, 10^{-5}, and 10^{-6} in order to determine the antimicrobial activity of the slash-resistant fabric at of 5, 10, 15, 20, and 25 % concentrations. Since the fabrics could not be fully immersed in the agar solution, the test was conducted separately for both faces of the fabric. Two fabrics were tested for each face, giving a total of four fabrics and 16 zones of inhibition points. An average of all the 16 points was recorded.

The Fig. 9.4 shows that the peak antimicrobial activity is attained at 10 % of recipe concentration. The rate of antimicrobial activity increases with the increase in concentration of recipe up to 10 %, and the increase is insignificant thereafter. The coefficient of determination (R2) value is least for log concentration of 10^{-5} at 0.8083 and is more consistent for lower bacterial concentration of 10^{-6} at 0.9556. It cannot be concluded from the results that the consistency will increase with decrease in bacterial concentration, as the investigation has been done at only three

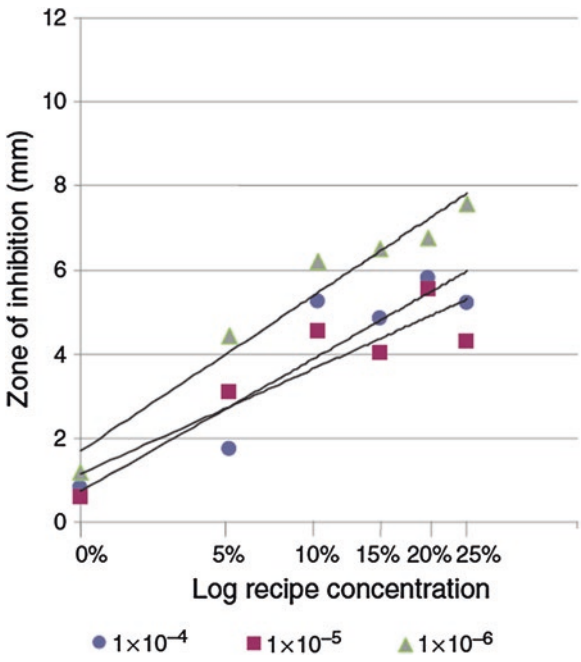

Fig. 9.4 Zone of inhibition of *S. Aureus* [18]

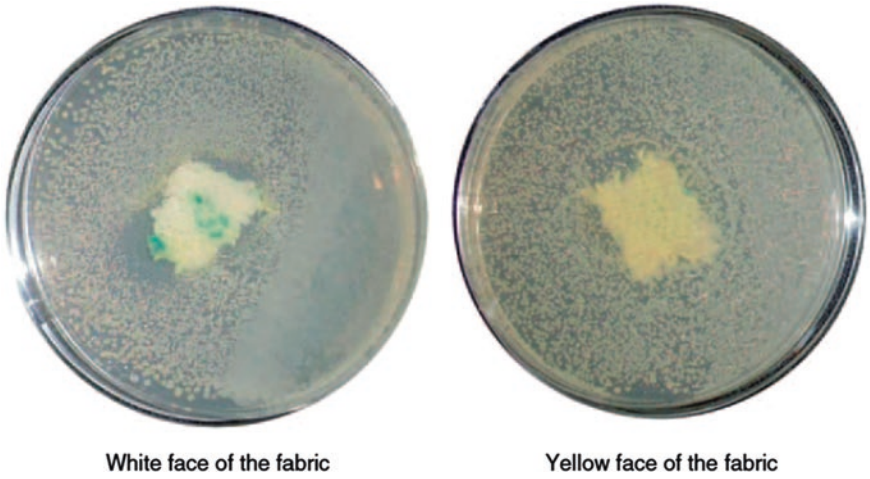

Fig. 9.5 Inhibition zone of control untreated fabric against *S. Aureus* [18]

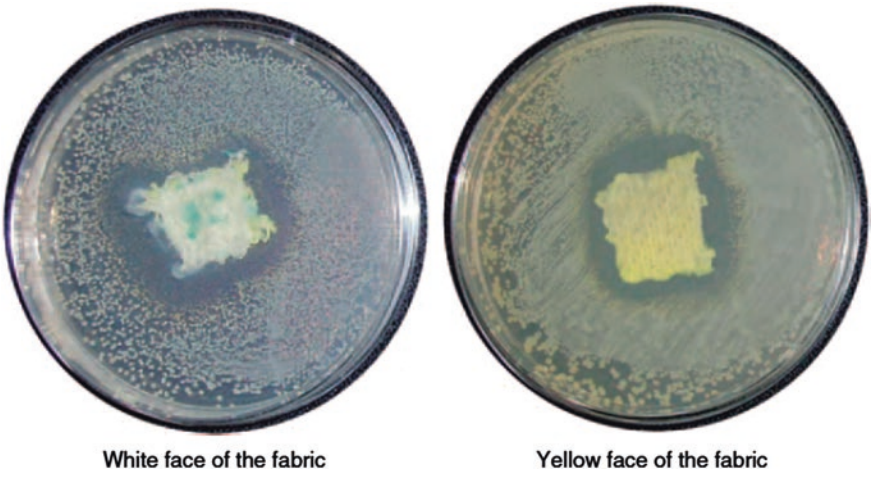

Fig. 9.6 Inhibition zone of treated fabric (10 % concentration)—*S. Aureus* [18]

dilutions. The optimum antibacterial activity can be obtained at 10 % concentration with zone of inhibition of 5.2, 4.6, and 6.2 mm at various bacterial dilutions.

Figure 9.5 shows the antibacterial activity of the control untreated fabric against *S. Aureus* at 10^{-4} dilution, and Fig. 9.6 shows the antibacterial activity of the fabric treated with 10 % concentration of the chemical formulation.

The inhibition zone attained at 15 % concentration is slightly lower than that of 10 % concentration and increases marginally at concentrations of 20 and 25 %. Concentrations of the formulation beyond 25 % could not be tested, since the saturation point had been reached.

9.12 Antimicrobial Activity Against Gram-Negative Bacteria

The various bacterial concentrations of *E. Coli* versus the extent of antimicrobial activity at various concentrations of the synergistic chemical formulation applied on the novel slash-resistant fabric have been plotted as depicted in Fig. 9.7. Despite the noncorrelation of the data between the measured zone of inhibition at various chemical concentrations and the log of various concentrations of bacteria, the values obtained establish significant antimicrobial activity against Gram-negative bacteria [18]. Figure 9.8 shows the antibacterial activity of the control untreated fabric against Gram-negative bacteria, *E. coli,* at 10^{-4} dilution, and Fig. 9.9 shows the zone of inhibition of the treated fabric at 10 % concentration against *E. Coli*. Here again, the influence of chemicals against the Gram-negative bacteria shows the peak antimicrobial activity, with zones of 5.2, 6.1, and 7.1 mm, at 10 % concentration of the antibacterial formulation.

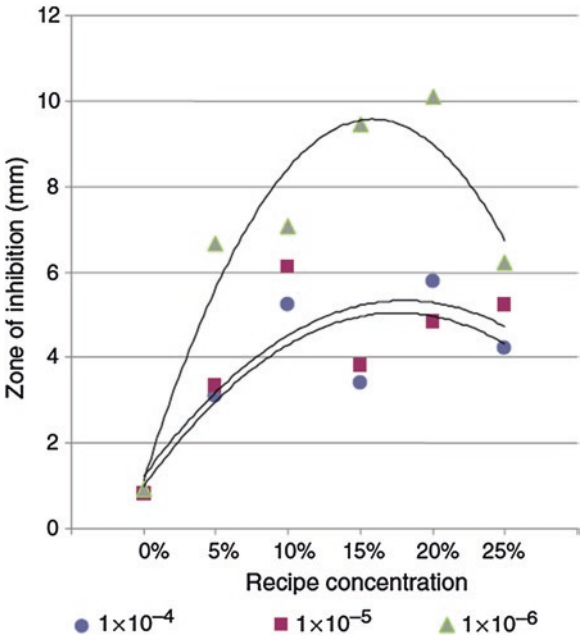

Fig. 9.7 Inhibition zone of *E. Coli* [18]

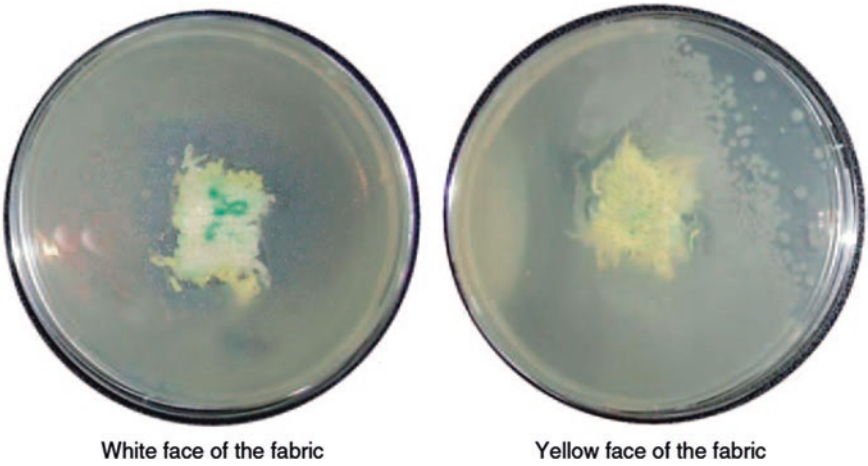

Fig. 9.8 Inhibition zone of control untreated fabric—*E. Coli* [18]

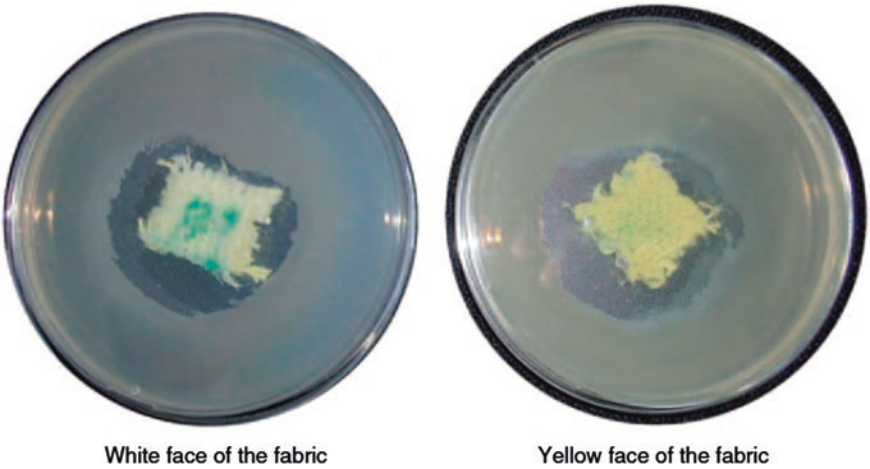

Fig. 9.9 Inhibition of treated fabric (10 % formulation)—*E. Coli* [18]

9.13 Durability of Antimicrobial Finish Against Gram-Positive Bacteria

The slash-resistant fabric consists of two layers with different yarn materials. One face is Kevlar and the other face with the composite WF 528. Both the yarns are different in absorption properties, and thus, the durability of the antimicrobial finish has been determined on both the faces of the fabric [18]. Figure 9.10 depicts the inhibition zone in mm against *S. Aureus* after 1, 5, and 10 washes, with and without a cross-linking (CL) agent, with Kevlar (Yellow) as the test face. The

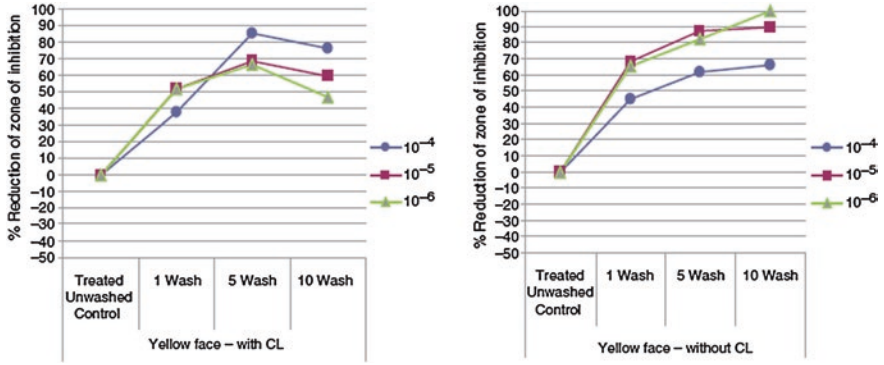

Fig. 9.10 Reduction of inhibition zone on Kevlar—with and without cross-linking agent—*S. Aureus* [18]

reduction in the zone of inhibition after every wash expressed as a percentage is shown graphically in Fig. 9.10.

Tests show that the percentage reduction in inhibition zone after washing is mostly higher in the case of fabrics without the CL agent. The average reduction at all dilutions is 85 % after 10 washes for the fabric without the CL agent, whereas the average reduction for the fabric treated with the CL agent is only 60 %. In the case of bacterial dilution of 10^{-6}, the percentage reduction in inhibition zone is 47 % after 10 washes with the CL agent and no antimicrobial activity is observed without the CL agent. The white WF 528 face shows a higher retention of the antimicrobial agents when a CL agent is used. The white WF 528 face exhibits a higher retention of the antimicrobial agents when a CL agent is used as compared with the antimicrobial activity on the yellow Kevlar face. The average reduction at all dilutions in the zone of inhibition is 37 % for the white face, whereas it is 60 % for the yellow Kevlar face (Fig. 9.11). In the case of treatments without the CL

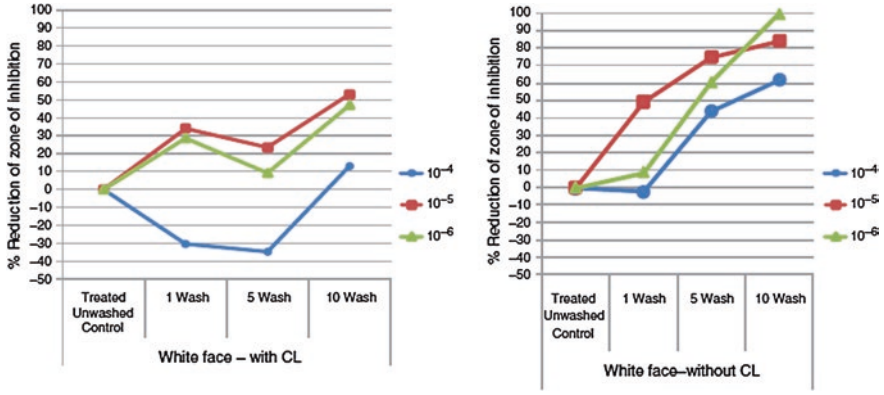

Fig. 9.11 Percentage reduction of inhibition zone on Kevlar (yellow) face with and without cross-linking agent—*E. Coli* [18]

agents, the percentage reduction in the inhibition zone is the same at 85 and 82 % for yellow face and white face, respectively.

When a fabric has been treated with an antimicrobial agent, its antimicrobial activity is supposed to be retained or get reduced with successive washings. However, in the case of bacterial dilutions at 10^{-4}, there has been an increase of 30 % in the antimicrobial activity after 1 and 5 washes. This suggests either an experimental error or a higher take-up of the antimicrobial chemicals at the particular portion of the fabric.

9.14 Durability of Antimicrobial Finish Against Gram-Negative Bacteria

The antimicrobial finish on Gram-negative bacteria has lesser durability than that on Gram-positive bacteria [18]. The reduction in antimicrobial activity increased to 100 % on both faces of the fabric, with and without the CL agent for bacterial dilutions of 10^{-6}, despite higher concentrations of bacteria exhibiting some antimicrobial activity. There has been no significant difference in the retention of the antimicrobial agents on the yellow face when a CL agent is used. The average percentage reduction in zone of inhibition is 88 % with CL agent and 86 % without CL agent (Fig. 9.11). An increase in activity by 11 % on the white WF 528 face has been observed when a CL agent is used indicating the durability of the antimicrobial (Fig. 9.12) and when compared to the antimicrobial activity on the yellow Kevlar face.

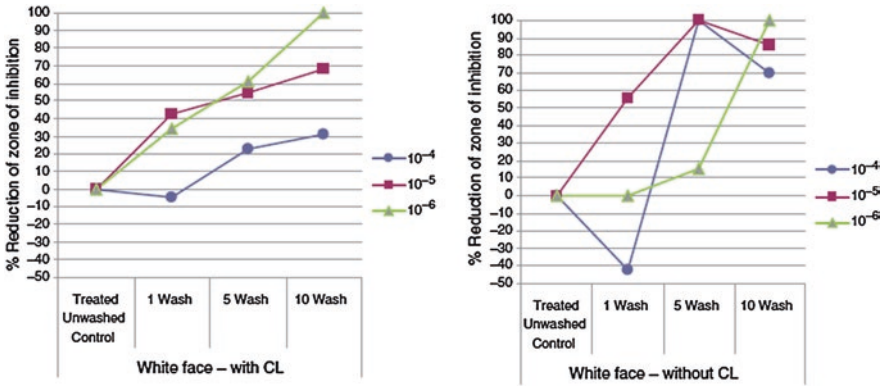

Fig. 9.12 Percentage reduction of inhibition zone on white (WF 528) face with and without cross-linking agents [18]

References

1. Wooding D (2007) Anarchy in UK: have the yobs taken over? The Sun 20:4
2. Anonymous (2006) Knife crime: in-effective reactions to a distracting problem. The Centre for Crime Justice Stud:20
3. Budd T (1999) Violence at work: findings from the British crime survey. Home Office, London
4. Youth Justice Board for England and Wales (2005) MORI youth survey 2004. Youth Justice Board for England and Wales, London, p 32
5. Anonymous (2008) B.B.C radio 4 news [Radio broadcast]. BBC, London
6. Buster C (2007) Body armor update. Law Ord 55(1):50–62
7. Bleetman A, Watson CH, Horsfall I, Champion SM (2003) Wounding patterns and human performance in knife attacks: optimising the protection provided by knife-resistant body armour. J Clini Forensic Med 10(4):243–248
8. Horsfall I, Prosser PD, Watson CH, Champion SM (1999) An assessment of human performance in stabbing. Forensic Sci Int 102(2–3):79–89
9. Chadwick EKJ, Nicol AC, Lane JV, Gray TGF (1999) Biomechanics of knife stab attacks. Forensic Sci Int 105:35–44
10. Fenne P (2005) Protection against knives and other weapons. In: Scott RA (ed) Textiles for protection. Woodhead Publishing, Cambridge, pp 652–662
11. Kanchi Govarthanam K, Anand SC, Rajendran S (2010) Development of advanced personal protective equipment fabrics for protection against slashes and pathogenic bacteria: part 1: development and evaluation of slash-resistant garments. J Ind Text 40:139–155. doi:10.1177/1528083710366722
12. Spencer DJ (2001) Knitting technology: a comprehensive handbook and practical guide, 3rd edn. Woodhead Publishing, Cambridge
13. Govarthanam KK, Anand SC, Rajendran S (2010) Development of advanced personal protective equipment for protection against slashes and pathogenic bacteria—part I—development and evaluation of slash resistant garments. J Ind Text 40(2):139–155
14. Rajendran S, Anand SC (1999) Development of a versatile antimicrobial finish for textile materials for healthcare and hygiene applications. In: Anand SC (ed) Medical textiles, proceedings of the international conference. Bolton, pp 24–25
15. Seventekin N, Ucarci O (1993) Damage caused by microorganisms to cotton fabrics. J Ind Text 84:304–313
16. Radford PJ (1973) Application and evaluation of anti-microbial finishes. Am Dyestuff Rep 62:48–59
17. Vigo TL (1994) Textile processing and properties: preparation, dyeing, finishing and performance. Elsevier, London
18. Kanchi Govarthanam K, Anand SC, Rajendran S (2011) Development of advanced personal protective equipment fabrics for protection against slashes and pathogenic bacteria part 2: development of antimicrobial hygiene garments and their characterization. J Ind Text 40(3):281–296
19. Broughton RM, Worley SD, Cho U, Lin J, Sun G (1999) Textiles with antimicrobial functionality. In: Book of papers, INDA Tec. INDA, Cary
20. Rigby AJ, Anand SC, Miraftab M (1993) Medical textiles: textile materials in medicine and surgery. Text Horiz:42–45
21. Manezes E (2002) Antimicrobial finishing for speciality textiles. Text Ind Trade J:35–38
22. Gao Y (2008) Recent advances in antimicrobial treatments of textiles. Text Res J 78(1):60–72
23. Gagliardi DD (1962) Antibacterial finishes. Am Dyestuff Rep 51(2):31–40 (Development of Antimicrobial Hygiene Garments 295)
24. Buchenska J (1996) Antibacterial polyamide fibres. Fibres Text Eastern Eur 4:53–59
25. Kawata T (1998) First permanently antibacterial and deodorant fibres. Chem Fibres Int 48:38–43

26. Williams JT, Painter P, Smith EJ, Walsh SE (2007) Comparison of antimicrobial textile treatments. In: Kennedy JF, Anand SC, Miraftab M, Rajendran S (eds) Medical textiles 2007: proceedings of the international conference on healthcare and medical textiles. Bolton, 16–18 July 2007
27. Thomas S, McCubbin P (2003) A comparison of the antimicrobial effects of four silver-containing dressings on three organisms. J Wound Care 12(3):101–107
28. Lashen ES (1971) New method for evaluating antibacterial activity directly on fabric. Appl Microbiol 21(4):771–773
29. Leonas KK (1997) Using laser scanning confocal electron microscopy to evaluate microorganism transmission through surgical gown fabrics. Medical textiles' 96 conference proceedings, Bolton Institute, UK, 17–18 July 1996. Woodhead Publishing, Cambridge, pp 60–65

Chapter 10
Surgical Gowns—Techno Economic Aspects and Innovations

10.1 Introduction

As the awareness on hygiene is increasing, the growth of medical textiles has enhanced during recent years. Diseases such as AIDS and hepatitis are on the increase, and it becomes important to develop understanding and find ways to protect from such serious diseases. The body of a patient who is to be operated can be a source of infection, and hence the doctors and their assistants who attend on them need protection from infection. Hence, such personnel use a protective garment known as surgical gown to protect from undesirable infection. But, a number of manufacturers and majority of the users of such protective clothing are not aware of the exact specification and performance needs of the fabrics used for this garment. If the fabric used in the manufacturing of the surgical gown has got pore sizes less than the size of the microbes, then the microbes cannot enter the body of the healthy person. But it might not be possible all the time to design a fabric with the particular pore size, which does not allow microbes to enter through the fabric, especially for the microbes such as virus, which is in the microlevel. For this purpose, a special woven structure has to be developed and a special antimicrobial coating needs to be applied to the fabric. But, it is evident with a coated material that the comfort property of the fabric deteriorates. During any minor surgery, the lack of comfort in the surgical gown is not of much significance. However, comfort is a crucial requirement during any major surgery over a long duration. Hence, it is necessary to apply a waterproof breathable coating to the fabric such that the water-based permeable fluids such as blood and serum cannot penetrate the surgical gown but air can pass through the fabric to maintain the comfort of the wearer. But it is also necessary to secure a perfect protection from viruses besides providing comfort. This chapter highlights the aspects related to the development, application and quality evaluation, and requirements of surgical gowns. It also discusses about the types of gowns available, their classification, technology of manufacture, test methods, their limitations, and future vision on the increasing need of human health and safety.

N. Gokarneshan et al., *Emerging Research Trends in Medical Textiles*,
Textile Science and Clothing Technology, DOI 10.1007/978-981-287-508-2_10

10.2 Basic Considerations in Surgical Gowns

Earlier surgical gowns have been used to protect the patients from the surgeons attending on them. Hence, an open-woven structure made from cotton, which was permeable and comfortable, was enough. However, with the appearance of infections related to the transmission of blood-borne pathogens, the need has changed over to protection of the surgeons and their assistants. Therefore, the surgical gown should protect the blood-borne infectious microbes from penetrating through the fabric and the fabric should be liquid proof. At the same time, the gown must provide comfort to the wearer by allowing heat and humidity to exchange between interior and exterior of the body. In other words, the fabric should be barrier resistant as well as comfortable to wear. Thus, there is a crucial need for the fabric to resist the penetration of liquids, such as blood, and also be noncontagious, flexible, and economical [1]. This is not easy to achieve. Despite some manufacturers claiming to achieve these functions, there exist a number of setbacks and constraints, which are highlighted in this chapter. Hence, the problems related to infection and diseases from pathogens and the comfort properties have prompted medical professionals to look into the clothing performance.

10.3 Infection and Transmission

Most of the post-surgical infections result from surgery, which happens due to the possibility of microorganisms attacking the open wound. Microorganisms can arise out of attendant staffs in the operation room, other patients, or even some objects or it could even be from the patients themselves. In clean operations, i.e., operations in sterile tissue and where hollow viscous is not entered the skin of operating room personnel and of the patient are the most important sources of microorganisms. In infection-prone operations, e.g., orthopedics and vascular implant surgery, the normal microbial skin flora is of significance as a cause of surgical site infection. Surgical gowns are used to prevent direct-contact transfer of infective agents from the surgical team to the operating wound and vice versa. When surgical gowns are made with appropriate material and techniques to create the required barrier, they could prevent dispersal of skin scales in the surgical room air [2]. Hence, the surgical gowns are gaining new interest owing to their protective property which offer barrier against very infectious viruses and bacteria. Surgical gowns are primarily intended to avoid transmission of pathogens. It is necessary to know the method of transmission so as to enable a fabric to prevent its occurrence [3, 4]. The pathogenic infections can get transmitted in a number of ways, such as contact, droplet, air-borne, and common vehicle transmission. There are two means through contact transmission can occur. The first is the direct-contact transmission involving a direct body-to-surface contact and physical transfer of microorganisms between an infected person with a susceptible host. An example would be touching blood, other potentially infectious materials (OPIM),

or patient tissues with ungloved hands. The second is the indirect-contact transmission that involves contact of a susceptible host with a contaminated intermediate object, such as contaminated instruments, dressings, or contaminated hands/gloves. An example would be contacting a used dental instrument or a removable patient appliance. Droplet transmission occurs during coughing, sneezing, talking, and so on. Transmission occurs when droplets containing microorganisms generated from the infected person are propelled a short distance through the air and deposited on the host's body parts such as nasal mucosa or mouth. An example would be contact with particles or spatter of patient body fluids. Air-borne transmission occurs by dissemination of either droplet nuclei or dust particles containing the infectious agent. Based on the environmental conditions, pathogens can be carried over a larger distance. The breathing in of minute particles from the body fluids of the patient is an example. Lastly, common vehicle transmission is related to microorganisms transmitted by contaminated items such as devices and equipment and carried away through different vehicles or transport systems.

10.4 Viruses, Bacteria, and Associated Diseases

The aforesaid discussions indicate that a surgical gown should protect the human body from blood-borne microorganisms and hence the fabrics should be produced such that the inter-yarn spaces should be less than the size of microorganisms. It therefore becomes necessary for the fabric manufacturer to know about the sizes of the different pathogens. The sizes of a range of bacteria and viruses causing serious diseases [5] are given in Tables 10.1 and 10.2 and would provide useful information to the fabric designers and subsequent processors, which would enable them to design appropriate fabrics for surgical gowns.

Table 10.1 Size of some highly infectious disease viruses [50]

Species	Size (μm)	Associated diseases
Bacteriophage ØX174	0.025–0.027 dia	Test virus used by Nelson
Hepatitis virus (HBV)	0.042–0.047 dia	
Adenovirus	0.07–0.09 dia	Respiratory infections
HIV	0.08–0.11 dia	Acquired immunodeficiency syndrome
Filovirus	0.08 dia	Ebola virus
Bunyaviridae	0.08–0.12 dia	Hanta virus
Orthomyxoviridae	0.08–0.12 dia	Influenza A, B, and C
Coronaviridae (SARS)	0.10–0.12 dia	SARS
Varicella-zoster virus	0.11–012 dia	Herpes
Cytomegalovirus	0.12–20 dia	Pneumonia, hepatitis, retinitis, encephalitis
Variola virus	0.14–26 dia 0.22–0.45 length	Small pox

Table 10.2 Size of some disease—bacteria [50]

Species	Size (μm)	Associated diseases
Serratia marcescens	0.45 dia	Extra-intestinal infections, nosocomial infections
Pseudomonas aeruginosa	0.50–1.0 dia 1.5–4.0 length	Endocarditis, pneumonia, osteomyelitis, nosocomial infections, meningitis, septicemia
Staphylococcus aureus	1.0 dia	Pneumonia, osteomyelitis, acute endocarditis meningitis, toxic shock syndrome, myocarditis
Mycobacterium tuberculosis	1.0–5.0 dia	Tuberculosis
Bacillus anthracis	1.0–1.5 dia 3.0–5.0 length	Anthrax infection

10.5 Comfort of Surgical Gown

The human body is exposed to varied environmental conditions and also to highly infectious hospital environment. The surgical gown has to cover the body and protect it against varying conditions of environment and also provide comfort to the wearer. Comfort is defined as the absence of discomfort or unpleasantness [6]. The movement of heat and water vapor through a garment are probably the most important factors in clothing comfort. If a garment provides too great a barrier to its passage, liquid moisture is formed by condensation of water vapor and the sensation of discomfort is increased, partly from a feeling of clamminess and partly because of the wet clothing clings [7–9]. The thermal comfort is promoted by the body's internal metabolism for production of heat, general level of activity, external temperature, insulating/permeable properties of fabric/clothing to moisture, water or air, and so on. The core temperature of human body remains 37 °C. The body generates heat continuously because of the metabolism of food and muscle activity and this heat is gets dissipated into the environment. The heat flow rate is dependent on the fabric properties and the temperature difference: The greater the difference the quicker heat is transformed. This characteristic is termed as temperature gradient. The heat transmission from the body happens through the three modes of conduction, convection, and radiation. The comfort as well as the barrier property of the surgical is mainly governed by the thermal conductivity, water vapor permeability, air permeability, and water impermeability.

10.6 Thermal Properties

At a skin temperature of 33–35 °C, the body experiences comfort and there would be no liquid perspiration. Hence, thermal comfort is fabric's capacity to maintain a skin temperature and permit transfer of body perspiration. Clothing that allows these conditions to remain when the environment changes and when the activities level increases will satisfy the basic requirement. The thermal comfort characteristics of a fabric are undermined by its thermal conductivity [10–14]. Moisture regain also influences the comfort phenomenon, as increasing moisture regain

increases thermal conductivity. Testing of thermal conductivity covers the determination of the overall thermal transmission coefficients due to the combined action of conduction, convection, and radiation. It measures the time rate of heat transfer from a warm, dry, constant temperature, horizontal flat-plate up through a layer of the test material to a relatively calm, cool atmosphere. Hence, it can be observed that heat transfer is crucial, since the human body has the tendency to get overheated under stressful working conditions. These are also measured as total heat loss (THL). THL is a measurement of a garment's ability to allow body moisture and heat to escape through all of its layers. The range at which the core body temperature is 'normal' versus at 'risk of death' is only 9–10 °F. With further changes as low as 3–4 °F, the human brain can be affected and poor decision making can result, along with extreme fatigue, exhaustion, loss of strength, and nausea. Employees can work with lesser risk and with greater physiological benefit and also be able to work safely and effectively, when the THL of the fabric is higher.

10.7 Breathability

The capability of a textile structure to permit water vapor passing out of the body through it and also prevent the entry of liquid to pass through it from outside is termed as breathability [15, 16]. The transmission of moisture vapor from the body considerably influences the comfort property in the following ways:

(a) The thermal energy generated by the human body gets dissipated mostly by evaporative cooling or loss of latent heat by the escape of moisture vapor.
(b) The inability of fabric to permit adequate moisture vapor diffusion causes accumulation of liquid or condensed water on the skin surface. The comfort property of the fabric is dependent on its breathability.

The moisture vapor transmission rate (MVTR) provides a measure of the breathability. It indicates the quantity of moisture that passes through a clothing assembly such as a dressing during a given time period. The higher the MVTR, the more effectively moisture is removed, preventing the accumulation of pools of moisture under the membrane. It is 'the steady water vapor flow in unit time through unit area of body, normal to specific parallel surfaces, under specific conditions of temperature and humidity at each surface.' The value is expressed in number of grams per square meter over a given period of time [1–3]. Another measurement, which is related with breathability, is THL. THL is a measure of a garment's ability to allow body moisture and heat to escape through all of its layers. The loss of water vapor through fabric is necessary to maintain balance of heat in the body and also comfort. Liquid moisture is formed the condensation of moisture vapor, which is caused by the barrier created by the fabric. This increases the sensation of discomfort, arising partially from a feeling clamminess and also partially due to wet clothing clings. Breathable fabrics have a wide range of applications that include rainwear, diver's clothing, footwear, mountaineering suits, skiwear, sportswear,

shoes, and more importantly surgical gown. In such applications, the resistance to penetration of liquid through fabrics is of considerable importance.

10.8 Air Permeability

The comfort property of the fabric is also influenced by air permeability. Any material which is permeable to air is also likely to be permeable to moisture vapor [17]. Hence, the air permeability is in general closely related to moisture–vapor permeability and the liquid moisture transmission. Fabrics made from cotton or wool undergoes swelling upon absorption of water vapor from the atmosphere. This would close off the pores in the fabric and thereby increase the resistance to convective flow through the material. Changes in fabric air permeability as a function of relative humidity are important for chemical protective clothing point of view.

10.9 Quantification of Comfort Parameters

A method has been developed to calculate the requirements that breathable fabric, which has to meet specific conditions. The following parameters have been considered [11]:

(a) The heat to be carried off by clothing (as a function of physical exertion)
(b) The estimated thermal resistance of clothing (thermal conductivity)
(c) The relative ambient humidity
(d) The ambient air velocity.

Assumptions:

1. Internal RH: 100 %.
2. External RH: 50 %.
3. Internal temp: 33 °C.
4. External temp: 20–30 °C.
5. Internal air exchange: 50 %.
6. External air speed: up to 4 m/s.
7. Garment thermal resistance: 1.4 clo.
8. Wearer: 70 kg man.

Subsequently, the necessary values for air and water vapor permeability have to be calculated for different levels of physical exertion and ambient temperatures. The fabric is supposed to be completely waterproof. The fabric permeability values for a surgeon in an operating room are mentioned in Table 10.3. When considering a surgeon who is working at moderate speed 20 °C at a moderate work pace. His clothing will feel comfortable, provided the air permeability is 100 L/m^2/min and the water vapor permeability 400 g/m^2/24 h. His clothing may be called breathable.

Table 10.3 Permeability of fabric necessary for maintaining equilibrium [50]

Work rate	Air flow rate (l/m²/min)			MVTR (g/m²/24 h)		
	10 °C	20 °C	30 °C	10 °C	20 °C	30 °C
Low	–	–	360	–	–	1020
Moderate	–	80	720	–	360	2076
High	–	320	1110	–	1392	3156
Very high	120	560	1470	640	2400	4140

10.10 Overview of Surgical Gown Materials Cotton/Cotton–Polyester

These are traditional materials for surgical gowns [18]. Even though they have wear comfort, the bigger pore size permits liquids and bacteria/viruses to pass through and thereby offers no protection/barrier against the microbes. Even with repeated impregnation of hydrophobic agents to create a good barrier, it cannot be made resistant to viruses, and also may not give the desired level of comfort. Compactly woven fabric comprising of a blend of polyester–cotton and also imparted with liquid-repellent fluorocarbon treatment are also available. Such a finish weakens with repeated washes and hence has to be re-imparted with the finish in order to sustain barrier effect.

10.11 Microfilament Fabrics

They are made of super fine polyester filaments, are closely woven, and are treated with a liquid repellent finish. Again, reliable barrier action is assured only with a hydrophobic treatment in each reprocessing cycle.

10.12 Multilayer Fabrics

Treble fabrics are used for surgical gown in order to attain a number of desired functions—outer layer designed to resist abrasion and puncture, middle layer providing exceptional barrier resistance to fluid penetration, and soft bottom layer adding comfort in addition to another layer of protection. Also, a tri-laminate is produced through combining a microporous membrane, bonded between an upper and lower layer of endless-fiber polyester. Mechanical stretched PTFE membranes are also used on surgical gown to resist fluid and virus to control transmission of infections.

10.13 Disposable- and Reusable-type Surgical Gowns

There are two types of surgical gowns that are being used and are disposable. The first type is known as single-use type and is made from nonwovens, while the second type which is of the reusable category made from wovens. Most single-use

products are sterilized by the manufacturer and delivered presterile to the user. But, some materials are suitable for hospital steam autoclaves, and hence nonsterile product ranges are also available.

10.14 Choice of Reusable Versus Disposables

The following factors should be carefully considered in decisions to use single-use versus reusable gowns [18–21]: Dual protection for both healthcare professionals and patients-placing has high importance on protection.

10.15 Judicious Selection of Gowns and Drapes

During the process of selection, assurance of asepsis, barrier effectiveness, comfort, economics, and environmental issues need to be given due consideration.

- Conforming to regulations and professional guidelines
- Precise evaluation of reusable materials. The ability of reusable gowns to resist strike-through varies with the number of uses, washings, and sterilization cycles.

10.16 Reviewing Costs

Precise evaluation of costs is not easy. A comprehensive evaluation of costs necessitates an appraisal of all related costs, some of which may initially not be apparent. The cost of gown varies with the amount of protection afforded. A high barrier and frequently reusable gown is required to perform a surgery with many risks and high blood count. A lower barrier disposable gown is utilized in the case of surgeries involving lesser risk [22]. Disposable gowns offer benefits in that hospitals can dispose off the contaminated textiles quickly, they reduce laundry costs, and they can be donned and doffed quickly in location such as emergency rooms [23]. Nonwoven disposables lighter than reusable ones and are also cooler [22]. Many researchers and manufacturers claim advantages and disadvantages in their own ways. According to recent reports, different authors describe benefits and constraints of disposable and reusable gowns in the following way [18].

10.17 Benefits and Constraints

Disposable (Single use): Benefits
As the products are used only once, there are no problems regarding damage to the barrier caused by reprocessing, and also the product quality is very consistent.

Moreover, there does not arise the necessity for in-house processing, enabling to have instrument-focused sterile services departments.

10.18 Synthetic Reusable Gowns

Benefits

Environment:
The reprocess ability of the gowns enables minimization of the quantity of clinical waste. This avoids the need to dispose off potentially hazardous and contaminated materials.

Cost:
Reduction of clinical waste helps to achieve substantial cost savings both in terms of incineration and the need to maintain a stock of single-use materials.

User/Wearer Preference:
Reusable materials may be preferred by clinicians with regard to aspects such as comfort, color, closer feel to cotton, and so on. The problem relating to comfort of gowns could be observed when surgeons find it objectionable to wear terming it as a 'papery' single-use gown.

10.19 The Constraints

The quality of reusable materials and the capacity of hospitals to monitor their use become questionable after repeated use. Owing to the high number of processing cycles, there are problems in maintaining a good barrier for the life of a reusable product and render it affordable. Products made from microfibers must be repeatedly impregnated in order to maintain a uniform barrier performance. Also key is the reliable recording of the frequency of processing for each individual surgical item. Hence, the potential problems related to reusable surgical items are as mentioned below [19, 20].

(a) Perception of less barrier protection
(b) Deterioration of barrier properties during laundering and sterilization, caused by factors such as wear, abrasions, and breakdown of fabric
(c) Irregularity in the product consistency involving multiple reprocessing. Lack of confidence in laundering and sterilization of reusable. Warnings from manufacturers regarding lack of assurance in performance or results
(d) Limited mandatory quality standards for laundries.

10.20 Other Parameters

A surgical to be produced is influenced by various other types of specifications [24, 25]. Some of these are highlighted below.

10.21 Types of Fabric Raw Materials

Despite the many types of fibers being used for surgical gowns, polyester appears to be the only fiber that prevails over the contrasting demands of comfort and barrier. Polyester surgical gowns are being utilized in surgeries of short durations, along with a small quantity of liquid.

10.22 Constructional Parameter

The suitability of the fabric for surgical gown for the intended application is influenced by the weave which can be plain weave or twill. As the twill weaves are having poor barrier effect in comparison with the plain weaves, they are not suitable for surgical gowns. Twill weave is particularly critical since it may have large pores between two adjacent yarns in the crossing points.

10.23 Sterilization Techniques

This is influenced by the kind of gown being used.

Gas- and irradiation-type techniques are being used for single-use-type gown, where low temperatures are preferred, whereas steam autoclave and dry heat methods are suitable in the case of reusable-type surgical gowns. A number of other factors that influence the property of the surgical gown such as filament fineness and cross section, filament yarns fineness and fabric density, fabric threads per inch, and fabric cover. Filaments with circular cross section exhibit better barrier effect since the packing density of the yarns made of circular cross-sectional filaments is far greater than any other cross-sectional shape of filaments. Also, the fabric having higher thread density, and thereby increasing the cover, exhibits enhanced barrier property.

10.24 Classification of Surgical Gowns

Classification Based on Level of Protection

Surgical gowns are classified into different categories based on the level of protection [26–29]. Four levels of protection are characterized based on the Association for the Advancement of Medical Instrumentation (AAMI). There is a system of classification for protective apparel and drapes used in healthcare settings based on liquid barrier performance. There are four tests that must be performed in order to establish the final AAMI classification:

(a) Spray impact penetration test;
(b) Hydrostatic head test;
(c) ASTM F1670; and
(d) ASTM1671.

The spray impact test is done to find whether the product is protective or nonprotective. The hydrostatic pressure test result indicates the level of protection from 1 to 3. The ASTM F1670 and F1671 are done for the products that are necessary to be fully impervious.

10.25 Four Classification Levels

Standardized test procedure and minimum performance levels have been fixed for gowns, drapes, and other protective apparel under these categories.

First level: The components of the critical zone should have a blotter weight gain not greater than 4.5 g, upon being tested for impact penetration.

Second level: When tested for impact penetration and hydrostatic pressure, critical zone components must have a blotter weight gain of not more than 1.0 g and a hydrostatic resistance of at least 20 cm.

Third level: The components of the critical zone should have a blotter weight gain not greater than 1.0 g and a minimum hydrostatic resistance of 50 cm, upon being tested for impact penetration and hydrostatic pressure.

Fourth Level: When tested for resistance to bacteriophage Phi-X174, critical zone components must show an AQL of 4 %.

The four levels of performance are related to the products' critical zones. The critical zones in a surgical gown are the areas that come in direct contact with blood, body fluids, and OPIM, which is most likely to occur, although areas outside the critical zones can be inadvertently splashed or sprayed as well. The front portion of a surgical gown (including the seam and other components) is expected to offer at least the minimum level of barrier performance (First level). Since the back of a gown intended for surgical applications is expected to stay dry, there is no liquid barrier performance requirement for that area. The four levels of performance are related to the products' critical zones. As the back of a surgical gown has to remain dry, liquid barrier performance is not necessary in the area.

10.26 The Design of Waterproof Breathable Fabrics

The design of a waterproof breathable fabric is crucial for the performance of surgical gown fabric in actual working conditions [30–32]. The problem associated with garments made from nonbreathable waterproof fabrics is that they cause condensation and accumulation on their inner surface, despite offering exceptional

protection against liquid or viruses. This problem arises because of the water vapor impermeability of the polymer coating. A buildup of moisture vapor inside the clothing may therefore cause discomfort. In the design of the surgical gowns, breathability is required to overcome this problem; breathability becomes necessary while designing gowns for surgical purposes. The garments can improve wearer comfort by reducing the buildup of perspiration inside of the clothing. When considering impervious blood- and virus-proof surgical gowns, closely woven fabrics alone are not adequate. A number of designs of water proof breathable fabrics are available such as microporous polymer membranes, solid polymer (monolithic) films, and bicomponent films.

10.27 Microporous Polymer Coating

The permeability of the polymer barrier determines the rate of dissipation of perspiration, when diffusion of water vapor through inter-yarn spaces, yarns, and fibers is severely reduced, due to lamination or coating with a continuous polymer membrane. The development of microporous structures having surface pores of much smaller dimensions than the inter-yarn spaces of woven fabrics has been an attempt to enhance the inherently low water vapor permeability of solid polymer membranes. A microporous barrier has microscopic holes through its polymer-based film. The microporous barrier layer 'breathes' primarily through a permanent air-permeable pore structure. The outside surface can repel even the finest water drop through surface tension effects. Air and water vapor can pass freely through the tortuous pathways provided that suitable concentration gradient exists between the inner and outer surfaces of the membrane. There are both PTFE (Teflon)-based and polyurethane-based microporous membranes. Different methods have been adopted for the production of microporous coatings and films.

10.28 Monolithic Coating

Barriers that adopt this technology have a continuous (no microscopic holes) polymer-based film or coating that does not permit flow of direct air or moisture vapor. The transmission of moisture vapor happens due to molecular diffusion as the moisture is absorbed by the membrane and released on the other side. The permeate dissolves on the surface of the membrane on the side of higher concentration and then diffuses across the film. The permeate desorbs and enters the surrounding airspace as a gas or vapor, as the vapor reaches the opposite surface. As the solid polymer-coated fabrics have no surface pores, they do not get affected by surface contamination and provide good barrier to blood-borne pathogens.

10.29 Comparison of Microporous Films with Monolithic Coating

Both technologies have their merits and demerits, some of which are mentioned as under [33, 34]:

(a) Monolithic coating are normally stiffer in handle as compared to microporous films.
(b) Microporous film has better breathability for the same thickness or weight of film and pore size.
(c) With regard to air permeability, monolithic coating and microporous films are found to be superior to bicomponent and hydrophilic films.
(d) Control of pore size and consistency of pore size is important for consistency of breathability and water proofness throughout the film.
(e) Continuous coating/lamination gives higher water vapor permeability than microporous films.
(f) Monolithic coating having no holes is less sensitive to possible deterioration.

10.30 Bicomponent Barrier Technology

It combines elements of both the microporous and the monolithic technologies in either an intimate or a layered manner. In layered constructions, the microporous and monolithic elements are simply applied one on top of the other. Both the technologies are intertwined in the case of intimate bicomponent constructions, thereby permitting a barrier to be created without any of the compromises normally present when either of the other two technologies is used individually.

10.31 Uncoated High-density Fabrics

The transmission of water vapor in the case of openly woven fabrics happens mainly through inter-yarn spaces and becomes relatively insignificant. Hence, fabrics having same open structure, weight, and thickness are supposed to exhibit same transmission rates without considering the type of yarn or fibers used. As the size of the inter-yarn spaces decreases, the secondary transmission mechanisms become more important. Hence, closely woven fabrics made from absorptive or hydrophilic fibers have greater transmission to water vapor than nonabsorptive and hydrophobic fibers of same structure. A number of high-density fabrics have been marketed recently [35]. They use yarns produced from microfibers of <1 decitex per filament. The demerit with this type of fabric is that it is unable to prevent blood-borne pathogens to pass through the fabric unless a specific method of treatment is adopted.

10.32 Polymer Coating/Lamination and Treatments for Breathable Barrier

A number of polymers and treatments can be used to achieve fluid proofness so as to get the desired barrier effect. This involves application of polymers such as polyurethane, PVC, PTFE membranes, acrylics, silicones, or fluorocarbons to the fabric. Fluorocarbons and silicones are water repelling agents and are temporary in nature [36]. Polyurethane offers many advantages and characteristics over many other polymeric materials, which make it suitable for use in surgical gowns. Polyvinylchloride suffers demerit with regard to flex properties, plasticizer migration, abrasion resistance, low temperature properties, cleanability, and so on, whereas polyurethane exhibits good chemical resistance, UV resistance and hydrolysis resistance, excellent low temperature flexibility, and excellent flex fatigue properties. In addition to the above, TPU offers excellent 'drape' properties, softness, and suppleness of hand. It also possesses much better moisture vapor transmission properties compared to PVC. High tensile strength and elongation combined with superior resistance to tearing and cutting make TPU exceptionally tough. These properties render it suitable for surgical gowns [37]. Also it is a temperature-sensitive kind of polyurethane, whose water vapor transport properties may undergo significant increase as the body temperature rises. The transition point in water vapor transport property of temperature-sensitive polyurethane can be controlled within the range of room temperature, specifically, through appropriate macromolecule design [38]. But this area is yet to be explored for its feasibility as a surgical gown. PTFE-based films having microporous structure are also used. Microporous structure is produced by mechanical fibrillation. The pore structure is produced by stretching the polymer film in both directions and annealed to impart microporous rips and tears all over the membrane.

10.33 Testing for Surgical Gowns

The performance of surgical gowns is evaluated by carrying out the following tests [27, 39].

10.34 Barrier Tests

(a) **Spray Impact Penetration Test Results**

This test measures the resistance of fabrics to liquid penetration by water spray impact. The tests enable to predict barrier performance in gown's critical zones and indicate how well the gown will perform when fluids fall or splash onto it. The seams are considered to be the weakest points even though all zones in a gown are considered as critical zone. When analyzing results from this test, higher numbers

indicate lower fluid resistance. The test is crucial since it simulates resistance to pressure spray or splash of fluids in clinical conditions. This type of 'arterial spurting' is often seen when an artery of a blood vessel is inadvertently compromised or damaged during tasks such as blood draw, I.V. changes and injections. Higher numbers from the test results indicate lower fluid resistance.

(b) **Hydrostatic Head Test Results**

These tests measure the resistance of fabrics to liquid penetration by water under constantly increasing hydrostatic pressure. The results enable in prediction of performance properties of the critical areas in the gown and indicate how well the gown will perform when fluid pressure is applied to it. Many procedures involve irrigation fluids, tissue fluids, or other liquids. A gown having high fluid resistance will provide barrier protection against the fluids even under application of pressure. For example, the healthcare worker's arm or torso may lean or rest against contaminated fluids during a procedure. The more stringent tests of this standard, ASTM F1670 and ASTM F1671, involve the use of body fluid and blood-borne pathogen stimulants according to time and pressure protocols that have been found to discriminate a higher level barrier performance in the laboratory setting. The less stringent tests, AATCC 42 and AATCC 127, involve the use of indirect (splash or spray) and direct contact with water according to time and pressure protocols.

(c) **Strength Test**

Personal protective equipments (PPE) come under quite a bit of stress during its actual usage. Product strength is measured by its resistance to tearing, puncturing, and breaking and by its ability to stretch.

(d) **Grab Tensile**

A measurement of a fabric's resistance to tearing under increasing pulling stress without an initial tear in the material. Higher numbers reflect superior performance (ASTM D5034).

(e) **Elmendorf Tear**

A measurement of a fabric's resistance to tearing under controlled force when there is an initial tear in the material (ASTM D1424).

(f) **Mullen Burst**

A measurement of the fabric's resistance to puncture under increasing pressure (ASTM D744).

10.35 Safety

All fabrics used in surgical gowns and drapes may burn. Manufacturers of gowns and drapes incorporate a caution label in the package. The rate of flame travel will vary with the specific material and can be measured using a standard test method.

10.36 Biocompatibility

Medical gowns have to undergo many tests that demonstrate the potential of the material to cause irritation to the skin, and include cytotoxicity (cell culture), primary skin irritation (shows the potential for irritating abraded skin), and dermal sensitization (shows the potential for eliciting allergic contact dermatitis).

10.37 Protection Against Microorganisms

The surgical gowns of the doctors and the nursing staff are open to the penetration of blood and serum of the patient in the surgical room. In practical testing of the surgical gown, it might not be possible all the time to go for testing with the human blood. In that case, synthetic blood- or particle-loaded liquids containing microspheres comparable with the sizes of bacteria can be effectively used for the purpose of testing. In the testing, actually the time necessary for the liquids containing the microspheres to pass from one side to the other side of the fabric is measured. The fabric having the highest penetration time is best for the surgical gowns. Bacteriophage penetration resistance is a test that assesses the effectiveness of materials used in protective clothing for preventing the penetration of a surrogate microbe (ØX174 bacteriophage) suspended in a simulated body fluid under conditions of continuous contact. This is a pass/fail test (ASTM F1671).

10.38 Comfort

While barrier effectiveness is foremost, if PPE is uncomfortable to wear, it is less likely to be used effectively. The discomfort may even interfere with the clinician's ability to do his or her job.

10.39 Air Permeability

It is a measurement of the air flow that can be maintained through a material at a specified pressure, which indicates the fabric's breathability and comfort during use (ASTM D737).

10.40 Stiffness

It is a measurement of the force of a fabric's resistance to flexing (i.e., folding or draping). The higher the force, the stiffer the fabric.

10.41 Moisture Vapor Transmission Rate

The most complicated testing concerns MVTR. The standard method used in the USA is ASTM E96-80. The upright cup, inverted cup, and desiccant methods are the common tests. The humidity range can be 50 or 100 %, and temperature can be 70 or 90 °F. The test figures vary widely depending upon the type of breathable system. Microporous coatings have excellent upright and desiccant cup values, but with the inverted cup, the hydrophilic membrane can produce much higher transmission rates [40]. Manufacturers tend to adopt testing methods that favor their system.

10.42 Storage Conditions

How the product is stored, can affect the polymers and fabrics used in the products, and therefore adversely affect barrier properties. Products should be stored in their original packaging in cool, dry environments and away from UV or fluorescent lights to help ensure the barrier effectiveness stability during storage. Stock should be rotated on a first in, first out basis.

10.43 Developments in Commercial Surgical Gowns

A reputed surgical gown manufacturing company 'Cardinal' has developed few novel kinds of surgical gowns [41, 42]. These are given as follows:

10.44 AstoundTM

AstoundTM surgical gown has a:

1. Tough outer layer designed to resist abrasion and puncture.
2. Middle layer providing exceptional barrier resistance to fluid penetration.
3. Soft bottom layer adding comfort in addition to another layer of protection.

10.45 SmartGownTM

The company claims that fabric reacts to increasing temperature by increasing its water vapor transfer rate. As the temperature rises, the amount of water vapor that escapes from the material also increases. The more water vapor that is allowed to

escape from the body of the fabric, the cooler and more comfortable the wearer will be. This happens due to little widening of the air gaps in the fabric with the rise in the temperature, which thus permits more water vapor to pass through. This gown is also designed with generously sized shoulder and sleeve area, which gives the wearer plenty of room to move and thus keep the air circulating perfectly which improves the comfort level. Another feature is that the main seams on the sleeves are also impervious, as the seam portion is the main cause for fluid transfer through it, on account of having small pores created by the sewing needle. The special proprietary sealing process creates a continuous bond along the length of the seam, eliminating the gaps that can occur with other sealing methods.

10.46 Smart SleeveTM

Cardinal also offers Smart SleeveTM surgical gowns, which combine elements from both Astound and SmartGownTM surgical gowns. The body of the gown is made from the same tri-layer fabric found in the Astound gowns, while the sleeves incorporate the breathable, impervious protection of the SmartGown fabric. Company claims that Smart Sleeve surgical gowns are classified as an AAMI Level 4, the highest rating established by AAMI.

10.47 Ahlstrom's Breathable Viral Barrier

A surgical gown with breathable viral barrier (BVB) has been developed wherein a membrane is sandwiched between inner and outer fabrics comprising of continuous fine filaments [42]. The inner layer provides a soft touch to the wearer's skin while the outer layer provides additional repellency and strength. The monolithic membrane technology has been used. As the inner membrane is a monolithic film (continuous without any holes), it offers good protection. The inner monolithic membrane is also breathable due to unique raw materials used in the construction. The film is breathable as water vapor in molecular state diffuses through the thickness of the film. The inner membrane responds to the rising body temperatures and resulting perspiration by increasing the rate of moisture transfer. It has been claimed that BVB fabric is lightweight, very strong, and low linting owing to the continuous fine filaments used in the reinforcing inner and outer layers. The inner membrane responds to the rising body temperatures and resulting perspiration by increasing the rate of moisture transfer.

10.48 Goretex PTFE Membrane

This consists of the process of mechanically expanding the polytetrafluoroethylene to form a microporous membrane and does not involve any chemical reactions [31]. Only low amounts of the polymer are needed to create this airy, lattice-like

structure, thus making the process highly efficient. It is claimed that use of the membrane offers a number of merits to the fabric. The polymer PTFE is extremely resistant to chemicals and ultraviolet radiation. It does not burn and has thermal stability between 250 and 280 °C and can also be recycled. The membrane is flex resistant even when being subjected to considerable mechanical stress. It is also highly biocompatible, harmonizing well with the body. It can also be safely disposed off with other household waste.

10.49 Best Practices for Selecting Medical Fabrics

A number of standards relating to the best practices for the selection of medical fabrics [43], surgical gowns and drapes, are available and are highlighted below:

(a) The materials used in surgical gowns and drapes should satisfy the requirements of safety and functionality in use by patients and healthcare workers.
(b) The selection of gown and drape products, both single-use and reusable, should be based on criteria specific to the products' function and use.
(c) Materials used for surgical gowns and drapes should be impermeable to blood and other body fluids, particulates, and microorganisms.
(d) Surgical gowns and drapes should have an acceptable quality level and be resistant to tears, punctures, and abrasions.
(e) The surgical gowns and drapes materials should be sterilized and reusable. The barrier properties should be checked after processing repeatedly.
(f) Surgical gowns and drapes should have combustion resistance.
(g) Surgical gowns and drapes should be comfortable and also be able to maintain the required body temperature.
(h) The surgical products should have a desirable cost-to-benefit ratio.

10.50 Organizations Imposing Relevant Standards

The following organizations have set standards for various tests related to surgical gowns

(a) AAMI—Association for the Advancement of Medical Instrumentation PB70: 2003: 'Liquid Barrier Performance and Classification of Apparel and Drapes Intended for Use in Health Care Facilities.'
(b) OSHA—Occupational Safety and Health Administration: 'Personal Protective Equipment' 2004.
(c) ORNAC (Operating Room Nurses Association of Canada): 'Recommended Standards and Guidelines, and Position Statements for Perioperative Registered Nursing Practice' 2003.

(d) CSA (Canadian Standards Association): 'Selection, Use, Maintenance, and Laundering of Reusable Textile Wrappers, Surgical Gowns, and Drapes for Health Care Facilities,' Z314.10-03.
(e) European Union Standard (Series 13795) regarding surgical drapes, gowns, and clean-air suites.
(f) AORN (Association of perioperative Registered Nurses): 'Standards, Recommended Practices, and Guidelines,' 2004.
(g) Centre for Disease Control and Prevention.
(h) FDA (Food and Drug Administration).

10.51 Setbacks of Available Gowns

Though manufacturers of surgical gowns make their claims about their products performance, it has not been proved clearly on the aspects [44]. Hence, the need is felt from both industry and surgical community to develop useful test methods that could be utilized in evaluating a material's barrier effectiveness 'under normal condition of use.' But, the tests, recommended by AAMI, are not in conformation to the stresses encountered during 'normal condition of use.' Hence, there is requirement to create test methods that would simulate the stresses occurring under 'normal condition of use' [45]. The effectiveness of protective clothing has to be done considering two aspects—liquid penetration and viral penetration as per ASTM procedures. Each test is rated on a pass/fail basis, with a 'pass' predicted on the material's ability to resist penetration at a level of two pounds per square inch (psi). A number of reports are available in the clinical literature indicating that the pressure exerted on surgical gowns under both in vivo and in vitro conditions are found to be far in excess of 2 psi [46–48]. Also, it should be noted that standard makes no mention of the level of protection that a 'pass' provides. Also it should be noted that this same AAMI group had several years earlier, stated that neither of the two tests (AATCC 42:2000 and AATCC 127:2000), which it has introduced in new AAMI standard entitled 'Liquid Barrier Performances and Classification of Protective Apparel and Drapes used in Health Care Facilities,' have been suitable for this purpose [49]. Surface tension is measured by a unit of dynes per centimeter. Whereas water used in both of the AATCC test measures around 72 dynes/cm, blood is around 42 dynes/cm (it is viscosity that makes blood thicker than water). Hence, liquids, such as blood, have a low surface tension and can penetrate fabrics more readily than those with a higher surface tension, such as water. Thus, in terms of interpreting the results of the tests for level 1, 2, and 3, they do not mean that under 'usual condition of use' they would protect against penetration of blood.

10.52 Medical Device Regulation Directives

Surgical gowns in a number of countries are not covered under Medical Device Regulation Directives. The European Medical Devices Directive 93/42/EEC

(introduced in 1995) has been in force in some countries such as UK since 1998 via the Medical Device Regulations (SI 2002 No. 618). According to this act, all medical devices placed on the market have to bear the CE mark, demonstrating that they meet the essential requirements of the Medical Devices Regulations. This includes surgical gowns and surgical drapes that are placed on the market as medical devices.

10.53 Future Outlook

From the aforesaid discussions, it is visualized that there are innumerable setbacks with regard to barrier effectiveness as well as comfort aspects [50]. But, future course of action for research would be to decide the type of research that is necessary and also the direction needed to evolve suitable standards and technology as well, which can satisfy the needs of the surgical community with regard to comfort and safety. The highlights of the discussions are given as under:

(a) There is need to refine the standards further through experimentation and collection of data under 'normal condition of use.'
(b) The factors relating to comfort, such as like breathability condition parameters, have to be determined objectively, i.e., extent of moisture vapor transmission and heat loss necessary and their conditions to specify minimum comfortable criteria.
(c) Classification based on protection once again is to be redefined based on various viruses' transmission control, going detail into pore sizes as well as under 'usual condition of use.'
(d) Research in fabric engineering design is required to attain different level of porosity and penetration force should be determined.
(e) It is necessary to optimize coating techniques, constituents, and application considering the various constructional and material constraints.

References

1. Nurmi S, Lintukorpi A, Saamanen A, Luoma T, Soinnen M, Suikkanen V-P (2003) Human, protective cloths and surgical drapes as a source of particles in an operating theatre. Autex Res J 3:394–399
2. European Standard EN 13795-1, Nov 2002
3. www.surgicenteronline.com/articles/4a1feat5.html
4. www.findarticles.com/p/articles/mi_m0MKX/is_6_73/ai_n8579069
5. www.emergencyfiltration.com/Technology/Microorganisms.htm
6. Slater K (1977) Comfort properties of textile. Text Prog 9(4):1–71
7. Ruckman JE (1997) Water vapor transfer in waterproof breathable fabrics part-1. Int J Clothing Sci Technol 9(1):10–22
8. Rees WH (1970) Comfort and the water vapor permeability of textiles. WIRA report 80
9. Rees WH (1971) Physical factors determining the comfort performance of textiles. In: 3rd seminar: textiles in comfort, Shirley Institute, Manchester

10. Dent RW (2001) Transient comfort phenomena due to sweating. Text Res J 71(9):796–806
11. Kannekens A (1994) Breathable coatings and laminates. J Coated Fabr 24:51–59
12. http://facta.junis.ni.ac.yu/facta/walep/walep99/walep99-14.pdf
13. Congalton D (1999) Heat and moisture transport through textile and clothing ensembles utilizing the 'Hohenstein' skin model. J Coated Fabr 28:183–196
14. Cheng KPS, Cheung YK (1994) Comfort in clothing. Text Asia 24:48–52
15. www.deerfieldurethane.com/breathablespaper9-5-02.pdf
16. Tanner JC (1979) Breathability, comfort and gore-tex laminates. J Coated Fabr 8:313–322
17. Gibson PW (1999) Water vapor transport and gas flow properties of textiles, polymer membranes, and fabric laminates. J Coated Fabr 28:300–327
18. www.molnlycke.net/…/Surgical/publications/MolnlyckeHealthCare/Moving_forward_from_ traditional_textiles.pdf
19. www.kca.com.au/healthcare/news/news01.htm
20. www.infectioncontroltoday.com/articles/231feat2.html
21. www.tx.ncsu.edu/jtatm/volume2issue2/vo2_issue2_abstracts.htm
22. Stanley L (1994) OSHA ruling still causing shifts in surgical gown marketplace. Health Ind J 115:16–18
23. Lickfield D (2001) Nonwovens in medical textiles. Int Fibre J 2:42–48
24. Abreu MJ, Cabeco Silva ME, Schacher L, Adolphe D (2003) Analysis of the surgical properties before and after irradiation: selection of the pertinent properties. Autex Res J 3:400–405
25. Aibibu D, Lehmann B, Offermann P (2003) Barrier effect of woven fabrics used for surgical gowns. In: 3rd Autex conference, Poland, pp 406–413
26. Association for the Advancement of Medical Instrumentation (2003) Liquid barrier performances and classification of protective apparel and drapes intended for use in health care facilities. ANSI/AAMI PB 70:2003. AAMI, Arlington
27. www.kchealthcare.com/docs/H7434_AAMI_Covergown.pdf
28. American Society for Testing and Materials (1992) Annual book of ASTM standards. American Society for Testing and Materials, Philadelphia
29. American Association of Textile Chemists and Colorists (1994) AATCC technical manual. AATCC, Research Triangle Park, NC
30. www.blauer.com/files/blauer/2004_Brochure223.pdf
31. www.gore-tex.co.uk/published/gfe_link/1021833151684.pdf
32. www3.interscience.wiley.com/cgi-bin/abstract/88012393/ABSTRACT
33. Kramar L (1998) Recent and future trends for high performance fabrics providing breathability and waterproofness. J Coated Fabr 28:106–115
34. Painter CJ (1996) Waterproof, breathable fabric laminates: a perspective from film to market place. J Coated Fabr 26:107–130
35. Lomax GR (1985) The design of waterproof, water vapor-permeable fabrics. J Coated Fabr 15:40–66
36. Roey MV (1991) Water-resistant breathable fabrics. J Coated Fabr 21:20–32
37. Samms J (2002) High moisture vapor transmission of thermoplastic polyurethane. Noveon Inc. Bull 11
38. Ding X, Hu J (2003) Temperature-sensitive polyurethane properties. Text Asia 33:42–45
39. www.infectioncontroltoday.com/articles/061room.html
40. Krishanan S (1992) Technology of breathable coatings. J Coated Fabr 22:71–79
41. www.cardinal.com
42. www.bbriefings.com/pdf/950/ahlstrom.pdf
43. www.surgicenteronline.com/articles/371feat3.html
44. Belkin NL (2005) 'False faith in the surgeon's gown' revisited. Bull Am Coll Surg 90:19–23
45. Bernard HR, Beck WC (1975) Operating room barriers: idealism, practicality and the future. Bull Am Coll Surg 60(9):16
46. Altman KW, McElhaney JH, Moylan JA, Fitzpatrick KT (1991) Transmural surgical gown pressure measurements in the operating theatre. Am J Infect Control 19:147–155

47. Smith JW, Tate WA, Yazdani S (1993) Determination of surgeon generated gown pressures during various surgical procedures in the operating room. Am J Infect Control 23(4):237–246
48. Telford GL, Quebbeman EJ (1993) Assessing the risk of blood exposure in the operating room. Am J Infect Control 21:351–356
49. Association for the Advancement of Medical Instrumentation (1994) Technical information report, selection of surgical gowns and drapes in health care facilities. AAMI TIR 11. AAMI, Arlington
50. Behera BK, Arora H (2009) Surgical gowns—an overview. J Ind Text 38(3):205

Chapter 11
Phosphorylated Cotton Chronic Wound Dressing

11.1 Introduction

In the treatment of acute as well as chronic wounds, woven and nonwoven gauze has been used over a long period of time [1]. Cotton and cellulose-based wound dressings are commonly being used in hospitals and nursing homes for wound care. Recently, modifications in fibers, yarns, and nonwovens have enhanced its quality and versatility in medical applications [2–5]. Chronic wounds pose a major problem worldwide [6]. For the 5 million Americans suffering from chronic open wounds, it is estimated that $5–7 billion per year is spent, and this is increasing at an annual rate of 10 % [7]. Chronic wounds are caused due to incomplete healing that happens when a wound gets arrested in the inflammatory stage of healing [8]. During the inflammatory stage of wound healing, an excess supply of neutrophils occurs [9]. As neutrophils possess an armament of biochemical weaponry that is used against bacteria, the release of destructive proteases from excess neutrophils becomes a threat to healing when a high concentration occupies the wound environment [10]. In this regard, the protease human neutrophil elastase found in high concentration in the chronic wound creates considerable protein destruction and prevents the wound from healing [11]. The design of wound dressings that selectively sequester proteases from the chronic wound has been based on the concept that molecular features of the protease including protein size, charge, and active site mechanism may be used to tailor the molecular design of the dressing material used to capture it [5, 11–15]. Initial studies have revealed how elastase substrate peptides could be tethered to cotton cellulose and used effectively to capture the protease in solution [13]. Commercial development of a mechanism-based wound dressing [16] that would offer an economic, highly effective product prompted that the product be based on a mode of action related to the ionic binding of cationic serine proteases and matrix metalloproteases to the dressing. Hence, a technique has been adopted

N. Gokarneshan et al., *Emerging Research Trends in Medical Textiles*,
Textile Science and Clothing Technology, DOI 10.1007/978-981-287-508-2_11

using phosphorylated cellulose, which involves a set of finishing chemistries for cotton modification that would be in tune with the prevailing concept of cotton textile processing.

11.2 Results of Findings

In commercializing phosphorylated cotton gauze, as a chronic wound dressing, the problems relating to the product and process with regard to the appearance, quality, and efficacy of the dressing need to be addressed [17]. The wound dressing development has been intended to maintain efficacy of protease sequestrant of the chronic wound dressing, and at the same time retaining desirable properties such as fabric whiteness, and uniform finishing treatment of the woven fabric. Protease sequestrant efficacy is defined as the ability of the modified dressing to lower human neutrophil elastase activity in the wound relative to untreated cotton dressing. Thus, the sequestrant efficacy of the dressing is a result of the dressing capturing proteases and removing them from the wound environment. Problems encountered in transferring the process finishing chemistry for the dressing modification from a stationary finishing process to a continuous process included the influence of fabric curing, sterilization, and water quality on the dressing's whiteness index and protease sequestrant efficacy. The continuous finishing process is shown in Fig. 11.1.

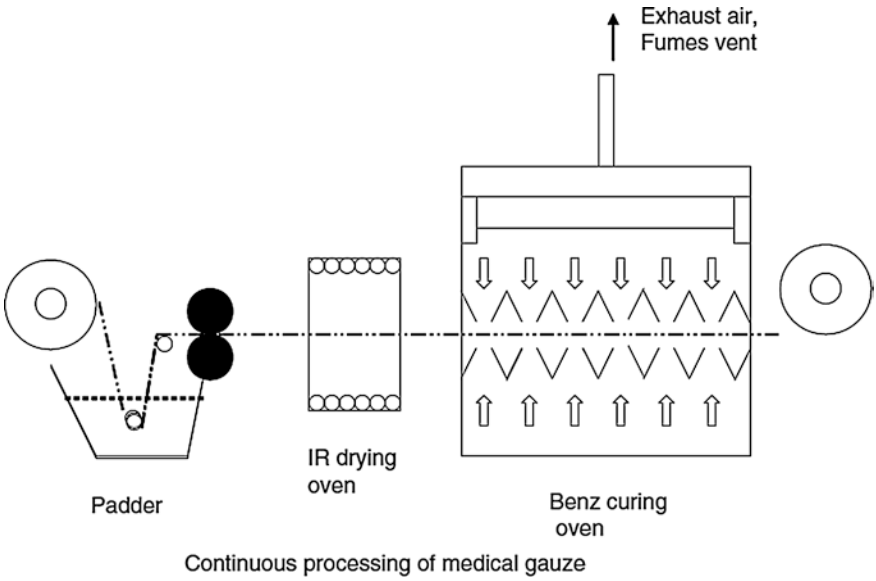

Fig. 11.1 Continuous finishing process [17]

In order to evolve suitable oven conditions for a continuous finishing process, dynamic oven conditions have been evaluated using a Benz oven. Dwell times in the Benz oven within a 160–170 °C temperature range were 6–7 min (Fig. 11.2).

The chemistry adopted in the phosphorylation finishing has been related to the high-temperature reaction of one of two reagents (SMP or DAP) in a formulation using urea (typically applied as 30 % of the total formulation). The biphasic reaction between the cellulose and the phosphorylating reagent is stimulated by urea (Fig. 11.3), and the release of ammonia from urea decomposition during the reaction required engineering the exhaustion of ammonia from the curing oven (see conditions stated in Fig. 11.2 inset).

Earlier research has reported on the influence of the two different finishes on the protease sequestrant efficacy of the phosphorylated cotton wound dressing [16]. The typical temperature range for evaluating the curing conditions with SMP was 160–175 °C. Sodium hexametaphosphate, which is a polymeric phosphate salt, can be cured on cotton in the presence of urea at a high temperature (160–170 °C) without yellowing of the fabric when compared to DAP (Fig. 11.4b, e). On the other hand, the DAP: urea finishing and curing gave higher add-ons (Fig. 11.4c, f), but even curing at lower temperature with these formulations gave rise to some slight discoloration of the cotton fiber as seen by the lower whiteness index in Fig. 11.4e. Evaluation of the phosphorylated cotton gauze's protease-lowering efficacy, when cured under stationary oven conditions, revealed that DAP: urea at a percent ratio by weight of 30:10 (urea:PO4) exhibited higher

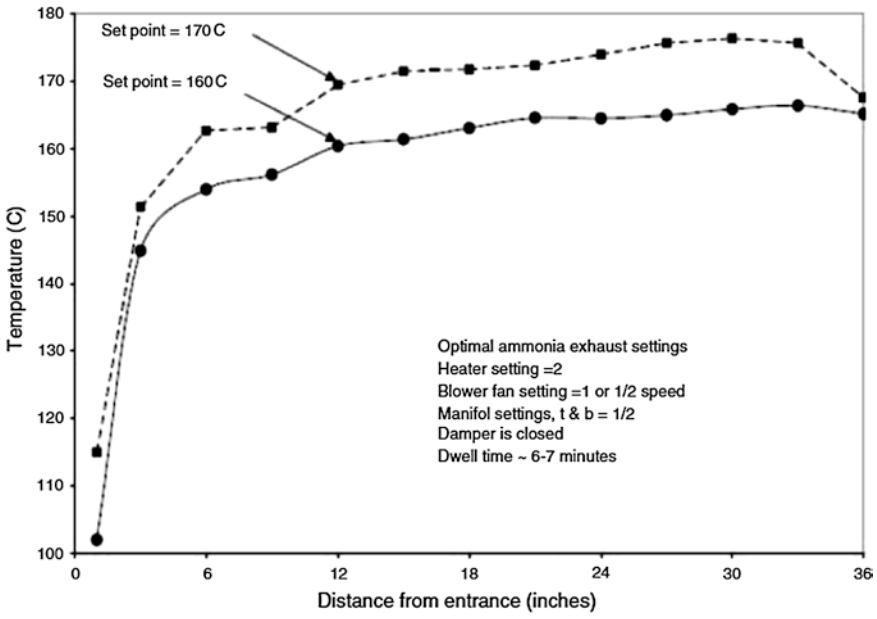

Fig. 11.2 Temperature profile of oven used for continuous process finishing [17]

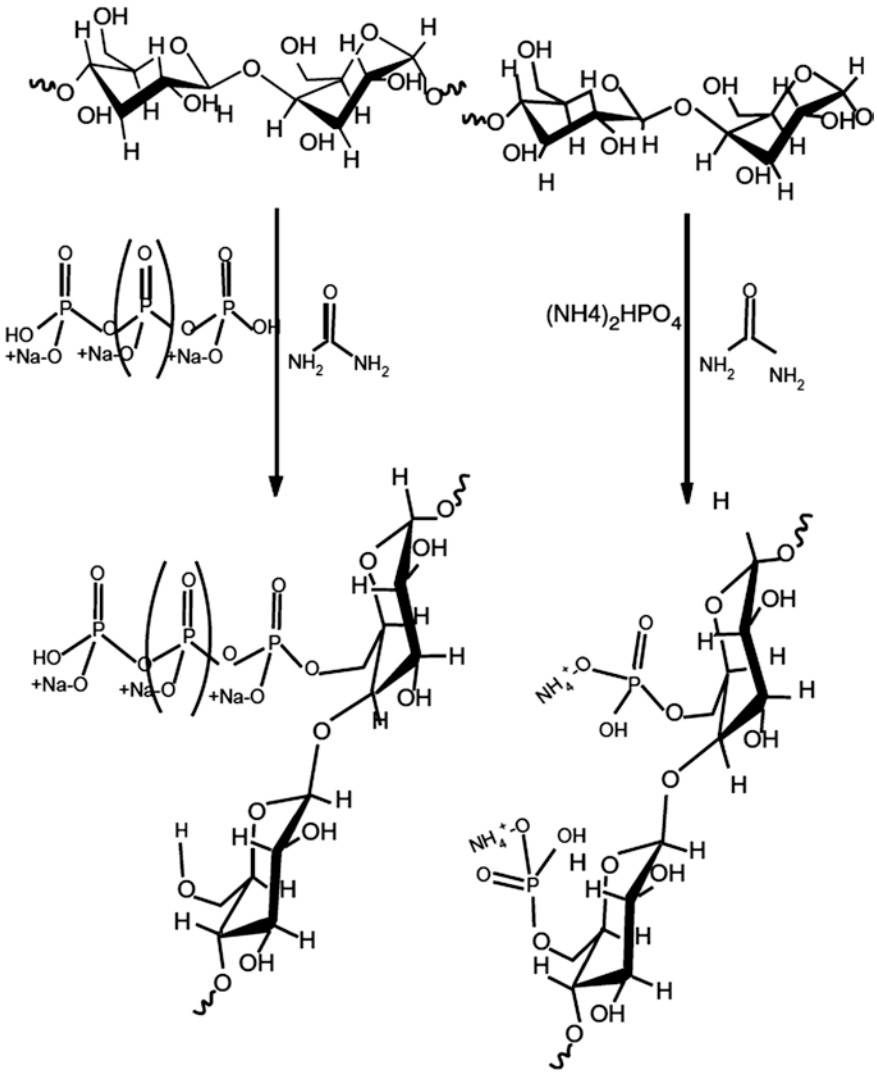

Fig. 11.3 Phosphorylation reaction of cellulose with SMP and DAP in presence of urea [17]

protease-lowering activity when compared to SMP as the phosphorylating reagent (Fig. 11.4a, d). The finding related to higher add-ons correlating with better protease sequestrant efficacy is consistent with earlier research, where the increase in cellulose phosphorylation has been correlated with an increase in protease sequestrant efficacy [16].

A number of formulations containing a combination of DAP and SMP have been cured on the cotton gauze, so as to enhance whiteness and retain efficacy.

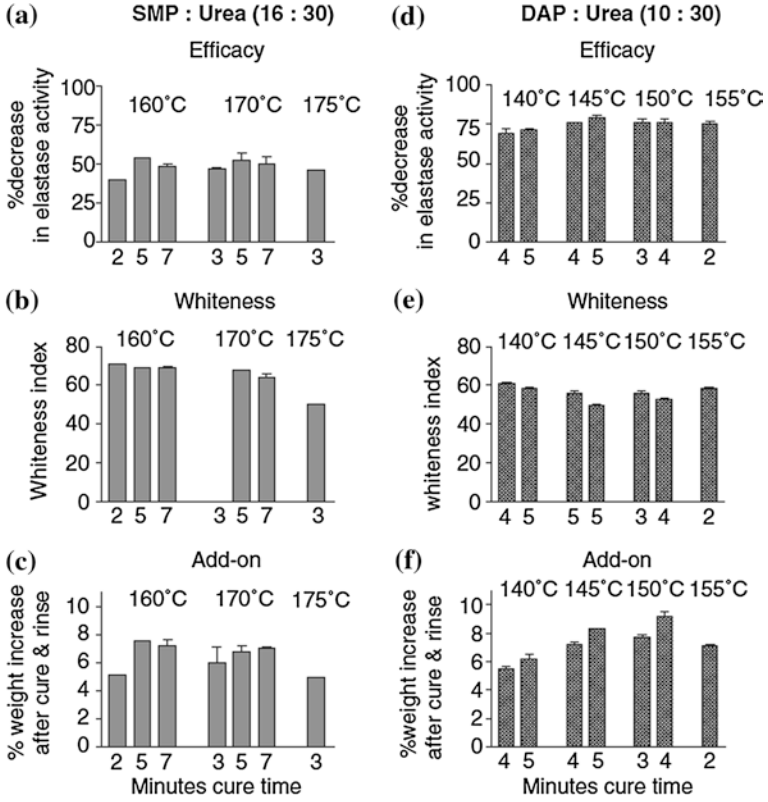

Fig. 11.4 Influence of phosphorylating formulations versus curing conditions (temperature and time) on efficacy (% elastase activity decrease compared to untreated control), whiteness, and add-on. *Solid bars* (**a**, **b**, **c**)—treated with SMP: urea (16:30); *crosshatched bars* (**d**, **e**, **f**)—treated with DAP: urea (10:30) [17]

Figure 11.5 depicts the influence of the combined formulation of DAP and SMP on efficacy and whiteness. The incorporation of SMP improved whiteness (Fig. 11.5b) but the higher protease sequestrant efficacy observed with DAP formulations was not retained with the inclusion of SMP (Fig. 11.5a).

The effective commercialization of the cotton wound dressing has been partially dependent on a reproducible cotton fabric product of acceptable whiteness. A number of phosphorylated cotton wound dressings, which had been treated under stationary finishing and curing conditions with either the SMP or DAP treatments, have been visually examined for whiteness based on standards of whiteness for cotton wound dressing products. The manufacturer's visual assessment of the dressing's whiteness was employed to determine a minimum acceptable whiteness index of 60 Fig. 11.4b, e which contrasts the fabric whiteness for both curing treatments. The SMP treatment gave a better whiteness index than the DAP treatment.

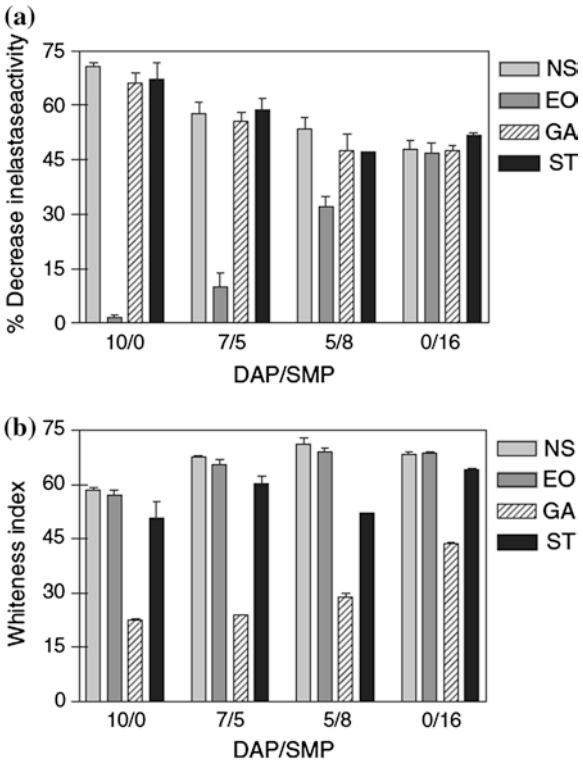

Fig. 11.5 Influence of the three types of sterilization on **a** efficacy (% elastase activity decrease compared to untreated control) and **b** whiteness of cotton gauze treated with urea and various combinations of DAP and SMP [17]. *NS* nonsterile; *EO* ethylene oxide; *GA* gamma irradiation; *ST* steam

But, the DAP treatments have been found to be acceptable to marginally acceptable for most of the samples tested, and they were generally more effective as a protease sequestrant (Fig. 11.4a, d). Figure 11.5 shows the influence of three kinds of sterilization on efficacy and whiteness. The type of sterilization utilized was found to play a major role toward choosing the appropriate process development of the phosphorylated cotton dressing. The phosphorylated cotton wound dressing samples have been evaluated for the influence of ethylene oxide sterilization conditions. The relationship of cotton dressing activity before and after sterilization is shown in Fig. 11.5a. In the case of the DAP-treated cotton, the ethylene oxide sterilization deleted virtually all of the observable protease sequestrant activity. The influence of ethylene oxide treatment on wound dressing activity could possibly happen through modification of the phosphorylated cotton with ethylene oxide. The modification mechanism of phosphate hydroxyl has not been clearly understood. But, the loss of dressing activity observed when ethylene oxide is used to sterilize DAP-treated cotton could possibly be due to one of the putative reactions (Fig. 11.6). Formation of the phosphate ester or enol removes the anionic charge from phosphorylated cellulose and thus the ability of the dressing to bind the cationic serine proteases and remove them from the wound environment. The reaction of phosphorylated cotton with ethylene oxide occurs with DAP and

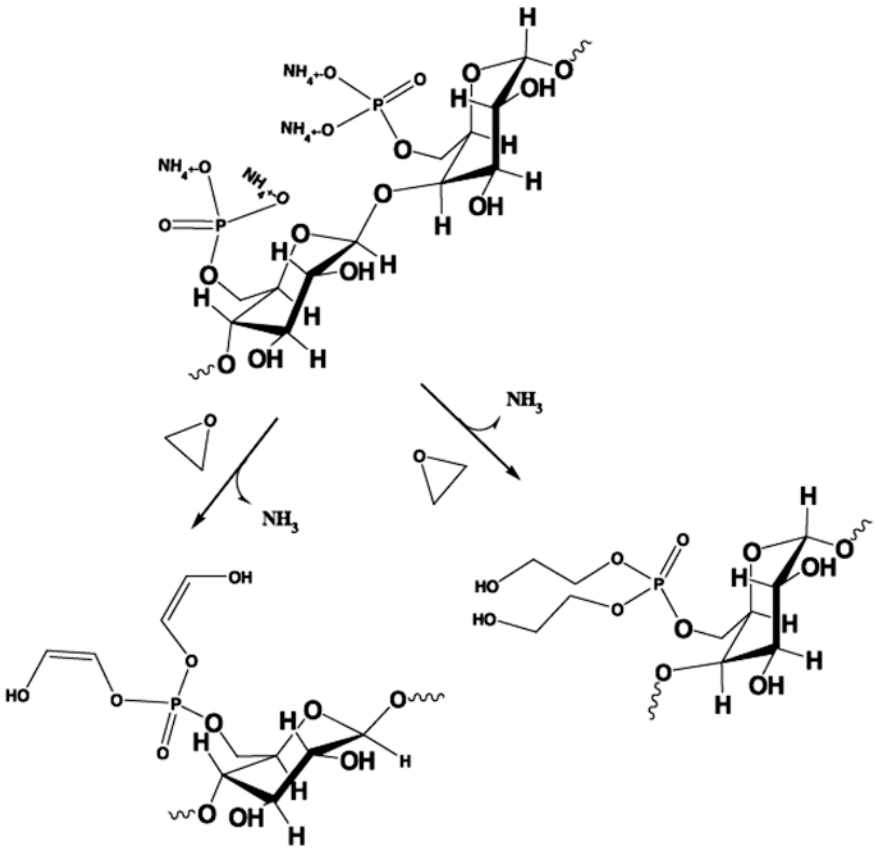

Fig. 11.6 Two independent reactions of ethylene oxide with phosphorylated cellulose [17]

not SMP-cured cotton. Hence, the free ammonia liberated can contribute partially to the driving force of the reaction owing to the ammonium counter ions on the phosphorylated cellulose. A comparison of FTIR spectra (Fig. 11.7) of ethylene oxide-sterilized and steam-sterilized dressings revealed two areas of the spectra that showed differences and serve as a corollary to the observed loss of protease sequestrant dressing activity. On comparing with untreated cotton, the spectrum of steam-sterilized phosphorylated cotton demonstrates a broad and significantly increased band of absorption centered at 1000 cm^{-1}. This increase in absorption can be ascribed to the P (O)–OH (single hydroxyl), which gives a strong stretching frequency signal centered near 1000 cm^{-1} [18]. Conversely, the spectrum of ethylene oxide-sterilized cotton exhibits a visible decrease in the intensity of this IR band centered at 1000 cm^{-1}. Of interest as well is the increased absorption and distinguishing bands that can be seen at 30–665 cm^{-1} and correlates to a close double bond (Fig. 11.6). The IR bands observed in this region of the spectrum suggest a phosphoenol ethylene analog of cellulose may account for masking of the

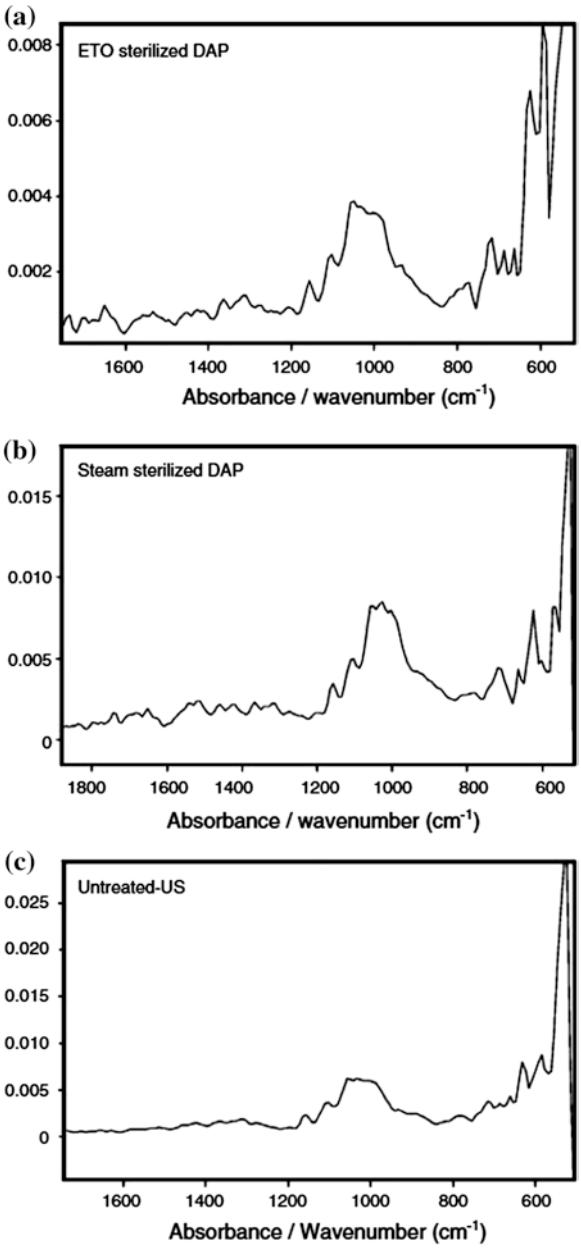

Fig. 11.7 FTIR spectra of sterilized phosphorylated cotton [17]. **a** IR spectrum of steam-sterilized dressing treated with urea:DAP (30:10), **b** IR spectrum of ethylene oxide-sterilized dressing treated with urea:DAP (30:10), **c** IR spectrum of untreated sterilized dressing

hydroxyls, as shown in Fig. 11.6. Bands belonging to the stretching frequencies of the cellulose structure itself obscure areas of the spectrum that might be directly correlated with a phosphate ester. Also, the dressings have been exposed to gamma irradiation and steam sterilization. Gamma irradiation was found to produce significant yellowing (Fig. 11.5b) of the phosphorylated cotton dressing even though protease sequestrant activity was essentially retained (Fig. 11.5a). Besides, steam sterilization proved effective comparatively (Fig. 11.5a) with only a small reduction in whiteness (Fig. 11.5b) when contrasted with similar nonsterile treatments. But it has been so decided not to employ steam sterilization treatment. Thus, process formulations that favored ethylene oxide sterilization have been selected. It has also been observed during the process of developing the phosphorylated cotton gauze that rinsing with city water reduces the elastase sequestrant efficacy of treated fabrics.

This effect was found to be variable and though it did not occur all of the time, when it did occur the desired activity could be restored with ammonium chloride. Earlier, it has been proved that the flame retardancy of phosphorylated cotton has been deactivated by calcium and can obstruct the efficacy of the FR finish after laundering [19]. Municipal water often contains calcium carbonate at levels of 100 ppm and is most likely the source of the inactivation of phosphorylated cotton. Interestingly, some cities use SMP to precipitate calcium from municipal water during purification treatments. The deionized water and municipal water rinses have been compared for their influence on protease sequestrant efficacy. Using available municipal water (having conductivity of 234) in the post-curing rinses has lead to reduced protease sequestrant efficacy as compared to use of deionized water. It was also found that three separate deionized water rinses are required to reduce the conductivity of the water within a range that was commensurate with optimal efficacy. The ratio of the formulation selected for pilot development of the cotton chronic wound dressing has been SMP:urea (16:30).

As diagramed in Fig. 11.1, the dressing was pad-dry-cured in a continuous process by applying this formulation to cotton gauze. The resulting effect of curing temperature on protease sequestrant capacity and whiteness is shown in Fig. 11.8. The temperature range and oven dwell-time were assessed as a function of the rate of curing in the continuous process. In this regard, it was found that a slower processing time of curing coupled with lower temperatures and thus longer oven dwell times promoted better protease sequestrant efficacy in the cotton gauze (Fig. 11.8). However, although there is a slight improvement in protease sequestrant activity with increased time at lower temperatures, the effect of curing conditions within the curing time and temperature range assessed was essentially equal. In the same way, industrial processing of the cotton gauze lead to a very similar profile, where the dressing has been observed to decrease protease activity by 40 % as compared to untreated controls (Fig. 11.9).

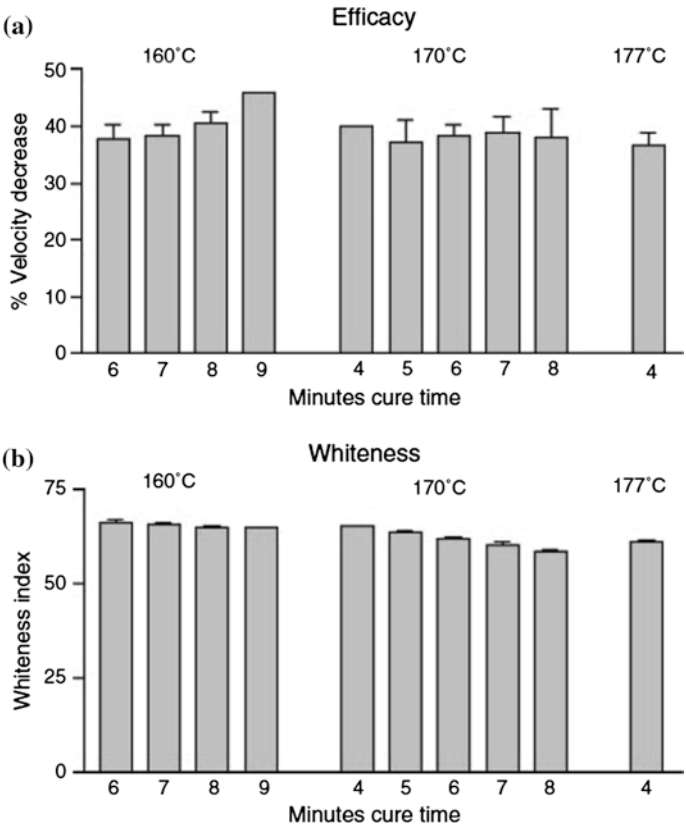

Fig. 11.8 Influence of curing time and temperature on **a** protease sequestration efficiency, **b** fabric whiteness of gauzes padded with 30 % urea:16 % SMP [17]

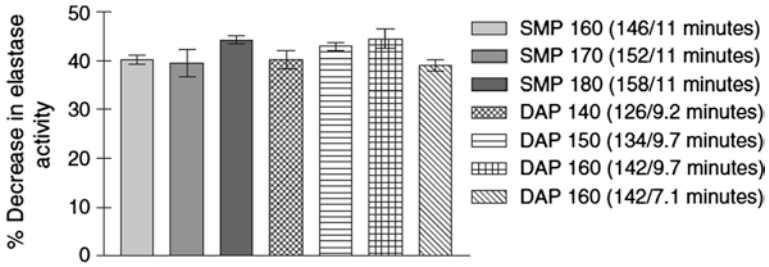

Fig. 11.9 Comparative protease sequestration efficiencies of two formulations applied on commercial pad-dry-cured equipment [17]

References

1. Elliot IMZ (1964) A short history of surgical dressings. Pharmaceutical Press, London
2. Goldthwait CF, Kettering JH, Moore M (1945) Semi elastic cotton gauze bandage fabric. Surgery 18(4):507–510
3. Parikh DV, Patience D (1998) Recommended standards for a new USP monograph on surgical spunlaced nonwoven fabrics. Pharm Forum 24(4):6627–6630
4. Edwards JV, Yager D, Bopp A, Diegelmann RF, Goheen S, Cohen IK (2001) Design, preparation, and activity of cotton gauze for use in chronic wound research, bioactive polymers. ACS Symp Ser 792:76–89
5. Edwards JV (2005) Future structure and properties of mechanism-based wound dressings. In: Edwards JV, Buschle-Diller G, Goheen SC (eds) Modified fibers with medical and specialty applications. Springer, The Netherlands, pp 11–33
6. National Pressure Ulcer Advisory Panel (2001) Pressure ulcers in America: prevalence, incidence, and implications for the future. An executive summary of the national pressure ulcer advisory panel monograph. Adv Skin Wound Care 14:208–215
7. Allman RM, Goode PS, Burst N, Bartolucci AA, Thomas DR (1999) Pressure ulcers, hospital complications, and disease severity: impact on hospital costs and length of stay. Adv Wound Care 12:22–30
8. Clark RAF (1996) Wound repair: overview and general considerations. In: Richard AFC (ed) The molecular and cellular biology of wound repair. Plenum Press, New York, pp 3–35
9. Diegelmann RF (2003) Excessive neutrophils characterize chronic pressure ulcers. Wound Rep Reg 11(6):490–495
10. Yager DR, Nwomeh BC (1999) The proteolytic environment of chronic wounds. Wound Rep Reg 7(6):433–441
11. Yager DR, Chen SM, Ward SI, Olutoye OO, Diegelmann RF, Cohen IK (1997) Ability of chronic wound fluids to degrade peptide growth factors is associated with increased levels of elastase activity and diminished levels of proteinase inhibitors. Wound Rep Reg 5:23–32
12. Edwards JV, Yager DR, Cohen IK, Diegelmann RF, Montante S, Bertoniere N, Bopp AF (2001) Modified cotton gauze dressings that selectively absorb neutrophil elastase activity in solution. Wound Rep Reg 9:50–58
13. Edwards JV, Batiste SL, Gibbins EM, Goheen SC (1999) Synthesis and activity of NH2- and COOH-terminal elastase recognition sequences on cotton. J Pept Res 54:536–543
14. Edwards JV, Eggleston G, Yager DR, Cohen IK, Diegelmann RF, Bop AF (2002) Preparation and assessment of citrate-linked monosaccharide cellulose conjugates with elastase-lowering activity design. Carbohydr Polym 50(3):305–314
15. Vachon DJ, Yager DR (2006) Novel sulfonated hydrogel composite with the ability to inhibit proteases and bacterial growth. J Biomed Mater Res 76A:35–43
16. Edwards JV, Howley PS (2007) Human neutrophil elastase and collagenase sequestration with phosphorylated cotton wound dressings. J Biomed Mater Res A 83A(2):446–454
17. Vincent EJ, Phyllis H, ValeriyY Allan L, Brian C (2009) Development of a continuous finishing chemistry process for manufacture of a phosphorylated cotton chronic wound dressing. J Ind Text 39(1):27–43
18. Silverstein RM, Bassler GC, Morrill TC (1991) Spectrometric identification of organic compounds, 5th edn. Wiley, New York, p 162
19. Reid JD, Mazzeno LW (1949) Preparation and properties of cellulose phosphates. Indus Eng Chem 41:2828–2831

Chapter 12
Treated Cotton Fabric for Moist Wound-Healing Dressings

12.1 Introduction

The pioneering research works done earlier provide the base for the introduction of moist wound healing concept [1, 2]. Moist wound healing enables to maintain the exposed wound tissue at optimum hydration [3]. This implies that wound tissues should be kept physiologically moist, but neither wet nor dry. The moist wound-healing dressings (also known as exclusive, semi-occlusive, advanced, or modern dressings) can be categorized into three kinds:

(a) Absorbent dressings that is very capable of absorbing and retaining fluids. Foams and calcium alginate dressings belong to this class and are suitable for wounds that produce excessive exudates. They help to prevent maceration of tissues and soiling of patient clothes and linen.
(b) Moist-maintaining dressings that can maintain the level of natural moisture of the newly forming tissues without active absorption. Hydrocolloid dressings and transparent film dressings belong to this class and are suitable for wounds that begin to granulate or fill in with new connective tissues, and their exudate levels decrease. The use of absorbent dressing could dehydrate the wound tissue during this phase of healing.
(c) Moisture-donating dressings that are used for wounds at the last stage of healing. They are covered by dry, dead tissues, which get dehydrated. The dead tissues have to be removed so as to permit optimal healing of wound. When the quantity of dead tissues is negligible, or the patient is unsuitable for surgical debridement, autolytic debridement is resorted to. Autolytic debridement is the digestion of dead tissues by the endogenous phagocytes and enzymes. This digestion is facilitated in moist wound environment. Examples are amorphous hydrogels and sheet or wafer hydrogels. Carboxymethylated (CM) cotton has been used as a cheaper option for alginate fibers in the production of absorbent wound dressings [4]. These dressings absorb exudates

N. Gokarneshan et al., *Emerging Research Trends in Medical Textiles*,
Textile Science and Clothing Technology, DOI 10.1007/978-981-287-508-2_12

from chronic wounds and retain a moist environment that simulates platelet activation and blood coagulation [5]. The coagulation of blood takes place due to the release of Ca ions in the wound area that occurs due to ion exchange process. The major demerit of these dressings is their inability to resist to bacterial infection. Actually, a dressing saturated with wound discharge is a favorable medium for the growth of pathogenic bacteria [6]. This can result in increasing the bioburden of the wound (the levels of bacteria and bacterial products). Investigation relating to the biochemical imbalances generally occurring in chronic, nonhealing wounds [3, 7, 8] revealed that the bioburden of wound is one of the biochemical aspects that results in stalling or nonhealing conditions. This chapter highlights the research study done to overcome this problem. This is achieved by treatment with tetracycline hydrate (TCH) or gentamicin sulfate (GS). CM cotton gauze fabrics of different contents of carboxyl groups in the form of various degrees of neutralization by Ca/Na cations are treated with different concentrations of TCH or GS. These fabrics are characterized by measuring their antibiotic content, swelling, and shrinkage. The in vitro release (of antibiotics) in phosphate-buffered saline (PBS) solution as well as antibacterial activities toward Pseudomonas aeruginosa (G−ve) and Staphylococcus aureus (G+ve) has been determined.

12.2 Findings of the Study

Carboxymethylation and Formation of Ca/Na carboxylate

Three levels of carboxyl contents have been achieved on cotton gauze fabric by changing the concentration of both of 'NaOH/monochloroacetic acid (MCA)' in the exhaustion bath as indicated in Table 12.1.

The increase of the concentration in the range investigated is coupled with increase in the carboxyl content. A carboxyl content of 72 meq/100 g exhibits no gelling in PBS in contrast to those of carboxyl contents of 170 and 220 meq/100 g. Accordingly, carboxyl groups of the first sample have been left in their Na salt, while the other two gelling samples have been made in Ca/Na forms under various degrees of neutralization, viz. 10/90, 20/80, and 30/70. Na form (sodium carboxylate) helps to absorb exudates at the initial phase of contact with the wound, and

Table 12.1 Effect of NAOH/MCA concentration on the carboxyl content of cotton gauze fabric and its swelling and gelling in PBS [9]

Conc. of NAOH/(MCA) Mol/lit/Mol/lit in the exhaustion bath	Carboxyl content of fabric	Swelling	Gelling of sodium form in PBS at 37 °C
(2.5)/(1.7)	72	430	No
(5.25)/(2.45)	170	900	Yes
(7.5)/(3.5)	220	945	Yes

Ca form restricts the absorption, so that the wound does not get desiccated and maintain moisture [9]. By the time [4], Ca is replaced by sodium according to the following equilibrium:

$$4(\text{Cell\_COO})2\text{Ca} + 2\text{Na}^{+}(\text{in wound fluids}) \leftrightarrow 2\text{Cell} - \text{COONa}^{+}\text{Ca}^{++} \quad (12.1)$$

The Ca cations precipitate by coagulating blood, and thus, the equilibrium of reaction 1 is shifted to the right-hand side, i.e., toward the formation of more sodium carboxylate. The latter is required to absorb the freshly produced exudates, which enables to maintain the moist environment at optimal level (neither dry nor wet). Gelling is required for the area of dressing in contact with the wound so as to reduce friction, or to eliminate it, so that the newly formed tissues are not aggravated by or adhered to the dressing [4]. The design of the dressing is to make it a multilayer. The layer in contact with skin should possess a high absorption capacity of exudates (high swelling) and good gelling behavior (without dissolution in the wound medium), and loaded with an antibiotic to resist local and invaded infections. The outer layer should also exhibit reasonable swelling so as to absorb any leakage of exudates, avoiding the need to manifest gelling, and loaded also with an antibiotic. Thus, the selection of CM cotton gauze fabric with carboxyl contents of 72, 170, and 220 meq/100 g. All manifest swelling (with varying extents), the first shows no gelling, and the rest are of gelling behavior.

12.3 TCH and G Contents of CM Cotton Fabrics

TCH or gentamicin content of various CM cotton fabrics with various degrees of neutralization (Ca salt) as a function of antibiotic concentration in the padding bath has been obtained. The antibiotic retention ability of the fabric increases with increasing concentration, independent of the carboxyl content, and the degree of neutralization [9]. The incorporation of antibiotics studied onto the fabric domain can be represented by equilibrium reactions 2 and 3. In reaction 2, TCH is exchanged between its complexes with PVP (a) and sodium carboxmethyl cotton (b) to yield cationically bound TCH carboxymethyl cotton (c). In reaction 3, G is cationically bound to CM cotton (V) as a result of exchange between its sulfate form (d) and cellulose sodium carboxylate.

$$\underset{a}{\text{PVP.TCH}} + \underset{b}{\text{Cell\_COONa}} + \text{H}_2\text{O} \leftrightarrow \underset{c}{\text{Cell.COOH}}\,.\text{TCH} + \text{PVP} + \text{NaOH}. \quad (12.2)$$

$$\underset{d}{\text{G.H}_2\text{SO}_4} + \text{Cell} - \text{COONa} \leftrightarrow \underset{e}{\text{Cell.COO}}\,\text{H.G} + \text{NaHSO}_4. \quad (12.3)$$

The increase in the carboxyl content causes increase in the ability of the fabric to hold TCH or G as a result of increasing the active sites of ionic binding (as shown by reactions 2 and 3). Also, for the same carboxyl content, TCH or G content reduces by increasing the degree of neutralization with Ca cations. This can

be interpreted in terms of both decreasing the extent of ionization of cellulose carboxyls (as a result of decreasing their Na form) and increasing the extent of cross-linking of the fabric structure by the divalent Ca cations that hinder the diffusion of TCH inside its structure. The data obtained reveal that, at the same set of conditions, the ability of the fabric to hold G is higher than that of TCH, which reflects differences between them regarding to solubility, functionality, chemical reactivity, size, molecular weight, and ability to form aggregates.

12.4 Swelling and Gelling

The effect of treating with various concentrations of TCH or GS on the swelling (or water uptake) and gelling of CM cotton fabrics of different carboxyl and Ca contents has been studied. The investigation has been done at physiological pH (7.4) in PBS at 37° ± 1 °C. The antibiotic content of the fabrics has been analyzed. The study shows that for the same set of conditions, the following inferences can be made.

(a) The untreated fabrics show slightly greater swelling than that of treated, and the degree of swelling reduces slightly by increasing the antibiotic concentration (and thus its content on the fabric),
(b) The greater the carboxyl content (Na salt), more is the fabric swelling, and
(c) The more the Ca content, lesser is the fabric swelling.

The latter can be related to the fabric cross-linking by Ca as well as reducing the carboxyl content. But, in any case, antibiotic-treated fabrics exhibit a wide margin of swelling ranging between 415 and 930 % (in case o TCH) and between 418 and 934 (in case of G), leading to varieties of choice in designing wound dressings based on them. It is also clear that all samples, except those having a carboxyl content of 72 meq/100, manifest gelling characteristic [9]. Thus, CM cotton fabrics having carboxyl contents of 170 and 220 meq/100 and treated with either of the antibiotics still have the ability to swell and gel, which is a prerequisite for those layers in contact with the skin in moist wound-healing dressings.

12.5 Shrinkage

The shrinkage of CM fabrics of various Ca contents as a function of treatment with TCH or GS has been studied. When the fabric shrinkage has been compared with swelling under identical conditions, it is found that shrinkage follows the same direction of swelling [9]. This implies that higher the swelling, larger is the extent of shrinkage. Logically, swelling results in increasing the fibers and yarn diameter, this in turns brings about a contraction in their lengths and hence leading to fabric shrinkage [10]. When the shrinkage of fabrics treated with TCH has

been compared with those treated with GS, under similar conditions, it has been found that the first is slightly lower than the first, which is actually in accordance with their swelling values. The dimensions of a dressing should be 5 cm more than the area of a wound. Hence, the total area of a dressing should take into account shrinkage value. This implies that the dimensions of the dressing should extend to 5 cm from the outer edges of the wound after shrinkage. Gelling of the layer next to the wound permits it to slide (upon shrinking) on it, not to force it to contract.

12.6 In Vitro Release of TCH and G

In vitro release of TCH or G up to 3 days, at physiological pH, of treated fabrics has been studied. It can be seen that the release follows a general pattern of a high initial release on the first day that slows down by prolonging the time up to 3 days [9]. TCH presents in two forms on the fabric (as shown by equilibrium reaction 2): a complex form with PVP (adhering loosely to the fabric) and ionically bound form with the carboxylate anions. As infected wounds have a polar nature, so at a pH value of 7.4 (of PBS that representing the physiological solution), the release of TCH can be manifested by reactions 5 and 6.

$$\mathrm{NaCl(in\ PBS)} \rightarrow \mathrm{Na^{+} + Cl^{-}} \tag{12.4}$$

$$\mathrm{PVP.TCH + Cl^{-}\_ \rightarrow PVP.Cl^{-} + TCH} \tag{12.5}$$

$$\mathrm{Cell - COOH.TCH + Na^{+} \rightarrow Cell - COONa + H^{+} + TCH.} \tag{12.6}$$

The release arises due to complex breakage (reaction 5) and sodium exchange (reaction 6). The high molecular weight of PVP (40,000) hinders the diffusion of the complex inside the fabric structure, and hence, it is most probably located at the surface layers of the fabric. Hence, the breakage of the complex is conducive during the initial stage of release, leading to higher initial release. By the time, the complex is depleted and the release is mostly due to sodium exchange. The gentamicin presents on the fabric in two ways (reaction 3), firstly, as unbound excess on the fabric surface in the form GS (d) and, secondly, as a cationically bound form with the carboxyl groups (e). The high initial release of gentamicin in a burst state on the first day can be attributed to the unbound form. The gentamicin is then released with a slower rate according to the following equilibrium reaction:

$$\mathrm{Cell - COOH.G + Na^{+} + Cl^{-} \rightarrow Cell - COO.Na + G.HCl}$$

The advantage of the mentioned pattern of release lies in fabric's capability to supply the wound with a high concentration of antibiotic at the beginning of occlusion, which resists pathogens already present in the wound. By the time, the fabric can supply the wound with lower amount of antibiotic to deal with any invading infection. Depending upon the initial TCH or G content of the fabric (which ranges from 2 to 184 mg/100 g in case of TCH and from 2 to 189 mg/100 g in

case of G), and the pattern of release, a physician can choose the suitable sample for the appropriate type of wound. Further investigation of the results of relating to in vitro release of TCH and G shows that for the similar set of conditions, the % release increases by:

i. Increasing the carboxyl and antibiotic content of the fabric, and
ii. Reducing the Ca content of the fabric.

The total release of TCH or G (in the 3 days) ranges from a maximum of 97 % (in case of a sample of 220 meq COOH/100 g and a Ca of 10 % neutralization that treated with 125 mg/L TCH) to a minimum of about 5.9 % (in case of samples of 72 meq COOH/100 g and treated with 1000 mg/L TCH).

12.7 Antibacterial Activity

The antibacterial activity, in terms of inhibition clear zone (ICZ), has been investigated for *S. Aureus* (G+ve) and *P. Aeruginosa* (G–ve), for the TCH- or GS-treated fabrics. It has been found that the treated fabrics inhibit the growth of bacteria around them with distances depending on their contents of antibiotic, carboxyl, and Ca. Untreated fabrics exhibit complete bacterial growth in virtue of achieving zero ICZs around them. The antibacterial activity that is seen is unevenly because of the release of TCH or G. Actually, the pharmacologic action of tetracycline is induced by diffusion through the bacterial cell wall into the inner cytoplasmic membrane where it binds with the 30S ribosome and inhibits protein synthesis [11]. G also inhibits protein synthesis due to 'irreversible' binding to specific 30S subunit proteins and 16S rRNA. This results in interference with the initiation complex, misreading of mRNA, so incorrect amino acids are inserted into the polypeptide leading to nonfunctional or toxic peptides and the breakup of polysomes into nonfunctional monosomes [12]. For a given set of conditions, it is normally known that the ICZ increases by increasing both of antibiotic concentration in the treatment bath and carboxyl content, while it decreases by increasing Ca content. It has been shown that the presence of Ca impairs the absorption of tetracycline in the stomach and the small upper intestine [13]. Accordingly, it is safe to assume that Ca cations can form complexes with TCH, which are of bigger size than TCH itself, thereby hindering its diffusion in agar, resulting in decreased ICZ. It can be also argued that Ca cations can form complexes with G, causing lower antibacterial activity [9]. It is also observed that the antibacterial activity follows a trend similar to that of antibiotic release. A comparison of data relating to the dependence of ICZ on TCH and GS concentrations shows that the antibacterial activity of TCH is different from that of G, this is due to differences between both with regard to solubility, functionality, chemical reactivity, size, molecular weight, and ability to form aggregates as well as mode of irreversible interaction with cell ribosome.

References

1. Winter GD (1962) Formation of a scab and the role of epithelialization of superficial wounds in the skin of the young domestic pig. Nature 193:293–294
2. Hinnman CD, Maibach HI (1963) Effect of air exposure and occlusion on experimental human skin wounds. Nature 200:377–378
3. Ovington GL (2007) Advances in wound dressing. Clin Dermatol 25:33–38
4. Parikh DV, Sachinvala ND, Calamari TA, Negulescu I (2003) Carboxymethylated cotton for moist wound healing. AATCC Rev 4(7):15–19
5. Attwood A (1989) Calcium alginate dressing accelerates split skin graft donor healing. Br J Plast Surg 42(4):373–379
6. Tereschenko LY, Shamolina II (1998) The use of celluloses to improve the sorption properties of cellulosic wound dressing. J Text Inst 89(3):570–578
7. Faalango V (2004) The chronic wound: impaired healing and solution in the content of wound bed preparation. Blood Cell Dis 32:88–94
8. Yudanova T, Reshetov IV (2006) Modern Wound Dressings: Manufacturing and Properties. Pharm Chem J 40(2):85–92
9. Abo- Shosha MH, Fahmy HM, Hassan FH, Adel MA, Khalil AA (2009) Tetracycline hydrate and gentamicine sulfate containing carboximethylated cotton fabric suitable for moist wound healing dressing: properties and evaluation. J Ind Text 38(4):341–360
10. Abdel Halim NA (2003) Effect of some constructions, pretreatment and finishing of woven cellulosic fabrics on some functional and care properties. PhD Thesis, Menoufia University, Egypt
11. Bickers DR, Hazeu PG, Lynch WS (1984) Clinical pharmacology of skin disease, vol. 7. In: Azarnoff DL (ed) Monographs in clinical pharmacology, chap. 6. Churchill Living Stone, New York, pp 130–162
12. www. DrugBank Gentamicin.mht, updated 01 Feb 2007
13. Olsen TG (1981) Therapy of acne. Med Clin North Am 66:851–871

Chapter 13
Use of Flared Textile Cuffs in Fenestrated Stent–Grafts

13.1 Introduction

In the era of technological developments, endovascular aneurysm repair (EVAR) is undoubtedly regarded as a competitive option to open surgery with brief duration of stay in hospitals, decreased 30-day mortality, and comparable long-term results [1, 2]. Modern devices can be used to treat more than 50 % of aneurysm patients, and this percentage is increasing with newer iterations [3]. But, the endovascular approach is considerably more complex in case of juxta-renal and perirenal aneurysms. Fenestrations offer potential solutions to aneurysms of complex anatomy. Unfortunately, they require sophisticated planning and the construction of customized stent–grafts that can take 6–8 weeks [4–7]. But, delay in customization, production, sterilization, and transportation in high-risk patients are not affordable (Fig. 13.1). Fenestration in the operating room before deployment holds some interest, but the sequence of unloading, fenestration, and reloading the stent–graft currently lacks reliability and quality control [8, 9]. The technique raises many questions, potential to also treat urgent or emergent patients due to the off-the-shelf design (Fig. 13.2). The underlying concept and initial testing of flared textile cuffs that can be immediately available off the shelf in case of emergency have been highlighted in this chapter. Four dissimilar prototypes of woven fabric tubes have been produced by compression molding and have been tested for their constructions, properties, and mechanical characteristics.

N. Gokarneshan et al., *Emerging Research Trends in Medical Textiles*,
Textile Science and Clothing Technology, DOI 10.1007/978-981-287-508-2_13

Fig. 13.1 Schematic representation of blood flow recanalization through an extensive abdominal aortic aneurysm and iliac aneurysm [10]

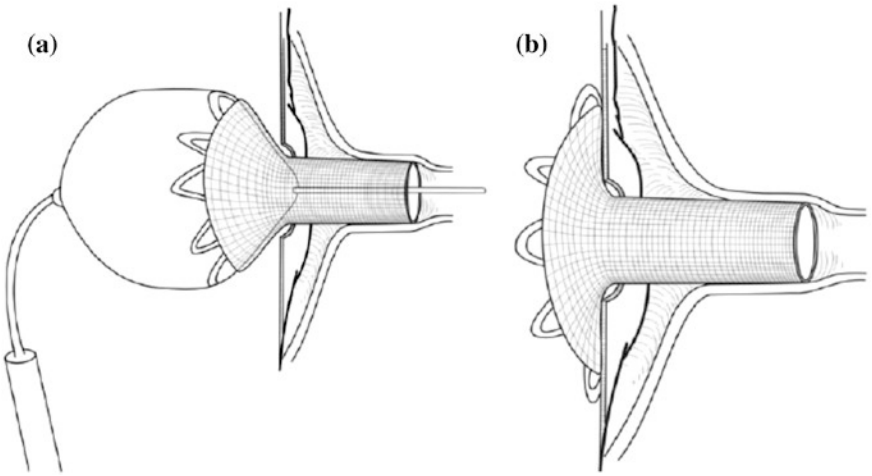

Fig. 13.2 Anticipated development of a flared textile cuff supported with an internal balloon-deployable bare stent **a** during deployment and **b** after deployment [10]

13.2 Fabrication of Flared Textile Cuffs

13.2.1 Fabrication of the Woven Fabric

Polyester multifilaments have been used as the raw material for the weaving process [10]. The multifilaments were used as warp yarns after special sizing. The fabrics have been woven and then desized and densified. The fabrics had either a plain (PW)

Table 13.1 Characteristics of the fabrics woven in comparison with fabrics of commercially available stent–grafts [10]

Models	Devices	Construction	Count of flat fabric after weaving (Warp × Weft) (/mm)
Control fabrics	V	Bistructure	–
	A	Plain	–
	C	Rib weave	–
	T	Twill	–
Experimental fabrics	PW1	Plain	$(6.6 \pm 0.2) \times (6.6 \pm 0.1)$
	PW2	Plain	$(7.4 \pm 0.3) \times (7.3 \pm 0.2)$
	TW1	Twill	$(6.3 \pm 0.2) \times (6.6 \pm 0.1)$
	TW2	Twill	$(7.5 \pm 0.2) \times (7.0 \pm 0.2)$

V Vanguard, *A* Anaconda, *C* Cook, *T* Talent

or twill (TW) fabric, and different fabric counts, giving four fabric sheets: PW1, PW2, TW1, and TW2. Table 13.1 gives the parameters for these fabric sheets.

13.2.2 Compression Molding

Compression molding has been used to obtain the flared cuff grafts [11] (Fig. 13.3). The grafts have been compressed into cuff shape by a mold after 10 min preheating at 160 °C in a hot air oven. The heat setting has been done in a hot air oven at 160 °C for half hour [10]. The prototypes have been prepared by cutting the top of the cuff-flare to form a tube.

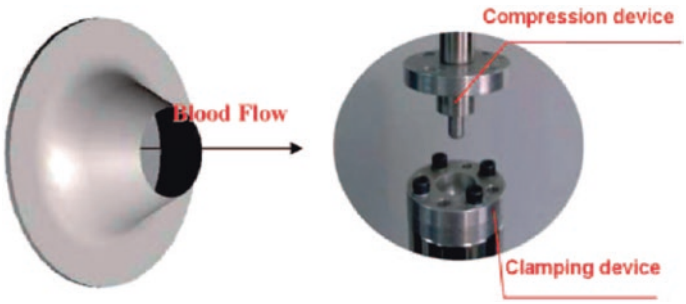

Fig. 13.3 **a** Flared cuff produced by compression molding. **b** In a machine fitted with a clamping device [10]

13.3 Textile Characterization of the Devices

Gross observations and light microscopy
The gross observations were conducted with a digital camera, and the characterization of the fabric structure has been done by optical compound microscope fitted with a charge-coupled device (CCD) camera [10].

13.3.1 Fabric Count

The density of the sample prototypes and fabric counts of each section have been determined according to the ISO 25539 standard [12]. The woven fabric count has been viewed under the optical compound microscope to count the number of ends and picks [10]. The fabric weight per square meter (g/m^2) has been calculated by the weight and area of the specimens [13].

13.3.2 Thickness

The graft thickness has been determined [14]. The diameter of the press foot of the thickness gauge is 6 mm, and the pressure was up to 22 kPa [10].

13.4 Morphology of the Flared Textile Cuffs

Figure 13.4 depicts the flared textile cuffs. The cuffs are divided into three sections: base, arc, and top. Its base is the fringe area of the cuff graft, used for opposition to the luminal surface of the aortic stent–graft, while its top is the extension to be deployed into the branching artery to maintain the blood flow. The arc is a transition area that permits its use for connecting fenestrations to various vessel diameters [10].

13.5 Structure Characteristics of Flared Textile Cuffs

The structural characteristics, including fabric count, fabric weight per square meter, thickness, and porosity of each part (base A, arc B, and top C), are shown in the Figs. 13.5 and 13.6. The fabric count, area density, and thickness of prototypes created by compression molding reduced progressively from the base A to top C, while the porosity increases gradually. The thickness of all section, of the flared cuff grafts particularly the arc and top, is lesser than or same as the commercial

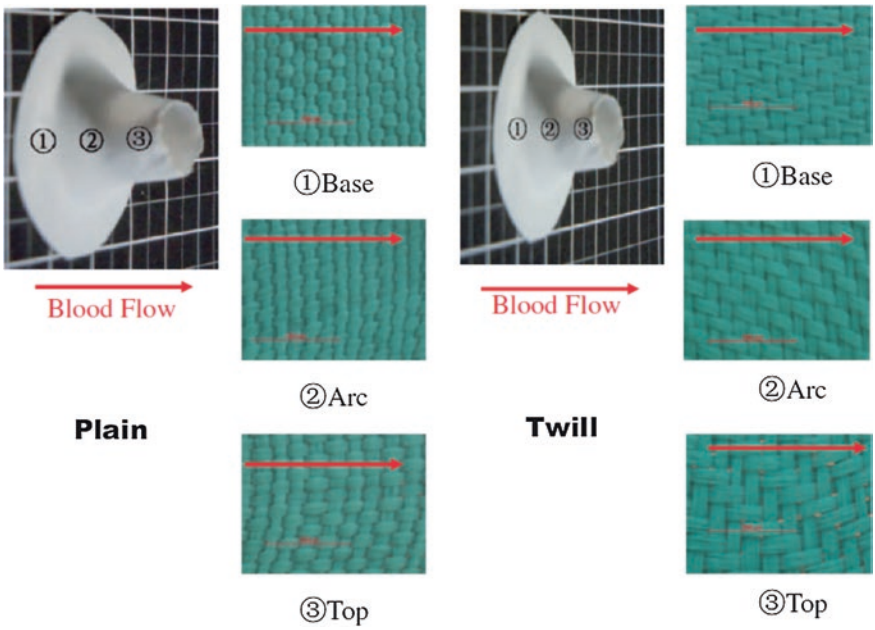

Fig. 13.4 Flared cuffs, made with a plain weave fabric (*left*) and a twill weave fabric (*right*) [10]

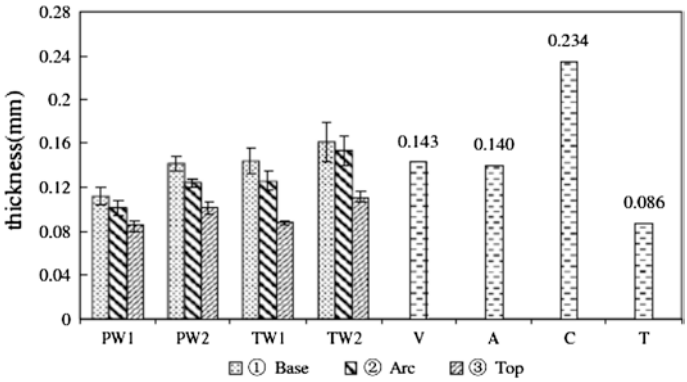

Fig. 13.5 Thickness of the different segments of the textile cuffs of the prototypes versus the thickness of the fabrics employed to manufacture commercially available devices [10]

references, Vanguard, Cook, Anaconda, and Talent [10]. The thickness of the plain weave fabric is slightly lesser than that of the twill weave with a similar fabric count, due to lesser float length and more interlacing points. The porosity of the bases of the prototype samples, used for sealing to the trunk graft, is much lower than the commercial reference. But, the porosity on the arcs and tops is almost the same as for commercial devices.

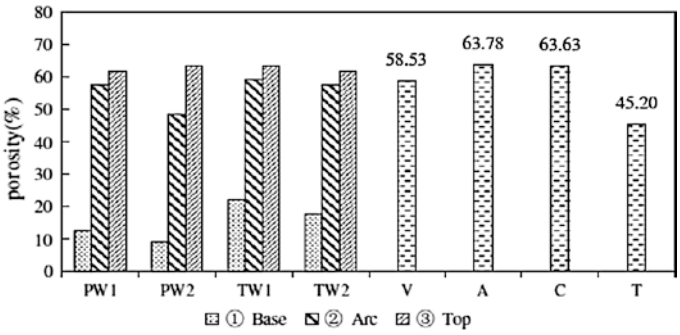

Fig. 13.6 Porosity of the different segments of textile cuffs [10]

13.6 Mechanical Characteristics of the Flared Cuff Graft

(a) **Burst strength**

The bursting strength of prototype samples (Fig. 13.7) reduced steadily from the base to the top due to the density gradient discussed previously. Also, textile grafts having greater fabric count exhibit higher bursting strength than the grafts of the same woven structure. The bursting strength of twill grafts is greater than that of plain grafts for same fabric count. In the case of fabrics that have low count, plain construction (top of PW1 and TW1) have greater bursting strength than that of twill construction due to a more stable construction. But, when the fabric count increases to a certain magnitude, plain or twill fabrics will both have stable constructions. Owing to its higher thickness, twill weave has higher bursting strength than plain grafts of a same count [10].

(b) **Radial strength**

The test results of the radial tensile force for the prototype grafts are shown in Fig. 13.8 and are same as the results of the bursting strength test. Grafts having greater fabric count have greater radial tensile strength than grafts having the same woven structure [10]. Twill woven grafts have higher radial tensile strength than that of plain grafts having same fabric count.

(c) **Elasticity**

As depicted in Fig. 13.9, the compression recovery values for the four prototypes exceed 85 % (Fig. 13.9). In the case of compression retention duration ranging between 20 and 120 s; the prototype (TW2) displays the greatest elastic recovery, with recovery of more than 95 % of the original diameter. The other three prototypes exhibited slightly lower results, maintaining a recovery of more than 85 %. But, on increasing the duration of compression retention, the immediate elastic recovery for the four prototypes showed perceivable differences (Fig. 13.9).

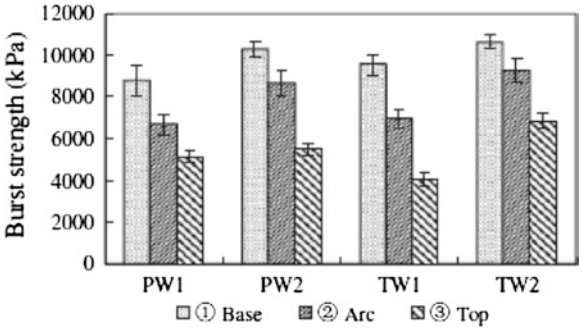

Fig. 13.7 Bursting strength of different segments of the textile cuffs [10]

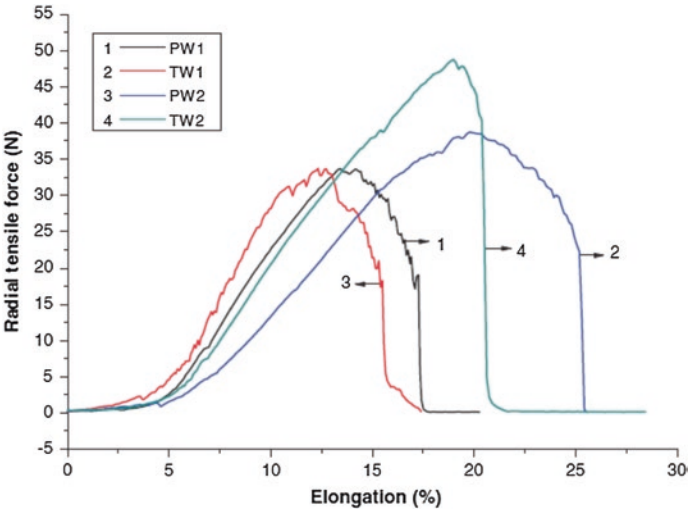

Fig. 13.8 Radial tensile strength of flared cuffs prototypes [10]

For compression, retention time is increased from 20 to 120 s and the immediate elastic recovery goes down from 92.1 and 92.2 % to 85.9 and 87.1 % for PW1 and PW2, respectively. Similarly, the immediate elastic recovery of PW2 and TW2 is maintained at 90.7 and 95.3 %, respectively. The grafts having greater fabric count have higher elasticity than the grafts with identical woven structure. The twill woven grafts showed higher elasticity in comparison with plain woven grafts of same fabric counts (PW1 < TW1 < PW2 < TW2). Consequently, TW2 would be easier to deploy during surgery. In summary, the TW2 prototype graft (with higher fabric count and twill weave) demonstrates the most optimal mechanical properties, including burst strength, radial tensile strength, and elasticity [10]. In addition, it also proves to present good structural characteristics that compare

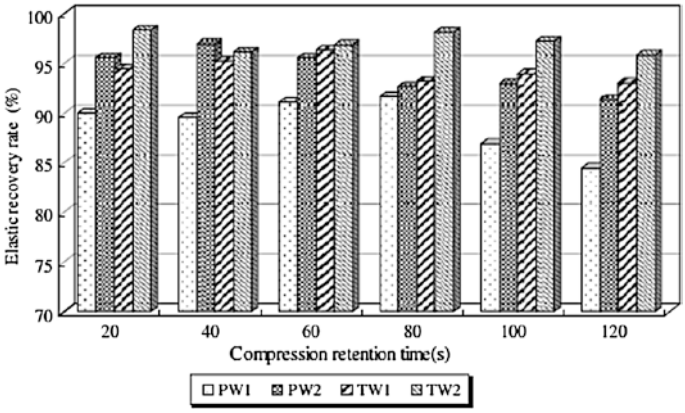

Fig. 13.9 Elastic recovery of the flared cuff prototypes exposed to radial compression with different durations of compressive retention [10]

favorably with commercial references. Hence, it shows good prospects for the application in fenestrated grafts.

13.7 Discussion of the Findings

Researchers have shown that [15] developments in the design of devices for EVAR are offering options for patients with complex anatomy in situation of urgency or emergency. Many patients can avail the facility of endovascular repair, with the increase in the availability of these types of devices [16–18]. The speed and the level of quality that will be attained will depend not only on aggressively pursuing new ideas, but also on cooperation and support from industry [11, 19]. The objective of these researches is to offer treatment options to patients with complex aneurysms and requiring immediate treatment. The flared cuffs have been particularly fabricated to be deployed through the fenestration of a stent–graft and to be supported by a balloon-deployable stent proximally flared upon delivery. The arc of this flared textile cuff can match a range of different diameters of proximal sealing zone in the fenestrated stent–graft and permits convenient, modular customization to match anatomy. The fenestration can have various diameters, but the flared structure will seal to the main stent–graft to ensure a continuous conduit preventing endoleak. The flared cuff is considered to be a new step in exploring the accessibility of fenestration grafts to frail patients having arterial anatomy that is complex [10]. The polymerization of shape memory polymers on polyester fibers offers very good potential due to their capacity for actuation [20]. Also, the possibility for reorientating branches without kinking enables better treatment of renal and other arteries. It will certainly add new devices in the highly diversified

armamentarium offered to surgeons [12–14].The flared polyester cuffs should compare well with existing fabrics used in endovascular prostheses with regard to safety, efficiency, and durability. The thickness of the polyester fabric is the most prominent characteristic. It should have a low profile so as to be easily inserted in a delivery catheter. In order to avoid blood leaking through the stent–graft, the porosity of the fabric should be low. However, greater porosity facilitates tissue in growth and the transportation of nutritive substances and metabolites to cells outside the stent–graft, especially endothelial cells. The flared cuff must have great stability. A little deformation in the structure happens due to the compression molding process. Tensile and shearing forces, arising from compression molding, act on fabrics to form the arc and the top. The structure of the base fabric remained unaltered after compression molding, while the elongation and slippage rate of the yarns in the top were larger than in the arc. Consequently, a gradient change of structure characteristics was formed, which can be considered to be advantageous. The decreasing density on the flared cuff graft can make it easier to deform and deploy during surgery, and the central area (the top) with lower density will adhere to the wall of the branch vessel to maintain blood flow. The bursting strength of the prototype samples reduces eventually from the base to the top. In addition, textile grafts with a higher fabric count have higher burst strength than grafts of the same weaving structure. Moreover, the bursting strength of twill grafts is greater than that of plain grafts of same fabric count. For fabrics that have a low count (top of PW1 and TW1), plain textiles may have higher burst strength than twill textiles due to a more stable construction. But, plain or twill fabrics can have stable construction, as the fabric count increases to a certain degree. Hence, twill will have higher bursting strength in comparison with that of the plain grafts because of higher thickness.

References

1. Dimick JB, Upchurch GR (2008) Endovascular technology, hospital volume, and mortality with abdominal aortic aneurysm surgery. J Vasc Surg 47:1150–1154
2. Greenhalgh RM, Brown LC, Powell JT et al (2010) The United Kingdom EVAR Trial Investigators, Endovascular versus open repair of abdominal aortic aneurysm. N Engl J Med 362:1863–1871
3. Hinchliffe RJ, Hopkinson BR (2007) Development of endovascular stent-grafts. J Eng Med 221:547–561
4. Greenberg RK, Sternbergh WC III, Makaroun M et al (2009) Intermediate results of a United States multicenter trial of fenestrated endograft repair for juxtarenal abdominal aortic aneurysms. J Vasc Surg 50:730–737
5. Ricotta JJ, Oderich GS (2008) Fenestrated and branched stent-grafts. Perspect Vasc Surg Endovasc Ther 20:174–187
6. Oderich GS, Ricotta JJ (2009) Modified fenestrated stentgrafts device design, modifications, implantation, and current application. Perspect Vasc Surg Endovasc Ther 21:157–167
7. Oderich GS, Farber MA, Sanchez LA (2011) Urgent endovascular treatment of symptomatic or contained ruptured aneurysms with modified stent grafts. Perspect Vasc Surg Endovasc Ther 23:186–194

8. Ouyang C, Liang H (2010) Urgent interventional bilateral renal artery fenestration for giant pararenal abdominal aortic aneurysm with upper digestive tract obstruction. J Vasc Surg 52:1048–1051
9. Starnes BW (2012) Physician-modified endovascular grafts for the treatment of elective, symptomatic, or ruptured juxtarenal aortic aneurysms. J Vasc Surg 56:601–607
10. Wang1 F, Li1 C, Wang1 L, Li1 C, Li1 Y, Lin1 J, Jing2 Z, Douglas3,4 G, Nutley5 M, Guidoin3 R (2014) Flared textile cuff to be apposed on the proximal sealing zone in fenestrated stent-grafts. Text Res J 84(3):279–289
11. Buchanan LW, Stavropoulos SW, Resnick JB et al (2009) Endovascular repair of aortic disease: a venture capital perspective. Semin Intervent Radiol 26:56–66
12. Nordon IM, Hinchliffe RJ, Manning B et al (2010) Toward an ''off-the-shelf'' fenestrated endograft for management of short-necked abdominal aortic aneurysms: an analysis of current graft morphological diversity. J Endovasc Ther 17:78–85
13. Nordon IM, Hinchliffe RJ, Holt PJ et al (2009) Modern treatment of juxtarenal abdominal aortic aneurysms with fenestrated endografting and open repair—a systematic review. Eur J Vasc Endovasc Surg 38:35–41
14. Mestres G, Riambau V (2012) Late performance of EVAR will be solved by newer endografts. In: Greenhalgh RM (ed) Vascular and endovascular controversies update. BIBA Publishing, a Division of BIBA Medical Ltd, London, pp 309–317
15. Farber MA, Oderich GS (2012) Physician made fenestrated compared with off-the-shelf fenestrated devices. In: Greenhalgh RM (ed) Vascular and endovascular controversiesupdate. BIBA Publishing, a Division of BIBA Publishing Ltd, London, pp 225–227
16. Greenberg R, Eagleton M, Mastracci T (2010) Branched endografts for thoracoabdominal aneurysms. J Thorac Cardiovasc Surg 140:171–178
17. Brozzi NA, Roselli EE (2012) Endovascular therapy for thoracic aortic aneurysms: state of the art in 2012. Curr Treat Options Cardiovasc Med 14:149–163
18. Bicknell CD, Cheshire NJW, Riga CV et al (2009) Treatment of complex aneurysmal disease with fenestrated and branched stent grafts. Eur J Vasc Endovasc Surg 37:175–181
19. Greenberg RK, Qureshi M (2010) Fenestrated and branched devices in the pipeline. J Vasc Surg 52:15S–21S
20. Zou Y, Lam A, Brooks DE et al (2011) Bending and stretching actuation of soft materials through surface-initiated polymerization. Angew Chem Int Ed 50:5116–5119

Chapter 14
New Orthopedic Support Material

14.1 Introduction

Recently, functional textiles for medical and related healthcare products have gained access in the textile field [1]. The textile industry has been equipped with medical knowledge and has enriched the textile fabrics due to their interaction with the skin [2]. Some significant applications of the textiles in medical field are artificial aortas and bandages. But, advanced functional textile drug delivery systems have not been developed till the end of the past century [3]. Orthopedic support materials have been used for protection and as support joints in different areas of the body. Knee supports, wrist supports, ankle supports, elbow supports, shoulder supports, and back supports are some good examples of these applications. Such supports are being used for cure or protection. The medical applications are suitable under the below-given conditions:

(a) Post-operative or traumatic irritations;
(b) Joint illnesses which are degenerative and inflammatory;
(c) Stressed ligaments and tendons; and
(d) Specific problems of different joints [4].

Transdermal drug delivery systems (TDDSs) have innumerable merits when compared with conventional pharmaceutical dosage forms. These include improved systemic bioavailability of active pharmaceutical ingredients, fewer administration frequency, longer duration of therapeutic action, reduction in side effects, and steady drug delivery profile [5]. A number of technologies have been adopted for preparation of TDDSs. One such technology involves the use of medicated textiles for delivering drugs to specific body sites [6]. Microencapsulation has gained interest in textile research during the recent years, since patent applications are increasing. The important areas of application of the microencapsulation process include durable fragrances, phase-change materials, dyes, fire retardants,

N. Gokarneshan et al., *Emerging Research Trends in Medical Textiles*,
Textile Science and Clothing Technology, DOI 10.1007/978-981-287-508-2_14

and antimicrobial agents [7]. This technique can also be used as an encapsulation method when it entraps active material within a protective matrix, which is essentially inert to the material being encapsulated [8]. Polymers are frequently used in microencapsulation studies. Ethyl cellulose is a water-insoluble polymer widely used in oral and topical pharmaceutical formulations [9]. It is especially used to prepare sustained-release medications of various types. In the absence of polymer swelling ability, ethyl cellulose becomes a key factor in such systems, because release kinetics would depend largely on the porosity of the hydrophobic compact [10]. Spray-drying encapsulation method has many merits and is being used in the preparation of microparticulate drug delivery systems. It is a well-established technology, involving readily available equipment and comparatively low-cost encapsulation [11]. This technique changes liquid feed into dry powder in a single stage and is suitable for the scaling-up of the microencapsulation and continuous particle processing operation, and can be used for a different materials [12]. Diclofenac sodium (DS), a sodium salt of 2-[(2,6- dichlorophenyl)aminophenyl]-acetic acid (Fig. 14.1), is a nonsteroidal anti-inflammatory drug (NSAID), commonly used for the long-term treatment of rheumatic disorders, such as osteoarthritis, rheumatoid arthritic, and ankylosing spondylitis [13]. Its use causes many unwanted serious side effects due to the long-term oral administration, such as stomach ulcerations, abdominal burning, pain, cramping, nausea, gastritis, and even serious gastrointestinal bleeding and poisoning of the liver. Though it is fully absorbed following oral administration, but in its elimination, half-life is relatively short, ranging between 1 and 2 h. Due to its biopharmaceutical and pharmacological properties, sustained-release formulations of DS are desirable that should maximize the therapeutic benefit and reduce the unwanted side effects, since the frequency of administration is lower, improving the therapeutic efficacy and patients' compliance [14–19]. This chapter highlights the preparation and characterization of DS microparticles and their application to orthopedic support materials. The spray-drying technique has been utilized in obtaining the microparticles and involved ethyl cellulose as a matrix material to control drug release. The morphology and particle size of the drug microparticles were optimized for impregnation of DS microparticles onto the orthopedic support materials. Lastly, investigations have been carried out on vitro drug release of microparticles and textile impregnated with microparticles.

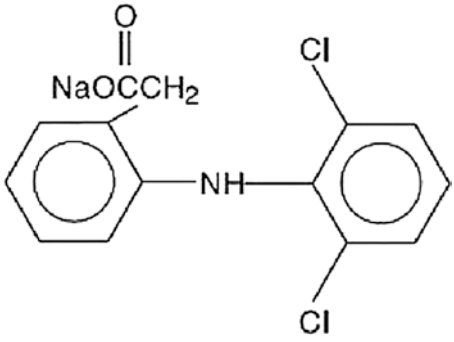

Fig. 14.1 Chemical structure of diclofenac sodium [25]

14.2 Characterization of Microparticles

(a) **Drug content and encapsulation efficiency**

Higher encapsulation efficiency values have been achieved for the microparticles having a drug: polymer ratio of 1:1. When the DS load of the microparticles was reduced from 36.82 to 10.77 %, the encapsulation efficiency dropped from 94 to 77 % [25].

(b) **Particle size and size distributions**

Figure 14.2 depicts the particle size and distributions of the prepared microparticles. The mean particle sizes of microparticles formed by (1:1), (1:2), and (1:4) formulations are 8.61, 9.68, and 8.44 mm with span values of 1.66, 2.23, and 1.82, respectively [25].

(c) **Particle morphology**

Figure 14.3 shows the scanning electron photomicrographs of spray-dried microparticles (1:1), (1:2), and (1:4). It can be observed that the spray-dried product is composed mainly of spherical-shaped particles and also the absence of

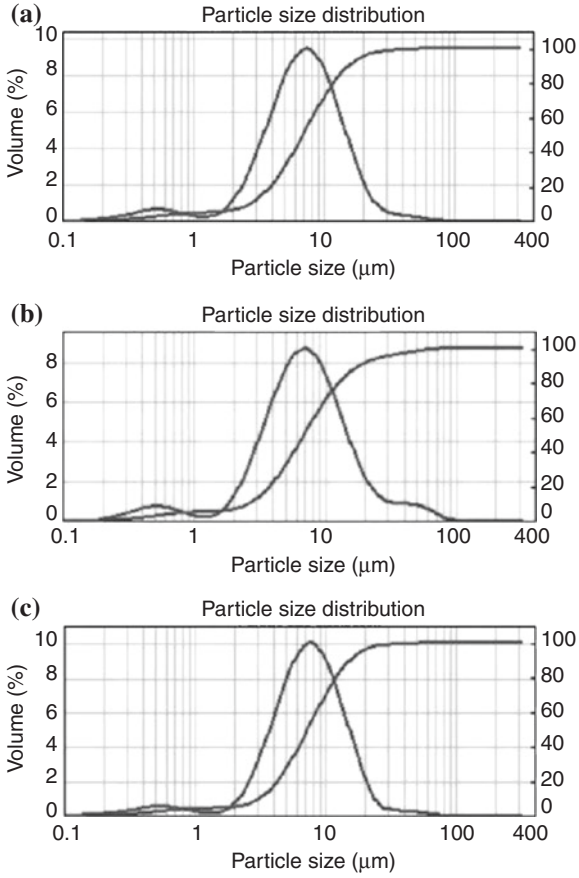

Fig. 14.2 Particle size distributions of microparticles: **a** (1:1); **b** (1:2); and **c** (1:4) [25]

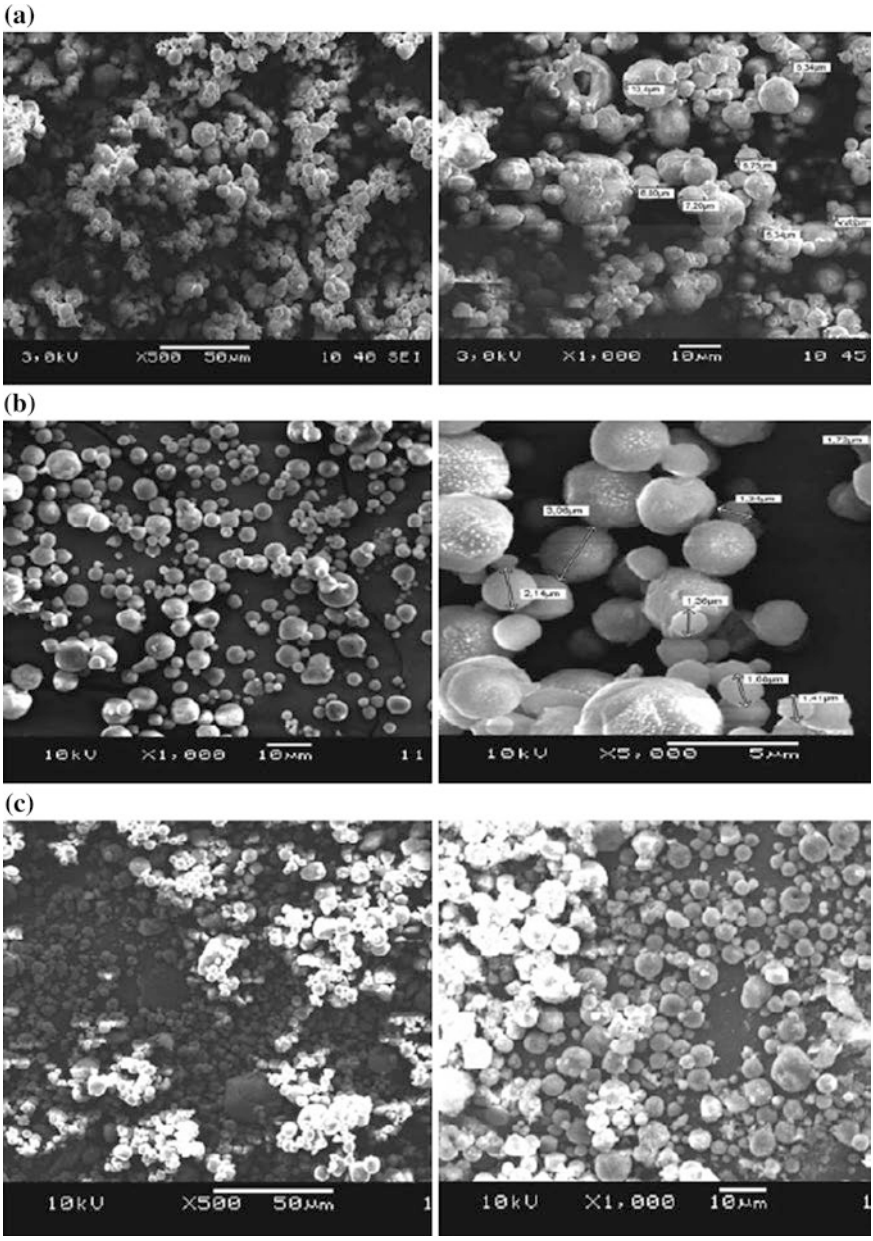

Fig. 14.3 Scanning electron photomicrographs of spray-dried microparticles: **a** (1:1); **b** (1:2); and **c** (1:4) [25]

agglomerates. They also indicate the formation of microparticles with homogeneous characteristics and smooth appearance and do not exhibit the presence of free drugs on the microparticles surfaces. These morphological characteristics show that the drug is dispersed through the microparticles [25].

(d) **Fourier transforms infrared spectroscopy**

Interaction between the drug and polymers is commonly brought about by identifiable changes in the FT-IR patterns. Figure 14.4 shows the FT-IR patterns of DS and microparticles, and characteristic peaks at 3387 cm^{-1} as a result of N–H stretching of the secondary amine, at 1572 cm^{-1} due to –C¼O stretching of the carboxyl ion, and at 744 cm^{-1} owing to C–Cl stretching were exhibited in FT-IR spectra of DS (Fig. 14.4a). The FT-IR spectra of drug-free microparticles containing ethyl cellulose show an asymmetric peak at around 2973–2925 cm^{-1}, which is due to C–H stretching (Fig. 14.4b). The peak at 1375 cm^{-1} is due to CH3 bending, and the small peak near 1450 cm^{-1} is due to CH2 bending [25]. The broad distinct peak near 1050 cm^{-1} may be due to the C–O–C stretch in the cyclic ether. The peaks of DS-loaded microparticles (Fig. 14.4c–e) were similar (but with lesser intensity) to the spectrum of DS. The peaks of various functional groups, as described in the IR spectrum of DS, were also present in the microparticles without any shift or change. These observations revealed the intact nature of the DS present in the microparticles. The absence of drug–polymer system interaction and the stability of the encapsulated drug in microparticles have been confirmed from these results. Identical observations with other drug/carriers have been reported by other researchers [20, 21].

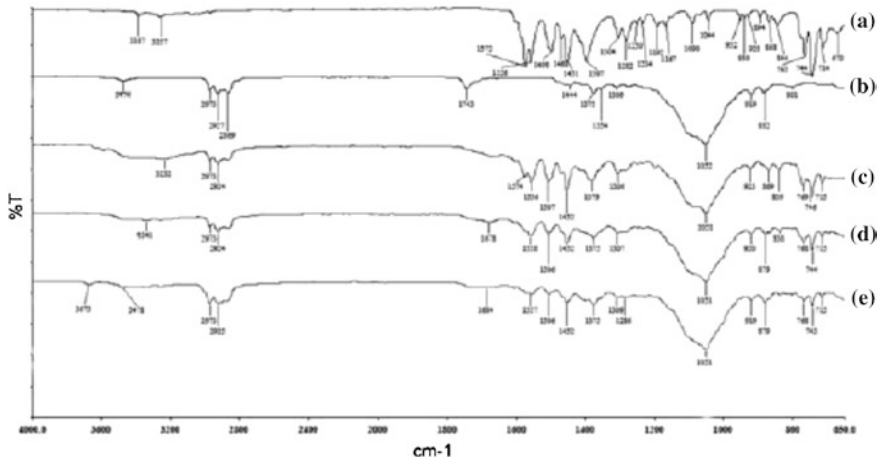

Fig. 14.4 Fourier transform infrared spectra of pure diclofenac sodium (**a**), 1:1 microparticles (**b**), 1:2 microparticles (**c**), and 1:4 microparticles (**d**) [25]

(e) **Differential scanning calorimetric**

Figure 14.5 shows the DSC thermograms of pure drug, drug-free microparticles, and drug-loaded microparticles. The DSC thermogram of pure drug (Fig. 14.5a) exhibits one endothermic peak. This sharp peak at 297.78 °C is due to melting of the drug. There has been no defined peak in the case of drug-free microparticles

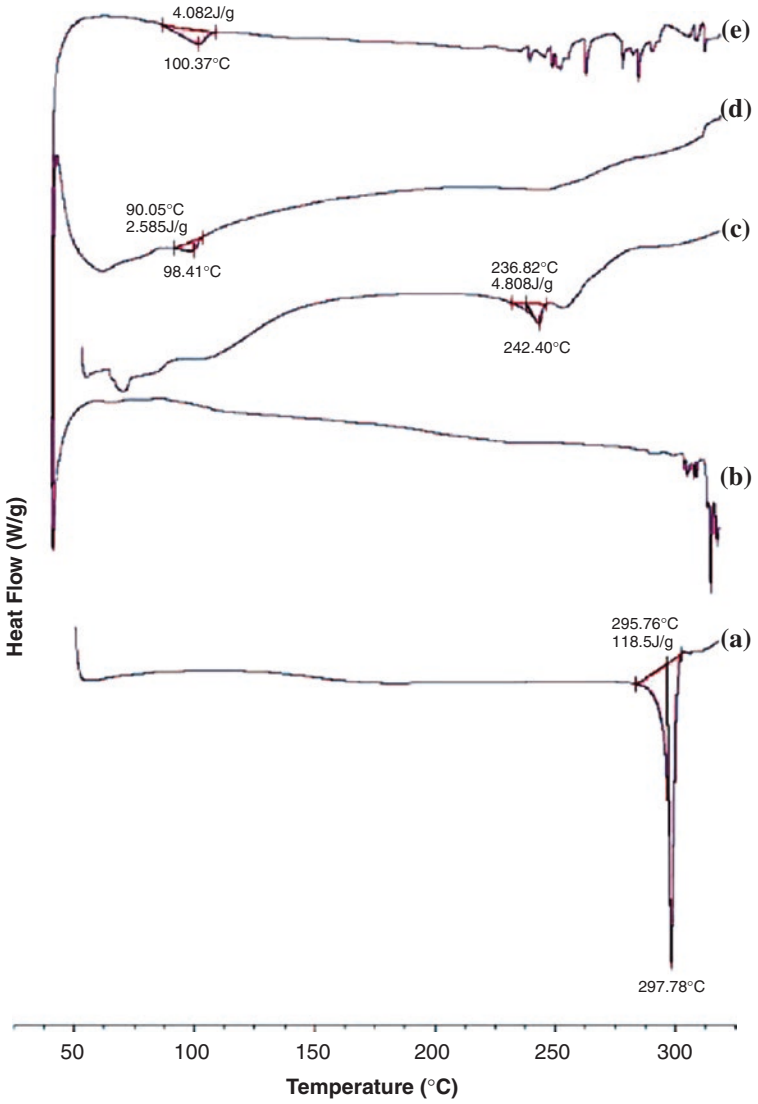

Fig. 14.5 Differential scanning calorimetry thermograms of diclofenac sodium (**a**), drug-free microparticles (**b**), drug:polymer ratio 1:1 microparticles (**c**), drug:polymer ratio 1:2 microparticles (**d**), and drug:polymer ratio 1:4 microparticles (**e**) [25]

(Fig. 14.5b). Small peaks have been noticed in the case of drug-loaded microparticles, at 242.4, 98.41, and 100.37 °C in 1:1, 1:2, and 1:4 microparticles (Fig. 14.5c–e), respectively [25]. This reveals that the drug has the amorphous distribution in the polymer matrix. Simultaneously, the results also revealed that there is no interaction between the drug and polymer systems. DSC results demonstrated the consistency with the findings obtained from FT-IR analysis. X-ray powder diffractometry.

(f) **X-ray powder diffractometry**

Investigations from X-ray diffraction patterns further proved the physical nature of the drug entrapped in microparticles. Figure 14.6a–e exhibits the XRD patterns of drug, drug-free microparticles, textile fabric, and textile impregnated with

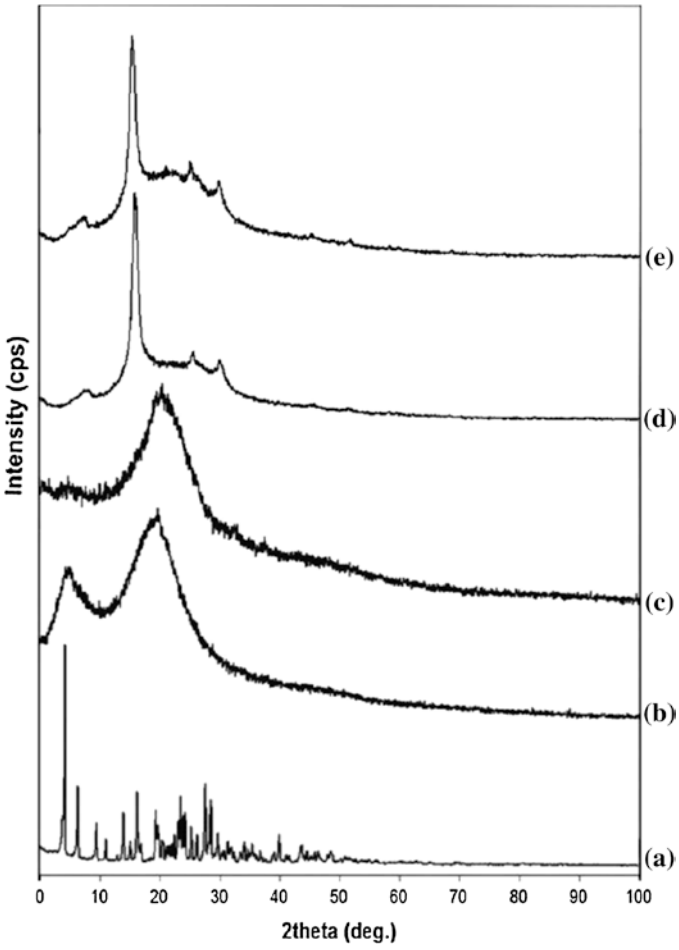

Fig. 14.6 X-ray diffraction patterns of diclofenac sodium (**a**), drug-free microparticles (**b**), microparticles composed of a drug:polymer ratio of 1:1 (**c**), textile fabric (**d**), and textile fabric impregnated with microparticles composed of a drug:polymer ratio of 1:1 (**e**) [25]

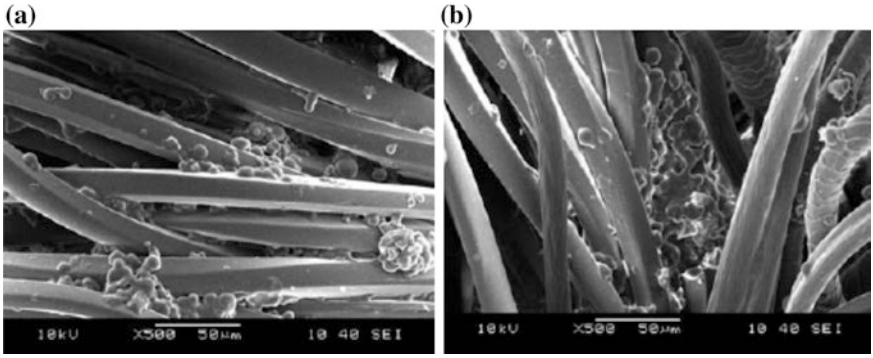

Fig. 14.7 Scanning electron photomicrographs of textile impregnated with microparticles [25]

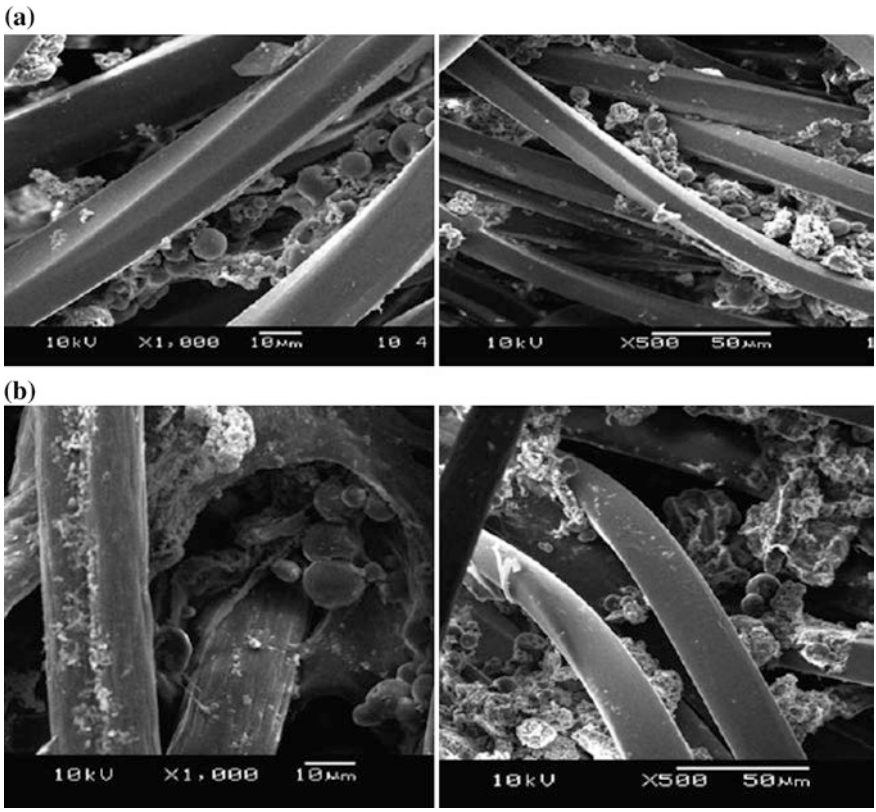

Fig. 14.8 Scanning electron photomicrographs of textile impregnated with microparticles washed for **a** 10 cycles and **b** 20 cycles in accordance with standard ISO 105 C06 [25]

microparticles, respectively. The X-ray diffraction patterns of DS exhibit sharp peaks owing to the crystalline nature of the drug. However, these drug peaks disappeared in the X-ray diffraction patterns of microparticles and the textile impregnated with microparticles (Fig. 14.6c, e).

The DS appeared to show its specific crystal peaks when it existed in a crystalline form, but could exist as a molecular dispersion after the drug was entrapped in the microparticles. Researchers [21, 22] observed identical patterns with other drug/carriers. This, in support of the DSC study, clearly reveals the amorphous form of entrapped drug in the microparticles. During the process of spray, a phase change often occurs and it may result in the production of amorphous substances [23].

(g) **SEM of textile impregnated with microparticles**

Textile materials applied with microparticle dispersions have been studied by using SEM. Figure 14.7 shows that the adhesion between textile fiber and microparticles has been effective as proved by SEM photomicrographs [25]. The microparticles between fibers are spherical shape as viewed under SEM (Figs. 14.7 and 14.8).

14.3 Studies on Air Permeability

The air permeability of textile materials is governed by parameters such as fabric structure, density, thickness, and surface characteristics, and is considered to be one of the important properties [25]. The air permeability test has been carried out to study the influence of microparticles on the air permeability properties of textile materials (Table 14.1).

Air permeability test results show that the air permeability value of the textile impregnated with microparticles has been somewhat reduced. This was because the microparticles fill in the space between fibers. By maintaining the concentrations of microparticles and the cross-linker on orthopedic support material constant, the air permeability values of the orthopedic support material impregnated with microparticles are not expected to change. The air permeability results also confirm this aspect. There is no significant difference between the air permeability values of the textile materials impregnated with microparticles prepared in different drug: polymer ratios. But, the air permeability values were observed to decline when compared with values of untreated orthopedic support material, since the cross-linking material forms cross-links and that it is a nanosized coating material.

Table 14.1 Air permeability values of textile materials impregnated with microparticles [25]

Sample	Air permeability values (mm/s)
Untreated orthopedic support materials	226
Orthopedic support material impregnated with microparticles composed of a drug: polymer ratio of 1:1	199.5
Orthopedic support material impregnated with microparticles composed of a drug: polymer ratio of 1:2	198
Orthopedic support material impregnated with microparticles composed of a drug: polymer ratio of 1:4	198.5

14.4 Laundering Test

Figure 14.8 shows the SEM photomicrographs of textiles containing microparticles that have been washed 10 and 20 times. It is seen that even after washing, the microparticles remain on the textile material. The drug-loaded microparticles continue to stay on the fabric, even after 20 washing cycles. The studies reveal that the microparticles have not been adsorbed on the surface of the textile material, but absorbed by it in the presence of the self-cross-linking agent, and bindings between microparticles and fibers have been able to withstand up to 20 launderings [25].

14.5 In Vitro Drug-Release Studies of DS Microparticles

The extent of drug release from microparticle formulations is depicted in Fig. 14.9. In vitro release, study of the microparticles has shown that the time for 100 % DS release has been extended to 90, 120, and 150 min for 1:1, 1:2, and 1:4 microparticle formulations, respectively, as compared with 60 min for pure DS. The studies show that increasing the polymer ratio reduces the rate of release. In the drug-release medium, all microparticle formulations showed an initial fast release due to the dissolution of the drug from the surface, but the release of the drug was extended up to 150 min depending on the polymer ratio. Greater channels are possibly created, with increased drug release from the microparticles, thereby leading to quicker rates of drug release [25]. Also, higher drug levels in the microparticle formulation create a higher drug concentration gradient between the microparticles and drug-release medium, thereby increasing the rate of drug release.

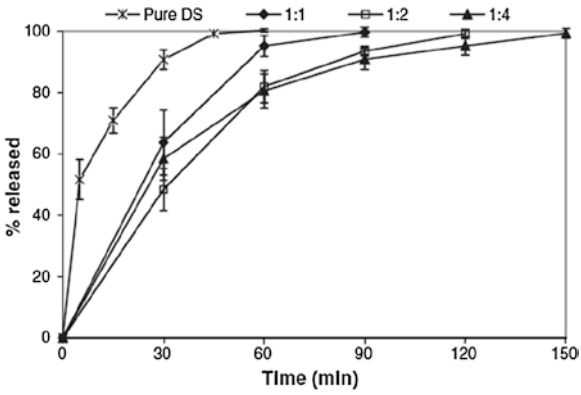

Fig. 14.9 In vitro diclofenac sodium (*DS*)-release profiles from pure drug and microparticles [25]

14.6 Textile Impregnated with DS Microparticles

Figure 14.10 depicts the findings of the in vitro release of textile impregnated with microparticles with different drug: polymer ratios in pH 7.4 phosphate buffer solutions at 37 °C. It could be observed that during the initial phase of the investigation of the drug release, for all formulations, a greater extent of DS (60–90 %) has been freed from the surface of the textiles. The smaller size of the microparticles (8.44–9.68 mm) can contribute to the quick release of the microparticles as well as the big surface area and amorphous characteristics of drug. Amorphous drugs have greater solubility in comparison with crystalline drugs and also have different physiochemical properties [24]. Therefore, fast dissolution of the encapsulated drug could take place immediately when the drug particle was exposed to the aqueous environment [25].

During the first hour, a burst effect has been revealed for all drug-release profiles [6]. The burst effect is possibly caused due to the quick dissolution of the drugs situated near the surface of the microparticles, as the DS is soluble in pH 7.4 phosphate buffer solution. The dissolution of the surface drug will result in channels, allowing the aqueous medium to penetrate into the matrix, leading to drug dissolution and subsequent drug release via the medium-filled channels. The phenomenon could possibly be explained as a considerable loading of the drug is situated in the vicinity of the microparticle surface, and this is released as the cavity size increases. After 1 h, there was a steady release of drug into the release medium for all formulations. On comparing the formulations, the drug-release ratio has been greater in 1:1 than in 1:2 and 1:4 during the first three hours ($p < 0.001$ for each point). In the case formulation 1:1, the drug release has been completed in the third hour, and in the case formulation 1:2, it was completed in the fifth hour. Completion of the drug release in formulation 1:4 was longer than eight hours. In formulation 1:2, drug release was higher than in formulation 1:4 in the fourth and fifth hours. Thus, it can be stated that the increase of drug loading created a faster drug release. Polymer concentration and drug-release behavior were directly proportional. To determine the mechanism of drug release, 1:2 and 1:4 microparticles

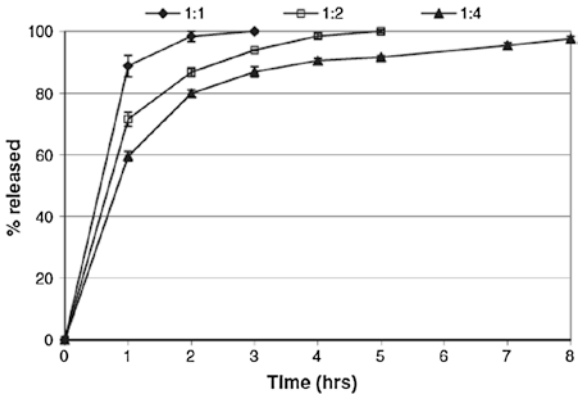

Fig. 14.10 In vitro diclofenac sodium-release profiles of textiles impregnated with microparticles [25]

and textiles impregnated with 1:2 and 1:4 microparticles, which have prolonged drug release, were subjected to release kinetic studies. Statistical analysis shows that the drug release from microparticles and textile-impregnated microparticles followed the first-order equation (concentration-dependent release of drug) rather than the Higuchi kinetic model (diffusion-controlled release of drug).

References

1. Fisher G (2002) Medical and hygiene textiles—continuing in good health. Tech Textil Int 11:10–16
2. Hippler U-C, Elsner P (2006) Biofunctional textiles and the skin. Curr Probl Dermatol 33:51–66
3. Nierstrasz VA (2007) Textile-based drug release systems. In: Langenhove LV (ed) Smart textiles for medicine and healthcare: materials, systems and applications. Woodhead blishing Ltd and CRC Press, Cambridge, pp 50–74
4. Horrocks AR, Anand SC (2003) Teknik Tekstiller El Kitabı. The Textile Institute, Tu¨ rk Tekstil Vakfı, Meta Basım Matbaacılık Hizmetleri, p 586
5. Zhan X, Tang G, Chen S et al (2006) A new copolymer membrane controlling clonidine linear release in a transdermal drug delivery system. Int J Pharm 322:1–5
6. Ma ZH, Yu DG, Branford-White CJ et al (2009) Microencapsulation of tamoxifen: application to cotton fabric. Colloids Surf B 69:85–90
7. Nelson G (2002) Application of microencapsulation in textiles. Int J Pharm 242:55–62
8. Re´ MI (1998) Microencapsulation by spray drying. Drying Technol 16:1195–1236
9. Dahl TC and Ethylcellulose (2006) In: Rowe RC, Sheskey PJ, Owen SC (eds) Handbook of pharmaceutical excipients, 5th edn. Pharmaceutical Press, London
10. Du¨ rig T, Harcum WW, Lusvardi KM et al (2003) Compaction characteristics of high ethoxyl, low viscosity ethylcellulose. Pharmaceutical Technology Report, 024, Hercules Incorporated, Aqualon Division, Wilmington, DE
11. Thies C (1996) A survey of microencapsulation processes. In: Benita S (ed) Microencapsulation methods and industrial applications. Marcel Dekker Incorporated, New York, pp 1–21
12. Broadhead J, Rouan SK, Rhodes CT (1992) The spray drying of pharmaceuticals. Drug Dev Ind Pharm 8:1169–1206
13. Sweetman SC (ed) (2002) Martindale: the complete drug reference. Pharmaceutical Press, London, pp 30–32
14. Rattes ALR, Oliveria WP (2007) Spray drying conditions and encapsulating composition effects on formation and properties of sodium diclofenac microparticles. Powder Technol 171:7–14
15. Sajeev C, Vinay G, Archna R et al (2002) Oral controlled release formulation of diclofenac sodium by microencapsulation with ethyl cellulose. J Microencapsul 19:753–760
16. Duarte ARC, Costa MS, Simplicio AL et al (2006) Preparation of controlled release microspheres using supercritical fluid technology for delivery of anti-inflammatory drugs. Int J Pharm 308:168–174
17. Ozgu¨ ney Sarıgu¨ llu¨ I, Karasulu HY, Kantarcı G et al (2006) Transdermal delivery of diclofenac sodium through rat skin from various formulations. AAPS PharmSciTech 7:39–45
18. ThakareMand Singh KK (2006) Preparation and evaluation of diclofenac sodium controlled release tablets using spray drying technology in aqueous system. Indian J Pharm Sci 68:530–532
19. Dangprasirt P, Ritthidej GC (1995) Development of diclofenac sodium controlled release solid dispersions by spray drying using optimization strategy I. Powder formulation. Drug Dev Ind Pharm 21:2323–2337

20. Bhise KS, Dhumal RS, Paradkar AR et al (2008) Effect of drying methods on swelling, erosion and drug release from chitosan-naproxen sodium complexes. AAPS PharmSciTech 9:1–12
21. Saravanan M, Bhaskar K, Maharajan G et al (2011) Development of gelatin microspheres loaded with diclofenac sodium for intra-articular administration. J Drug Target 19:96–103
22. Desai KG (2005) Preparation and characteristics of high-amylose corn starch/pectin blend microparticles: a technical note. AAPS PharmSciTech 6:E202–E208
23. Corrigan OI, Holohan EM (1984) Amorphous spray-dried hydroflumethiazide—polyvinylpyrrolidone systems: physiochemical properties. J Pharm Pharmacol 36:217–221
24. Okonogi S, Yonemochi E, Oguchi T et al (1997) Enhanced dissolution of ursodeoxycholic acid from the solid dispersion. Drug Dev Ind Pharm 23:1115–1121
25. Merih Sariisik, Mesut Arici, Özlem Topbas, Sinem Yaprak Karavana, Cihat Öztürk, Gökhan Ertan (2013) Design of orthopedic support material containing diclofenac sodium microparticles: preparation and characterization of microparticles and application to orthopedic support material. Textile Research Journal 83:1030. Originally published online 19 April 2013 doi: 10.1177/0040517512464292

Chapter 15
Polydioxanone Weft-Knitted Intestinal Stents

15.1 Introduction

In the case of patients with intestinal cancers, intestinal blockage and stenosis have been noticed in clinical conditions [1]. Investigations have shown that stents can alleviate intestinal obstruction and stenosis [2, 3]. For over thirty years, the metal stents have been used for the treatment of the obstruction and stenosis of bowel and vessels [4]. The metal stents pose problems in further treatment and reduce image quality of magnetic resonance imaging. In the treatment of obstruction and stenosis, biodegradable stents can offer an alternate option. The major advantage of biodegradable stents is different from other kinds of stents in that they can prevent serious long-term complications and do not require removal, thus avoiding further surgeries and potential morbidity [5]. The aliphatic polyesters, such as polylactic acid, poly(L-lactide), poly (lactic-co-glycolic acid), and polydioxanone (PDO), are the very commonly used biodegradable polymers for stents [6]. PDO has many merits over other polymers, such as good flexibility and elasticity, appropriate absorption rate, suitable biocompatibility, and minimal inflammatory response [7–9]. The stents mainly give mechanical support for obstructed intestines, which can restore intestinal lumen and waste flow smoothly. Therefore, it is important to investigate and optimize the mechanical properties of stents. Various models have been used to study the mechanical properties of stents. These are structural mechanical models, such as the Bernoulli–Euler beam theory and the Coulomb torsion theory. In the recent literatures, numerical modeling is often adopted, that is, using finite element method (FEM) analyses to expand stents by imposing pressure to the internal stents struts or by enlarging a rigid cylinder inside the stents in displacement control [10, 11]. Despite a good deal of progress being reported on the influence of weft-knitting parameters on the mechanical properties of intestinal stents, only little literature has been focused on this aspect [12]. For the weft-knitted stents, the advantage is that they can easily be removed

N. Gokarneshan et al., *Emerging Research Trends in Medical Textiles*,
Textile Science and Clothing Technology, DOI 10.1007/978-981-287-508-2_15

by pulling one yarn to unravel the structure. A number of production parameters influence the mechanical performance and geometrical properties of weft-knitted stents [13]. The radial force and circumferential strength of the stents are strongly influenced by a number of yarn, fabric, and process factors [14, 15]. Using fractional factorial design of experiments, we can identify these effects of different parameters (factors) and determine the optimal process settings using these factors [16, 17]. A level of factorial design has been used to estimate the error [16, 17]. This chapter identifies the effect of weft-knitting parameters on the mechanical properties of stents using the statistical modeling method and also suggests optimum parameter settings. The human intestine has been studied for intra-abdominal and intra-intestinal pressure, by adopting an intestine physical model. The complete factorial design has been used to identify the most appropriate factors and the optimum processing parameters for the stent mechanics.

15.2 The Physiological Mechanism of Intestinal Stents

The implantation of the stents into the intestine lumen avoids the obstruction and stenosis. They can withstand the force from the radial direction during the function process. The radial force is exerted perpendicular to the centerline or axis of an object. The utility life of the stents is dependent on proper radial force as they withstand the compression in the abdomen of patients. The circumferential strength is simulated using expanding force by solid wastes in the intestine. The fixation of the stent in an intestine diagnosed with stenosis is shown in Fig. 15.1.

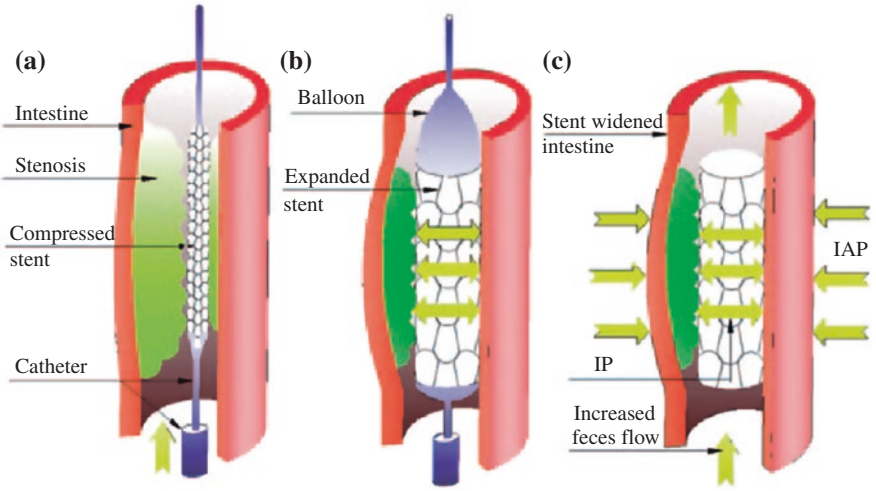

Fig. 15.1 Placement process and mechanical function of the intestinal stent [18]. **a** Deflated balloon catheter and closed stent inserted into the *narrow* intestine. **b** Inflated balloon expanding the stent and compressing the tumor to restore the lumen size of the intestine. **c** Compressed tumor and widened intestine

As can be seen, the implanted stent is compressed due to the abdominal pressure during function process, and hence, it requires suitable radial force to restore its tubular shape against the compression. Similarly, the stent bears the expansion by the intestinal pressure because of the solid feces and movements of the intestine. Thus, the choice and design of stents with appropriate circumferential strength and radial force become crucial.

15.3 Circumferential Strength and Radial Force of Intestinal Stents

Figure 15.2 indicates the intestinal pressure distribution of the human intestine [18–20]. As shown, the pressure in the intestine is between 0.5 and 4 kPa. The pressure values in the small and large intestine range between 1.5–1.9 and 2.1–2.8 kPa, respectively [19]. It can be seen that both the diameter and intestinal pressure of the small intestine are smaller than that of the larger intestines, which means that the diameter and mechanical properties of larger intestinal stents are larger and better than those of small intestinal stents. The pressure hidden inside the abdominal cavity is known as abdominal pressure. The pressure is significantly impacted by the required radial force of intestinal stents implanted. The radial force tested is to determine the force exerted by a stent on the vessel in the deployed state during expansion and compression. Hence, stents with greater

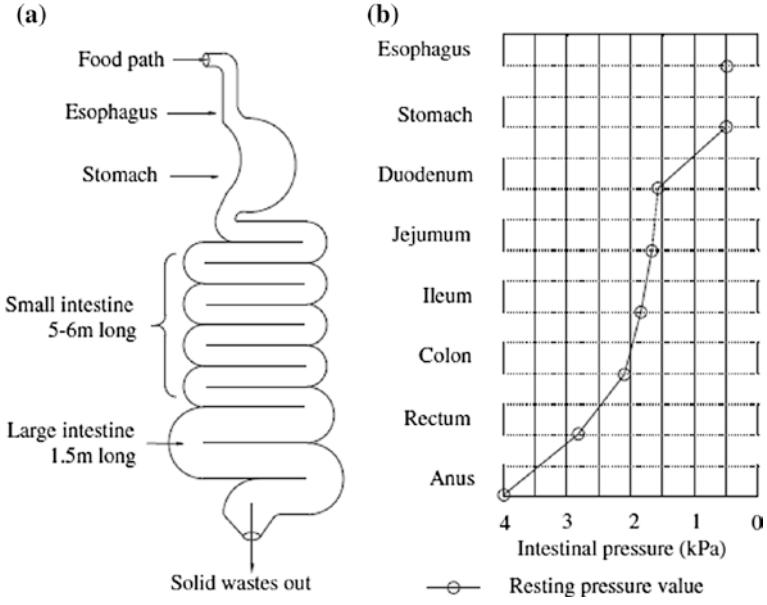

Fig. 15.2 Pressure distribution values in the human intestine [18]. **a** The human digestive system. **b** Intestinal pressure distribution

radial force should be used on patients with higher pressure. The normal human abdominal pressure value is between 2 and 8 kPa. In the case of patients with serious abdominal conditions, the pressure value can go above 30 kPa. Surgical decompression is recommended in patients with moderate or severe pressures [21]. The radial force and circumferential strength can be calculated [22]. The minimal and maximum circumferential strength and radial force of both small and large intestinal stents have been calculated. In the case of small intestinal stents, the circumferential strength and radial force are lower than those for large intestinal stents.

15.4 Synthesis of the Polymer

A conventional bulk ring-opening polymerization technique has been used to synthesize PDO polymer. The PDO yarn has been manufactured by an extrusion process accompanied by a drawing process to form a self-reinforced structure (Fig. 15.3). Two PDO yarns having linear densities of 100 ± 10 and 150 ± 10 tex have been chosen, which are suitable for the needle size in the machine.

15.5 Preparation of Stent Samples

A special type of circular weft-knitting machine has been used for knitting the PDO yarns. The length and diameter of stents can be adjusted based on the computed tomography (CT) analysis of the intestine with stenosis or obstruction in patients. In the investigation discussed herein, the length (60 mm) and radius (10 mm) of stents have been set as the general size of metal stents available commercially. The factors significantly affecting the radial force and circumferential strength have been decided by the use of 2n factorial design. Four factors have been selected—stitch cam setting (mm), fabric tension (cN), yarn tension (cN), and yarn linear density (tex). These factors have been selected since the weft-knitting machine for producing the intestinal stents is not a commercialized one. It is difficult to control the stitch density or loop length using an electronic device automatically. The four factors are easier for optimization, in comparison

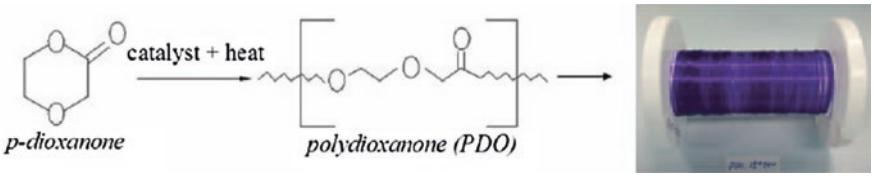

Fig. 15.3 Method of synthesis for PDO yarn [18]

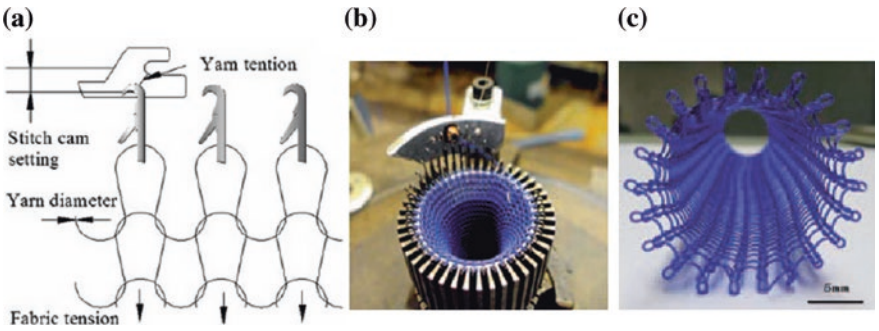

Fig. 15.4 Principles of weft knitting for PDO stent [18]. **a** Weft-knitting principle. **b** Weft-knitting machine cylinder. **c** Prototype biodegradable PDO yarn

with other factors on the machine. The influence of the stitch cam setting on the fabric mechanics has been discussed [23]. This parameter is adjusted by the stitch cam position with a negative yarn filling system. For this special weft-knitting machine with small diameter, it is quick to evaluate the effect of this parameter. The yarn and fabric tension have been determined when they are loaded by external force. All of these factors mutually impact on the final mechanical performance of stents in this special case. All the factor levels have been chosen considering the operation limits of the experimental machines and the yarn properties. An experimental matrix with 2n factorial design (n is the number of factors, each run at two levels) has been selected [24], and a total of 16 different weft-knitted stent samples have been produced [18, 23, 24] (Fig. 15.4).

15.6 Mechanical Properties of Polydioxanone Yarns

The measurement of tensile properties of the adopted yarns has been done adopting the British standards. Twenty readings have been obtained for every yarn with identical testing conditions so as to obtain reliable average data [18]. The yarns have been pretensioned to remove the stress for maintaining the standard test condition for all samples. Figure 15.5 depicts the tensile curves of PDO, polypropylene, and polyester yarns.

The elongation (X-axis) and tenacity (Y-axis) of three types of yarns given in Fig. 15.5 were calculated using Eqs. (3) and (4), respectively. It is shown that PDO has a much better tensile property; therefore, PDO could be more suitable for intestinal stents in terms of mechanical property:

$$\text{Elongation } (\%) = \frac{E \times 100}{L}$$

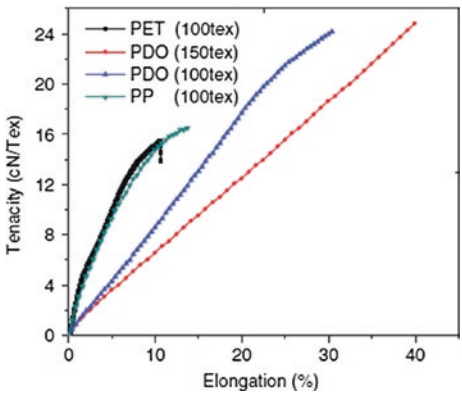

Fig. 15.5 Tensile properties of polydioxanone(PDO), polyethylene terephthalate(PET), and polypropelene [18]

where L is initial length of specimen (mm) and E is the increase in length of the specimen (mm):

$$\text{Tenacity(cN/Tex)} = \frac{F_{\max}}{F}$$

$F_{\max}$ is the maximum force of the test specimen in cN and T is linear density in tex, measured on the same package.

15.7 Mechanical Property Characterization for Weft-Knitted Stents

In order to determine the force exerted by a stent on the vessel after it has been fixed to the intestine, during expansion and compression, it is subjected to prior radial force test as per suitable British standards [9]. The radial force has been determined by measuring the force required to change the diameter of the stent using a modified compression instrument. The machine was set up as shown in Fig. 15.6a, b, for performing the radial force test and circumferential strength as well [18]. Samples were subjected to area loads at standard room temperature (20 ± 2) °C and relative humidity 65 %, and their circumferential strength was measured at head speed (5 mm/min) and full scale (5000 N).

15.8 Mechanical Performance Prediction of Weft-Knitted Stents

The basic parameters and properties of knit fabrics such as stitch density, fatigue resistance, compliance, and elastic recovery become important in the evaluation of intestinal stents. In order to minimize the possibility of stent migration, the stitch

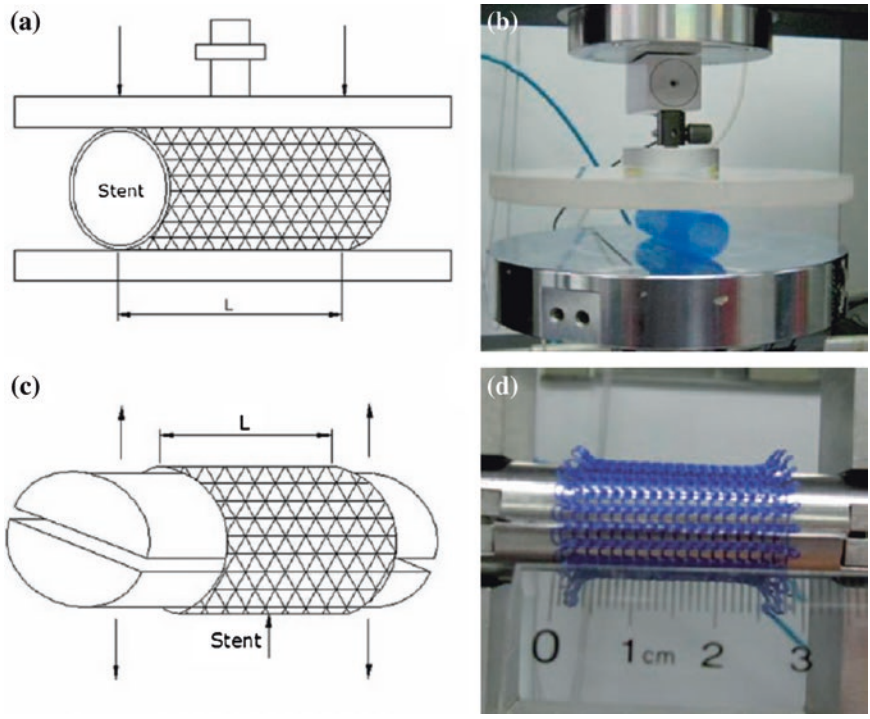

Fig. 15.6 Measurements of radial force and circumferential strength [18] (**a**) and (**b**) modified instruments for testing radial force

density was set as for the general metal stents in the market. Four factors have been selected for inclusion in the quadratic (second-degree) polynomial models to model each response by the best ANOVA technique. A p value is the probability (within a 95 % confidence interval) that the factor has a significant impact on the response. According to the p value corresponding to the terms of the proposed models, the results from the analysis show that the stitch cam setting, fabric tension, yarn tension, and yarn linear density have a significant effect on radial force and circumferential strength. The coefficient of determination is an indicator to indicate the value of response changes when the value of the variable increased by one (code value) and other variables do not change. The values of stitch cam setting and fabric tension exhibit a negative coefficient that means the values of yarn radial force or circumferential strength reduced, whereas two factors increased [18]. On the other hand, the values of yarn tension and yarn linear density show a positive coefficient that means the values of Y1 and Y2 increased when two factors increased. Data have been obtained for the prediction models for Y1 and Y2 and help to evaluate the effect of each variable to responses Y1 and Y2. The ANOVA indicates that regression models are adequate due to high coefficient of determination R2. The R2 values of Y1 and Y2 are 99.08 and 98.72 %, respectively. It

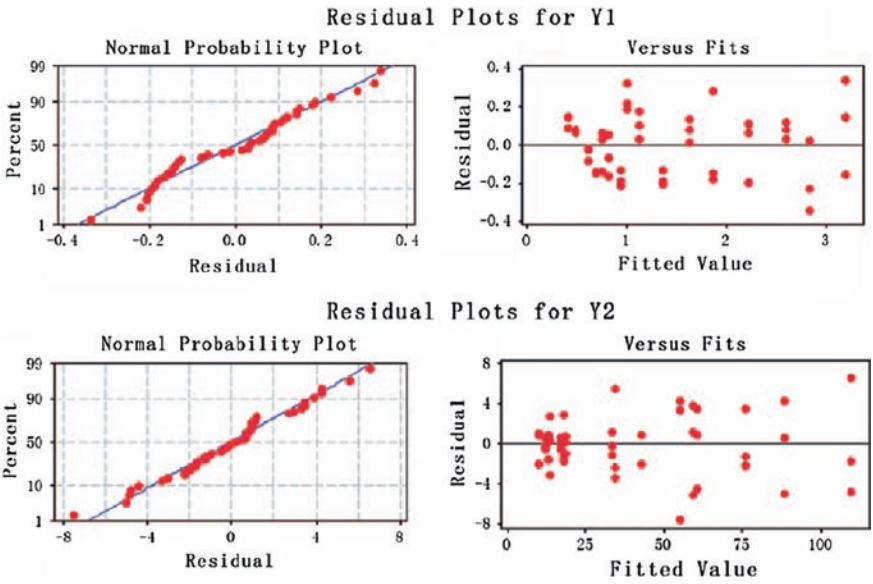

Fig. 15.7 Normal plots of residual and residual versus fits [18]

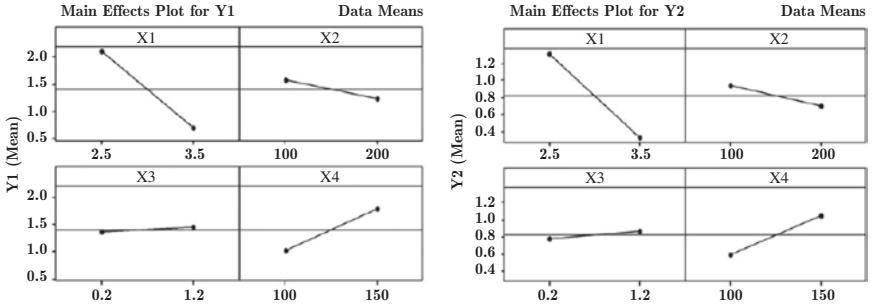

Fig. 15.8 Main effect plots for radial force and circumferential strength of weft-knitted stents [18]

suggests that the proposed models of Y1 and Y2 can describe 99.08 and 98.72 % of the variation in the data. The normal plot of residual and residual versus fits for Y1 and Y2 is indicated in Fig. 15.7. The models show a good fit. Hence, the proposed model is acceptable. The influence of stitch cam setting, fabric tension, yarn tension, and yarn linear density on radial force and circumferential strength is depicted in Fig. 15.8. The results indicate that the yarn tension and yarn linear density are the most important factors for stent mechanical properties. In particular, the radial force and circumferential strength of stents can be increased when

the stitch cam setting and fabric tension decreased, or yarn tension and yarn linear density increased.

15.9 Optimization of Weft-Knitted Stent Performance

The mechanical properties of weft-knitted stents have been optimized by optimizing textile parameter settings. The contour plot method has been used to indicate the values and processing parameters for every desirable response. The stitch cam setting, fabric tension, and yarn linear density have been selected as three of the most representative significant parameters for two responses. Each contour plot includes the response and the related two factors; other factors were given at constant values. The constant value can be held at low, middle, and high levels. The maximum value of the response should be different when selecting various levels, because of the different coefficients in the regression model of each response. Points having similar response are connected to produce contour lines of contour responses. The two crucial textile parameters for each weft-knitted stent performance have been identified from main effect plots (Fig. 15.8). Contour plots show that the stitch cam setting and fabric tension can result in optimal values of radial force and circumferential strength for weft-knitted stents. On observing the circumferential strength, the area showing highest circumferential force is indicated as the darkest gray zone (>100 cN/mm). From the calculated values for the radial force of small and larger intestinal stents, the settings for the stitch cam setting, fabric tension, and yarn linear density can be selected in the specific areas of the plots. As an instance, in the areas (stitch cam setting of 2.8–3.1 mm and fabric tension up to 205 cN, or stitch cam setting of 2.6–2.8 mm and yarn linear density up to 125–145 tex, or fabric tension lower than 105 cN and yarn linear density in the range of 105–116 tex), the optimized radial force can be higher than 2.0 cN/mm. Several combinations of weft-knitting parameters are available, which result in a large scale of radial force and circumferential strength for stents. Hence, further optimization of the parameter setting and minimization of the optimum range is required. The radial force and circumferential strength are considered to be very important for intestinal stents, based on the investigation of physiological mechanism. The correlation between radial force and circumferential strength of 12 fabrics is shown in Fig. 15.9, and it clearly shows a close relationship between radial force and circumferential strength of weft-knitted stents. Hence, the circumferential strength is much easier to achieve to high value than radial force. For example, the column value of sample Q5 given in Fig. 15.9 is the highest radial force of 5.5 cN/mm and its circumferential strength can also reach the highest of 165 cN/mm. It would imply that the stent is much more likely to squash than rupture. Hence, it is necessary to ensure that the radial force of the stent is adequate during the fixation of the stent.

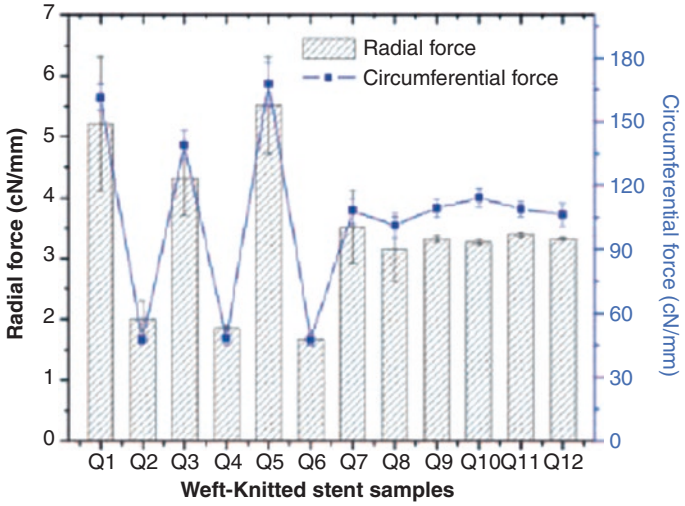

Fig. 15.9 Relation between radial force and circumferential strength of the weft-knitted stents [18]

15.10 Validation of the Statistical Models

Based on the calculated circumferential strength and radial force values, in the fabrication of small intestinal stents with the necessary radial force between 1.3 and 2.5 cN/mm, and circumferential strength between 20 and 50 cN/mm (the value range is higher than the minimum required due to the intrinsic property of the weft-knitted stents), it is possible to predict the process parameters for the stent using the proposed models. The overlaid contour plots indicate that the predicted values of the stitch cam setting and fabric tension can result in desirable values of radial force and circumferential strength (Fig. 15.10). Although yarn linear density is the significant factor to radial force, this factor has not been selected because of the current limitation of yarn spinning machine. If the yarn tension and yarn linear density were held at 1.2 cN and 150 tex, respectively, it can be concluded that using a stitch cam setting between 3.2 and 3.4 mm and fabric tension between 140 and 160 cN, it could be a good compromise to obtain compliant weft-knitted stents with minimum long-term rupture risk and good performance. Based on the predicted process parameters, another three groups of fabrics have been fabricated to validate the statistical models [18]. The radial force and circumferential strength of these fabrics have been determined and compared with the values predicted theoretically. The results show that there is still small variance between predicted values and actual values from the actual experiments. This is due to the fact that the weft-knitted structure of stents can cause slippage of loops. In the fabrication and

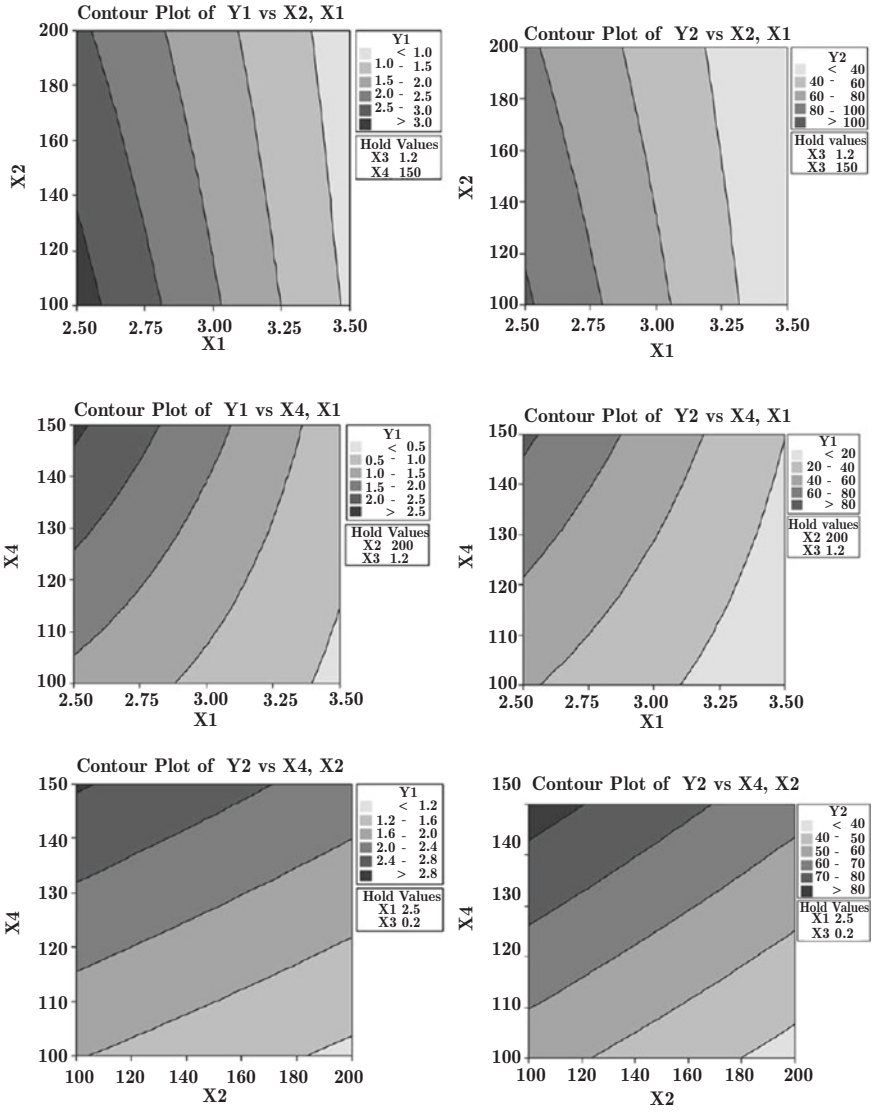

Fig. 15.10 Contour plots of Y_1 and Y_2 versus stitch cam setting, fabric tension, and yarn linear density [18]

the measurement process, errors can be caused due to both the loop slippage and flexible structure of stents. As illustrated in the introduction, the FEM has been used by researchers in simulation of stent mechanics. However, the stent structural models are all solid models in which these stent loops are connected by the solid mode. The loop slippage has not been highlighted. Hence, based on this work,

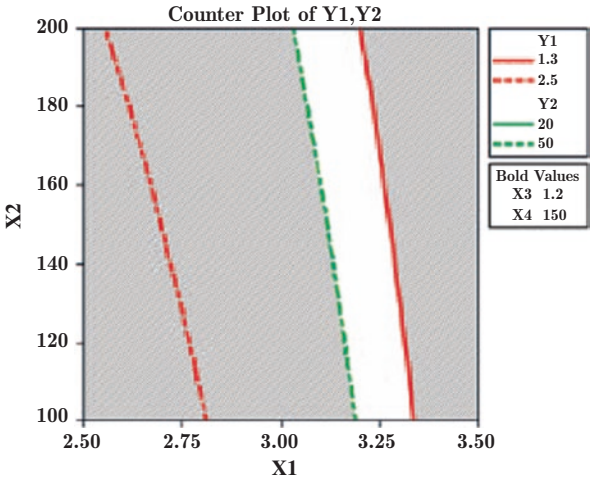

Fig. 15.11 Contour plot of radial force with various fabric tensions and cam settings [18]

modeling actual geometry structure for stent use, the FEM is recommended to improve the accuracy of prediction for stent mechanics in the future (Fig. 15.11).

References

1. Watson A, Shanmugam V, Mackay I et al (2005) Outcomes after placement of colorectal stents. Colorectal Dis 7:70–73
2. Mauro MA, Koehler RE, Baron TH (2000) Advances in gastrointestinal intervention: the treatment of gastroduodenal and colorectal obstructions with metallic stents. Radiology 215:659
3. Khot U, Lang AW, Murali K et al (2002) Systematic review of the efficacy and safety of colorectal stents. Br J Surg 89:1096–1102
4. Vearick SB, Michelon M, Schaeffer L et al (2007) Development and in vivo testing of a nitinol tracheal stent. J Biomed Mater Res B 83:216–221
5. Stivaros S, Williams L, Senger C et al (2010) Woven polydioxanone biodegradable stents: a new treatment option for benign and malignant oesophageal strictures. Eur Radiol 20:1069–1072
6. Zilberman M, Nelson KD, Eberhart RC (2005) Mechanical properties and in vitro degradation of bioresorbable fibers and expandable fiber-based stents. J Biomed Mater Res B Appl Biomater 74:792–799
7. Saito Y, Minami K, Kobayashi M et al (2002) New tubular bioabsorbable knitted airway stent: biocompatibility and mechanical strength. J Thorac Cardiovasc Surg 123:161
8. Rejchrt S, Kopcov M, Brtov J (2009) Intestinal biodegradable stents. Initial experience in the Czech Republic. Folia Gastroenterol Hepatol 7:7–10
9. Kontio R, Ruuttila P, Lindroos L et al (2005) Biodegradable polydioxanone and poly (l/d) lactide implants: An experimental study on peri-implant tissue response. Int J Oral Maxillofac Surg 34:766–776
10. De Beule M, Van Impe R, Verhegghe B et al (2006) Finite element analysis and stent design: reduction of dogboning. Technol Health Care 14:233–241
11. Hall GJ, Kasper EP (2006) Comparison of element technologies for modeling stent expansion. J Biomech Eng 128:751

12. Van Der Merwe H, Daya Reddy B, Zilla P et al (2008) A computational study of knitted nitinol meshes for their prospective use as external vein reinforcement. J Biomech 41:1302–1309
13. Yuksekkaya ME, Adanur S (2009) Analysis of polymeric braided tubular structures intended for medical applications. Textil Res J 79:99–109
14. Fatkić E, Geršak J, Ujević D (2011) Influence of knitting parameters on the mechanical properties of plain jersey weft knitted fabrics. Fibres Textil East Eur 19:88
15. Choi MS, Ashdown SP (2000) Effect of changes in knit structure and density on the mechanical and hand properties of weft-knitted fabrics for outerwear. Textil Res J 70:1033–1045
16. Nakarani M, Patel DJ, Bhimani DR et al (2010) Design and optimization of mucoadhesive hydrophilic matrix tablet containing atenolol using central composite design. Acta Pharmaceutica Sciencia 52:400–409
17. Annadurai G (2000) Design of optimum response surface experiments for adsorption of direct dye on chitosan. Bioproc Eng 23:451–455
18. Li G, Li Y, Lan P, He X, Hu H, (2011) Polydioxanone weft-knitted intestinal stents: fabrication and mechanics optimization. Textile Res J 83(20):2129–2141
19. Martinez-de-Juan J, Saiz F, Ponce J et al (1998) Retrieval of the small intestinal pressure from time-frequency analysis of the electroenterogram. Proc IEEE EMBS Hong Kong 3:1505–1508
20. Yan R, Yan G, Guo X et al (2010) A practical measuring system for intestinal pressure activity and its clinical application. Biomed Signal Process Control 5:82–86
21. Wittmann DH, Iskander GA (2000) The compartment syndrome of the abdominal cavity: a state of the art review. J Intensive Care Med 15:201–220
22. Mokhtar S, Abdessalem SB, Sakli F (2010) Optimization of textile parameters of plain woven vascular prostheses. J Textil Inst 101:1095–1105
23. Spencer DJ (2001) Knitting technology. In: A comprehensive handbook and practical guide, CRC, Boca Raton, Florida
24. Montgomery DC, Myers RH (2002) Response surface methodology. In: Process and product optimization using designed experiments, 2nd edn. John Wiley & Sons, Hoboken, New Jersey

Chapter 16
Nonwoven Cellulose Substrates for Modern Wound Dressings

16.1 Introduction

The wounds caused by burns and pressure sores and of acute and chronic nature generally excrete exudates in high quantities. Despite the fact that exudation the natural response of the body's defense mechanism, it can prevent wound healing and provide an effective medium for microbial growth [1]. These wounds require specific treatment, as improper treatment can result in serious infections or even prove fatal [2]. The key for successful wound treatment is to ensure the surrounding area of the wound, as well as the healthy part of the skin, is protected from infection by opportunistic bacteria [3, 4]. These infections can be prevented by the use of presently available antimicrobial creams, foams, hydrogels, hydrocolloid and polymer films, and textile medical dressings [5, 6]. Even though silver has been used as an antimicrobial agent for more than 2000 years, the proof of its potential cytotoxicity is much more recent [7–10]. There have been a number of research studies on silver recently, which has paved the way to new technological solutions at enable a safe silver attachment or alternative means of antimicrobial activity [11–14]. The moisture present in the wound becomes one of the crucial factors that influence the wound healing capacity [15]. Functional materials that enable this are hydrophilic medical dressings which, due to their characteristics (increased absorption of the exudate's hydrophilic components), are capable of absorbing the exudate and some other impurities from the wound [16]. In the treatment of pressure sores and burns, cellulosic materials and their derivatives are being used as host materials in medical dressings. In order to improve the hydrophilicity of cellulosic materials, standard chemical procedures are used in the textile industry, i.e., mercerization. Various kinds of other cellulose material modifications are mentioned in the literature. Among these are heat treatment, combination of cellulose materials with other moieties (e.g., silane derivatives), and regeneration of cellulose derivatives to pure cellulose [17–19]. One of the normally adopted techniques is an alkaline treatment that results in

N. Gokarneshan et al., *Emerging Research Trends in Medical Textiles*,
Textile Science and Clothing Technology, DOI 10.1007/978-981-287-508-2_16

a better and quicker binding of reagents, as well as a softer feel [20, 21]. Alkaline treatment causes changes in the structure of the cellulose material, which lead to its increased hydrophilicity, but simultaneously affect the material's mechanical properties. The procedure requires the use of huge quantities of chemicals (sodium hydroxide) and thus poses an environmental problem. Gas plasma process offers more ecologically acceptable options to chemical processes [22–24]. The plasma technique enables homogenous surface treatment; its main advantage is maintaining technological parameters (mechanical properties), while improving the hydrophobic and hydrophilic properties of the material [25–28] depending on the input gases used. The objective of the topic discussed in this chapter is to explore various techniques for modifying the host cellulosic material so as to achieve satisfactory antimicrobial activity and suitable hydrophilicity. The use of the solgel process enabled binding with commercially available silver chloride nanoparticles on the host material and helps achieve a satisfactory antimicrobial effect. The choice of a suitable method for the attachment of silver chloride nanoparticles was based on one earlier studies, where comparison has been made on the influence of differently chemically modified solgel systems on the adsorption of these nanoparticles and their release from viscose nonwoven [29]. A commercial solgel system has been adopted since the same formulation was already effectively attached onto a cellulose-based fabric and due to the fact that such materials have a better possibility to be used in commercial wound dressings during the times to come [30, 31]. The greatest attention was paid to finding the optimum modification processes of the cellulosic nonwoven in order to enhance its hydrophilic properties. The techniques used to verify the hypotheses are scanning electron microscopy (SEM), in vitro release studies with Franz diffusion cell, atomic absorption spectroscopy (AAS), antimicrobial activity testing, powder contact angle method, water retention value, atomic force microscopy (AFM), dynamic light scattering (DLS), and mechanical properties determination.

16.2 Topography and Morphology of Surface

SEM technique with low magnification has been used for studying the longitudinal views of single fibers (Fig. 16.1) [32]. Evidently, the surface of the sample does not reveal that any site-specific changes can be observed on any sample surface. The entire changes in the surface caused by the used treatments appear to be almost evenly distributed over the whole fiber surface. Several fibers from different parts of the treated nonwoven samples were examined with SEM and mentionable discrepancies could not be found (addition).

The SEM images with a higher magnification show the samples having differences between the treatment procedures exhibited in a more pronounced manner (Fig. 16.2). The extent of change, resulting from different fiber treatment, varies from no morphological changes at all to highly altered surface features. The samples P, SP, and ASP, appear to exhibit most significant changes, where plasma treatment was the final procedure [32].

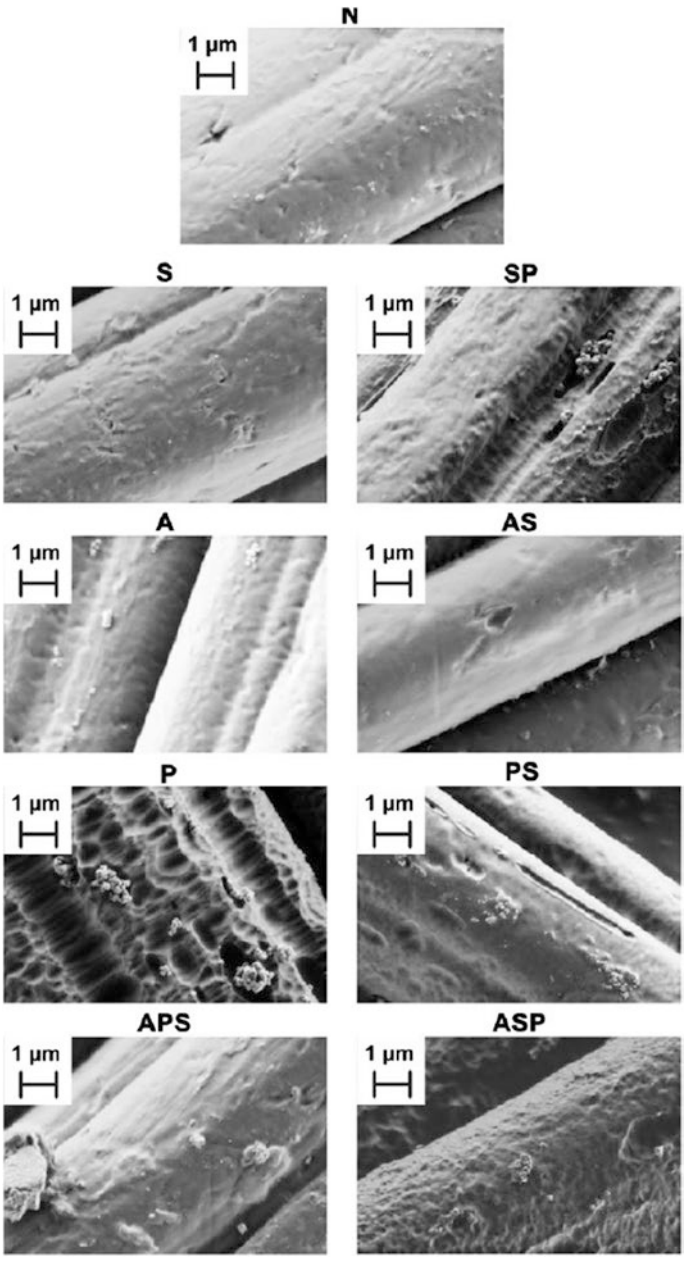

Fig. 16.1 Microscopic views of untreated and differently treated viscose nonwoven (low magnification) [32]

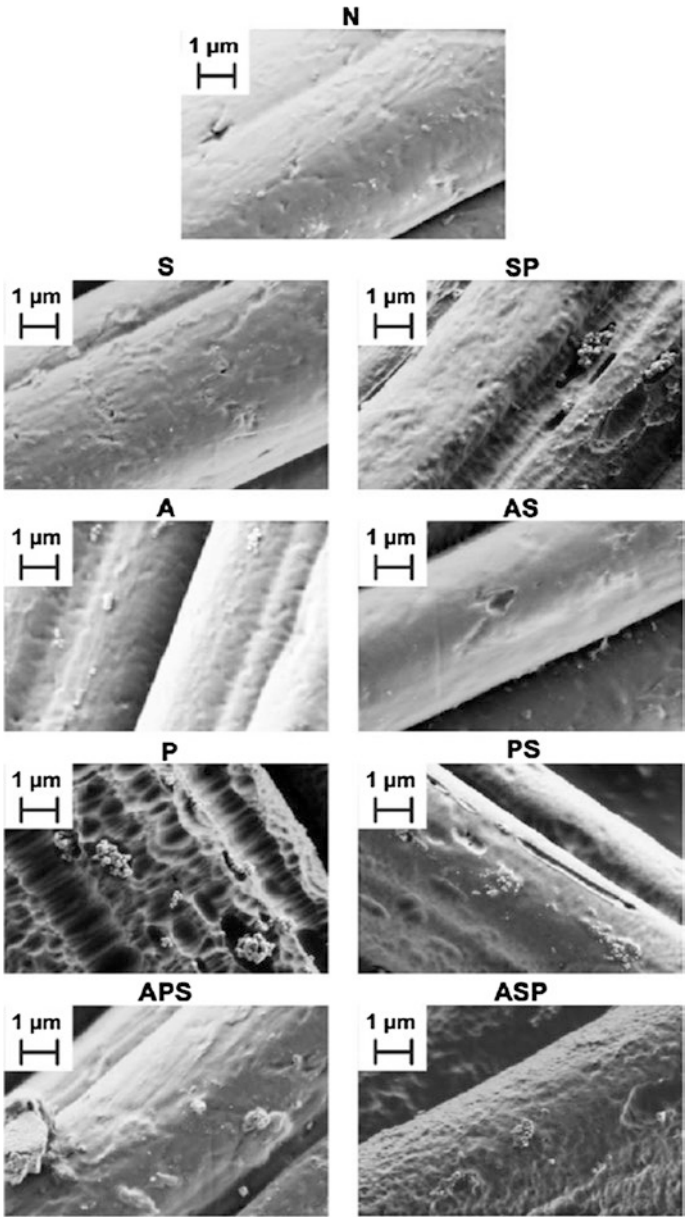

Fig. 16.2 SEM micrographs of the untreated and differently treated viscose nonwoven with high magnification [32]

This is due to the fact that plasma treatment not only leads to surface functionalization, but also affects the surface due to etching, that follows procedure of the plasma treatment. Of all the samples, sample P shows holes on the surface having a diameter of some hundred nm. The other two samples, where plasma treatment was the final preparation step (SP and ASP), experienced less rigorous changes. Samples in which the final attachment of silver chloride nanoparticles through the solgel process (S, AS, PS, APS) show a smoother surface compared to untreated samples. The same is also true for samples where plasma treatment was used prior to the attachment (samples PS and APS). In these samples, the plasma-induced changes are less pronounced when compared to the samples where the silver nanoparticle attachment was not applied. It can be noticed particularly on the edges of holes and surface bumps, where these appear to be more rounded. The areas in which various features (such as holes, bumps, and channels) can be noticed before treatment are now for the most part covered with thin surface films. This effect leads to an overall reduced surface roughness in comparison with the untreated sample (in the case of S and AS) or the samples P and AP (in the case of samples PS and APS). The latter is a result of the used solgel procedure for the attachment of silver particles (the surface of fibers is first covered with a thin layer of the solgel solution, which is evenly distributed over the surface. It is then transformed to the gel state and leads to a smoother surface, as can be seen in Figs. 16.2 and 16.3). The least pronounced effect on the surface is due to treatment with sodium hydroxide, which exhibits no observable effect on the surface of treated fibers. The sodium hydroxide treatment produces a reaction with cellulose, thereby forming sodium cellulose. Silver particles could not be observed on the surface of the fibers, probably due to their incorporation inside the surface solgel films. Also EDS and FTIR techniques have been used to add to the overall inter-operation of structural and morphological changes. The EDS technique has been unsuccessful due to the experimentally proven threshold for observation of silver on the surface, which has been shown to be above 600 ppm. The incorporated amount in the samples is far less, while FTIR could not deliver explicit proof about any surface changes due to the complex nature of the cellulose-based samples and the absence of observable interactions between silver and cellulose.

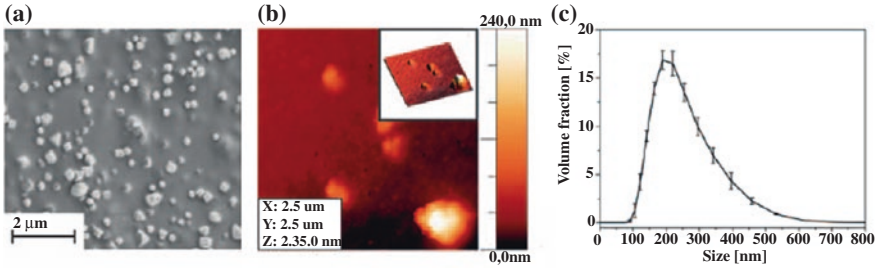

Fig. 16.3 Silver particle size determination with **a** SEM, **b** AFM, and **c** DLS [32]

16.3 Determination of Surface Silver Concentration and In Vitro Silver Release Evaluation

The quantity determination of the incorporated silver revealed that all silver-treated samples (S, PS, SP, AS, ASP, and APS) showed a concentration above the threshold, required for producing the antimicrobial effect (0.060 mg/g) [33]. The concentration of silver for these samples ranged between 0.077 and 0.141 mg/g.

16.3.1 In Vitro Silver Release Studies

The cytotoxicity of silver is a relatively new approach that has recently paved the way for alternative methods of producing antimicrobial effect, i.e., by amino acid-based antimicrobial agents [34–40] or finding ways to safely attach silver in wound care products [2, 13, 41]. Regarding the latter, it is very necessary to ensure that after long-term use of the product, the silver release is prevented to an extent, as otherwise it can cause cytotoxic effect. Investigation has been done regarding the limit value of silver release from commercial medical dressings at which an antimicrobial effect has still been noticed. It has been shown that if less than 2 mg/L of silver is released within 24 h, no significant cytotoxic effect can be observed [10]. This value was taken into account during preparation of silver-coated fibrous substrates in such a way that its release would not exceed the limit value, and thereby a safe antimicrobial effect is achieved [32]. The solgel process has been used to bind silver nanoparticles safely on cellulose fibrous material. This proved to be extremely efficient since the silver release from treated samples (as determined with Franz diffusion cells) and the measurements of the silver concentration in the solution after the release showed that, regardless of the sequence/combination of the used sample treatment processes, the concentration of silver release was very low. The entire measured data revealed silver concentration values below the detection limit, which is less than 0.05 mg/L. This investigation also established that silver cytotoxicity not only depends on the concentration of the bound silver in the dressing, but also on other factors, particularly the method of silver binding in the dressing and its affinity to moisture [10]. Medical dressings with greater hydrophilicity thus release less silver into the wound and are also less toxic to human cells since the bacterial kill zone in such instances is transferred to the interior of the dressing. On this basis, it is possible to conclude that a lower silver release was achieved in samples that had been alkaline and plasma-treated in order to increase hydrophilicity, as opposed to those without pretreatment prior to solgel coating. Further measures have been taken in order to ensure complete safety toward the silver's potential cytotoxic effect. Emphasis has also been shown to the size of the attached silver nanoparticles, as it is known that the skin presents a rather big barrier for bigger particles. Commercial nanoparticles are a suitable choice, as their size, ranging from 100 nm to 500 nm, can permeate the skin [30].

The size of silver nanoparticles in a suspension iSys Ag has been confirmed by several techniques. The SEM, AFM, and DLS techniques have been used to measure the size values of silver particles. Figure 16.3 shows the images obtained with the microscopy techniques, along with the particle size distribution.

The results obtained with different methods match and can also be confirmed with data from the published literature. Hence, even if silver chloride particles are released, they cannot penetrate into the body. The methods of measurement and release of silver are found to be suitable for the safety assessment of medical dressings with attached silver. But, it does not answer the effect of treatments for improving hydrophilicity on the silver release from fibrous viscose nonwoven. This aspect has been discussed in more detail in the foregoing sections.

16.3.2 Reduction of Bacteria

The antimicrobial activity of untreated and treated viscose fibrous samples has been studied. The studies reveal that there has been no decrease in the bacteria *Staphylococcus Aureus*, *Escherichia. Coli*, and *Pseudomonas Aeruginosa* in the untreated viscose sample, whereas there has been a decrease of *Enterococcus Faecalis* has been 77 %. The viscose nonwoven alkaline-treated sample also does not exhibit antimicrobial activity against *E. Coli, E. Faecalis,* and *P. Aeruginosa*, while the decrease of *S. Aureus* has been 99 %. Plasma treatment has effectively decreased the number of *S. Aureus* and *E. Faecalis* bacteria, whereas an increased antimicrobial effect has been noticed on *E. Coli* and *P. Aeruginosa*. As the antimicrobial activity is not to be expected after the oxygen plasma treatment and after the alkaline treatment where the alkali has been rinsed from the material, the obtained results could be seen as an error in the chosen antimicrobial testing method [32]. According to the standard, after the bacterial suspension has been incubated with the sample, bacteria are excluded from the material by adding 100 ml of distilled water and shaking for 1 min. Thereby discrepancies in the number of bacteria released into the water from more or less hydrophilic samples could occur. Despite the hydrophobic properties of the bacterial cell membrane, the result obtained with the antimicrobial test indicates the adsorption of bacteria to the viscose nonwoven, since the plasma-treated sample, that is the most hydrophilic, showed a reduction in two out of four bacterial strains [42]. The decrease has been seen in only one bacterial strain, in the case of the alkaline-treated and the reference samples. The antimicrobial effect of all the silver-treated samples is evident. Silver, which is known to effectively destroy numerous microorganisms (broad-spectrum effect), also destroyed the *S. Aureus* bacteria in investigation done. These microorganisms have the potential to cause many human diseases from skin infections (impetigo or scabbing, postural rash, boils, carbuncles, skin abscesses, etc.) to life-threatening diseases such as pneumonia, meningitis, osteomyelitis, endocarditis, toxic shock syndrome, bacteremia, and septicemia. *S. Aureus* is one of the five most common pathogens in hospital infections and

often causes postoperative wound infections [43]. All the silver-treated dressings also inhibited the *E. coli* bacteria, which is best known as intestinal bacteria, but can cause infection in almost any organ or anywhere in its host due to its opportunistic character; namely it takes advantage of other bacterial infections in the body for its own growth. All infections result in bacteremia and subsequently to sepsis and septic shock [44, 45]. All samples of viscose nonwoven, except the alkaline-treated sample, effectively decreased *E. Faecalis* bacteria, which are connected to endocarditis and bacteremia, urinary tract, blood circulation, and postoperative wound infections [46–48]. Also, they are resistant to many types of antibiotics [49]. Silver-treated medical dressings can destroy *P. Aeruginosa* bacteria that cause infection of burns and open wounds. The solgel system without silver may also contribute to a lesser extent to the antimicrobial activity, as some studies represent the silanols as a novel class of antimicrobial agents [50]. Considering the present and other studies [2, 6, 11, 13, 29, 42, 51], and because of silver's great efficiency, finding better methods for binding of silver, while simultaneously ensuring suitable hydrophilicity, is a more favorable approach than completely denouncing silver due to its possible cytotoxicity. The use of super hydrophilic materials in combination with silver binding techniques adopting the solgel process has made it possible.

16.3.3 Water Contact Angles and Water Retention Values

Medical dressings are expected to possess hydrophilicity, as it enables absorption of exudates, bacteria, and other impurities from a wound [32]. Figure 16.4 depicts the hydrophilic properties of the untreated and differently treated samples as water contact angles and water retention values. The water retention experiments have been carried out in quadruplicate; accordingly, the results are presented as averages with standard errors. It can be seen from the figure that all the treatment combinations enhanced the hydrophilic properties of viscose nonwoven. But, each treatment contributed differently to the reduction in the contact angle between the material and water (samples A, P, and S).

The sequence of treatments and their combinations also had varied effects on the contact angle. Contribution of an individual treatment in combination with others is not the same as the result of an individual treatment. A decrease of 35 % in the contact angle has been observed in the alkaline-treated sample A compared to the reference sample. The biggest reduction in the contact angle is noticeable in the plasma treatment (sample P) and amounts to 67 %. The viscose nonwoven silver-treated samples have been least affected in hydrophilic properties and had the minimum contact angle. The contact angle was reduced by 19 %. To ensure wound healing, a medical dressing has to have an excellent hydrophilic as well as antimicrobial activity. Hence, research also focused on finding the right combination of the mentioned treatments. As shown in Fig. 16.4, the sample AS, which first underwent alkaline and then antimicrobial treatment,

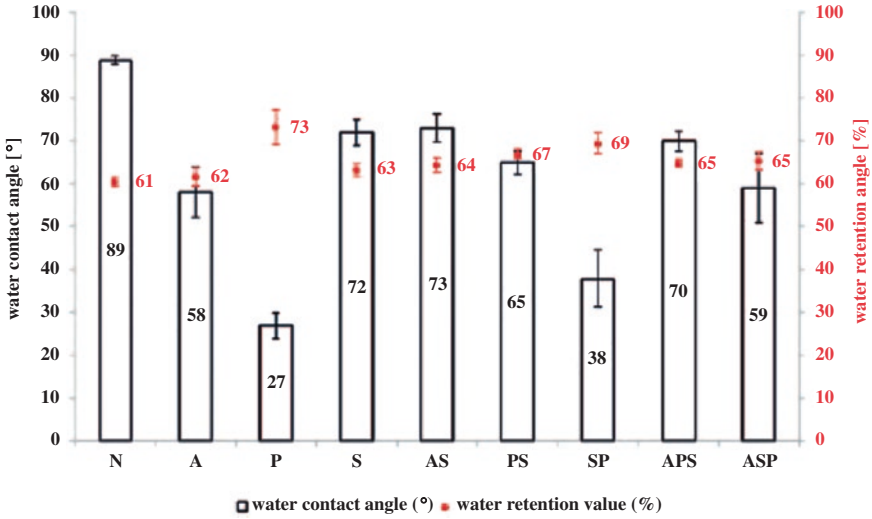

Fig. 16.4 Hydrophilic properties for the untreated and differently treated samples of cellulose nonwoven [32]

does not exhibit such good hydrophilic properties as it did after the alkaline treatment alone (sample A). The contact angle has decreased by 18 % compared to the reference sample and is practically the same as in the sample S. Thus, it can be concluded that the solgel process nullified the effect of the alkaline treatment, expanded the structure of cellulose fibers, and hence enabled the access to the amorphous regions of the fibers interior [50]. This can be attributed to the overlaying of viscose fibers with the solgel coating, which prevented water penetrating through the surface of the fibers and into their interior. Similar results are observed when comparing the samples P and PS, which were plasma-treated to get hydrophilicity. Applying oxygen plasma with a high density of neutral oxygen atoms that react with the surface of the viscose material results in two different effects. Firstly, it creates new oxygen-rich functional groups (among other—COOH groups), and secondly, it enlarges the openings on the fiber surface [22, 23]. This can be observed in Figs. 16.2 and 16.3 (especially for sample P). Combined effect of the etched surface and the presence of hydrophilic functional groups on the surface is an excellent hydrophilicity of the modified material. Further treatment of such material using the solgel system would most likely make the fiber surface more waterproof, as in the sample AS. Also, the combination of both techniques to increase the material's hydrophilicity and subsequent treatment using silver (sample APS) did not significantly reduce the contact angle. The sample SP showed different results for that was first treated with the solgel system and subsequently plasma-treated. The measurements of contact angle and the SEM micrograph analysis have revealed that the oxygen plasma treatment resulted in changes of the previously solgel-coated fibers. The

sample P showed less significant changes compared to the previously untreated material. The reason for this is most likely in the chemical composition of the iSys LTX binder, whose components are of organic–inorganic origin. As it has been proved that a satisfactory reduction in the contact angle (57 %) is reached with a combination of treatments, i.e., first a solgel coating, followed by a plasma treatment (sample SP), the same or improved results were expected in the case of the sample ASP. But, no improvement in the hydrophilic properties has been noticed with the alkaline pretreatment of the sample, as the contact angle of the finally treated sample has decreased by only 34 %. The cause of the increased contact angle—as compared to the sample SP—could lie in the greater concentration of the solgel system that was adsorbed to the previously alkaline-treated material. Initial investigations have revealed an increase of three times in the concentration of the adsorbed solgel reaction mixture. But, additional studies will be required to find a statistically significant correlation between the treatment effect and the mentioned solgel adsorption. The alkaline treatment, which is known to effect the inter-molecular hydrogen bonds between cellulose chains, is expected to loosen the fibers' structure and open its pores [52, 53]. The latter could have had an effect on the greater solgel precursor absorption that plasma could not modify as successfully as the untreated viscose surface. Comparison of samples P and SP showed similar effect. The influence of the different treatments on the contact angles, as explained above, are mostly confirmed by the comparison of the water retention results (Fig. 16.4). The water retention value for the sample A stands out, since it could be expected to be slightly by higher, given the results of the contact angle measurements. The sample P showed the greatest water retention percentage. The plasma and alkaline treatments create difference in the degree of retained water and contact angle values. The contact angle has a more pronounced effect and creates hydrophilic groups on the surface of the material and in its interior as well. In order to achieve greater hydrophilicity with alkaline treatment, a higher alkali concentration should be used. The pores of the cellulosic fibers that were initially enlarged with alkaline swelling get closed due to the high drying temperature that subsequently follows the alkaline treatment (70 °C). The influence of high temperature on cellulose has also been reported, wherein it has been found that heat treatment increases surface hydrophobicity and reduces swelling capacity of cellulose model thin films [17]. As the solgel system covered the fiber surface and blocked its pores with applied antimicrobial coatings, the improvement in water retention of all the samples has been insignificant. Only plasma slightly modified their hydrophilicity (sample SP).

16.3.4 Mechanical Properties

The tensile properties of differently treated viscose samples have been measured in terms of breaking force and elongation [32]. These factors are considered to be crucial as the investigation aims to develop medical dressings that must not tear

during application or removal from the wound. This creates additional pain for the patient and also further damages the already sensitive wound and surrounding tissue. The breaking force for differently treated viscose samples, measured in horizontal and longitudinal directions, is presented in Fig. 16.5.

The elongation in longitudinal and horizontal directions is presented for all samples, depending on the treatment used (Fig. 16.6). When the untreated sample and modified ones have been compared, it is found that all treatment procedures increased the breaking force of the material [32].

Among them, the sample ASP, which underwent first the alkaline, then the antimicrobial, and in the end the plasma treatment, exhibits the greatest breaking force in the horizontal and the longitudinal direction. The breaking force increased to the same extent for samples A and APS, followed by the sample AS. All the samples have been subjected to alkaline treatment which most likely tangled together the viscose fibers in the nonwoven fabric during the intensive rinsing of the alkali solution, rather than damaged the smooth surface of the fibers. Hence, there is increased friction between the rough surfaces of individual fibers during breaking force testing and it becomes more difficult to separate the tangled fibers that eventually results in increased breaking force. Subsequent application of the solgel system (sample AS, Figs. 16.2 and 16.3) most likely fills in the rough surface of the fibers and softens the fibers due to the addition of a wetting agent. It also enhances the fiber smoothness. It can be inferred from the test results that etching of the fiber surface by plasma treatment (sample P) enhances the friction between the fibers during the breaking force testing, even though this effect is not as significant as in the case of the alkaline-treated fibers. The plasma treatment that follows the alkaline treatment etches the surface further and loses

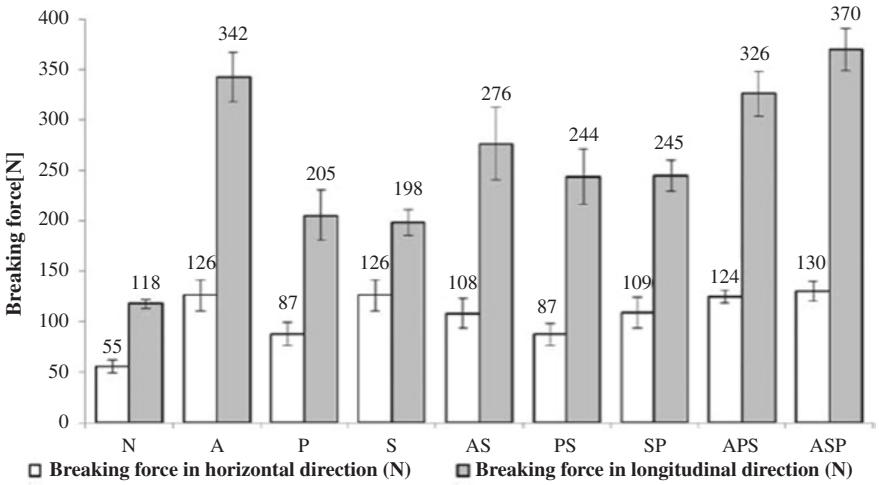

Fig. 16.5 The breaking force in horizontal and longitudinal direction of untreated and treated viscose samples [32]

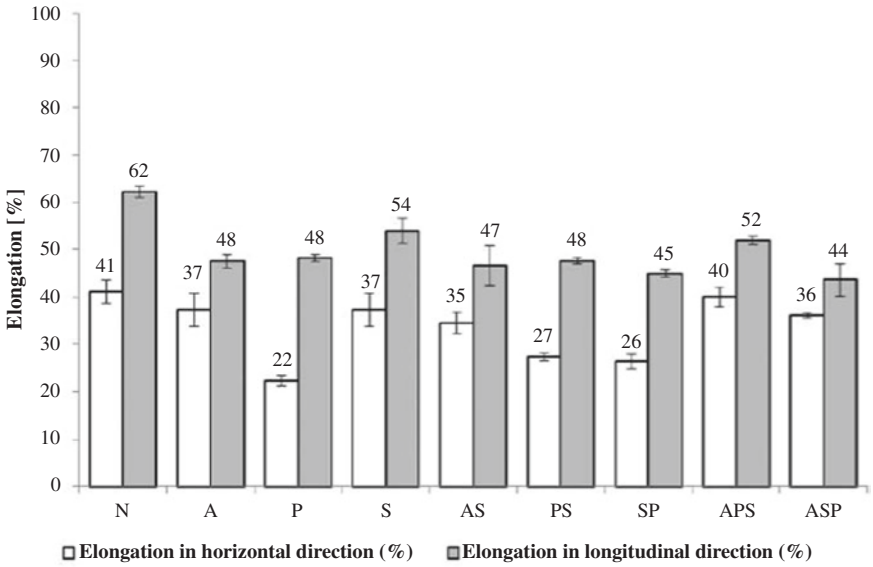

Fig. 16.6 The elongation at break at horizontal and longitudinal direction of untreated and treated viscose samples [32]

smoothness even after the solgel treatment (sample APS, Figs. 16.2 and 16.3), unlike in the case of the sample AS. When the application of solgel coating is followed by plasma treatment, it increases the sample surface roughness and thus improves friction between fibers. The solgel-coated fibers are not completely smooth as the breaking force value of the sample S has increased nearly twice as against the untreated sample. As expected, all the treatment methods reduced the elongation at break of the viscose nonwoven (Fig. 16.6) because of the breaking force measurement results. But, the differences are not as prominent. The plasma treatment had the biggest effect on the reduction of the elongation at break of the viscose nonwoven, as well as the greatest morphological effect on the surface of the fibers (Figs. 16.2 and 16.3). The antimicrobial treatment affected the elongation at break the least, among all treatments. The viscose nonwoven that was chosen as the input material has very good tensile properties on its own since it is used in the production of medical dressings. The most important finding from the performed set of tensile testing is that none of the treatments worsened these properties. Overall, all the treatment combinations improved the breaking force. The alkaline treatment had the greatest effect in this regard; therefore, the samples AS, APS, and ASP are most suitable for a potential medical dressing that includes antimicrobial treatment. Among these samples, the most pronounced reduction in the elongation at break was observed with the sample APS. The sequence of treatment used with this sample appears to be well most promising, considering the tensile properties.

16.3.5 Air Permeability

Maintaining the moisture of the wound surface is basic requirement of open wound treatment. The air permeability, apart from hydrophilicity, also affects the moisture of the wound, as it significantly contributes to an optimum 'breathing' of the wound and the evaporation of fluids from the wound [32]. When air permeability of a wound dressing is high, it could dry out the wound and cause death of the cells and thereby produce an undesirable effect on the rate of wound healing [51]. The air permeability values of untreated and differently treated samples of viscose nonwoven are shown in Fig. 16.7.

Sample A permeated the least air in comparison with the reference sample; air permeability was reduced by 62 %. This could be attributed to not only in the influence of the alkaline treatment on the cellulosic material that resulted in fiber swelling, but also in the whole process of alkaline treatment. During intensive rinsing of alkali swelling solution, the fibers in the nonwoven fabric got tangled and hence decreased the air permeability due to the closing of fiber-to-fiber interstices. This assumption is confirmed by comparing all the samples, whereby it is clear that all the samples that included alkaline treatment have lower air permeability than the reference sample. The plasma treatment contributed the most to the increase in air permeability of the material (sample P). This phenomenon is most likely due to in the etching of the fiber surface. The thinner fibers could have been burned by the plasma and hence reduced the density of fiber web. Comparison of samples S, AS, and PS also indicates that plasma has a permanent effect on air permeability since it was maintained even after the solgel treatment. The plasma

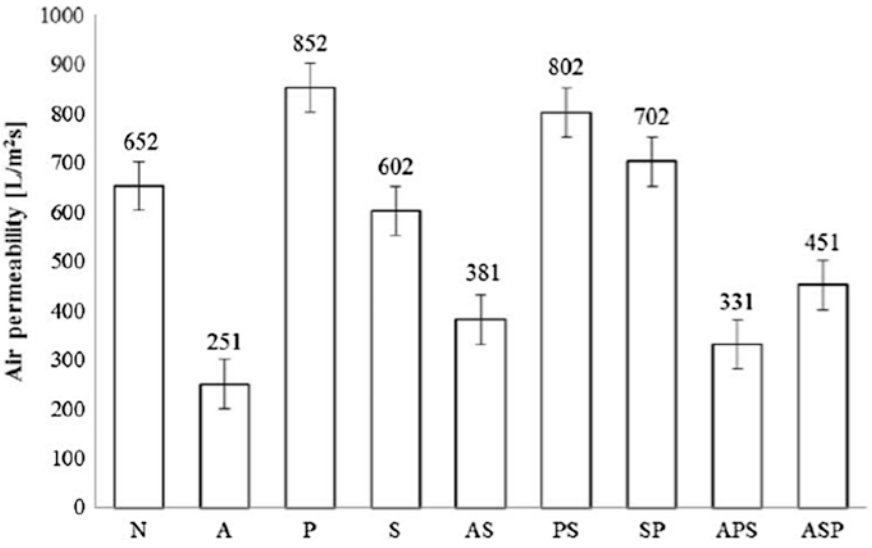

Fig. 16.7 Air permeability for untreated and differently treated viscose samples [32]

treatment did not significantly increase the air permeability of the previously alkaline-treated samples, where rinsing caused a permanent entanglement of the fibers, when the sample A has been compared with those of samples APS and ASP. Treatment of the material with the solgel process affected the air permeability only slightly. The air permeability was only minimally reduced, which is speculated to result from the addition of Kollasol wetting agent and a slight thickening of the fibers due to a layer of a binder and nanoparticles. But nonetheless, applied solgel coatings preferably embed individual fibers only with little or no surplus silane coatings filling out the inter-fiber voids in the fibrous network. It is necessary that medical dressings besides maintaining moist surface of wound should possess hydrophilicity and also be capable of absorbing exudates, bacteria, and other impurities from a wound. The decrease in air permeability is an advantageous aspect that contributes to a faster wound healing. The samples AS, APS, and ASP prove to be best suited for potential medical dressings.

References

1. Widgerow AD (2011) Chronic wound fluid—thinking outside the box. Wound Repair Regener 19:287–291
2. Parikh DV, Fink T, DeLucca AJ et al (2011) Absorption and swelling characteristics of silver (I) antimicrobial wound dressings. Text Res J 81:494–503
3. Moucha CS, Clyburn T, Evans RP et al (2011) Modifiable risk factors for surgical site infection. J Bone Joint Surg 93:398–404
4. Rojas I-G, Padgett DA, Sheridan JF et al (2002) Stress-induced susceptibility to bacterial infection during cutaneous wound healing. Brain Behav Immun 16:74–84
5. Petrulyte S (2008) Advanced textile materials and biopolymers in wound management. Danish Med Bull 55:72–77
6. Leaper DJ (2006) Silver dressings: their role in wound management. Int Wound J 3:282–294
7. Wei L, Tang J, Zhang Z, Chen Y, Xi T (2010) Investigation of the cytotoxicity mechanism of/silver nanoparticles in vitro. Biomed Mater 5:044103
8. Kim Y-J, Yang S, Ryu J-C (2010) Cytotoxicity and genotoxicity of nano-silver in mammalian cell lines. Mol Cell Toxicol 6:119–125
9. AshaRani PV, Low Kah Mun G, Hande MP et al (2008) Cytotoxicity and genotoxicity of silver nanoparticles in human cells. ACS Nano 3:279–290
10. Burd A, Kwok CH, Hung SC et al (2007) A comparative study of the cytotoxicity of silver-based dressings in monolayer cell, tissue explant, and animal models. Wound Repair Regener 15:94–104
11. Liu J, Sonshine DA, Shervani S et al (2010) Controlled release of biologically active silver from nanosilver surfaces. ACS Nano 4:6903–6913
12. Kokura S, Handa O, Takagi T et al (2010) Silver nanoparticles as a safe preservative for use in cosmetics. Nano Med 6:570–574
13. Eid KA, Azzazy HM (2012) Controlled synthesis and characterization of hollow flower-like silver nanostructures. Int J Nanomed 7:1543–1550
14. Seetharaman S, Natesan S, Stowers RS et al (2011) A PEGylated fibrin-based wound dressing with Antimicrobial and angiogenic activity. Acta Biomater 7:2787–2796
15. Breitwieser D, Moghaddam MM, Spirk S, et al (2013) In situ preparation of silver nanocomposites on cellulosic fibers—microwave vs. conventional heating. Carbohyd Polym 94: 677–686

16. Breitwieser D, Spirk S, Fasl H et al (2013) Design of simultaneous antimicrobial and anticoagulant surfaces based on nanoparticles and polysaccharides. J Mater Chem B 1:2022–2030
17. Mohan T, Spirk S, Kargl R et al (2012) Exploring the rearrangement of amorphous cellulose model thin films upon heat treatment. Soft Matter 8:9807–9815
18. Spirk S, Ehmann HM, Kargl R et al (2010) Surface modifications using a water-stable silanetriol in neutral aqueous media. ACS Appl Mater Interfaces 2:2956–2962
19. Kargl R, Mohan T, Köstler S, et al. (2012) Functional patterning of biopolymer thin films using enzymes and lithographic methods. Adv Funct Mater 23(3): 308–315
20. Young RA (1986) Structure, swelling and bonding of cellulose fibers. In: Young RA, Rowell RM (eds) Cellulose, structure, modification and hydrolysis, Wiley, New York, pp 102–107
21. Lewin M, Sello SB (1983) Handbook of fiber science and technology. M. Dekker, New York, pp 1–4 and 9. (Textile Research Journal 84(1):110)
22. Stana-Kleinschek K, Persin Z, Maver T (2011) Modification of non-woven cellulose for medical Applications using non-equilibrium gaseous plasma. Mater Technol 45:253–257
23. Persin Z, Stenius P, Stana-Kleinschek K (2011) Estimation of the surface energy of chemically and oxygen plasma treated regenerated cellulosic fabrics using various calculation models. Text Res J 81:1673–1685
24. Vesel A, Mozetic M, Strnad S et al (2009) Plasma modification of viscose textile. Vacuum 84:79–82
25. Shen L, Dai JJ (2007) Improvement of hydrophobic properties of silk and cotton by exafluoropropene plasma treatment. Appl Surf Sci 253:5051–5055
26. D'Agostino R, Favia P, Fracassi F () Treatments NASIoP and deposition of P. plasma processing of polymers. Kluwer Academic Publishers, Dordrecht, Boston
27. Titov VA, Shikova TG, Rybkin VV et al (2006) Modification of polyethylene, polypropylene and cotton using an atmospheric pressure glow discharge with liquid electrolyte cathode. High Temp Mater Process 10:467–477
28. Titov VA, Rybkin VV, Shikova TG et al (2005) Study on the application possibilities of an atmospheric pressure glow discharge with liquid electrolyte cathode for the modification of polymer materials. Surf Coat Tech 199:231–236
29. Pivec T, Persin Z, Maver T et al (2012) Binding silver nanoparticles onto viscose non-woven using different commercial sol-gel procedures. Mater Tehnol 46:75–80
30. Tomsic B, Simoncic B, Orel B et al (2009) Antimicrobial activity of AgCl embedded in a silica matrix on cotton fabric. Carbohyd Polym 75:618–626
31. Klemenčič D, Tomšič B, Kovač F et al (2012) Antimicrobial cotton fibres prepared by in situ synthesis of AgCl into a silica matrix. Cellulose 19: 1715–1729
32. Pivec T, Persˇin Z, Kolar M, Maver T, Dobaj A, Vesel A, Maver U, Stana-Kleinschek K (2014) Text Res J 84(1) 96–112
33. Hribernik S, Pivec T, Kurečič M et al (2012) Optimization of the sol–gel-assisted procedure for binding of silver onto modal fibres. In: 7th central European conference 2012 fibre-grade polymers, Portorose, Slovenia pp 265–271
34. Pasupuleti M, Schmidtchen A, Malmsten M (2012) Antimicrobial peptides: key components of the innate immune system. Crit Rev Biotechnol 32:143–171
35. Malmsten M, Davoudi M, Walse B et al (2007) Antimicrobial peptides derived from growth factors. Growth Factors 25:60–70
36. Malmsten M (2011) Antimicrobial and antiviral hydrogels. Soft Matter 7:8725–8736
37. Infante MR, Perez L, Pinazo A et al (2004) Amino acid-based surfactants. CR Chim 7:583–592
38. Clapes P and Infante MR. Amino acid-based surfactants: enzymatic synthesis, properties and Potential applications. Biocatal Biotransform 2002; 20: 215–233
39. Su HL, Lin SH, Wei JC et al (2011) Novel nanohybrids of silver particles on clay platelets for inhibiting silverresistant bacteria. PLoS One 6: e21125
40. Beighton D (1984) The influence of saliva on the hydrophobic surface-properties of bacteria isolated from oral sites of macaque monkeys. FEMS Microbiol Lett 21:239–242

41. Kluytmans J, van Belkum A, Verbrugh H (1997) Nasal carriage of Staphylococcus aureus: epidemiology, underlying mechanisms, and associated risks. Clin Microbiol Rev 10:505–520
42. Russo TA, Johnson JR (2003) Medical and economic impact of extraintestinal infections due to Escherichia coli: focus on an increasingly important endemic problem. Microbes Infect 5:449–456
43. Murray BE (1990) The life and times of the Enterococcus. Clin Microbiol Rev 3:46–65
44. Hidron AI, Edwards JR, Patel J, et al (2008) NHSN annual update: antimicrobial-resistant pathogens associated with healthcare-associated infections: annual summary of data reported to the National Healthcare Safety Network at the Centers for Disease Control and Prevention 2006–2007. Infect Control Hosp Epidemiol 29: 996–1011
45. Amyes SG (2007) Enterococci and streptococci. Int J Antimicrob Agents 29(3):S43–S52 Pivec et al. 111
46. Lyczak JB, Cannon CL, Pier GB (2000) Establishment of pseudomonas aeruginosa infection: lessons from a versatile opportunist. Microbes Infect 2:1051–1060
47. Kim YM, Farrah S, Baney RH (2007) Membrane damage of bacteria by silanols treatment. Electron J Biotechnol 10: 252–259
48. Kim YM, Farrah S, Baney RH (2006) Silanol—a novel class of antimicrobial agent. Electron J Biotechnol 9:176–180
49. Blunder M, Hurkes N, Spirk S et al (2011) Silanetriols as in vitro inhibitors for AChE. Bioorg Med Chem Lett 21:363–365
50. Krässig HA (1993) Cellulose: structure, accessibility, and reactivity. Gordon and Breach Science, Yverdon
51. Vesel A (2008) XPS study of surface modification of different polymer materials by oxygen plasma treatment. Inform Midem 38:257–265
52. Roy D, Semsarilar M, Guthrie JT et al (2009) Cellulose modification by polymer grafting: a review. Chem Soc Rev 38:2046–2064
53. Field FK, Kerstein MD (1994) Overview of wound healing in a moist environment. Am J Surg 167:2S–6S

Chapter 17
PET Implants for Long-term Durability

17.1 Introduction

Polyethylene terephthalate (PET) finds a broad range of medical applications, of which implants are one such. But, many human deaths have been reported due to PET graft failures, and the actual number of deaths from PET graft failures is feared to be much more than those officially recorded, as fear of litigation could prevent reporting of failures [1–6]. The graft failures can also be attributed to other causes. Of these, the surgical failures of grafts can be due to causes such as thrombosis and infection, rather than the failure of the textile material, or death of elderly patients from natural causes or causes other than graft failure [5]. In vivo, both circumferential and longitudinal cracks have been noticed on the ruptured polyester and polypropylene implants [7–11]. The premature rupture of PET implants is caused by a number of factors such as repetitive pulsatile blood flow pressure, high blood pressure, and body fluid environments [5]. These physiological stresses on implant materials can be continuous or intermittent; for example, an anterior cruciate ligament (ACL) graft encounters constant stress [12]. Also, all vein grafts undergo arterial pulse pressure [13]. The average time for implant failures is usually 7.0 years, but it ranges from 12 months to 19 years. It has been found that residual stress in textile implants created during textile processing (spinning, winding, warping, sizing, and weaving) causes the formation of cracks and the deterioration in mechanical properties through chemical degradation [14]. Low-temperature cast coagulation technique has been used in an attempt to minimize the residual stress during production and formation of cracking during use. But, these implants still have produced stress cracks in vivo because of hydrolytic degradation [15]. Alkalis and amines have long been used to understand the fine structures of apparel-grade PET [16, 17]. Apparel-grade polymers and processing equipment have been used in the earlier developed PET implants. But, advances in spinning and polymer technology (spin finish, process machineries) have enabled production of high-tenacity

N. Gokarneshan et al., *Emerging Research Trends in Medical Textiles*,
Textile Science and Clothing Technology, DOI 10.1007/978-981-287-508-2_17

PET for medical applications where long-term durability is necessary [18, 19]. PET yarns for industrial applications (medical applications, geosynthetic applications) require complex drawing and heat treatment in order to obtain the required tenacity, extensibility, thermal shrinkage, orientation, and crystallinity of fibers [20]. As for instance, the tenacity and extensibility of apparel-grade polyester is 26 cN/tex and 30–40 %, respectively, while the value is 85 cN/tex and 7 % for industrial-grade fiber [21]. In the USA and Canada, the implant failures have to be compulsorily be documented with the Federal Drug Administration (FDA) and Health Canada, respectively, outlining 'event description' and 'manufacturer narrative,' as well as deterioration of effectiveness of the medical device which has caused death or serious deterioration in the condition of a patient [22, 23]. It is not legally required to submit laboratory test results for performance evaluation simulating accelerated physiological conditions. The previous investigation showed that alkaline degradation of PET under applied loading conditions produced surface cracks when the applied load was above the yield load at room temperature [24]. The investigation discussed herein utilizes two loading conditions (applied load and preload) and three aqueous chemical solutions (sodium hydroxide, sulfuric acid, and ammonium hydroxide) to determine if the in vivo formation of circumferential and longitudinal cracks in PET implants can be predicted before implantation. Moreover, the investigation has used empirical equations to calculate the approximate lifetime of the PET implants made from high-tenacity medical-grade polymer.

17.2 Changes in Properties of NaOH-Treated PET

PET-A and PET-B samples have been treated in aqueous NaOH in relaxed state and under applied loads as well, and the weight loss (%), breaking load (cN), and breaking load (%), and also the surface characteristics have been determined. The weight loss (%) in both the cases increased with increasing duration of treatment [25]. A similar trend in weight loss (%) increase with treatment time has been noticed for the samples treated with aqueous NaOH in applied loading and preloading conditions. But, the weight loss (%) of the applied-loaded and preloaded samples has been found to be greater than the relaxed samples under the same conditions of treatment. As an instance, after 4 days of treatment in aqueous NaOH, the relaxed PET-A samples (PET-A/NaOH/zero load) lost 15.3 % weight, whereas the applied-loaded samples (PET-A/NaOH/246 MPa applied load) lost 20.2 %, and the preloaded samples (PET-A/NaOH/246 MPa preload) lost 19.4 % weight. One reason for the slight increases in weight loss (%) for the stressed and prestressed samples was the increase in surface area, or reduction in linear density of the fiber due to stress, as the relationship was found to be inverse between weight loss (%) in alkaline medium and fiber decitex (weight loss (%) α 1/sqrt d: d is the fiber decitex) [26]. The reduction in breaking load (%) in the case of the relaxed samples treated in aqueous NaOH has been found to be similar to the corresponding weight loss (%), except for the 96-h-treated samples. The

96-h-treated samples in the relaxed condition (PET-A/NaOH/zero load) produced a higher breaking load (%) than the corresponding weight loss (%). The reduction in the breaking load (%) in the case of the applied-loaded (PET-A/NaOH/246 MPa applied load, PET-B/NaOH/246 MPa applied load) and preloaded samples (PET-A/NaOH/246 MPa preload; PET-B/NaOH/246 MPa preload) has been found to be much greater than the corresponding weight loss (%). The reason for the higher breaking load (%) for the applied-loaded and preloaded samples than the relaxed samples is highlighted in the scanning electron micrograph section.

17.3 Changes in Properties of Sulfuric Acid and Ammonium Hydroxide-treated Poly (Ethylene Terephthalate)

In the case of PET—samples treated with sulfuric acid and ammonium hydroxide—the weight loss (%), breaking load (cN), and breaking load loss (%) have been measured. There has been an insignificant weight loss (%) for sulfuric acid-treated samples in relaxed and applied loading states [25]. But, the breaking load loss (%) was significantly higher for all three conditions and increased with the increasing duration of treatment. For example, the sample (PET-A/sulfuric acid/246 MPa applied load) treated with 5 % sulfuric acid for 96 h lost 70 % of the breaking load. A similar trend in weight loss (%) and mechanical loss (%) was observed with the ammonium hydroxide-treated samples. The extent of influence on the mechanical properties of PET by the aqueous solution of ammonium hydroxide is dependent on the solution concentration and stressing conditions. While the weight loss (%) of ammonium hydroxide-treated samples was unchanged, the breaking load loss (%) increased with the increasing applied loading conditions and concentration of ammonium hydroxide. As an instance, at 2 % ammonium hydroxide and 246 MPa applied load, the reduction in breaking load has been 23.5 % compared to 69.1 % for 5 % ammonium hydroxide under similar treatment states. The data obtained for weight reduction (%) match with those published in the literature, as no weight loss (%) has been obtained when PET was treated in aqueous ammonia at 30 °C for 10 days and n-butylamine at 21 °C for 72 h [17, 27]. But, a small amount of weight loss (3.3 %) has been reported when polyester was treated with 10 % (w/w) aqueous solution of ethanolamine for 6 h at 100 °C [17].

17.4 Scanning Electron Micrographs

Figures 17.1 and 17.2 depict the scanning electron micrograph (SEM) photographs for the virgin (untreated) PET-A and PET-B samples. There are no cracks or grooves observed in these two PET samples [25].

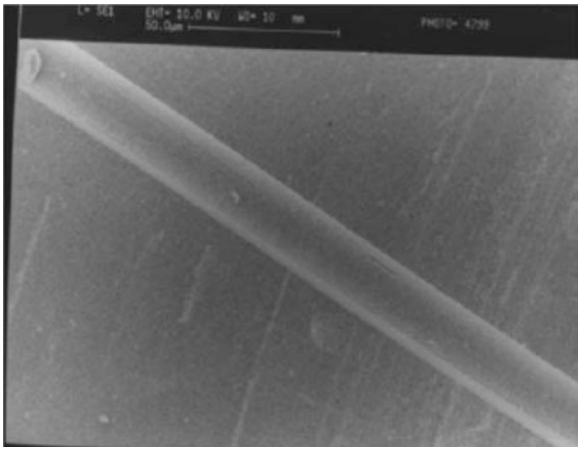

Fig. 17.1 Scanning electron micrograph of virgin PET-A [25]

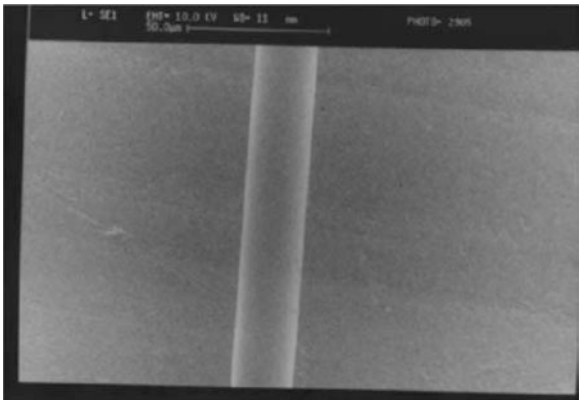

Fig. 17.2 Scanning electron micrograph of virgin PET-B [25]

The surface appearance of the PET-A sample treated in the relaxed condition (PET-A/caustic soda/zero load) for 96 h with 10 % caustic soda (weight loss: 15.3 %). The overall fiber surface treated with alkali in the relaxed condition is rougher than the surface of the virgin PET sample. Even though no circumferential cracks have been observed on this micrograph (Fig. 17.3), a few longitudinal pits can be seen. These longitudinal pits are similar to those obtained in the alkaline hydrolyzed PET samples containing titanium dioxide [28] and are responsible for the larger breaking load loss (%) than the corresponding weight loss (%). Conversely, the micrograph of PET-B (PET-B/caustic soda/zero load) treated in the relaxed state for up to four full days in 10 % caustic soda (weight loss: 18.5 %) did not produce any longitudinal or circumferential cracks. There have been no noticeable longitudinal pits as samples of PET-A (PET-A/caustic soda/zero load) have been treated for up to 72 h (weight loss: 11.9 %) in the relaxed condition with 10 % caustic soda. The surface characteristics of PET are different for different

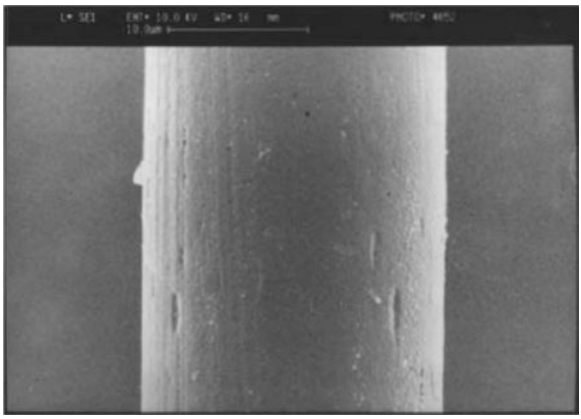

Fig. 17.3 Scanning electron micrograph of PET-A treated in the relaxed state with 10 % NaOH, 96 h [25]

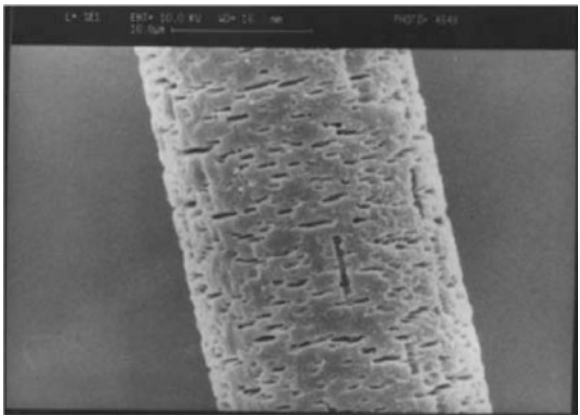

Fig. 17.4 Scanning electron micrograph of PET-A treated with 10 % NaOH, 96 h/2000 g load [25]

loading conditions and PET types. Longitudinal cracks have been noticed in the PET-A samples (not visible in SEM photographs) as the applied load was below yield load (<246 MPa) of PET, and no visible cracks in either direction have been seen in the PET-B samples (not seen in SEM photographs), except the treated samples of 4 full days with 123 MPa applied loading condition, which shows the onset of crack formation. But, as the applied load exceeded the yield load of 2000 g or 246 MPa, severe circumferential and longitudinal cracks have been created in the PET-A samples (Fig. 17.4), and longitudinal cracks have been observed in the PET-B sample (Fig. 17.5). The length and width of the cracks increased with the severity of the hydrolysis. The yield load was determined by the 'slope threshold' method using an Instron Universal Strength Tester and was found to be 1220 g for PET-A and 1240 g for PET-B. The longitudinal cracks have been more pronounced in the stressed PETA sample (Fig. 17.4: PET-A/caustic soda/246 MPa applied load) than the relaxed PET-A sample (Fig. 17.3: PETA/caustic soda/zero load) under identical hydrolysis conditions. The longitudinal crack patterns

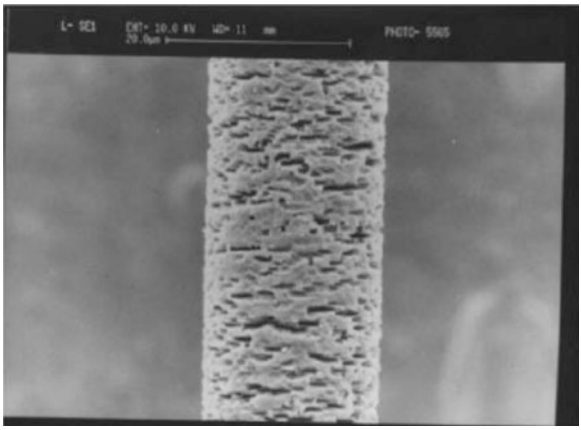

Fig. 17.5 Scanning electron micrograph of PET-B treated with 10 % NaOH, 96 h/2000 g load [25]

(crack length, width, and frequency) are different for PET-A (Fig. 17.4) and PET-B (Fig. 17.5) for similar treatment conditions. The difference in dimensions of crack size in PET-A and PET-B arises from the presence of different size crystals, which depend on the processing history. The size and number of crystal formation are influenced by the rate of heat-setting and cooling (nucleation rate). It is known that smaller and more numerous crystals are formed with a high nucleation rate, while larger and fewer crystals are formed with a slow nucleation rate [21]. The circumferential and longitudinal cracks in the stressed PET samples are similar to those observed in the ruptured PET implants in vivo that resulted in numerous human deaths [7, 9, 10]. There have been no cracks when samples have been treated under loading conditions in water alone (micrograph not shown).

The circumferential cracks have been created due to the applied load, which exceeded the yield load and alkaline environment, and the longitudinal cracks in the PET-A sample could possibly have arisen from surface defects or due to the presence of titanium dioxide, as the sample is bright and contains about 0.1 % TiO_2, although titanium dioxide should not be used in medical-grade PET as it damages cell membranes [29]. Alternatively, the PET-A sample might have manufacturing defects, possibly from the heat-setting treatments.

As the surface defects can be identified by the treatment of PET with caustic soda in relaxed and applied loading conditions, further studies have been conducted to find whether other loading conditions and chemicals could be used to detect such defects in PET implants before their implantation into the human body. One such loading condition was ‘preloading’ the PET samples before their treatment with the alkaline solution. A residual stress is generated in the samples by the preloading condition. The residual stress in the textile structure is created in two ways: (a) during conversion of fibers to yarns and yarns to fabrics spinning/winding/warping/weaving) and (b) during normal functioning in the human body because of intermittent pulsatile forces. It is reported that the residual stress in the textile structure is responsible for premature rupture of small-caliber straight tubes (bifurcated grafts, femoro-popliteal grafts and axillo-femoral grafts). Figure 17.6

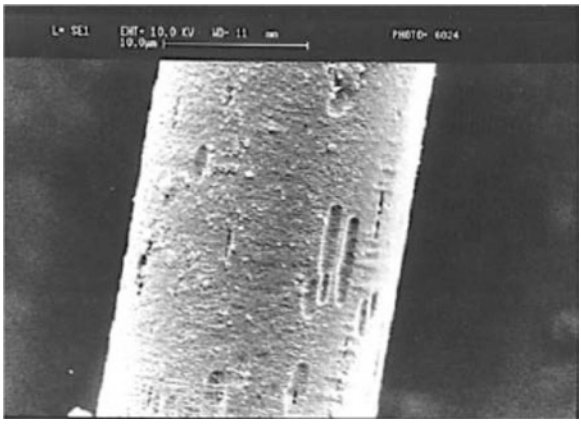

Fig. 17.6 Micrograph of prestressed sample (prestressed for 48 h) treated with 10 % NaOH in relaxed condition, 40 °C for 96 h [25]

shows the scanning electron micrographs obtained from the prestressed sample of PET-A (PET-A/NaOH/246 MPa preload) treated in 10 % alkaline solution at 40 °C. Both circumferential and longitudinal cracks can be seen in this micrograph. In contrast, only circumferential cracks are present in the PET-B prestressed (PET-B/caustic soda/246 MPa preload) sample (micrograph not shown). The longitudinal cracks in the prestressed sample (Fig. 17.6) are much wider and deeper than the relaxed sample (Fig. 17.3) [25].

But, the longitudinal and circumferential cracks are far less pronounced than those in the 246 MPa applied-loaded samples (Fig. 17.4). The longitudinal cracks in the prestressed sample are far more pronounced than the circumferential cracks. It appears that the longitudinal cracks in all three alkaline-treated PET-A samples (relaxed: Fig. 17.3, applied loaded: Fig. 17.4 and preloaded: Fig. 17.6) are parallel to each other and the angle between the longitudinal cracks and fiber axis is approximately 2°–5° (Fig. 17.6). Similar longitudinal pits and craters have been observed in the explanted Vanguard stent–grafts [7]. The surface of the virgin polyester fiber normally has many flaws or cracks, which are absent in the scanning electron micrographs (Figs. 17.1 and 17.2), but can be seen using very high magnification in the form of fine surface topography [30]. The molecular force in the case of PET along the transverse direction is much weaker in comparison with the molecular force in the longitudinal direction, and, in thermotropic polyesters, the circumferential strength is only 20 % of the longitudinal strength and the modulus is less than 10 % of the longitudinal value [31, 32]. As the fiber is subjected to stress, the stress concentration at the tip of each crack increases the magnitude of the crack. The line of maximum stress in the whole fiber is across a plane 90 to the fiber axis, and locally, it is along the line of the crack opening. These two directions usually coincide to give circumferential cracks when the fiber is under stress during alkaline hydrolysis [33]. Moreover, circumferential cracks are formed during aqueous alkaline treatment in the loaded state, as the load becomes more than the yield load because of the transformational changes of the fiber [24, 34]. This conformational change exerts strain on the ester bonds that break easily due to the weakest bond energy of C–O in the ester bond [35]. As for the longitudinal

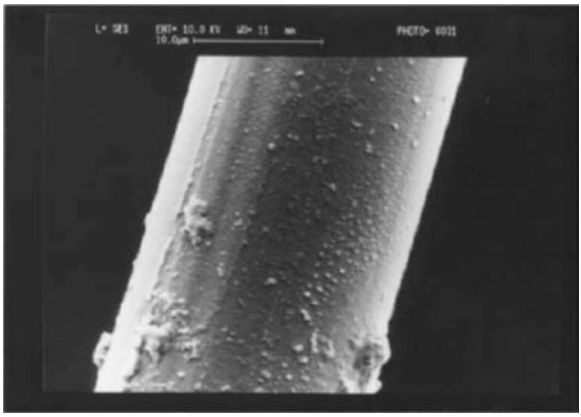

Fig. 17.7 Micrograph of 2000 g stressed sample treated with 5 % H_2SO_4, 40_C/48 h [25]

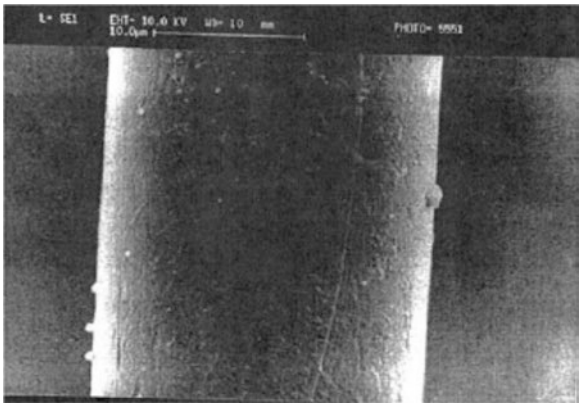

Fig. 17.8 SEM of PET having 5% NaOH at room temperature in relaxed state (120 days)

cracks in the applied-stressed and prestressed samples, the load beyond yield load increases the shear stress in the inherent defects of the fiber, thereby overcoming the circumferential forces responsible for longitudinal cracks. These longitudinal cracks stay in the fiber and help in the penetration of hydroxide ions, increasing the depth and length of the longitudinal cracks [36]. Though the pH of the blood (7.4) is far lesser than that of the caustic soda, however, the similar level of applied loading and preloading conditions can be encountered by implants in the human body. In the case of PET-A samples treated with 5 % sulfuric acid, the cracks have not been noticed in the relaxed (not in figure) and the stressed states as well (Fig. 17.7: PET-A/sulfuric acid/246 MPa applied load).

The same surface characteristics have been noticed in the case of the PET-A samples treated with 2 % (not in figure) and 5 % ammonium hydroxide in the relaxed state (PET-A/ammonium hydroxide/zero load [25] (Fig. 17.8).

The smooth appearance of the acid and ammonium hydroxide-treated samples with 246 MPa loading conditions was surprising, as both PET-A samples (PETA/ sulfuric acid/246 MPa applied load; PET-A/ammonium hydroxide/246 MPa applied

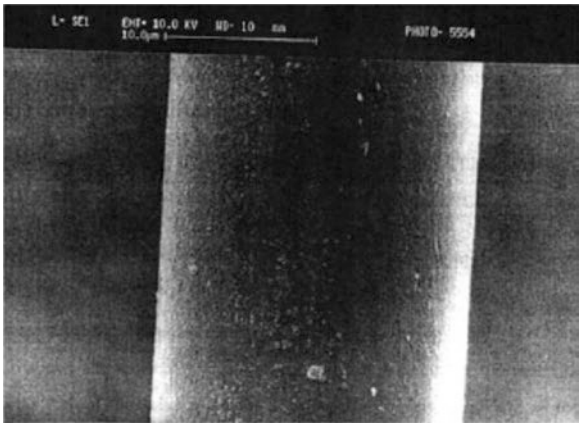

Fig. 17.9 Scanning electron micrograph of PET1 treated with 5 % ammonium hydroxide, at room temperature, 120 days, under 1 kg load [25]

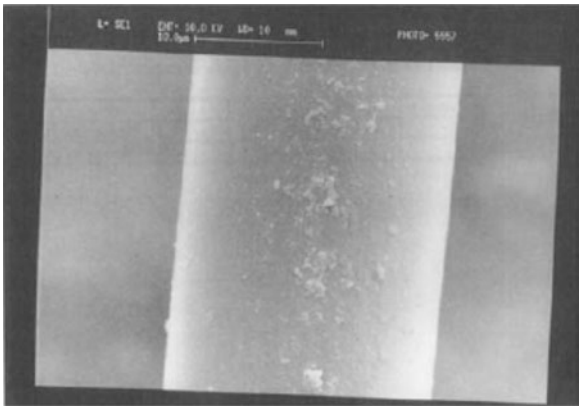

Fig. 17.10 Micrograph of 2000 g stressed sample treated with 5 % NH_4OH, room temperature/120 days [25]

load) lost about 70 % breaking load. The findings indicate that the reaction of sulfuric acid and ammonium hydroxide in relaxed and stressed states (below and above yield loads) occurs all over the actual substance of the fibers with a gradual chemical degradation of PET and splitting of linkages in the long-chain polyester molecules. In the case of polyester treated with neat n-butylamine at 21 °C for 72 h, however, the formation of spiral, helical, circumferential, and longitudinal cracks on various amine-treated polyesters has been reported [17, 37].

17.5 Proposed Chemical Reaction

The degradation effect of caustic soda on the properties of polyester fibers arises because of chemical reaction [25]. The hydroxide anions react with the carbonyl oxygen atoms of the ester group to form one hydroxyl and one carboxylate end

group in the aqueous alkaline and relaxed states [21]. Under the relaxed state, the highly ionized compound cannot readily diffuse into the nonpolar polyester. Hence, hydrolysis is confined to the polyester surface, and only the diameter of the fiber is decreased, but the tenacity does not change. The diffusion of the hydroxyl groups takes place as its size is much smaller than the cracks in PET (3.56 Å), and also because of the crack formation under stressing conditions, and particularly above the yield stress is apparently much smaller than the cracks in PET [38]. This diffusion of hydroxyl ions inside PET results in the removal of more PET layers in stressing samples than the relaxed samples, which leads to more weight loss, and the reaction produces one hydroxyl and one carboxylate end group as given below:

$$\mathrm{R{-}COO{-}CH_2CH_2{-}O^{-OH^-}} \rightarrow \mathrm{RCOO + OH^-}$$

A hydroxyl and a carboxyl end group is formed due to protonation of the in-chain oxygen atom of the ester group, followed by the reaction with water in the acid media [21].

$$\mathrm{R - COO{-}CH_2CH_2{-}O^{-H+}} \rightarrow \mathrm{RCOO^- + OH^-}$$

The protonation takes place in the case of ammonium hydroxide, as the ammonium ion (NH_4^+) is slightly acidic and dissociates into H^+ and NH_3. As the concentration of ammonium hydroxide is relatively low, more ammonium ions are formed in the bath as compared to the hydroxide ions, and hydrolysis takes place in a manner similar to acid hydrolysis [39]:

$$\mathrm{NH_4^+ \rightarrow H^+ + NH_3}$$

17.6 Calculation of Poly(Ethylene Terephthalate) Implant Lifetime

It has been earlier reported that the weight loss (%) of medical-grade PET roughly fits the ICI formula given in Eq. (17.1) [27]. An empirical equation relating loss in breaking load with treatment time and applied load for a particular concentration and treatment temperature of caustic soda has also been reported [24]. The generic empirical equation is given in Eq. (17.2). Eqs. (17.3) and (17.4) have been computed statistically for PET-A and PET-B, respectively, at 40 °C and 10 % NaOH concentration using breaking load (cN) data [24]

$$\text{Weight loss}(\%) = \frac{0.47t\left(x^2 + 6x\right)}{1.082^{110-r}\,\text{sqrt.}\,d} \tag{17.1}$$

where t is the time in hours, x is the concentration of NaOH (%), T is the temperature in °C, and d is the decitex of the fiber.

$$Y = \beta_0 + \beta_1 T + \beta_2 L^2 \tag{17.2}$$

where Y is the predicted breaking load (cN), T is the treatment time (days), and L is the applied load (g).

$$\begin{aligned} Y &= 47.1 - 3.44T - 2.26 * 10^{-6}L^2 \\ R^2 &= 0.85, \quad S = 2.88, 95\,\%\ \text{confidence lim} = \pm 6 : 27 \end{aligned} \tag{17.3}$$

$$\begin{aligned} R^2 &= 0.90, \quad S = 3.56,\ 95\,\%\ \text{confidence lim} = +7 : 77 \\ Y &= 56.4 - 4.79T - 4.36 * 10^{-6}L^2 \end{aligned} \tag{17.4}$$

In Eqs. (17.3) and (17.4), R^2 is the coefficient of determination, S is the standard deviation about regression, and 95 % confidence limits for the predicted breaking load Y are given by $\_t0.025S$, where $t0.025$ is obtained from probability points of the t distribution table using n_2(¼12) degrees of freedom [25].

Using Eq. (17.3) for PET-A, the lifetime for 50 % loss in breaking load for the 'zero applied loading' condition would be only 7 days in 10 % NaOH at 40 °C. As the dependence of NaOH concentration with the weight loss (%) is ($x_2 + 6x$) as per Eq. (17.1), and assuming the rate of weight loss is proportional to breaking load loss, the lifetime can be calculated using the lower concentration of alkali that is likely to be encountered by PET implants. Thus, the lifetime will be about 50 years in zero loading condition considering 0.01 % or 0.0025 M NaOH (pH < 11). Similarly in the case of the PET-B sample, the lifetime would be about 45 years, considering Eq. (17.4) and taking the dependence of NaOH ($x_2 + 6x$), in 0.0025 M NaOH at 40 °C. As the pH of blood is only 7.4, physiological fluids alone cannot be responsible for the premature rupture of PET implants, as reported in a number of medical literatures. But, when a premature rupture takes place, the important contributing factor is possibly the site-specific physiological loads that exceed the polymer yield load. The use of apparel-grade PET materials can be another reason for premature rupture of PET implants since it has been observed that the retrieved PET implants in different hospitals have been produced from semi-dull, round cross-sectional, textured multifilament, Type 56T Dacron [40]. This specific polyester was apparel grade and not meant to be used for implants. The textured and semi-dull polyesters degrade faster than the clear (bright) and flat filament polyester yarns [17]. The research investigation discussed herein could be the first to compute the lifetime of PET implants. But, in this work, the empirical equations have been computed for applied loading and alkaline (NaOH) conditions only, as PET implants encounter alkaline conditions in the human body due to the slightly alkaline nature of blood and physiological stress. Further, only breaking load was used for computing the empirical equations. The lifetime can also be calculated by the use of other mechanical properties such as elongation, constant stress (creep), constant strain (stress relaxation), and work of rupture. Elongation may be a more sensitive property to monitor than breaking strength, because elongation is associated with low molecular weight chains that degrade faster than high molecular weight chains. Certain types of PET

implants are subjected to constant stress in the human body, and in such implants, it is more suitable to use creep data for lifetime prediction. In the case of implants that are fixed and immovable, the lifetime requires to be computed using constant strain data. In the case of hypertensive patients, work of rupture is very suitable. In the calculation of lifetime, a number of other relevant polymer properties such as hardness, molecular weight, and carboxyl group formation can prove useful, based on the area in which the implant is situated in the body.

References

1. Zarins C, Arko F, Crabtree T et al (2004) Explant analysis of AneuRx stent grafts: relationship between structural findings and clinical. J Vasc Surg 40:1–11
2. Chakfe N, Riepe G, Dieval F et al (2001) Longitudinal ruptures of polyester knitted vascular prostheses. J Vasc Surg 33:1015–1021
3. Wilson S, Krug R, Mueller G et al (1997) Late disruption of Dacron aortic grafts. Ann Vasc Surg 11:383–386
4. Jones AP, Sidhom S, Sefton G (2007) Long-term clinical review (10–20 years) after reconstruction of the anterior cruciate ligament using the Leeds-keio synthetic ligament. J Long-Term Eff Med Implants 17:59–69
5. Damme H, Depre M, Creemers E et al (2005) Intrinsic structural failure of polyester (Dacron) vascular grafts. A general review. Acta Chir Beig 105:249–255
6. Dieval F, Chakfe N, Wang L et al (2003) Mechanisms of rupture of knitted polyester vascular prostheses: an in vitro analysis of virgin prostheses. Eur J Vasc Endovasc Surg 26:429–436
7. Chuter TAM (2009) Durability of endovascular infrarenal aneurysm repair: when does late failure occur and why? Semin Vasc Surg 22:102–110
8. Trippestad A (1985) Late rupture of knitted Dacron double velour arterial prostheses. Acta Chir Scand 151:391–395
9. Berger K, Sauvage LR (1981) Late fibre deterioration in Dacron arterial grafts. Ann Surg 193:477–491
10. Yashar JJ, Richman MH, Dyckman J et al (1978) Failure of Dacron prostheses caused by structural defects. Surgery 84:659–663
11. Clave A, Yahi H, Hammou JC (2010) Polypropylene as a reinforcement in pelvic surgery is not inert: comparative analysis of 100 explants. Int Urogynecol J 21:261–270
12. Conner C, Morris R, Vallurupalli S et al (2008) Tensioning of anterior cruciate ligament hamstring grafts: comparing equal tension versus equal stress. J Arthroscopic Relat Surg 23:1323–1329
13. Baird RN, Abbot WA (1976) Pulsatile blood-flow in arterial grafts. Lancet 308:948–950
14. White SR, Hann HT (1992) Process modeling of composite materials: residual stress development during cure. Part I. Model formulation. J Comp Mater 26:2402–2422
15. Henryk J, Salacinski R, Tai RJ et al (2002) In vitro stability of a novel compliant poly(carbonate- urea) urethane to oxidative and hydrolytic stress. J Biomed Mat Res 59:207–218
16. Collins MJ, Zeronian SH, Semmelfyer M (1991) The use of aqueous alkaline hydrolysis to reveal the fine structure of poly(ethylene terephthalate) fibres. J Appl Polym Sci 42:2149–2161
17. Zeronian SH, Collins MJ (1989) Surface modification of polyester by alkaline treatments. Textil Prog 20:1–26
18. Guidoin R, King M (2004) Ind Fabr Products. Review 89:58–63
19. East AJ (2005) In: McIntyre JE (ed) Synthetic fibres: nylon, polyester, acrylic, polyolefin. Woodhouse Publishing Ltd, Cambridge

20. Falkai BV (1996) Developments in the production of industrial PET filaments. Asian Textil J 5:26–38
21. McIntyre JE (1998) Polyester fibres. In: Lewin M, Pearce EM (eds) Handbook of fibre science and technology: fibre chemistry, vol IV. M. Dekker, New York, pp 1–73
22. Implants and Prosthetics (2011) US Food and Drug Administration, http://www.fda.gov/MedicalDevices/ProductsandMedicalProcedures/ImplantsandProsthetics/default.htm (Accessed 20 Jan 2011)
23. Medical Devices Regulations, SOR/98-28, Health Canada, http://canlii.org/en/ca/laws/regu/sor-98-282/latest/sor-98-282.html (accessed 15 Feb 2011)
24. Rahman M, East G (2006) Effect of applied stress on the alkaline hydrolysis of poly(ethylene terephthalate) at 40_c: relevance to medical textiles. J Appl Polym Sci 102:4814–4822
25. Mashiur Rahman, In vitro study of poly (ethylene terephthalate) implants for long-term Durability. Textile Res J 83(9);893–903
26. Rahman M (1997) Alkaline degradation of polyester geotextiles. PhD thesis, The University of Leeds, UK
27. ICI Technical Manual (1966) The effect of alkalis. Section B2, UK, pp 1–3
28. Solbrig C, Obendorf S (1991) Alkaline hydrolysis of titanium dioxide delustred poly(ethylene terephthalate) yarns. Textil Res J 61:177–181
29. Valant J, Drobne D, Novak S (2012) Effect of ingested titanium dioxide nanoparticles on the digestive gland cell membrane of terrestrial isopods. Chemosphere 87:19–25
30. Holmes SA, Zeronian SH (1995) Surface area of aqueous sodium hydroxide hydrolyzed high- speed spun poly(ethylene terephthalate) fibers. J Appl Polym Sci 55:1573
31. Morton WE, Hearle JWS (2008) Physical properties of textile fibres, 4th edn. Woodhouse Publishing, Cambridge, pp 509–558
32. Jaffe M, East AJ (2007) Polyester fibres. In: Lewin M (ed) Handbook of fibre chemistry, 3rd edn. CRC Press, Boca Raton
33. Hearle JWS, Lomas B, Cooke WD, et al (1989) Chapter 4: brittle tensile fracture. In: Fibre failure and wear of materials. Ellis Horwood, Chichester, pp 33–39
34. East GC, Rahman M (1999) Effect of applied stress on the alkaline hydrolysis of geotextile poly(ethylene terephthalate). Part 1: room temperature. Polymer 40:2281–2288
35. Ding W, Ju D, Chai W (2010) The effect of working pressure on the chemical bond structure and hydrophobic properties of PET surface treated by N ion beams bombardment. Appl Surf Sci 256(22):6876–6880
36. Hearle JWS, Lomas B, Cooke WD et al (1989) Chapter 7: axial splits. In: Fibre failure and wear of materials. Ellis Horwood, Chichester, pp 54–59
37. Holmes SA (1996) Surface defect geometry/tensile failure relationships of aminolyzed poly(ethylene terephthalate). Textil Res J 66:214–218
38. Stern K, Amis E (1958) Ionic size. Chem Rev 59:1–64
39. Britto DT, Herbert J, Kronzucker HJ (2002) NH4 + toxicity in higher plants: a critical review. J Plant Physiol 159:567–584
40. King MW, Zhan Ze and Guidoin R (2001) J Textil Appa Tech Manag 1:1 (Rahman 903)

Chapter 18
Garments for Respiratory Protection in Hazardous Environments

18.1 Introduction

Firefighting is a very risky task. The demands of firefighting equipment are very high and necessitate specific material properties. The factors involved in the design of protective clothing and respiratory protection are available in the literature [1, 2]. In terms of striking an optimal compromise, which is important due to the high level of potential hazards that are involved, it is often not possible to make a one size-fits-all decision. Practical demonstration has been done to determine whether the structural firefighting should also carry equipment specialized for fighting wildfires [3]. As the respiratory tract of the human body strongly influences the control of body temperature, and accounts for about 10 % of heat loss from the body, selection of appropriate respiratory protection is of paramount importance [4, 5]. The choice becomes increasingly important at high ambient temperatures when the ambient vapor pressure exceeds that of the skin as the cooling effect from sweating is inhibited under those circumstances. In the case of highly exertive situations, firefighters are unable to wear proper respiratory protection due to the increased difficulty to breathe and heat stress. The use of handkerchiefs and bandannas is ineffective in providing relief, unless the fabrics hold an electrostatic charge for the entrapment of respirable particles. During the First World War, electrostatically enhanced filter media have been developed for respiratory protection. They are sealed in a container wherein the particle ranges between 0.1 and 1 μm [6]. Various forms of electrostatic media have since been described and characterized [7], and while nonwoven filter structures currently dominate the market for highly charged media, it has been shown that such filters can also be manufactured in woven or knitted form for use in apparel [8–10]. One application that is of particular interest to this work is the use of electrostatic filter materials for the protection of trained and private individuals involved in the fighting of wildfires. If it is possible to use the superior effectiveness of such

N. Gokarneshan et al., *Emerging Research Trends in Medical Textiles*,
Textile Science and Clothing Technology, DOI 10.1007/978-981-287-508-2_18

filters to trap smoke particles, this protection can be achieved while imposing only a relatively low physiological stress on the wearer. Performance, however, varies strongly with the choice of materials that are used for making the electrostatic filter medium because only some fiber materials can take on and retain large amounts of electrostatic charge. A range of materials have been reported [11] to produce highly charged webs that retain stored charge over periods of many years [12, 13]. In firefighting, it is critical that materials resistant to high temperatures are used in order to avoid scalding should a person come into contact with a naked flame. Only a few publications on electrostatically enhanced filter media have so far given consideration to the aspect of high temperature [14]. This investigation is aimed specifically at high-temperature polymers that are used to date in PPE for firefighters or emergency personnel. These include polybenzimidazole (PBI), polyimide-amide (two different forms of Kermel), meta-aramid (Nomex), and para-aramid (comparable to Dupont's Kevlar). Performances are compared to polypropylene (PP) blended with wool (Merino), which is another fiber that is currently used in firefighter apparel. Results of investigations showed differences in performance for different fiber blends. Some of these blends attained best practice filtration performance.

18.2 Materials Used

Electrostatic blends of Merino wool and polypropylene have been previously investigated [15]. The studies indicate that such fiber blends can develop high levels of electrostatic charge and that the charge remains unchanged in the filter medium for several years. To extend the range of electrostatic blends investigated to include high-temperature and high-performance polymeric fibers, the new polymeric fiber materials were combined with either wool or polypropylene as the second component because these fibers had shown remarkable performance in previous experiments [16].

18.3 Fiber Details

The fiber properties of the Merino wool, polypropylene, and high-temperature polymer fibers have been considered. More information pertaining to the fiber properties has been obtained from fiber length profiles which are determined using a fiber array sorter and from fiber diameter measurements. Data pertaining to material densities, maximum operating temperatures, glass transition temperatures, and melting points are available from the literature. Wool being a nonthermoplastic fiber is characterized by a degradation temperature rather than a melting point. The properties of the various fibers clearly outlines the potential performance improvement that could be achieved in terms of the operating temperature, particularly

over polypropylene, if it was possible to use these materials successfully in electrostatic fiber blends [16].

18.4 Processing Equipment

The nonwoven filter media have been produced on a small-scale process involving two types of fibers that were blended into a loose web before carding. More entanglement has been permitted by use of needle punching, so as to increase the mechanical strength of the web. Batches of typically 100–150 g were blended on a flat surface and processed on a small-scale processing line in two stages, web formation followed by web consolidation. Web formation was carried out using a card that comprised of a single swift (1000 mm wide, 1525 mm diameter, with card wire), three worker sets, a single doffer, and a doffer fly-comb. A corona bar was located at a distance of 50 mm from the fly-comb. Web consolidation was done on a Hunter fiber locker (needle punch) with a 300-mm by 300-mm needle board with 1000 needles (40 gauge, 3 in. long, barb configuration 322). Needle penetration was 12 mm, and the drive speed was adjustable. The width has been restricted to 300 mm.

18.5 Results of Findings

The study is directed toward a specific type of electrostatic filter media, which are webs made from a blend of two different fiber materials. The electrostatic charge is created in the web due to rubbing of the fibers with each other. The rubbing action results in a selective accumulation of positive electrostatic charge on one type of fiber material (e.g., wool) and negative electrostatic charge on the other (e.g., polypropylene) under a process called ‘triboelectric’ charge separation. These clusters of accumulated charge become an electrostatic field that attracts fine dust particles to the fiber surfaces where they are captured. The accumulation of charge in the filter medium can be very stable in the right circumstances, particularly at moderate to low relative humidity, and can remain there for many years.

18.5.1 Filter Media

The physical properties of manufactured filter media have been evaluated. The blend ratio shows differences in fiber diameter, and material density for each fiber combination and the needling density have been set to achieve thickness of 5 mm. The basis weight and porosity have no specific bearing, but are shown for

information. Variations in pressure drop arise due to design-driven differences in the respective web structures and are affected during dust loading by the penetration of the medium and the fiber surface smoothness (e.g., affected by scales on wool). They are undesirable, but can only be avoided if fiber diameters are matched and fiber surfaces smooth.

18.5.2 Fiber Cleanliness and Surface Charge

Wool fibers have a natural waxy coating on their surface and can store electrostatic charge. But it is necessary to remove this wax due to its stickiness that binds fibers together. Synthetic fibers and clean scoured wool fibers are generally coated with spin finishes to suppress electrostatic charge, which disrupts the flow of fiber through the processing equipment. These surface finishes cause electrostatic charge to dissipate and therefore need to be removed prior to triboelectric charging of the filter medium. A number of spin finishes are soluble in water and can be removed by water-based scouring. Figure 18.1 depicts an infrared ATR spectra obtained from meta-aramid (AM) fibers both before and after DCM Soxhlet extraction.

The presence of surface active agents on the fibers has been seen in the form of CH_2 stretching vibrations. Carbonyl (C=O) stretching vibrations have also been seen often. Aliphatic esters have been usually seen on the high-temperature polymer fibers, upon analyzing the extract residues. This is consistent with the spectra obtained from the fiber surface (Fig. 18.1). Analysis of the extract obtained from the carbonized wool (not shown) revealed residual wool wax and surfactant to be the major surface contaminants. The extract residue from the polypropylene

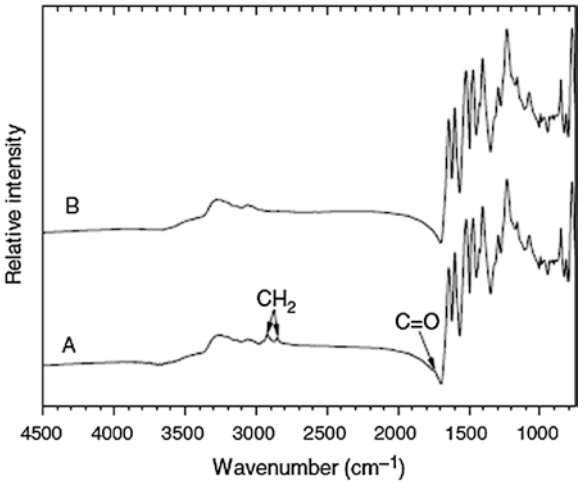

Fig. 18.1 Infrared ATR spectra of (*A*) as received AM and (*B*) AM after DCM Soxhlet extraction. Showing loss of CH_2 and C=O functional groups after extraction [16]

showed the presence of a POE (polyoxyethylene) fatty acid ester-based spin finish. In all cases, these were no longer identified after extraction. It would be reasonable to anticipate an effect from the natural presence of surface charged species on some of the materials. For example, the surface of wool in its natural state is weathered and will thus have negatively charged sulfonate groups present from the oxidation of the amino acid cystine. This negative charge can be easily transferred through contact with the surface of a suitable electron-accepting material, thus leaving the wool surface positively charged. Hence, wool acquires a position on the positive charge accepting side of the 'triboelectric series [11, 12, 17]. The surface of carbonized wool carries increased levels of negative charge as sulfate groups due to the carbonizing treatment [18]. A perceivable overall decrease in the fiber's positive charge can be observed. The stability of stored electrostatic charge was assessed by means of nondestructive clean filter testing. Figure 18.2 depicts temporal changes of filter penetration for a duration of 75 days for two high-temperature polymers, Nomex (AM) and Kermel Beige (PIAP), where samples were stored in sealed plastic bags at less than 65 %RH between individual repeats of tests. Each high-performance polymer fiber has been blended separately with polypropylene fibers or with wool and processed.

PIAP blended with PP shows a very high performance (low penetration) that is stable over time. But, the same polymer blended with wool shows a drastic decrease in performance with the penetration increasing to about 65 % before settling on a performance level. The wool blend with AM is exhibiting a temporal performance decay that is similar to that of PIAP but settles on 70 % penetration. The blend of AM with PP is also decaying, but settles on a lower penetration of about 40 %. As it is usual for some of the stored electrostatic charge to dissipate over a period of about 3 days after manufacturing, even if the fiber blend is electrostatically stable, it is not possible to clearly infer on the AM-PP blend merely on the basis of this measurement. Further information from dust loading experiments may shed some light on this.

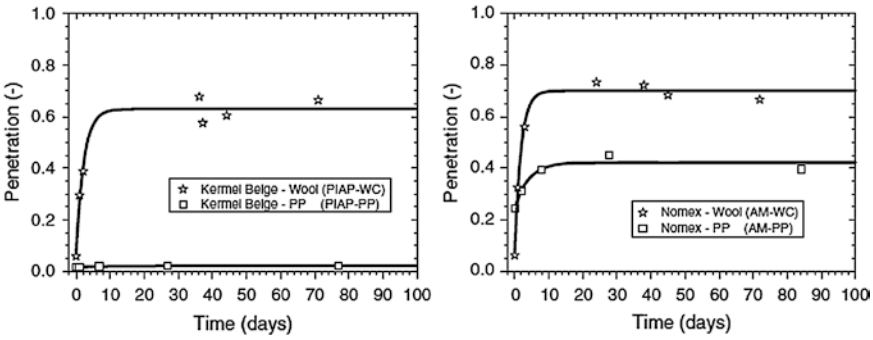

Fig. 18.2 Temporal changes in the penetration of fine particles of 0.3–0.5 mm diameter for blends of PP or WC with PIAP (*left*) and AM (*right*) [16]

18.5.3 Dust Loading Performance

The deposition of dust in most filter media causes the penetration to decrease and the pressure drop to increase due to clogging [19]. But, if a filter medium contains high levels of electrostatic charge, the effect of the charge becomes the dominating influence over all other particle capturing processes and influences the change in penetration dramatically. Under such circumstances, the penetration increases rather than decrease, due to the effect of stored charge is being reduced by the accumulation of dust in the filter medium. As the dust load in the filter medium increases, the effect of clogging is strengthening and eventually becomes the new dominant effect which causes the penetration to decrease again [20–25]. The filter performance has been characterized so as to satisfactorily account for this relatively complex behavior by plotting the penetration and pressure drop as a dependence of the cumulative dust load challenge, which is the amount of fine particle dust that the medium has been subjected to. Figure 18.3 exemplifies this aspect.

Past experience has shown that in the case of uncharged media, the quality factor Q remains in the vicinity of a characteristic value Q_0, which depends slightly on the construction of the filter test instrument. The value of Q_0 is approximately 7 kPa^{-1} for the 'dust loading' test and about 20 kPa^{-1} for the nondestructive 'clean filter' test. From previous results, it appears that this relationship shows surprisingly little dependence on fiber diameter in the range of 100 nm–100 mm (based on comparisons of meltblown and electrospun media) and a porosity of the medium within 0.80–0.96 [26]. Electrostatically enhanced media, on the other hand, can reach Q-values that are 10–100 times higher than Q_0 while they are in a clean state. But, with dust accumulation in the filter structure, the effect of electrostatic charge is decreased due to a charge shielding effect [27]. This effect is reflected in the dependence of the quality factor Q on dust load, as shown at the bottom of Fig. 18.3, which shows the value of Q falling continuously until it reaches an asymptotic value in the vicinity of Q_0, where the medium is fully discharged. This dependency is typical of highly charged electrostatic filter media, although there are some exceptions as illustrated in the discussion of results. Figure 18.4 shows the performance of P1-rated filter masks of melt blown polypropylene versus electrostatic wool–polypropylene filter medium. The filter masks investigated are model 8710 from 3 M and FR 5710 used by fire authorities in Australia. The latter mask has the lowest penetration of the three media compared and performs close to a P2 rating but imposes also the highest breathing resistance on the wearer, as expressed by the pressure drop [28].

The electrostatic medium shows the least pressure drop and complies with a P1 rating for dust loads above 10 gm^{-2}. It is well known that the electrostatic charge inside of a suitably designed triboelectric filter medium will remain there almost indefinitely [27]. An important criterion that should be satisfied to achieve this is to avoid adding charge depleting chemicals to fiber surfaces or to remove these chemicals as highlighted in the previous section. Satisfying this criterion will however not essentially always result in a highly charged triboelectric medium. The

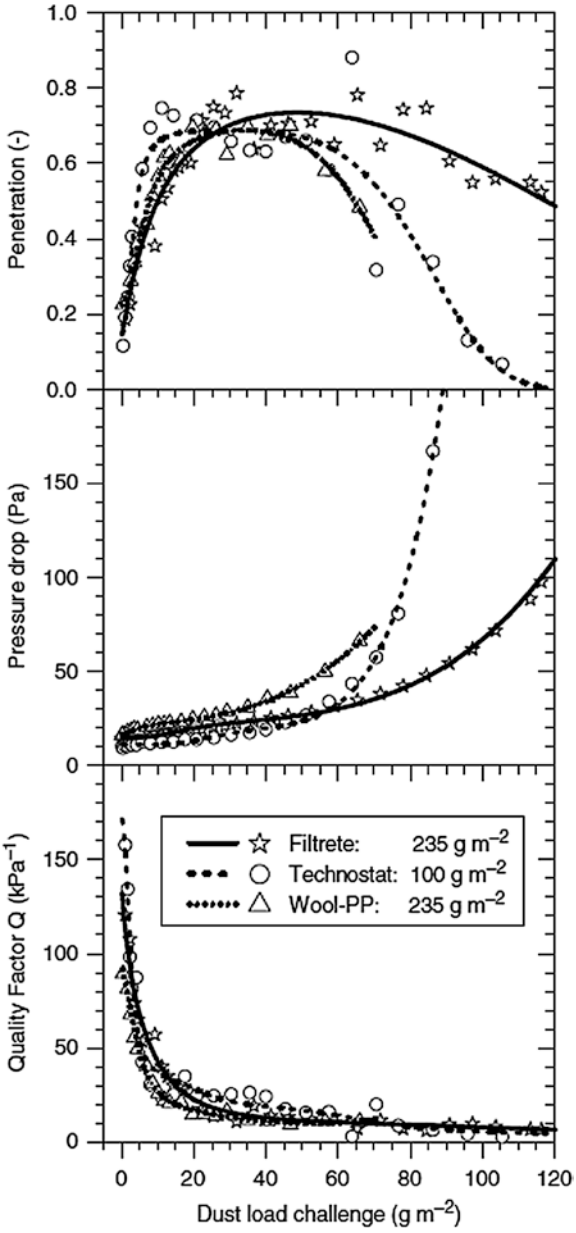

Fig. 18.3 Some examples of filter performances obtained from three types of electrostatic media: a polypropylene split-fiber electret (FiltreteTM), an all synthetic triboelectric medium (Technostat_) and a triboelectric blend of Merino wool and polypropylene (Wool–PP). The *plots* show from the *top* changes in penetration, pressure drop, and quality factor as a function of dust load challenge [16]

combination of fiber materials used also has a very significant influence on the outcome as will become more obvious from the dust loading results that are presented below [29]. Figure 18.5 shows changes in penetration and pressure drop with increasing quantities of collected dust.

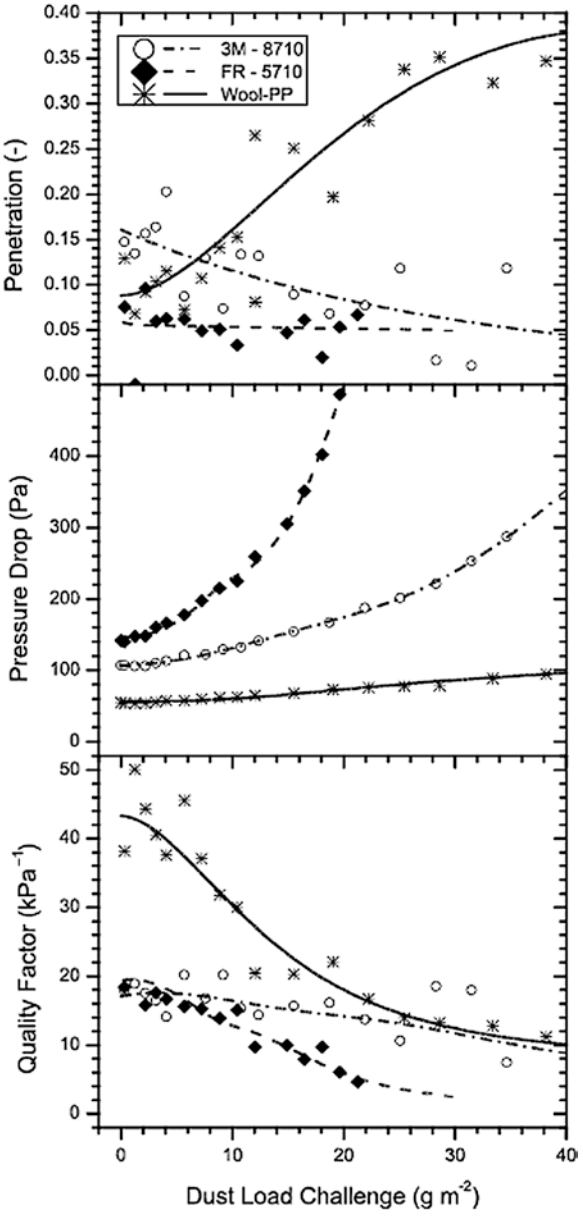

Fig. 18.4 Comparitive evaluation of dust load filter performances of P1-rated dust masks 3M 8710 and FR 5710 with an electrostatic wool–polypropylene blend filter medium [16]

Results of four high-temperature polymers blended with polypropylene, PP, (left-hand side) or wool, WC, (right-hand side) illustrate clearly the initial rise of the penetration to a specific maximum, from which it continues to diminish monotonically until clogged. The pressure drop increases monotonically at the same time, due to continuously increasing dust load collected by the medium.

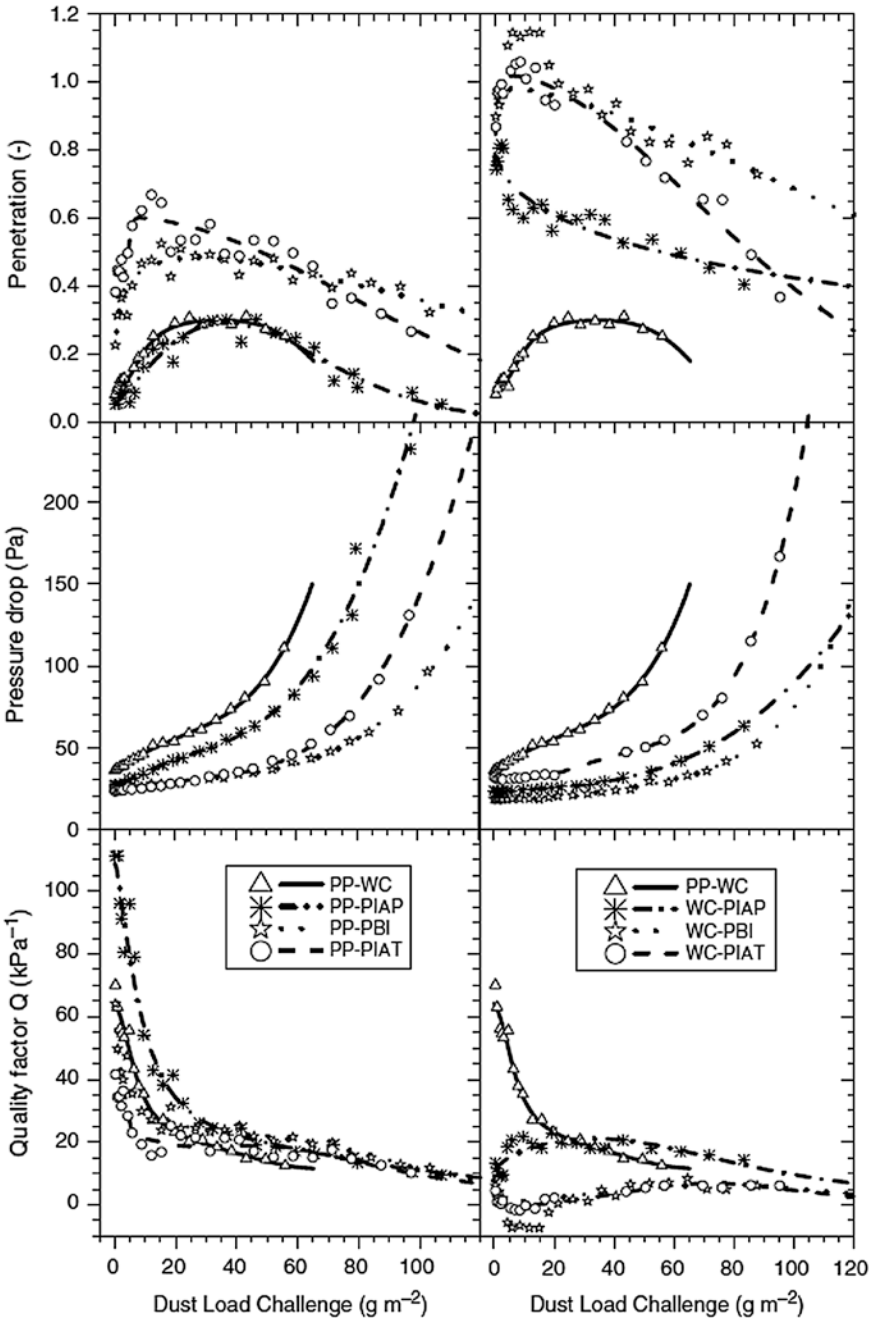

Fig. 18.5 Dust load dependencies for penetration, pressure drop, and quality factor of various high-temperature fiber blends with polypropylene PP (*left column*) and wool WC (*right column*) [16]

The quality factor given below is used to simultaneously track penetration and pressure drop changes of the filter medium, as it changes also with increasing dust load.

$$Q = \frac{-\ln(P)}{\Delta p}.$$

where Q is the quality factor and Δp is the pressure drop.

This quantity is generally fairly constant for essentially uncharged filter media, as is the case for the WC–PIAT blend in Fig. 18.5. Strongly enhanced media like WC–PP, on the other hand, can initially reach quality factor values more than 10 times higher due to electrostatic charge. The quality factor then drops to an asymptotic value close to that of an uncharged medium. All quality factor curves of fiber blends containing polypropylene (left-hand column) follow this behavior. But, in the wool fiber blends (right-hand column), only the blend of wool with polypropylene shows high levels of electrostatic charge. All other blends commence in the vicinity of the discharged value Q and Q_0 from where some blends reach slightly higher values for a period of time (e.g., WC–PIAP), while others drop (e.g., WC–PIAT), but only to return to Q_0 as the media lose the effect from electrostatic charge. In the case of the blends of WC–PBI and WC–PIAT, the measured penetration attains values greater than 1, which is reflected in the negative quality factor values. This behavior is seen on many occasions where filter media with nonpermanent charge have been tested. One possible explanation is that the filter medium is actively releasing some of the collected test dust back into the airstream. Dust loading performances of electrostatic fiber blends that contain aramids (AM, AP) are shown in Fig. 18.6.

A typical strong electrostatic enhancement is obtained for para-aramid fibers (AP) blended with polypropylene (PP), while results for the respective blend with wool (WC) suggest the presence of low levels of unstable charge. Meta-aramid (AM) fiber blends, on the other hand, have shown quite unusual performance patterns that have not been seen for any other fiber combination. The penetration of AM blends with both PP and WC, remained remarkably constant for dust loads up to 70 gm^{-2} in the case of PP–AM, and even higher for WC–AM. The initial quality factor of 30 kPa^{-1} is not terribly high, but it remains significantly elevated for the duration of the test, up to 120 gm^{-2}. This implies an intermediate performance level of permanent electrostatic charge that is for some reason only weakly affected by charge shielding [27]. Moreover, the blends of AM with WC and PP with WC are the only wool-containing blends that show significant levels of electrostatic charge.

18.5.4 Discussion of the Findings

The range of electrostatic filter media used can be grouped into three main categories based on their penetration maxima from dust loading performance testing.

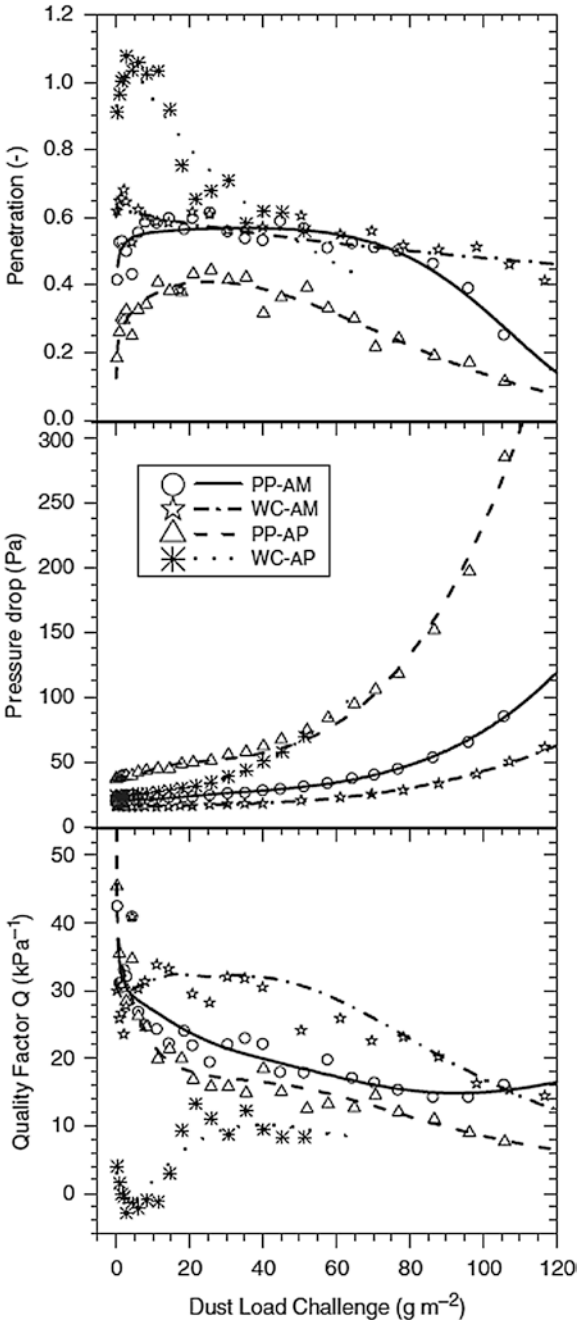

Fig. 18.6 Dust load dependencies for penetration, pressure drop, and quality factor of aramid blends (meta-aramid AM, para-aramid AP) with polypropylene (PP) or wool (WC) [16]

But, as the pressure drop has to be included with the penetration in the performance assessment, the corresponding grouping based on quality factor Q is also done. It is interesting to note that there is a group of filter media that perform to an intermediate level for which the stored electrostatic charge is perfectly stable over time. Such media do not match with the performance of the very best fiber blends. This is quite different to the media that exhibit low performances, where electrostatic charge is unstable and generally decaying over a period of a few days. A subgroup in the intermediate performance group shows unusual charge depletion characteristic. The quality factor is not particularly high for the filter medium as new, but it remains at that level for accumulated dust loads of 80 gm^2 or more. Hence, the medium has an unusually high 'dust holding capacity,' as the expected 'standard' behavior would be a continuous, asymptotic reduction of the quality factor into the vicinity of Q_0 where the medium is discharged. These media all have meta-aramid (Nomex) as one of the blended components. It would be convenient if it was possible to predict which blends generate high levels of quasi-permanent electrostatic charge and would hence be suited for the manufacture of high-performance filter media. The storage of electrostatic charge locally on fiber surfaces and the conditions under which they remain quasi-permanently attached has however been a scientific challenge for some time [11, 12, 17, 30, 31]. It has been suggested that the 'triboelectric series' of polymers, from which it is possible to determine for a combination of fiber polymers which one is likely to attract the positive charge and which one the negative, can provide some useful guidance in this regard. A number of polymers, like poly(ethylene terephthalate) (PET), readily accept charge when they are rubbed against a surface, but subsequently lose this charge within a period of hours to a few days. It has been suggested that the quasi-permanence of electrostatic charge, or the lack of it, is dependent on the electrical resistance of the polymer material, which must be very high for a material to preserve electrostatic charge over very long durations [32]. But, Merino wool appears to oppose this principle by producing quasi-permanently charged filter media in a blend with polypropylene, while the electrical conductance is fairly high because of the huge quantity of moisture that the fiber can absorb from ambient air [33]. In effect, while the triboelectric series may give some indication of the chargeability of a certain combination of fiber materials, the situations which enable the permanence of stored electrostatic charge are still now evading any successful prediction. Hence, it is required to determine the blends that perform best as electrostatic filter media through experiments. This can be done by monitoring the filtration performance to fine particle challenges over the useful service life of the medium. For the design of actual products such as bandannas, flexible respirators, and respirator canisters, it is necessary to consider, in addition to the filtration performance, other factors that are relevant to its use. The high-temperature polymers discussed herein are familiar to the firefighter apparel market, and properties relating to mechanical strength and abrasion resistance have been investigated by their manufacturers. But, the requirements of a respiratory protective device are different to those of apparel as breathability is a prime consideration. The electrostatic filter media can be manufactured as stretchable knits with fine particle

penetration remaining below 0.5 (50 %) at any time during loading with dust [10]. Also, there is no obvious obstacle to the production of electrostatic weaves. In this regard, it is possible to change from respirators as add-on devices to fully integrated all-apparel solutions. While the filtration performance is not as good as that of optimized respirator cartridges, it is still highly superior to nonelectrostatic materials being used in apparels. It can be useful during prolonged exposure to low or medium levels of smoke particles where individuals would not wear a half-face respirator so as to preserve stamina and energy. Electrostatic filter materials will furthermore provide some thermal protection after short exposure to high temperature. When polypropylene is used as one of the components, the smoke particle protection will probably cease after exposure to high temperature for a significant time duration. This leads to reduction in protection from smoke particles. However, the high-temperature component of the fiber blend can maintain the thermal protection and mechanical integrity. But, because of its low melting point, the presence of polypropylene in a filter medium to be used in firefighting applications makes the wearers susceptible to scalding if they come into contact with a naked flame, as indicated by flame spread tests. A blend of meta-aramid (AM) with wool (WC) is the only material found that contains no polypropylene and shows a stable electrostatic charge. However, even such blend fails the flame spread test, which is probably because of the presence of the wool. The filtration performance of this material is only average, but still interesting, particularly due to its unusual charge dissipation behavior and the suggestion that its performance shows only a minor dependence on the load of captured dust. On the basis of higher glass transition temperatures, it may also have a superior high-temperature filtration performance over other materials, but has not yet been proved. When considering results of polyimide-amides, it is interesting to observe that the ‘as is’ technical-grade material of the polymer, Kermel Tech (PIAT), belongs to the intermediate filtration group, while the dyed apparel-grade material, Kermel Beige (PIAP), matches the benchmark performances set by commercial products such as the wool/polypropylene blend. It would mean that the dye used plays a key role in the overall electrostatic properties of the material.

References

1. Havenith G, Heus R (2004) A test battery related to ergonomics of protective clothing. Appl Ergonomics 35(1):3–20
2. Chemical substances and biological agents—studies and research projects. Wildland Firefighter Health Risks and Respiratory Protection Consultant Claire Austin. R-572. Montre´ al: Institut de recherche Robert-Sauve´ en sante´ et en se´curite´ du travail (IRSST), 2008. http://www.irsst.qc.ca/files/documents/PubIRSST/R-572.pdf
3. Executive fire officer program. Structural Firefighters Use of Wildland Personal Protective Clothing and Equipment on Florida Wildfires District Manager, Florida Division of Forestry, Jacksonville, Florida USA C Bruce Jr. Hill. Emmitsburg, USA: National Fire Academy, US Fire Administration (USFA), 2000. http://www.usfa.dhs.gov/pdf/efop/efo29732.pdf

4. Burch GE (1945) Rate of water and heat loss from the respiratory tract of normal subjects in a subtropical climate. Arch Internal Med 76(5):315–327
5. Jones JG (1991) The physiological cost of wearing a disposable respirator. Am Ind Hyg Assoc J 52(6):219–225
6. Hansen NL (1932) Method for the manufacture of smoke filters or collective filters. Britain 384,052. 1 Dec 1932
7. Brown RC (1989) Effect of electric charge in filter materials. Filtr Sep 26:46–51
8. Garwanska R, Lekova V (1996) Development and study of electret fibrous materials for medical purposes. Fibres Text Eastern Eur 4(1):60–61
9. Schutz JA, Kyratzis I (2007) Aerosol protection: washable electrostatic barrier fabrics for fine particle scavenging. In: International conference on individual protective equipment, Melbourne. 16–19 Oct 2007, IPE 2007
10. Schutz JA, Kyratzis I (2007) Aerosol protection: washable electrostatic barrier fabrics for fine particle scavenging. In: International conference on individual protective equipment, Melbourne. 16–19 Oct 2007, IPE 2007
11. Smith PA, East GC, Brown RC, Wake D (1988) Generation of triboelectric charge in textile fiber mixtures and their use as air filters. J Electrostatics 21(1):81–98
12. Brown RC, Smith PA (1999) Triboelectric charging of filters and charge configuration. In: Stenhouse JIT, Gradon L, Marijnissen JCM (eds) Electret filters, production and properties. Delft University Press, Delft, pp 19–28
13. Schütz JA, Humphries W (2010) A study of wool/polypropylene nonwovens as an alternative to the Hansen filter. Textile Res J 80(13):1265–1277
14. Smith PA (1989) Electrically charged fibres in air filtration. Text Horiz 9:38–40
15. American society of heating refrigerating and air-conditioning engineers. Method of testing general ventilation air-cleaning devices for removal efficiency by particle size (ANSI Approved). Standard 52.2-1999. ASHRAE 2000
16. Schutz JA, Church JS (2011) Respiratory protection for physiologically straining environments. Textile Research Journal 81(13) 1367–1380
17. Schütz JA, Maxwell JM, Huson MG (2001) 3.7 hunt for charges in electret filters with a scanning probe microscope. Section 3: nonwoven composites and new applications. In: TANDEC 11th annual international nonwovens conference. The University of Tennessee, Knoxville, Textiles and Nonwovens Development Center (TANDEC)
18. Zhao W, Pailthorpe MT (1987) A study of wool carbonizing. 4. Surface-barrier effects in rapidly carbonized wool. Textile Res J 57(10):579–582
19. Davies CN (1973) Air filtration. Academic Press Inc., Ltd, London
20. Baumgartner H, Löffler F (1987) Particle collection in electret fibres filters—a basic theoretical and experimental study. Filtr Sep 24(5):346–351
21. Lethimäki M, Heinonen K (1994) Reliability of electret filters. Build Environ 29(3):353–355
22. Walsh DC, Stenhouse JIT (1997) The effect of particle size charge and composition on the loading characteristics of an electrically active fibrous filter material. J Aerosol Sci 28(2):307–321
23. Bostock GJ (1999) Electret filters for respiratory protection. In: Stenhouse JIT, Gradon L, Marijnissen JCM (eds) Electret filters, production and properties. Delft University Press, Delft, pp 59–68
24. Podgórski A (1999) Selected problems in the modelling of aerosol filtration in fibrous filters. In: Stenhouse JIT, Gradon L, Marijnissen JCM (eds) Electret filters, production and properties. Delft University Press, Delft, pp 95–106
25. Walsh DC, Stenhouse JIT (1998) Parameters affecting the loading behavior and degradation of electrically active filter materials. Aerosol Sci Technol 29(5):419–432
26. Schütz JA (2008) Interdependence of fine particle filtration performance and dust load for electrostatic media. Filtration 8(3):252–258
27. Stenhouse JIT, Walsh DC (1999) Experimental measurements of filter loading characteristics. In: Stenhouse JIT, Gradon L, Marijnissen JCM (eds) Electret filters, production and properties. Delft University Press, Delft, pp 85–93

28. Committee SF/10 industrial respiratory protection. Respiratory protective devices. AS/NZS 1716:1994. NSW. Australia: Standards Australia, 1994
29. Brown R (1984) Air filters made from mixtures of electrically charged fibres. In: Vanbrabant R, Weiler R (eds) Electrical and magnetic separation and filtration technology. Koninklijke Vlaamse Ingenieursvereniging, Antwerpen (Royal Flemish Society of Engineers)
30. Baumgartner H, Löffler F, Umhauer H (1986) Deep-bed electret filters—the determination of single fiber charge and collection efficiency. IEEE Trans Electr Insul 21(3):477–486
31. Schwan R (1989) Einfluss der morphologie und elektrostatik von synthesefasern auf die filtertechnischen eigenschaften moderner filtermedien (Influence of morphology and electrostatic charges of synthetic fibres on operating charcteristics of modern filter media). Melliand Textilberichte 70:577–581, 653–659 (English edition, 1989); 8: E246–E248, E277–E280
32. Tsai PP, Wadsworth LC (1996) Effect of polymer properties on the electrostatic charging of different media structures for air filters. Society of Plastics Engineers Technical Papers, pp 3642–3651
33. Brown RC, Wake D, Smith PA (1994) An electrically augmented filter made from conducting and dielectric fibers. J Electrostat 33(3):393–412

Chapter 19
Ammonia Plasma Treatment of Viscose Wound Dressings

19.1 Introduction

There has been a long history regarding the application of textile wound dressings. Viscose fiber has been widely used in woven and nonwoven textiles as well. Despite the fact that viscose outscores other similar fibers such as lyocell, and modal, with respect to sorption capacity and wet ability rate, these properties are well below those of alginate fibers. The absorption characteristics of cellulosic materials can be enhanced by a number of techniques and chemical processes [1–7]. But, the properties of the treated materials get degraded by such chemical processes. The low-temperature gaseous plasma offers an eco-friendly option. This medium exists as thermodynamically non-equilibrium state of gas [8–11]. The charged particles attain particular kinetic energy by getting accelerated in electrical fields. A number of electrical discharge methods are available for producing plasma, and electrode-less high-frequency discharges are more common as they permit production of many neutral excited reactive particles that include radicals, neutral atoms, and molecules excited to both electronically and vibrationally excited states [12]. Light particles (electrons) can follow changes in the local electrical field in such discharges so they gain kinetic energy well above the energy of random movement at room temperature, but heavy particles (neutral as well as positively and negatively charged atoms and molecules) cannot, providing the electric field frequency is more than about 1 MHz. The electrons can transfer only a small amount of their kinetic energy to heavy particles and hence remain essentially at room kinetic temperature. In the gas phase, neutral atoms are often stable at considerably less pressure. They do not get lost by heterogeneous surface recombination, under the absence of metallic electrodes.

N. Gokarneshan et al., *Emerging Research Trends in Medical Textiles*,
Textile Science and Clothing Technology, DOI 10.1007/978-981-287-508-2_19

They are not lost, and hence, the dissociation fraction of gaseous molecules at room kinetic temperature can attain a sufficiently high percentage [8–10]. The reason for good stability of atoms at low pressure is a low probability for three-body collisions that can only lead to recombination of atoms to a parent molecule in the gas phase. The created plasma particles are highly reactive and hence create a conductive medium for the surface modification, like functionalization of organic materials and formation of nanostructured materials without affecting the bulk properties of solid materials [13–16]. In the past, the traditional theory has always been that wound should be kept dry so that a scab may form over the wound: The wound should be exposed to the air and sunlight as much as possible. The distinct demerits with these principles are that the scab, composed of the dehydrated exudate and drying dermis, pose a physical barrier to healing which is then delayed, since the epidermal cells cannot move through the scab formed. The temperature at the wound surface exposed to air decreases, resulting in peripheral vasoconstriction affecting the flow of blood to the wound and thereby delaying further healing. Earlier it has been shown that the wound healing under moist conditions healed faster than the wounds under dry conditions, open to air [17]. The removal of excessive exudate from the wound without allowing the wound to dry out, thereby maintaining a moist environment alone, is an insufficient benefit in modern wound dressings. Additional properties promoting wound healing are required, for example, the ability to prevent infection. The use of biologically active polymers through either by binding drugs onto them or by introducing various functional groups enables to check bacterial or fungal growth on fabric. The quality and quantity of protonated amino groups have a good effect on the antimicrobial properties of functionalized fiber-oriented polymers [18, 19]. Many metal ions have antimicrobial activity [20–22] but are either very toxic or not safe for patients [23–26] and the environment. Considering the aforementioned aspects, the wound infection control in the wound environment can be beneficial, and wound dressings having both properties are desirable. Most available procedures combine different functionalization steps one after another, that is, for improving sorption [1–7] and antimicrobial properties [27–38]. Also, more than 400 individual advanced hydrophilic wound dressings, including 25 alginates, 55 foams, 50 hydrocolloids, 51 hydrogels, and 24 transparent films [39] and dressings that contain and release antimicrobial agents at the wound surface, are available in the market [40]. However, there is a small literature available addressing a one-step procedure resulting at the same time in an excellent adsorption and bacterial load management, which leads to longer wear time of dressings and quicker wound healing. The influence of environmentally friendly treatment on hydrophilicity and antimicrobial activity has been discussed herein, and an attempt was made to define the practical balance between high hydrophilicity and antimicrobial activity. The surface composition and morphology of viscose after plasma treatment can be changed based on the gases used and the duration of the treatment [41–43]. Considering this aspect, viscose nonwoven fabric has been exposed

to ammonia gas at various time durations. X-ray photoelectron spectroscopy has been used to study the surface properties, while atomic force microscopy has been used to determine the morphological changes. The antimicrobial activities have been measured by adopting the AATCC test method, and the influence of plasma modification on the hydrophilicity of viscose has been assessed by monitoring the water rise and contact angle [44].

19.2 Surface Chemical Composition

The effectiveness of producing nitrogen functionalities onto sample surface has been studied by utilizing the X-ray photoelectron spectroscopy. The spectra have been obtained for untreated and ammonia plasma-treated viscose samples (Fig. 19.1). The Fig. 19.1b exhibits a typical spectrum for a sample exposed to ammonia plasma for 20 s yarn. The same spectra have been obtained for samples treated with plasma at other exposure times (not discussed herein). The elemental survey spectrum of the ammonia plasma-treated viscose sample shows an N peak with a binding energy (BE) of 399.2 eV, which is a good evidence for the presence of nitrogen atoms on surfaces [45]. The detailed data from XPS scans on different surfaces have been obtained. The O/C ratio for untreated sample slightly differs from theoretical value. The difference arises due to surface contaminants along with small amounts of C–C carbons practically found on all measured samples [46, 47]. The data relating to higher atomic percent carbon and lower atomic percent oxygen for a short duration of plasma exposure have been gathered. It has been observed that atomic percent nitrogen attains a value of 10 %. This value does not reflect the real content of nitrogen on the surface of the sample, since the escape depth of photoelectrons should be taken into account. The real concentration of N-atoms on the surface is probably higher. Longer duration of treatment and lower discharge power favor high nitrogen, as pointed out by other researchers [48]. But it is necessary that a high-resolution scan signal could also be acquired and properly charge

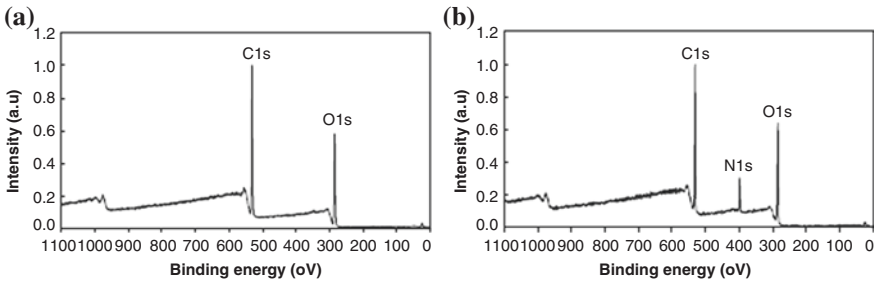

Fig. 19.1 X-ray photoelectron spectroscopy spectra of **a** nontreated, **b** and ammonia plasma-treated viscose sample for 20 s [45]

compensated to establish the peak BE. However, the technique is not useful in this specific case, owing to the rich morphology of the particular samples. Best results using high-resolution XPS spectra have been obtained for almost flat and homogeneous surfaces, as available from literature, and the rich morphology leads to broadening of peaks. Hence, the characterization of materials using high-resolution XPS on the C1s peak fails in cases of heterogeneous materials with complex morphology [49].

19.3 Surface Morphology

The application of ammonia plasma treatment on the surface morphology changes has been studied using atomic force microscopy (AFM). The 3D AFM images of untreated as well as plasma-treated viscose samples using ammonia gas for 100 s yarn are shown in Fig. 19.2.

It can be seen that there is a substantial difference between untreated and plasma-treated samples [45]. The morphology of the plasma-treated sample appears much richer. This type of behavior has been noticed in a number of polymers [50]. However, the phenomenon is clearly understood. One possible explanation is that the small in homogeneity of the original material reflects in selective etching, since the etching rate depends on the degree of crystallinity of polymers, as demonstrated by Junkar et al. [51]. Recently, a number of complex mechanisms have been reported [52]. The nanosurfaces which are rough and functionalized do not permit for accommodation of bacteria.

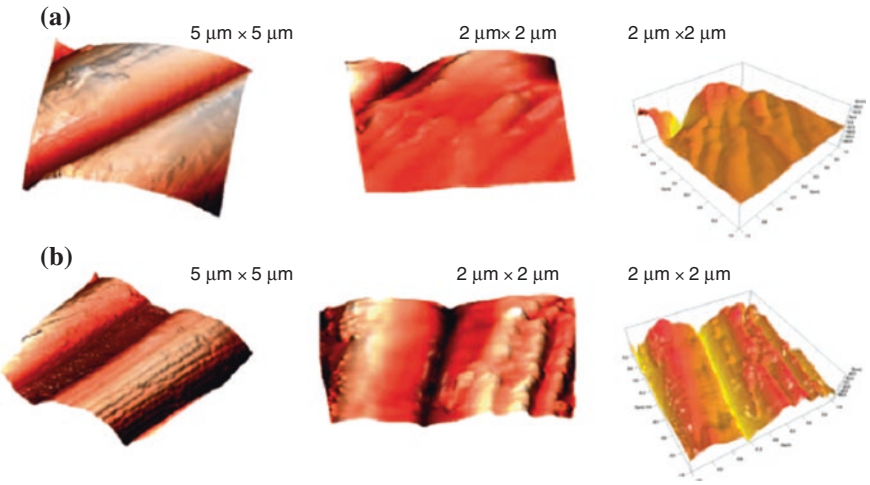

Fig. 19.2 X-ray photoelectron spectroscopy spectra of nontreated (**a**) and NH_3 plasma-treated viscose sample for 20 s (**b**) [45]

19.4 Hydrophilic Properties

Figure 19.3 shows the rise of water in untreated and plasma-treated viscose samples based on the duration of exposure to ammonia gas [45]. The curves are plotted as terms of gained mass versus time. The absorbency capacities presented as the amount of liquid uptake in equilibrium are also shown in the figure. The untreated sample exhibited the slowest water rise, as the complete wetting was noticed only after about 100 s. The quantity of water uptake in equilibrium was about 0.98 g.

The ammonia plasma-treated samples attained the equilibrium value quicker. Even a brief treatment for 20 s permitted for reaching the equilibrium uptake in a much lesser of about 20 s. The above figure showing water uptake imply a monotonous decrease of the time required for attaining equilibrium with increasing duration of plasma treatment. The duration is only a few seconds for prolonged plasma treatment and the equilibrium amount of water uptake more than 1 g. On the other hand, in the initial stage of water uptake, the mass^2 data plotted versus time, as presented in Fig. 19.4, are fitted by straight lines, according to the modified Washburn equation.

During the initial water uptake for the first three seconds, the curves show the minimum imbibition of water as indicated by the untreated sample. In the case of all ammonia-treated samples, the rate of water uptake was quicker and was based on the duration of plasma treatment. For short duration of treatment, the differences between samples are very significant, and for longer duration of treatment, the difference is less significant. In the case of absorbent nonwoven materials, the absorbency rate is also an important performance parameter to be taken into account. The figure four indicates the absorbency rate, which is plotted as mass^2 versus

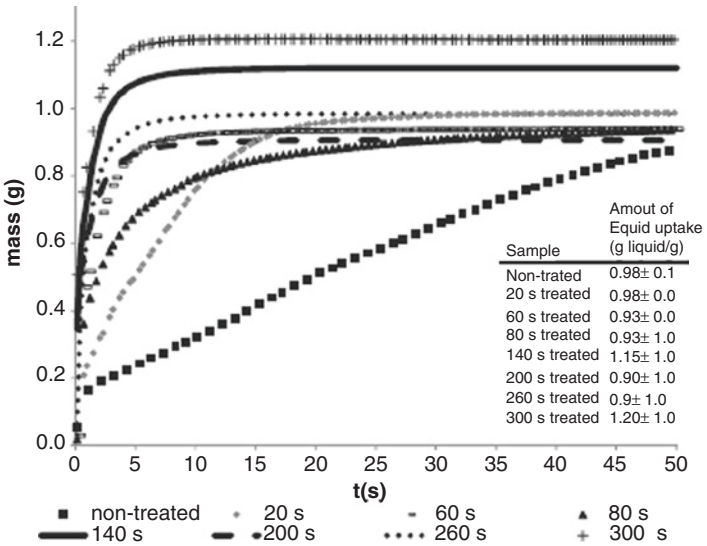

Fig. 19.3 Water rise of untreated and plasma-treated viscose samples at various exposure times to ammonia gas—20, 60, 80, 140, 200, 260, and 300 s [45]

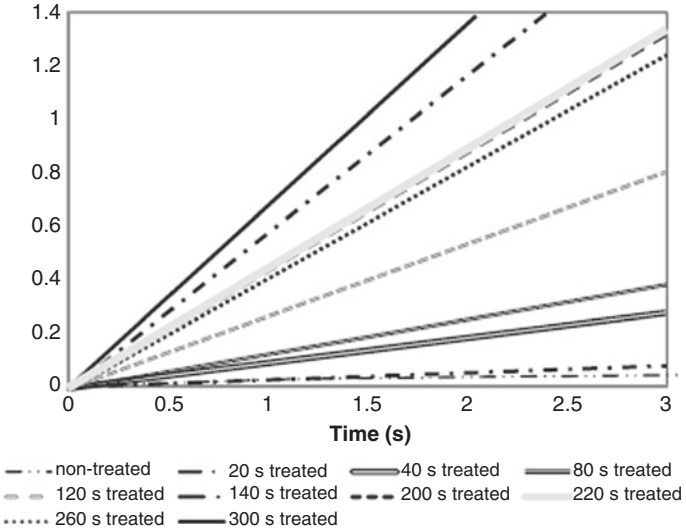

Fig. 19.4 Square mass data of water rise on untreated and plasma-treated viscose samples at various durations of exposure to ammonia gas—20, 40, 80, 120, 140, 200, 220, 260, and 300 s [45]

time. The absorbency rate is governed by the balance between the forces exerted by the capillaries and the frictional drag offered by the fiber surfaces.

The above figure exhibits a marked increase in the absorbency rate. The results shown in Fig. 19.5 demonstrate a dramatic increase of the absorbency rate by

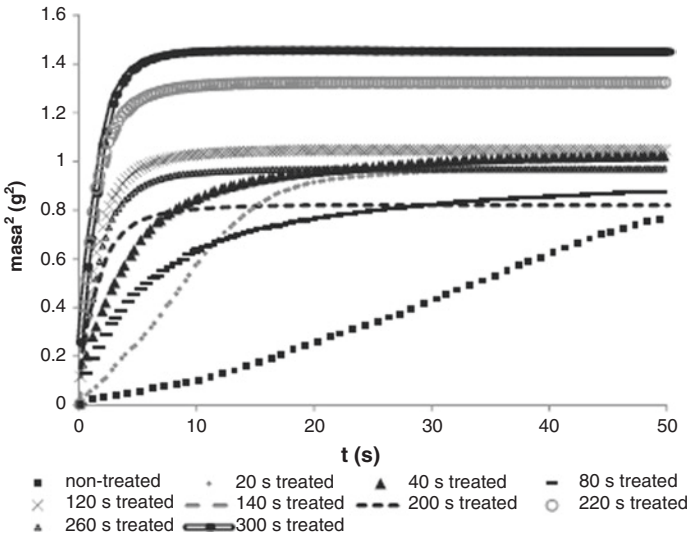

Fig. 19.5 Absorbency rate of nontreated and plasma-treated samples depending on exposure time to ammonia gas, that is, 20, 40, 80, 120, 140, 200, 220, 260, and 300 s [45]

plasma-treated material versus the untreated material. The duration of treatment influences the absorbency rate of the plasma-treated material. The absorbency rate increases with the increase in the duration of exposure. The plasma treatment improves the hydrophilicity. The nontreated sample shows a water contact angle of about 89°. The contact angles constantly decreased with increasing plasma exposure time up to about 140 s. Thereafter, the contact angle remains fairly constant at the value of about 40°. Apparently, some kind of saturation of surface wettability is observed at long durations of treatment.

19.5 Antimicrobial Activity

The ammonia plasma-treated viscose and untreated viscose materials have been compared for a range of bacteria. *Staphylococcus Aureus and Enterococcus Faecalis* (Gram-positive) and *Escherichia coli and Pseudomonas Aeruginosa* (Gram-negative) have been tested in the investigation [45]. All the four bacteria have been selected as they are known to be common wound pathogens having higher antibiotic resistance, rendering them difficult to treat. Only the materials exposed to ammonia gas for 60 and 300 s are being considered, as reduction (R) after 24 h of tested bacteria incubation. The AATCC test method 100–1999 shows the percent of reduction as result $R¼0$ or $R < 60$ in the situation where the sample does not possess bacteriostatic characteristics. The mentioned was evident by non-treated sample, except the 77 % reduction with *E. Faecalis* was a surprise. Viscose material treated with plasma, irrespective of used treatment time, showed antimicrobial properties by Gram-positive bacteria, which has been more pronounced for *S. Aureus*. The duration of exposure of the plasma had considerable effect by Gram-negative bacteria, as the reduction was clearly visible only for viscose materials imparted by ammonia gas for 300 s.

19.6 Discussion of Findings

19.6.1 Effect of Plasma Parameters

The plasma is abundant in reactive particles that are charged and neutral as well. In addition, the plasma created in hydrogen-containing gases is a good source of ultraviolet (UV) radiation. Despite the fact that the UV radiation is not really visible from the optical spectrum presented in Fig. 19.6, it exists due to the following reasons. Firstly, very intensive hydrogen atomic lines are observed in the spectrum. The lines originate from transitions of H atoms from the higher to the first excited states (Balmer series). As usual, the highest line, marked Ha, corresponds to the transition from the second to the first excited state of hydrogen atoms [45]. If these transitions are intensive, even more intensive will be the transitions to the

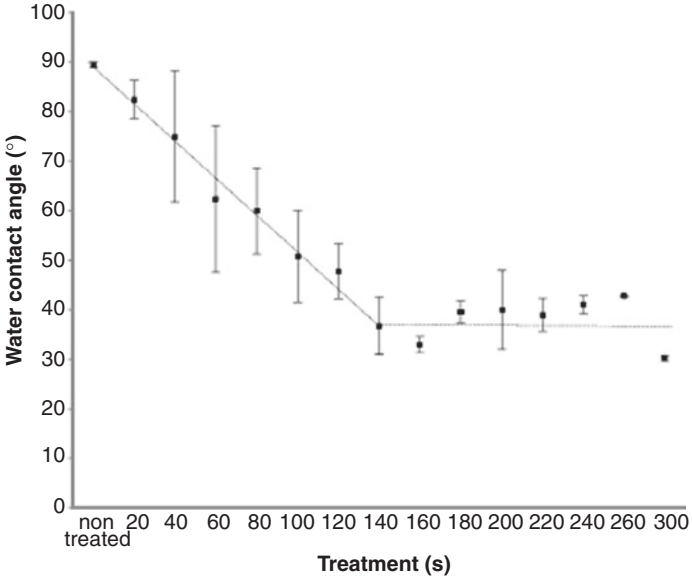

Fig. 19.6 Water contact angles of nontreated and plasma-treated viscose samples depending on exposure time to ammonia gas, that is, 20, 40, 60, 80, 100, 120, 140, 160, 180, 200, 220, 240, 260, and 300 s. To make the dependency hydrophilicity versus exposure time clearer, the *dashed line* is added as an eye guide [45]

ground state (Lyman series). Namely, H atoms do not have metastable excited states, so the excitation of any state is due to the direct transfer of kinetic energy of electrons (electron impact excitation) (Figs. 19.7 and 19.8).

Moreover, strong radiation can arise from the relaxation of excited molecules formed by heterogeneous surface recombination of H atoms. This recombination certainly appears in the experimental system and is proved by the mass spectrum presented in Fig. 19.2.

The proof for such intensive UV radiation has been reported recently [53]. This emission is not noticed in Fig. 19.1, since the sensitivity of the optical spectrometer in the UV range is much lower than in the visible range, and the fact that transmission of borosilicate glass for light quanta reduces quickly with reducing wavelength in the UV range. Energetic photons are thus present in the reactor and cause destruction of molecular bonds in the materials, leading to formation of free radicals on surfaces [54]. The depth of photon penetration is not large but large enough to modify viscose material not only on the surface but also in the bulk of the material. The plasma has positively charged molecules and atoms. The ions are accelerated across the sheath next to the sample and cause modification of surface functionalities on the surface of the samples. Considering a flat surface and the possibility for interaction between an impinging ion and a carbon atom on the surface was 1, the surface can saturate with ion-induced functionalities in a short duration that can be estimated considering the flux of ions onto the surface and

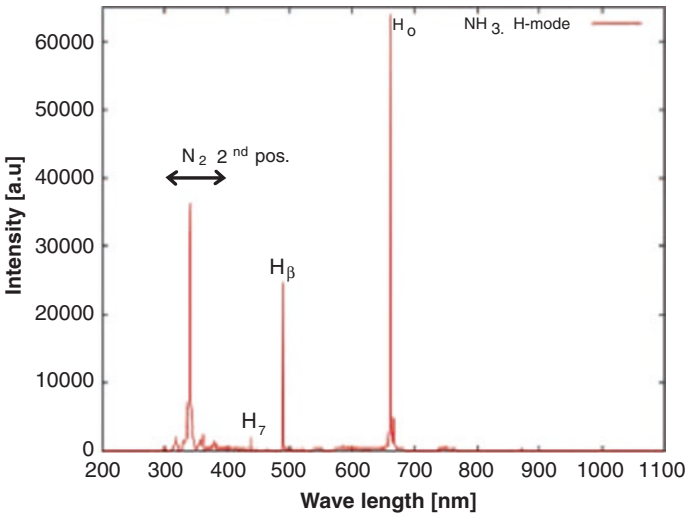

Fig. 19.7 A typical optical spectrum of plasma created in NH_3 gas at the pressure of 150 Pa and radio frequency power of 100 W [45]

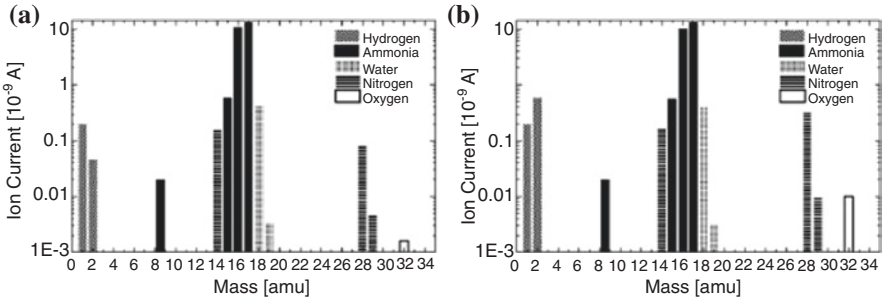

Fig. 19.8 Two mass spectra of NH_3 gas in equilibrium state (**a**) and in plasma state (**b**) [45]

the surface density of atoms in solid materials. The required duration for saturation in the upper approximation is thus solely 0.05 s. Practically, the surface is very rough due to fibril structure of the sample, so the real surface area is orders of magnitude larger than the geometrical time. However, if ions were responsible for modification of the surface properties, the saturation would appear in a much shorter duration of treatment than about 140 s. In surface modifications, ions are not apparently the only plasma particles responsible. Besides charged particles whose density in plasma has been determined with the double electrical probe, neutral reactive particles are also present in the plasma.

A substantial number of ammonia molecules dissociate in plasma at reasonably high RF power (Fig. 19.9). The molecular density is about 4×10^{22} m^{-3} at the

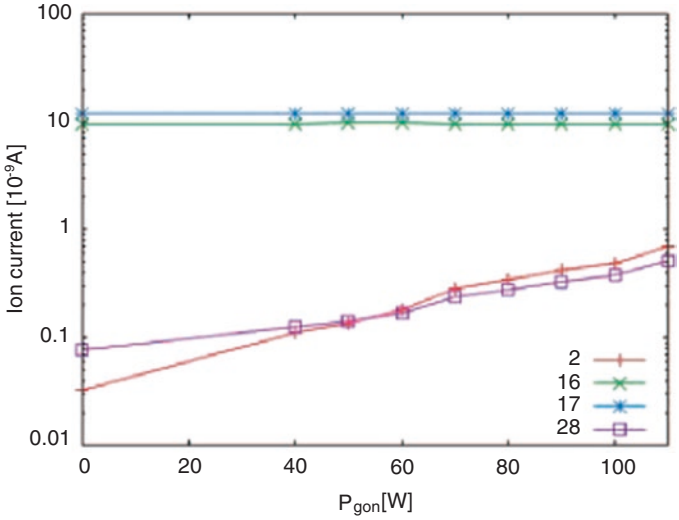

Fig. 19.9 The height of typical mass peaks versus the power of the radio frequency generator [45]

pressure of 150 Pa. The density of reactive nitrogen atoms is about 1×10^{21}, thus five orders higher than the density of ions, and they definitely play a role in functionalization of the materials [45].

19.7 Plasma Surface Chemical Modifications

The nitrogen-containing functional groups are influenced by ammonia plasma, and the distribution and density of the functional groups can be suitably altered with plasma parameters. In the case of many materials, the saturation of the materials with nitrogen has been noticed even after a short exposure to an atmosphere filled with N-atom [55]. The XPS results just confirm this theory, since the surface of our samples contains a substantial amount of nitrogen as revealed from Fig. 19.8. Efforts to achieve a high-resolution C1s peak failed because of the nature of the samples, as well attenuated total reflectance (ATR). Fourier transform infrared (FT-IR) spectroscopy cannot be used to identify the chemical groups if the thickness of a plasma polymer material is in the micrometer range [56, 57]. Hence, extraction of the exact functional groups appearing on the viscose samples upon ammonia plasma treatment has not been possible. According to the relevant literature, a variety of functional groups may appear on the surfaces and the effect of post-plasma oxidation could convert amines into amides [58]. But it is intriguing to note that the oxygen concentration on the surface as shown from the XPS results dropped by almost a factor of 2 for prolonged

plasma treatment. This significant reduction in oxygen concentration can be explained by the formation of oxygen-free nitrogen-functional groups, particularly when considering the chemical structure of nontreated viscose and the final depth resolution of XPS devices [45].

19.8 Changes in Surface Topography

Plasma particles can be etched on polymer materials in a very selective manner [53, 54]. A significant increase in the surface roughness can be observed on the surface morphology (Fig. 19.5) of the plasma-treated sample in comparison with untreated material. While the fibers are rather flat prior to plasma treatment, they obtain rich morphology after the treatment. The morphological change certainly has an effect on both adsorption and absorption of water and other fluids. The results summarized in Figs. 19.3 and 19.8 are therefore explained by combined effects of surface functionalities and roughness. The two factors influence the contact angle of a liquid on a solid surface. Increased roughness allows for excellent hydrophilicity of materials with high surface energy. The high merit of weakly ionized plasma created by electrode-less high-frequency discharges is that the neutral reactive particles abound and their density attains values over $10^{21}m^{3.11}$. The neutral atoms play a crucial role in etching, as excellent functionalization of the sample surface is easily obtained even by gaseous ions from plasma. The synergistic effects of ions and neutral nitrogen atoms allow for etching of polymer materials even at room temperature. This etching is restricted to the fibers on the very surface of the samples, as the ions cannot penetrate through inter-fibril spaces. Neutral atoms, on the other hand, easily penetrate deep into pores due to poor probability for heterogeneous surface recombination. Despite not being as reactive as ions, they also cause slow etching of polymer materials and can modify surface morphology of fibers even within the bulk of materials. Recently, it has been that neutral atoms can etch polymers at room temperature without the presence of any ions [59]. Hence, the etching enables increased roughness of fibers, which is a certainly advantageous.

19.9 Plasma-Induced Hydrophilicity

Hydrophilic properties are not only based on the functionalization of the sample on the surface, but also on the functionalization of the bulk of the material as well [45]. The used nonwoven samples were a few millimeters thick and composed from randomly oriented viscose fibers. Hence, it is necessary to modify the bulk of the sample so as to achieve optimal hydrophilicity. A big difference is seen between nontreated and ammonia plasma-treated samples. The water rise (defined as the squared mass gain in a unit time) is rather low in the case of untreated

material. During the initial 3 s, it is only about 0.04 $g^2\ s^{-1}$. As the untreated materials are moderate in hydrophobic properties, the rise is rather low. For the next sample tested (treated with plasma for 20 s), the water rise is improved significantly and is about 0.16 $g^2\ s^{-1}$ during the first 3 s of uptake time. The water rise curves keep increasing with increasing plasma treatment time, and for treatment times exceeding, say, 140 s, the material saturates with water already in a few seconds of uptake time (Fig. 19.3). The corresponding initial water rise curves approach values above 1 $g^2\ s^{-1}$, which are about 30× larger values than for untreated material. This significant improvement in the water rise cannot be explained merely by improved adsorption of water on the surface of samples, but bulk effects need to be considered. Obviously, the prolonged treatment of samples with plasma permits for optimization of the hydrophilic properties of viscose material. The optimization is explained by the modification of surface properties throughout the bulk of the sample. The high-energetic photons penetrate deep into materials and cause bond scission in solid material. Such interaction results either in reorganization of the atoms in cellulose material or in chemical interaction with hydrogen and nitrogen atoms that abound in plasma reactor. Moreover, neutral atoms in the ground state can form functional groups on the surface of polymers even in the absence of UV radiation. Namely, experiments performed in late flowing afterglows, where only the most stable particles created in plasma (predominantly neutral atoms in the ground state apart from metastable molecules with long radiation relaxation times) are present, showed similar results in terms of polymer surface functionalization as the experiments in plasmas themselves [59]. Hence, the functionalization in the bulk is influenced by diffusion of neutral reactive plasma particles, and it explains the rather slow improvement of the water rise versus plasma treatment time (Figs. 19.3 and 19.4). The sorption properties should improve in a second plasma treatment if functionalization of the surface alone is considered. Here, it is worth mentioning that there is not a strict parallelism between the water uptake amount and the exposure time of samples with ammonia gas. The deviation is roughly within the limits of statistical errors that are presented in Fig. 19.3. Considering the systematic error, which is also estimated to about 10 %, the curves lay well within the total error for this sort of measurements. The poor parallelism between the water uptake amount and the plasma exposure time can thus be explained with the accuracy of this particular experimental procedure. The contact angle of untreated material (Fig. 19.5) is rather high at about 90°. Even a short exposure to plasma for 20 s results in a drop of the contact angle for several degrees and the contact angle keeps reducing monotonously (almost linearly) with increasing treatment time until it attains an angle of 40° after roughly 140 s of plasma treatment. Further, the water contact angle remains fairly the same. Obviously, some kind of saturation appears after 140 s of plasma treatment. Considering upper considerations, it is possible to conclude that this treatment time permits for throughout functionalization of the material and further exposure does not affect the wettability of the samples. The structural geometry of the textile material also affects the penetration of the fragmented gas particles into the voluminous textile. The nonwoven sample has

many fibers disorderly gathered together, which also forms spacing between fibers. At low pressure, the mean free path (the distance traveled by a molecule or atom between successive collisions) in the gas phase is higher than the textile distances, and the collision of gas molecules with the fiber surface is enhanced as compared to gas–gas collision, thus favoring a good penetration of plasma species into the textile. This implies that the obtained hydrophilicity of the plasma-treated sample has improved significantly because of the loosely structured nonwoven material [60].

19.10 Plasma-Enhanced Antimicrobial Properties

The reduction rate for untreated material is zero, while surprisingly enough a 77 % reduction for *E. Faecalis* has been evident, within the tolerance limits of experimental error. Plasma treatment for smaller duration shows a sufficient antimicrobial effect as long as *S. Aureus* is the merit. Longer duration of exposure to ammonia gas showed adequate antimicrobial effect for Gram-negative bacteria and does not seem to affect the growing of *E. Faecalis*. The observed effect cannot be explained directly, as the interaction between the bacterial cell wall and plasma-treated materials is generally unknown [45]. The nitrogen-rich functional groups on the surface of viscose materials may cause a stress to bacteria and thus inability to grow and multiply in such an environment [18, 19]. The stress is due to particular interactions between nitrogen-containing functional groups and the bacterial receptors, but any discussion on exact mechanisms is out of scope here. As the type and concentration of various nitrogen-containing functional groups cannot be seen from XPS results, any further discussion is not valid. *E. Coli* and both Gram-positive cultures are nonmotile, while *P. Aeruginosa* is a motile bacteria. Hence, the reason for ''discrepancy' in reduction, irrespective of used treatment, could be in bacteria cell size and shape [46]. *S. Aureus* is cocci of 1 mm diameter and mostly arranged like irregular clusters [61]. *E. Faecalis* is a spherical bacterium of cell size 0.5–1 mm and seen as singly or in pairs with short chains. Both Gram-negative bacteria are straight or slightly curved rods, 1.5–2 mm long and stacked up next to each other. While the smaller individual bacteria such as *E. Faecalis* could easily get through the porous sample, larger arrangement settled cultures appearing as clusters or pairs have been unable to do so.

19.11 Factors Influencing Bacteria Adhesion

The very complex process of bacterial adhesion is influenced by a number of factors including the environmental factors, such as the associated flow conditions, the presence of serum proteins or antibiotics, the bacterial properties, and the material surface characteristics [62]. The factors influencing bacteria adherence

to a biomaterial surface include chemical composition of the material surface charge, hydrophobicity, and simply surface roughness or physical configuration [63–72]. The bacterial adhesion and proliferation are influenced by surface chemistry. Materials having various functional groups alter bacterial adhesion in a manner based on material hydrophobicity and charge. Upon altering or modifying the surface chemistry by plasma treatment (as an example), the bacterial adhesion to these surfaces gets hampered [71, 73–76]. It has been shown that decreased bacterial adhesion happens due to significant alteration in the hydrophilicity (i.e., decreasing of contact angle) [71, 76]. It has been found that the irregularities of polymeric surfaces promote bacterial adhesion and biofilm deposition, whereas the ultrasmooth surface does not favor bacterial adhesion and biofilm deposition [77]. It occurs because a rough surface has a greater surface area and the depressions in the roughened surfaces provide more favorable sites for colonization. The surface morphology exhibited a significant increase in surface roughness (Fig. 19.5b), whereas the data obtained show satisfactory antimicrobial effect. Similar results have also been obtained [78]. A small increase in surface roughness showed a significant increase in bacterial adhesion, while larger roughness increase had no significant effect in bacterial adhesion compared to the smooth surface. This can be attributed to the nonlinear dependence of bacterial adhesion on surface roughness, which provides scope for further investigations, like broader range of surface roughness, surface area measurement, or analysis of surface configuration. Generally, bacteria with hydrophobic properties prefer hydrophobic material surfaces; the ones with hydrophilic characteristics prefer hydrophilic surfaces. But, the surface hydrophobicity of a material plays a more important role in bacterial adhesion than bacterial surface hydrophobicity. The bacteria are negatively charged in aqueous suspension. The surface charge of bacteria varies according to bacterial species and is influenced by the growth medium, the pH and the ionic strength of the suspending buffer, bacterial age, and bacterial surface structure. But, the relative contribution of bacterial surface charge to bacterial adhesion is not clear. As bacterial adhesion is a very complicated process influenced by a number of factors, such as bacterial-material properties and environment and, moreover, the experimental evaluation of the relative contributions of such factors is extremely difficult, more investigations are necessary to get better knowledge of the mechanisms of bacterial adhesion.

References

1. Hengstberger M, Kaltenecker O, Oppermann W (1999) Vliesstoffe mit superabsorbierenden Eigenschaften. Tech Text 42:295–297
2. Junping J, Xin L, Dequan Z et al (2010) Doping/dedoping process induced wettability switching of polyaniline-coated conductive textile. Acta Polym Sin 2:192–198
3. Hyde GK, Stewart SM, Scarel G et al (2011) Atomic layer deposition of titanium dioxide on cellulose acetate for enhanced hemostasis. Biotechnol J 6:213–223
4. Durso DF (1978) Chemical modification of cellulose—a historical review. In: Rowell RM, Young RA (eds) Modified cellulosics. Academic Press, New York, pp 23–37

5. Freytag R, Donzé JJ (1983) Alkali treatment of cellulose fibres. In: Lewin M, Sello SB (eds) Handbook of fiber science and technology: volume I: chemical processing of fibers and fabrics, fundamentals and preparation, part A. Marcel Deckker, Inc., New York, pp 91–121
6. Fengel D, Wegener G (1984) Reactions in alkaline medium. In: Fengel D, Wegener G (eds) Wood, chemistry, ultrastructure, reactions. Walter de Gruyter, Berlin, pp 66–105
7. Lewin M (1984) Bleaching of cellulosic and synthetic fabrics. In: Lewin M, Sello SB (eds) Handbook of fiber science and technology: volume I: Chemical processing of fibers and fabrics, fundamentals and preparation, part B. Marcel Deckker, Inc., New York, pp 91–243
8. Belmonte T, Pintassilgo CD, Czerwiec T et al (2005) Oxygen plasma surface interaction in treatments of polyolefines. Surf Coat Technol 200:26–30
9. Donkó Z, Hartmann P, Kutasi K (2006) On the reliability of low-pressure dc glow discharge modelling. Plasma Sources Sci T 15:178–186
10. Gaboriau F, Cvelbar U, Mozetic M et al (2009) Comparison of TALIF and catalytic probes for the determination of nitrogen atom density in a nitrogen plasma afterglow. J Phys D Appl Phys 42:055204–1–055204–5
11. Mozetic M. Extremely non-equilibrium oxygen plasma for direct synthesis of metal oxide nanowires on metallic substrates. J Phys D Appl Phys 44:174028–1–174028–9
12. Gorjanc M, Bukovsek V, Gorensek M et al (2010) CF4 plasmaand silver functionalized cotton. Text Res J 80:2204–2213
13. Canal C, Gaboriau F, Villeger S et al (2009) Studies on antibacterial dressings obtained by fluorinated post-discharge plasma. Int J Pharm 367:155–161
14. Belmonte T, Arnoult G, Henrion G et al (2011) Nanoscience with non-equilibrium plasmas at atmospheric pressure. J Phys D Appl Phys 44:363001
15. Kong MG, Keidar M, Ostrikov K (2011) Plasmas meet nanoparticles—where synergies can advance the frontier of medicine. J Phys D Appl Phys 44:174018–174032
16. Levchenko I, Kumar S, Yajadda M et al (2011) Self-organization in arrays of surface-grown nanoparticles: characterization, control, driving forces. J Phys D Appl Phys 44:174020–174028
17. Winter GD (1962) Formation of the scab and the rate of epithelization of superficial wounds in the skin of the young domestic pig. Nature 193:293–294
18. Fras L, Ristić T, Tkavc T (2012) Adsorption and antibacterial activity of soluble and precipitated chitosan on cellulose viscose fibers. J Eng Fiber Fabr 7:50–57
19. Fras Zemljic L, Sauperl O, But I et al (2011) Viscose material functionalized by chitosan as a potential treatment in gynecology. Text Res J 81:1183–1190
20. Lee AR, Huang WH (1995) Zinc sulphadiazines: novel topical antimicrobial agents for burns. J Pharm Pharmacol 47:503–509
21. Pecharromán AECC, Moya EAJSS (2006) Antibacterial activity of copper monodispersed nanoparticles into sepiolite. J Mater Sci 41716:5208–5212
22. Cady NC, Behnke JL, Strickland AD (2011) Copper-based nanostructured coatings on natural cellulose: nanocomposites exhibiting rapid and efficient inhibition of a multidrug resistant wound pathogen, *A. baumannii*, and Mammalian cell biocompatibility in vitro. Adv Funct Mater 21:2506–2514
23. Fraser JF, Cuttle L, Kempf M et al (2004) Cytotoxicity of topical antimicrobial agents used in burn wounds in Australasia. Anz J Surg 74:139–142
24. Percival SL, Bowler PG, Russell D (2005) Bacterial resistance to silver in wound care. J Hosp Infect 60(1):1–7
25. Percival SL, Slone W, Linton S et al (2011) Use of flow cytometry to compare the antimicrobial efficacy of silver-containing wound dressings against planktonic Staphylococcus aureus and Pseudomonas aeruginosa. Wound Repair Regen 19:436–441
26. Percival SL, Thomas JG, Slone W et al (2011) The efficacy of silver dressings and antibiotics on MRSA and MSSA isolated from burn patients. Wound Repair Regen 19:767–774
27. Chekmareva IA (2002) Experimental study of reparative regeneration processes in the wound treated with bioactive dressings. Bull Exp Biol Med 133:192–195

28. Hart J, Silcock D, Gunnigle S (2002) The role of oxidized regenerated cellulose/collagen in wound repair: effects in vitro on fibroblast biology and in vivo in a model of compromised healing. Int J Biochem Cell B 34:1557–1570
29. Wu YB, Yu SH, Mi FL et al (2004) Preparation and characterization on mechanical and antibacterial properties of chitosan/cellulose blends. Carbohydr Polym 57:435–440
30. Baohua L, Hu J, Meng Q (2009) Nonwoven supported temperature- sensitive poly(N- isopropylacrylamide)/polyurethane copolymer hydrogel with antibacterial activity. J Biomed Mater Res B 89B(1):1–8
31. Jing A, Zhang H, Zhang J et al (2009) Preparation and antibacterialactivity of electrospun chitosan/poly(ethylene oxide) membranes containing silver nanoparticles. Colloid Polym Sci 287:1425–1434
32. Madhumathi K, Sudheesh Kumar PT, Abhilash S et al (2010) Development of novel chitin/nanosilver composite scaffolds for wound dressing applications. J Mater Sci Mater Med 21:807–813
33. Watthanaphanit A, Supaphol P, Tamura H et al (2010) Wetspun alginate/chitosan whiskers nanocomposite fibers: preparation, characterization and release characteristic of the whiskers. Carbohydr Polym 79:738–746
34. Watanakunakorn C, Glotzbecker C (1978) In vitro activity of carbenicillin, ticarcillin, sisomicin and netilmicin alone and in combination against Pseudomonas aeruginosa. Antimicrob Agents CH 24:343–346
35. Kontogiannopoulos KN, Assimopoulou AN, Tsivintzelis I et al (2011) Electrospun fiber mats containing shikonin and derivatives with potential biomedical applications. Int J Pharm 409:216–228
36. Gilbert P, Moore LE (2005) Cationic antiseptics: diversity of action under a common epithet. J Appl Microbiol 99:703–715
37. Zemljic Fras L, Persin Z, Stenius P (2009) Improvement of chitosan adsorption onto cellulosic fabrics by plasma treatment. Biomacromolecules 10:1181–1187
38. Mikhaylova A, Liesenfeld B, Moore D et al (2011) Preclinical evaluation of antimicrobial efficacy and biocompatibility of a novel bacterial barrier dressing. Wounds 23:24–31
39. Kudej RK (2012) Management of challenging wounds: moist wound healing. In: Proceedings ACVS 2012 veterinary symposium, Washington, DC, 11 Jan–11 Mar 2012, pp 646–650
40. Ovington LG (2007) Advances in wound dressings. Clin Dermatol 25:33–38
41. Kienberger F, Ebner A, Gruber HJ et al (2006) Molecular recognition imaging and force spectroscopy of single biomolecules. Acc Chem Res 39:29–36
42. Maver U, Žnidaršič A, Gaberščček M (2011) An attempt to use atomic force microscopy for determination of bond type in lithium battery electrodes. J Mater Chem 21:4071–4075
43. Kan CW (2007) Surface morphological study of low temperature plasma treated wool—a time dependence study. In: Méndez-Vilas A, Díaz J (eds) Modern research and educational topics in microscopy: vol 2. ©FORMATEX, Spain, pp 683–689
44. AATCC Test Method 100–1999, assessment of antibacterial finishes on textile materials: AATCC technical manual 75 (2000) Technical manual of the american association of textile chemists and colorists 1999, AATCC, Triangle Park, NC, pp 147–149
45. Persin Z, Zaplotnik R, Kleinschek KS (2013) Ammonia plasma treatment as a method promoting simultaneous hydrophilicity and antimicrobial activity of viscose wound dressings. Text Res J 84(2):140–156
46. Peršin Z, Maver U, Pivec T, Maver T, Vesel A, Mozetič M, Stana-Kleinschek K (in press) Novel cellulose based materials for safe and efficient wound treatment. Carbohyd Polym, special issue: biopolymers for life
47. Washburn EW (1921) The dynamics of capillary flow. Phys Rev 27:273–283 (2nd Series)
48. Persin Z, Vesel A, Stana Kleinschek K et al (2012) Characterisation of surface properties of chemical and plasma treated regenerated cellulose fabric. Text Res J 80:2078–2089
49. Sissko Johansson L, Campbell J, Koljonen K et al (2004) On surface distribution in natural cellulosic fibres. Surf Interface Anal 36:706–710

50. Beamson G, Briggs D (1992) High resolution XPS of organic polymers—the Scienta ESCA300 Database. Wiley, Chichester
51. Favia P, Stendardo MV, d'Agostino R (1996) Selective grafting of amine groups on polyethylene by means of NH_3–H_2 RF glow discharges. Plasmas Polym 1:91–112
52. Mozetic M (2012) Application of X-ray photoelectron spectroscopy for characterization of PET biopolymer. Mater Tehnol 46:47–51
53. Junkar I, Vesel A, Cvelbar U et al (2009) Influence of oxygen and nitrogen plasma treatment on polyethylene terephthalate (PET) polymers. Vacuum 84:83–85
54. Junkar I, Cvelbar U, Vesel A et al (2009) The role of crystallinity on polymer interaction with oxygen plasma. Plasma Process Polym 6:667–675
55. Kontziampasis D, Constantoudis V, Gogolides E (2012) Plasma directed organization of nanodots on polymers: effects of polymer type and etching time on morphology and order. Plasma Process Polym 9:866–872
56. Kregar Z, Bišćan M, Milošević S et al (2012) Interaction of argon, hydrogen and oxygen plasma early afterglow with polyvinyl chloride (PVC) materials. Plasma Process Polym 9:1020–1027
57. Ishikawa K, Sumi N, Kono A et al (2011) Synergistic formation of radicals by irradiation with both vacuum ultraviolet and atomic hydrogen: a real-time in situ electron spin resonance study. J Phys Chem Lett 2:1278–1281
58. Holmes-Farley SR, Reamey RH, Nuzzo R et al (1987) Reconstruction of the interface of oxidatively functionalized polyethylene and derivatives on heating. Langmuir 3:799–815
59. Vesel A, Kolar M, Doliska A et al (2012) Etching of polyethylene terephthalate thin films by neutral oxygen atoms in the late flowing afterglow of oxygen plasma. Surf Interface Anal 44:1565–1571
60. Hossain MM, Herrmann AS, Hegemann D (2006) Plasma hydrophilization effect on different textile structures. Plasma Process Polym 3:299–307
61. Cvelbar U, Mozetic M, Hauptman N et al (2009) Degradation of staphylococcus aureus bacteria by neutral oxygen atoms. J Appl Phys 106:103303–1–103303–5
62. An YH, Friedman RJ (1997) Laboratory methods for studies of bacterial adhesion. J Microbiol Meth 30:141–152
63. Cordero J, Munuera L, Folgueira MD (1996) The influence of the chemical composition and surface of the implant on infection. Injury 27:S–C34–37
64. Kiremitci-Gumustedereliogl u M, Pesmen A (1996) Microbial adhesion to ionogenic PHEMA, PU and PP implants. Biomaterials 17:443–449
65. Gottenbos B, van der Mei HC, Busscher HJ (2000) Initial adhesion and surface growth of *Staphylococcusepidermidis* and *Pseudomonas aeruginosa* on biomedical polymers. J Biomed Mater Res 50:208–214
66. Tegoulia VA, Cooper SL (2002) *Staphylococcus* aureusm adhesion to self-assembled monolayers: effect of surface chemistry and fibrinogen presence. Col Surf B Biointerf 24:217–228
67. Buczynski BW, Kory MM, Steiner RP et al (2003) Bacterial adhesion to zirconium surfaces. Col Surf B Biointerf 30:167–175
68. Henriques M, Azeredo J, Oliveira R (2004) Adhesion of *Candida albicans* and *Candida dubliniensis* to acrylic and hydroxyapatite. Col Surf B Biointerf 33:235–241
69. Speranza G, Gottardi G, Pederzolli C et al (2004) Role of chemical interactions in bacterial adhesion to polymer surfaces. Biomaterials 25:2029–2037
70. Gottenbos B, Grijpma DW, van der Mei HC et al (2001) Antimicrobial effects of positively charged surfaces on adhering Gram-positive and Gram-negative bacteria. J Antimicrob Chemother 48:7–13
71. Balazs DJ, Triandafillu K, Chevolot Y et al (2003) Surface modification of PVC endotracheal M tubes by oxygen glow discharge to reduce bacterial adhesion. Surf Interf Anal 35:301–309
72. Scheuerman TR, Camper AK, Hamilton MA (1998) Effects of substratum topography on bacterial adhesion. J Col Interf Sci 208:23–33

73. Francois P, Vaudaux P, Nurdin N et al (1996) Physical and biological effects of a surface coating procedure on polyurethane catheters. Biomaterials 17:667–678
74. Davenas J, Thevenard P, Philippe F et al (2002) Surface implantation treatments to prevent infection complications in short term devices. Biomol Eng 19:263–268
75. Whitehead KA, Colligon JS, Verran J (2004) The production of surfaces of defined topography and chemistry for microbial retention studies, using ion beam sputtering technology. Intern Biodeter Biodegrad 54:143–151
76. James NR, Jayakrishnan A (2003) Surface thiocyanation of plasticized poly(vinyl chloride) and its effect on bacterial adhesion. Biomaterials 24:2205–2212
77. Scheuerman TR, Camper AK, Hamilton MA (1998) Effects of substratum topography on bacterial adhesion. J Col Interf Sci 208:23–33
78. Taylor RL, Verran J, Lees GC et al (1998) The influence of substratum topography on bacterial adhesion to polymethyl methacrylate. J Mater Sci Mater Med 9:17–22

Chapter 20
Sutureless Atrial-mitral-valve Prosthesis

20.1 Introduction

The recent years have seen the development of interventional heart valve therapies [1–4], while there is commercially available prosthesis to treat aortic and pulmonary valves [5–8]. Regurgitation is the most common mitral valve disease in Western countries. The recent trend focuses on the reconstruction of valve rather than replacement, owing to many reasons. The preservation of the subvalvular apparatus, which is necessary for ventricular performance, is an important aspect to be considered. Since mitral valve therapies do not give satisfactory results in comparison with interventional aortic or pulmonary valve placements, mitral valve therapy remains a task of open heart surgery [9–12]. The interventional placement of a biological valve in the mitral position has been partially investigated [13, 14]. This is due to the fact that this valve presents a challenging anatomy to anchor a biological heart valve. In order to solve this problem, a hollow body has been created, which is equipped with a heart valve that utilizes all surrounding structures inside the heart to anchor or permit the additional valve to cure the underlying disease. The main requirements for such prosthesis were as follows: self-expansion after compression in all dimensions and adaption to the atrial wall with approximated blood tightness through the prosthesis wall to allow exclusion of the left atrium. Hence, a new complex hollow body has been designed, which is made of nitinol and polyvinylidene fluoride. A certain number of prosthesis prototypes have been built, and its functionality has been tested in vitro and its overall performance has been studied in a porcine model of mitral incompetence.

20.2 Requirements of the Prosthesis

The required prosthesis should completely cover the left atrial wall from the pulmonary veins down to the mitral annulus and contain a biological heart valve (Fig. 20.1).

N. Gokarneshan et al., *Emerging Research Trends in Medical Textiles*,
Textile Science and Clothing Technology, DOI 10.1007/978-981-287-508-2_20

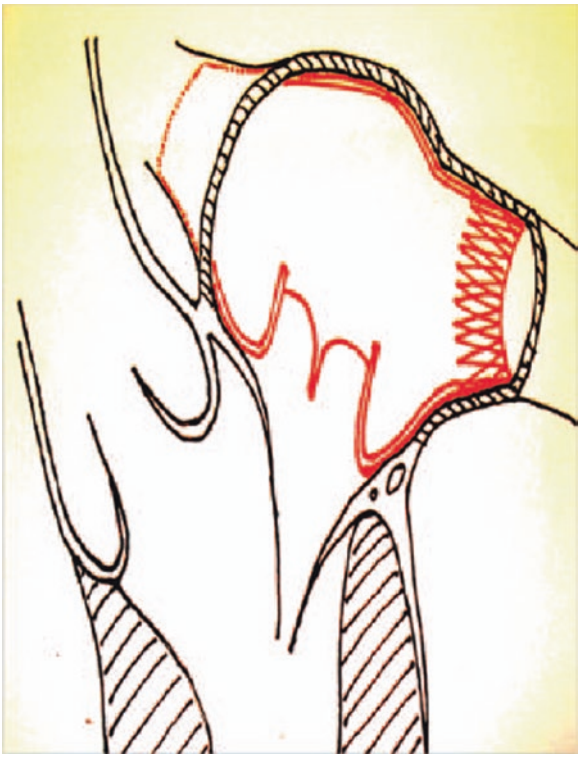

Fig. 20.1 Prosthesis shown schematically (in *red*) with additional valve in left porcine atrium with two pulmonary veins [18]

The following characteristics have been decided from prosthesis:

(a) Compressible with good self-expansion after release;
(b) Compression stability vertical to the valve plain; and
(c) Approximated blood tightness and low thrombogenity inside.

A single-wall design has been decided based on a number of earlier studies [18]. The hollow body of the prosthesis has been designed for prosthesis wall, from a warp-knitted fabric of polyvinylidene fluoride. The external frame has been made from Nitinol, so as to achieve stability and self-expansion. The polyvinylidene fluoride polymer (of medical grade) has been melt spun into multifilament fibers with 30 filaments and having a yarn titer of 320 dtex. Warp-knitting technology has been adopted so as to produce a blood tight and elastic textile structure. The warp-knitted fabrics besides having the possibility of adjusting the design parameters such as size, shape, Young's modulus, and porosity of the textile structure have the additional merit of being fray proof. A double raschel warp-knitting machine has been used for the purpose and is capable of producing 3D textiles of varied yarn materials and counts. A two-bar tricot pattern has been selected for the fabrication of a dense structure having the required elastic properties (Fig. 20.2).

Appropriate needle gauge has been chosen and the loop density adjusted suitably. The polyvinylidene fluoride yarns have been designed considering the above

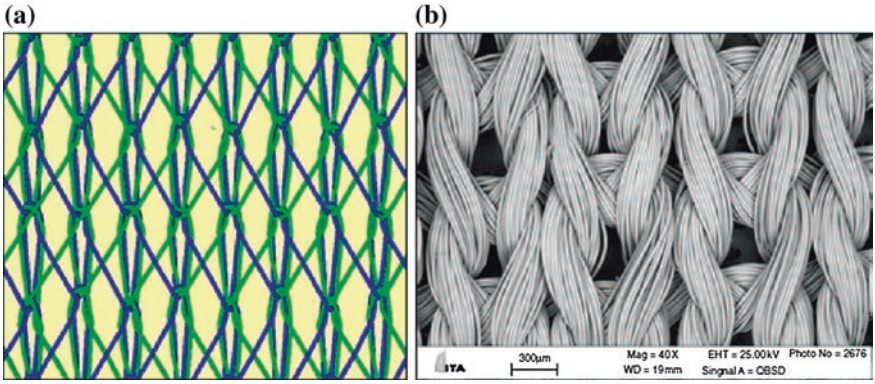

Fig. 20.2 **a** CAD sketch of warp-knitted two-bar tricot binding, **b** SEM photograph of two-bar tricot binding [18]

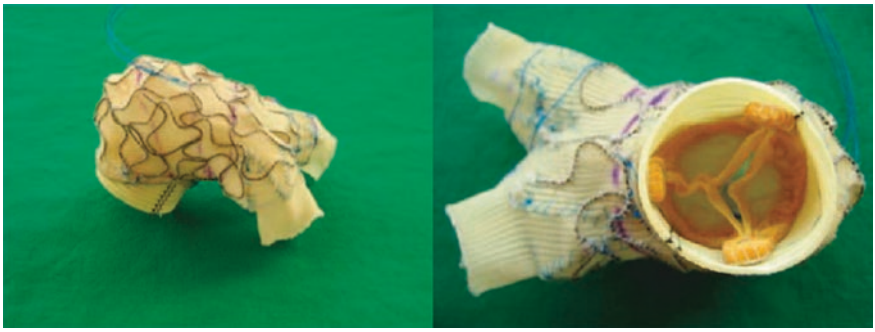

Fig. 20.3 Pictures of a prosthesis prototype with integrated biological valve [18]

parameters and have been converted into a tubular bifurcation. Polyvinylidene fluoride shows better properties than polypropylene, which is normally used in cardiac surgery [15–17]. Medical-grade nitinol wire with a diameter of 200 mm has been used to produce the external skeleton. The Nitinol has been tempered in the super elastic phase at 500 °C for 15 min. Hence, the Nitinol wire was fixed to the desired shape using a mold representing the porcine left atrium from the pulmonary veins as far as the mitral valve. Subsequently, the super elastic Nitinol skeleton in the shape of the porcine left atrium was sutured onto the PVDF tubular bifurcation fitting the mold, whereas the two branches fitted the pulmonary vein ostia. The polyvinylidene fluoride Nitinol composite structure which is assembled forms a new self-expandable hollow body customized to the porcine anatomy. The prototypes so developed have been made up of a biological heart valve and Nitinol brackets joining the prosthesis rim up to the pulmonary vein stents (Fig. 20.3). The load from the valve is displaced through the Nitinol skeleton to the atrial wall and the pulmonary vein ostia. Eight such prostheses have been produced.

All prostheses have been first observed and tested in the pulsatile circulatory mock loop simulator. Hence, an elastic silicone model of the porcine left atria has been created, including the pulmonary veins and the upper portion of the mitral valve. It has been possible to directly see the behavior of prosthesis and function of the valve inside the model atrium due to the clarity of the silicone and water. The prostheses were compressed, inserted via the mitral valve part of the model atrium, and released again. The model has then been connected to the simulator with an inlet through the pulmonary veins and an outflow through the mitral valve, and pulsatile circulation established. The pulsatile circulatory mock loop simulator worked at heart rates ranging between 70 and 110 bpm and cardiac outputs of 2, 4, 5, and 7 l/min. It has been filled with saline. Positioning of the hollow body, its stability and the function of the embedded valve prosthesis have been monitored. Eight pigs, each weighing 70 kg, have been used in the animal trials.

20.3 Results of the Findings

All the prosthesis has been studied in vitro in the circulatory simulator before [18]. A good evaluation of the overall prosthesis performance has been enabled by the method of constructing the simulator coupled with the transparent model atrium (Fig. 20.4). The procedure of prosthesis implantation could also be controlled by visual inspection by considering simulation in the silicone atrium. The compression and release of the two extensions and the main body has been done separately through development of a method. The fully compressed prosthesis measured about 1.5 cm × 9.5 cm. After insertion of the prosthesis into the atrium first, the two extensions were released one after the other followed by the release of the main body. The prostheses fitted to the model atria very well. The expanded prostheses had no dislodgements in both the cases of without pumping and with maximal pumping of 7 l/min. The prostheses lay tightly on the model annulus in all cases. The valve re-expanded inside the prosthesis, and no signs of stenosis or insufficiency

Fig. 20.4 Prothesis in the circulatory simulator [18]

have been noticed. In one case, the suture fixation between prosthesis body and the biologic valve became insufficient with time and further pumping. The problem has been rectified after resuture. All eight animals survived after the operation, CPB time and the follow-up of 90 min without CPB. All the animals could be surgically implanted with the prosthesis through the longitudinal atriotomy. Tight closure of the fragile atrial wall was sometimes challenging. The atrial fibrillation happened during implantation on one instance but has been effectively treated. After termination of CPB and a brief compensatory period, hemodynamics reached a steady state comparable to preprocedural conditions in all animals. There has been no significant pulmonary hypertension or a v-wave in the wedge pressure, in particular. In spite of attempting a number of acoustic windows in each animal, only a restricted access to echocardiography has been possible. But, some small, ever-changing acoustic windows permitted gross; nevertheless, some small, always changing acoustic windows allowed gross echocardiography insights.

The prostheses exhibited good adaption to the atrial wall, and no relevant movement of the prostheses has been observed. The native as well as the biological mitral valve moved almost synchronously (Fig. 20.5). There has been no evidence for left ventricular outflow tract obstruction in any case. Even though a higher grade mitral regurgitation has been observed at the posterior leaflet of the native valve (artificial defect), the inadequacy jet has been stopped at the additional valve. The biological valve itself appeared with a normal movement of the cusps and without regurgitation and stenosis. It has not been possible to gather information regarding paravalvular leakage or rather tightness at the atrial wall, even by the use of echocardiogram. Fluoroscopy has been performed through the pulmonary artery as an angiography as well as a ventriculogram from the apex of the left ventricle. Such radiographic studies illustrate complete patency of the pulmonary veins into the atrium and straight passage of the contrast medium into the ventricle. No relevant regurgitation over the biological valve could be seen. A slight deposit of contrast medium has been observed in the area of the anterior

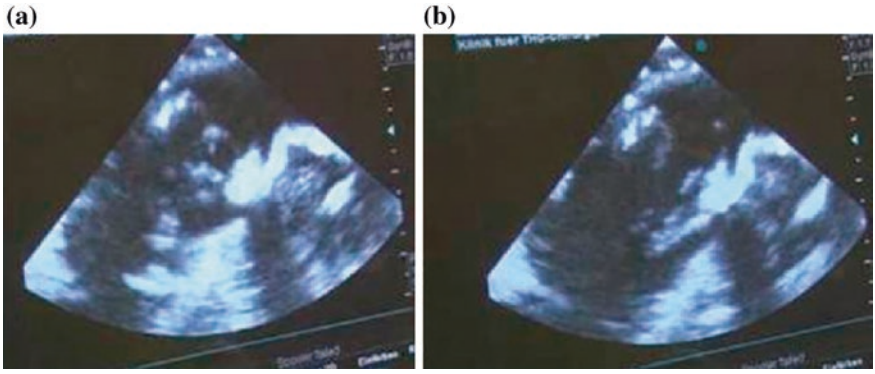

Fig. 20.5 Ultrasound image of the prosthesis [18]. **a** Closed additional valve inside the prosthesis, **b** open additional valve inside the prosthesis

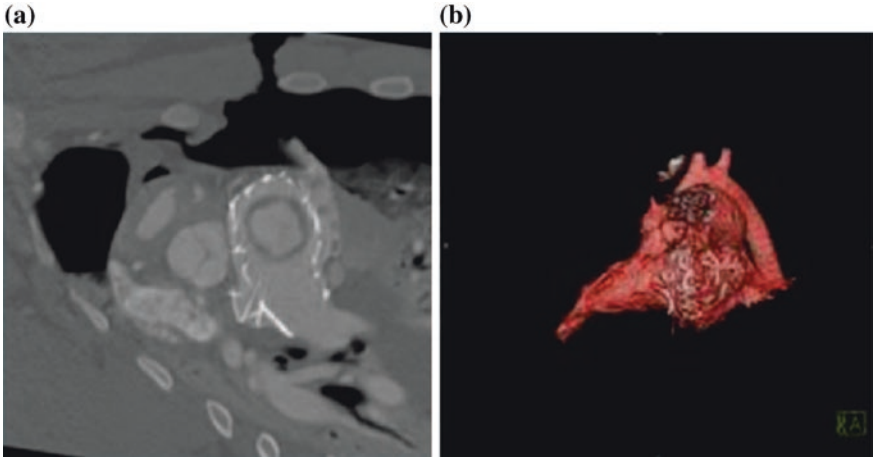

Fig. 20.6 **a** CT scan illustrating extended prosthesis in a single plane, **b** 3D reconstruction [18]

mitral leaflet between the atrial wall and the prosthesis. After restoration of coagulation capacity, no relevant hemodynamic changes occurred indicating severe clot formation or valve thrombosis. As a result of difficult visualization, the last four animals were subjected to a CT scan.

In the study, the appropriate position of the prostheses in the left atrium can be checked well (Fig. 20.6). Nevertheless, precise information regarding paraprosthetic leakage was not possible just as before. Autopsy showed a right (intended) overall position of the prosthesis in all cases. The prosthesis body was pressed on the mitral valve annulus, and in three animals, a slight gliding of the prosthesis into the mitral valve was seen. Apart from, in one case, there being a dissolved skeleton strut, there was no trauma to intracardiac structures.

The restriction of the mobility of the mitral valve leaflets or left ventricular outflow tract obstruction could not be identified (Fig. 20.7). In one instance, the

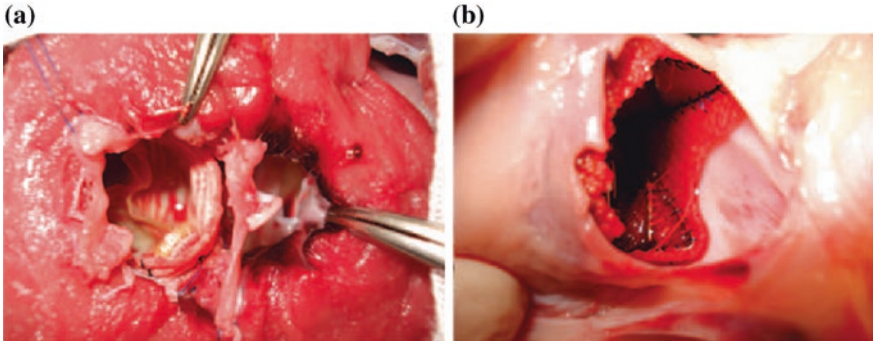

Fig. 20.7 Autopsy samples showing correct position of the prosthesis [18], **a** without outflow tract obstruction, **b** unobstructed pulmonary veins

malfunction of the prosthesis could not be observed clinically. There has been occlusion of the right pulmonary vein due to improper release of the prosthesis extension. In another instance, a small tear in the right pulmonary vein was caused by a sharp dissolved strut CT scans exhibiting expanded prosthesis in one plane (left) and in the 3D reconstruction (right). Figure had to be recognized.

The extension of the prosthesis could be identified at the appropriate position of the pulmonary vein, for all the animals tested, and adequately drained the pulmonary vein. The thrombus has not been identified inside the complete prosthesis.

20.4 Discussion of the Findings

Surgical repair has been considered to be the most effective treatment in mitral valve disease [18]. Interventional therapy for diseases of the mitral valve has shown remarkably good results in the case of patients with high risk, particularly in the treatment of aortic stenosis. A number of interventional approaches for repair of the mitral valve have been proposed, and some of them are under implementation [9, 18–20]. The interventional placement of a prosthetic valve in the mitral position is rarely investigated because the issue of anchoring is very challenging. The objective behind the interventional mitral valve therapy was to develop a complex self-expanding hollow body for the whole left atrium to allow a suture less positioning of a biological heart valve in the mitral position. This hollow body should exclude the entire left atrium and tighten directly above the valve up to the inflow of the pulmonary veins. A flexible textile material that could adjust to the surrounding structures inside the heart has been used, so as to satisfy the above-mentioned criteria for the prosthesis. Also, the textile surface should be biocompatible without major thrombotic characteristics. A warp-knitted structure made from polyvinylidene fluoride has been selected so as to permit the best 3D fitting of the textile body, since it is a biocompatible material suited for surgical purposes [16, 17]. Although the PVDF used was not completely tight for blood (a slow but quantitative not relevant passage of blood through the PVDF was observed), a functional tightness of the valve was achieved. The initial blood tightness can be enhanced further by either preclotting of the prosthesis or textile coating (external) with degradable biomaterials such as gelatin or collagen. It has been considered in growing of the endocardium and hence further fixation is enabled. Despite the preference for an inner skeleton pressing the polyvinylidene fluoride against the atrial wall, the skeleton of Nitinol has been sutured very close to the textile body from the outside for practical reasons. Nevertheless, by the use of these two materials, the creation of a rather complex textile hollow body, with not only self-expansion properties but also a feature to press the valve on the annulus to transmit the load from the valve up to the pulmonary vein ostia, was possible. All of the prostheses produced were subjected to the pulsatile circulatory mock loop simulator. A transparent silicone model of the left atrium has been made specifically for the purpose. This allowed visualization of the prosthesis and

its behavior in circulation like in an aquarium. Only minor impairments of the prostheses, such as a dehiscence of the biological valve from the prosthesis body, have been visible after a duration of 3 h. Taken together, the stability of the prosthesis in the atrium and the function of the biological valve could be demonstrated. The prostheses have been effectively implanted on eight animals. An open access to the heart has been selected (which requires CPB) since the issue of transcatheter implantation has not found to be relevant for a proof of the overall concept. From the circulatory standpoint, the implanted prostheses had to function quite well; otherwise, circulation would have been massively depressed. Unfortunately, visualization of the prosthesis with its valve proved unexpectedly difficult, and this made thorough evaluation of the prostheses complex. Nevertheless, taking all of the visualizations together, it was possible to demonstrate that the prostheses filled the complete left atrium tightly, that the biological valve worked, and that the overall position of the prostheses in relation to the insufficient native valve was as intended. These findings were confirmed by the autopsies of these animals. Remarkably, in the autopsies, despite the custom-made character of the prostheses, there was no relevant thrombus formation on or inside the prostheses. This indicates that the material PVDF together with Nitinol seems to be a very promising combination which can used for larger complex implants inside the heart. When the constraints on the investigation have been considered, the duration for which the new prostheses have been subjected to load conditions has been quite brief when compared to the actually required durability over the years. This can also apply when considering the potential side effects (such as perforation of the heart wall) of such prosthesis inside the heart. Future long-term investigation shall only be able to answer these questions.

References

1. Andersen HR, Knudsen LL, Hasenkamm JM (1992) Transluminal implantation of artificial heart valves. Description of a new expandable aortic valve and initial results with implantation by catheter technique in closed chest pigs. Eur Heart J 13:704–708
2. Bonhoeffer P, Boudjemline Y, Qureshi SA et al (2002) Percutaneous insertion of the pulmonary valve. J Am Coll Cardiol 39:1664–1669
3. Cribier A, Eltchaninoff H, Bash A et al (2002) Percutaneous transcatheter implantation of an aortic valve prosthesis for calcific aortic stenosis: first human case description. Circulation 106:3006–3008
4. Spillner J, Börgermann J, Reppenhagen G, Er-Xiong L, Reidemeister JC, Friedrich I (2005) An experimental approach to reversible ‘endovascular aortic valve placement’. J Heart Valve Dis 14(4):546–550
5. Cribier A, Eltchaninoff H, Tron C et al (2006) Treatment of calcific aortic stenosis with the percutaneous heart valve: mid-term follow-up from the initial feasibility studies: the French experience. J Am Coll Cardiol 47:1214–1223
6. Grube E, Laborde JC, Gerckens U et al (2006) Percutaneous implantation of the corevalve self- expanding valve prosthesis in high-risk patients with aortic valve disease: the siegburg first-in-man study. Circulation 114:1616–1624
7. Walther T, Simon P, Dewey T et al (2007) Transapical minimally invasive aortic valve implantation: multicenter experience. Circulation 116(11 Suppl):I240–I245

8. Khambadkone S, Bonhoeffer P (2004) Nonsurgical pulmonary valve replacement: why, when, and how? Catheter Cardiovasc Interv 62:401–408
9. Mack MJ (2006) New techniques for percutaneous repair of the mitral valve. Heart Fail Rev 11:259–268
10. Herrmann HC, Rohatgi S, Wasserman HS et al (2006) Mitral valve hemodynamic effects of percutaneous edge-to-edge repair with the MitraClip™ device for mitral regurgitation. Catheter Cardiovasc Interv 68:821–828
11. Silvestry FE, Rodriguez LL, Herrmann HC et al (2007) Echocardiographic guidance and assessment of percutaneous repair for mitral regurgitation with the Evalve MitraClip: Lessons learned from EVEREST I. J Am Soc Echocardiogr 20:1131–1140
12. Block PC (2005) Percutaneous mitral valve repair: are they changing the guard? Circulation 111:2154–2156
13. Goetzenich A, Dohmen G, Hatam N et al (2009) A new approach to interventional atrioventricular valve therapy. J Thorac Cardiovasc Surg 140:91–102
14. Ma L, Tozzi P, Huber CH, Taub S, Gerelle G, von Segesser LK (2005) Double-crowned valved stents for off-pump mitral valve replacement. Eur J Cardiothorac Surg 28(2):194–198
15. Laroche G, Marois Y, Schwarz E, Guidoin R, King Mand Douville Y (1995) Polyvinylidene fluoride monofilamentsutures: can they be used safely for long-term anastomosesin the thoracic aorta? Artificial Organs 19(11):1190–1199
16. Mary C, Marois Y, King MW et al (1998) Comparison of theinvivo behavior of polyvinylidene fluoride and polypropylenesutures used in vascular surgery. ASAIO J 44(3):199–206
17. Klinge U, Klosterhalfen B, Ottinger AP, Junge K, Schumpelick V (2002) PVDF as a new polymer for the construction of surgical meshes. Biomaterials 23(16):3487–3493
18. Spillner J, Goetzenich A, Amerini A, Holtmannspötter O, Deichmann T, Schmitz C, Autschbach R, Dohmen G (2011) New sutureless 'atrial- mitral-valve prosthesis' for minimally invasive mitral valve therapy. Text Res J 81:115–121
19. Rosengart TK, Feldman T, Borger MA et al (2008) Percutaneous and minimally invasive valve procedures: a scientific statement from the American Heart Association. Circulation 117(13):1750–1767
20. Bajona P, Katz WE, Daly RC, Zehr KJ, Speziali G (2009) Beating-heart, off-pump mitral valve repair by implantation of artificial chordae tendineae: an acute in vivo animal study. J Thorac Cardiovasc Surg 137(1):188–193

Chapter 21
An Innovative Test Method for Medical Stockings

21.1 Introduction

In the treatment of lymphedema on long-term basis and prevention of recurrence of venous diseases, medical compression hosiery is the commonly used type of compression [1–3]. Such a treatment reduces the necessity of medication and shortens the duration of treatment in the case of venous insufficiency [4, 5]. For each specific patient, a complex interaction of physical properties and construction parameters influences the suitability of compression hosiery, which is supposed to ensure both comfort during wearing and an appropriate level of compression. The extent to which the patient can manage and tolerate compression hosiery depends on the venous disease stage (shape and size of the limb), the patients' build (tall, short, normal, obese), and activity (mobility, age, lifestyle). During the application of compression, it is necessary that the greatest pressure should be at the ankle and reduced at the upper part of the limb, so as to ensure a gradual compression. Apparel products require multifunctionality and superior comfort performance and also able to satisfy the physiological and psychological needs. The garment fit and pressure comfort are considered to be crucial factors [6, 7]. The European standard specifies the requirements for medical compression hosier, including custom-made hosiery knitted from elastic threads, and indicates the testing method for compressive properties. It is suitable for medical compression hosiery used in the treatment of venous and/or lymphatic diseases of the leg. It also specifies that the raw material used for compression hosiery includes a stretchable yarn, made by covering an elastic core of polyurethane with other types of fibers. However, this standard indicates no testing method for correlation assessment between pressure values and the compression perception during wearing. The correlation between compression perception and pressure values has been investigated, which enable development of hosiery and socks that provide wearing comfort. The pressure perception changes depending

N. Gokarneshan et al., *Emerging Research Trends in Medical Textiles*,
Textile Science and Clothing Technology, DOI 10.1007/978-981-287-508-2_21

on the wearing duration and the fitting of each individual consumer [9]. The tensile deformation of medical stockings has been studied by many researchers at different levels of applied stress. The correlation between the results obtained by using different test methods is an important matter and is highly desirable for medical products. The relationship between uniaxial behavior and biaxial behavior is not clear [10]. In the case of fabrics with small rigidity, the test results are agreeable [11, 12]. The use of medical stockings involves stress in more than one direction during wearing, implying the necessity to test the elastic fabrics in at least two directions. It has been shown that when a fabric is uniaxially extended at a bias angle, the data for situations in which one or both of the tensile stress components are negative (as for the compressive stockings) could be important both for the manufacturing process and the subsequent use of knitted hosiery [13]. The research in the area has been done highlighting results of earlier works [14–17]. This chapter discusses the post-wearing compression preservation and the correlation between the size of medical stockings and the patient's dimensions for best fitting and uses a new approach based on the grab method. This chapter aims to examine a new testing method for assessing the capacity of ready-made compression hosiery to retain its designated compression after repeated wearing–washing cycles, as well as to prove that there is a connection between fit and size of medical compression hosiery, depending on the particular shape of the limb. According to the presented results, the following observations were made.

21.2 Medical Stockings

Medical compression stockings for the treatment of venous diseases have been knitted on circular weft-knitting machines [18]. The degree of compression has been controlled by the amount of elastomer incorporated in the product and by the 3D knitting system. Two interwoven elastic yarn systems comprising of inlay and body yarns have been knitted together. A package of 22 versions of medical stockings was produced. Various values of compression level have been obtained for each version, with a pressure profile decreasing from the ankle (with maximum level of 30 mm Hg) to the thighs. This kind of hosiery is classified in the moderate compression classes (Ccl II), with 23–32 mm Hg compression at the ankle [8]. The measuring point details have been shown in Table 21.1 [8]. Figure 21.1 illustrates the connection between the measured regions of the leg and the compression zones considered in the earlier experiments [1, 14–16].

Four compression zones have been considered and gradually achieved:

- CZ1—ankle level, where maximum compression is developed (point B, 100 %);
- CZ2—calf level with intermediate compression (point C, 70 %)
- CZ3—above-the-knee level with medium compression (point E, 50 %);
- CZ4—thigh level with minimum compression (point F, 40 %).

Table 21.1 Areas of compression for medical stockings [18]

Measuring point	Description of the measuring point	Compression zone	Description
a	Sole of the foot at the heel		
A	Forefoot at the base of the toes		
B	Ankle at the point of its minimum girth	CZ1 (with point B)	Ankle circumference at smallest girth
B1	Point at which the achilles tendon changes into the calf muscles		
C	Calf at its maximum girth	CZ2 (with point C)	Calf circumference at largest girth
D	Just below the tibia		
E	Center of the patella and over the back of the knee	CZ3 (with point E)	Between D and F
F	Between center point of the crotch and E point	CZ4 (with point F)	Thigh circumference at largest girth
G	5 cm below center point of the crotch, with the patient in the upright position		

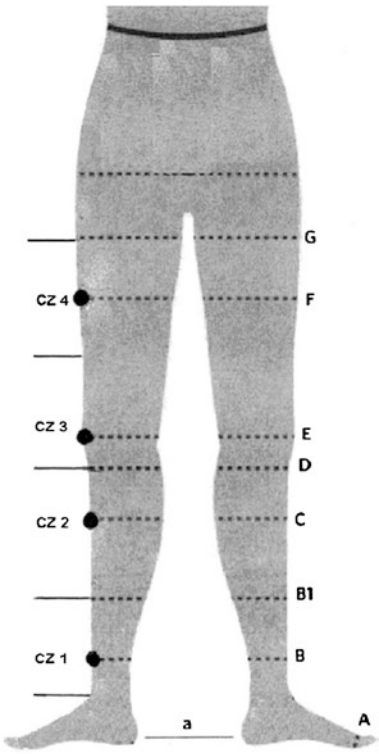

Fig. 21.1 Illustration of the compression zones along the leg [18]

21.3 Results of the Findings

The degree of compression of the medical stockings has been quantified by considering a reversely proportional dependence between the relative elongation and degree of compression [17]. The experimental results obtained with the triaxial tensile testing performed with the grab method and graphically illustrated by the polar graphs indicate the stocking reaction to the applied loads, on the four analyzed compression areas [18]. The triaxial disposal of the mean values of the evaluated deformations for the fabrics selected along the stocking leg before use is depicted in Fig. 21.2a, b (tested for the minimum and the maximum load). The same characteristics for the samples picked out along the stocking leg used by each of the two patients after 15 and 30 wearing–washing cycles are represented in Fig. 21.3a, b for patient 1 and Fig. 21.4a, b for patient 2, respectively, and also Figs. 21.5a, b and 21.6a, b.

21.4 Discussions of the Findings

The research investigation aimed to evaluate a new testing method for assessing the capacity of ready-made compression hosiery to retain its designated compression after repeated wearing–washing cycles and also to establish that a relationship exists between fit and size of medical compression hosiery, based on the specific shape of the limb [18]. The following observations have been made based on the test results. The experimental results obtained for the triaxial testing of the stockings are depicted graphically in Figs. 21.2, 21.3, 21.4, 21.5, and 21.6 and permit estimation of the deformation distribution along the leg. Irrespective of whether the stocking is new or used, the grab tests in the wale–course and bias directions explain the

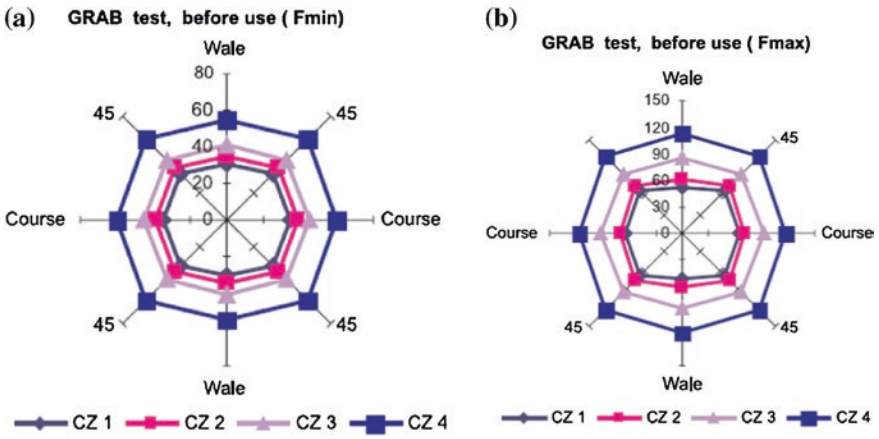

Fig. 21.2 Variation of triaxial deformation on the compression zones before use: **a** minimum force; **b** maximum force [18]

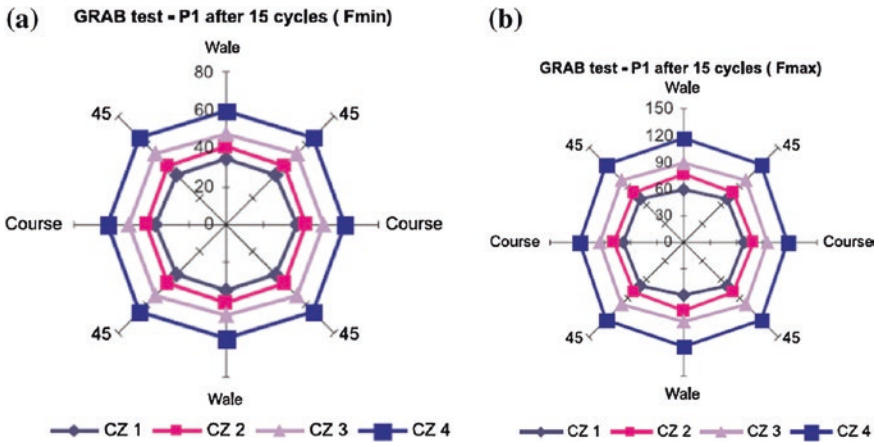

Fig. 21.3 Variation of triaxial deformation on the compression zones, patient 1 after 15 wearing–washing cycles. **a** Minimum force; **b** maximum force [18]

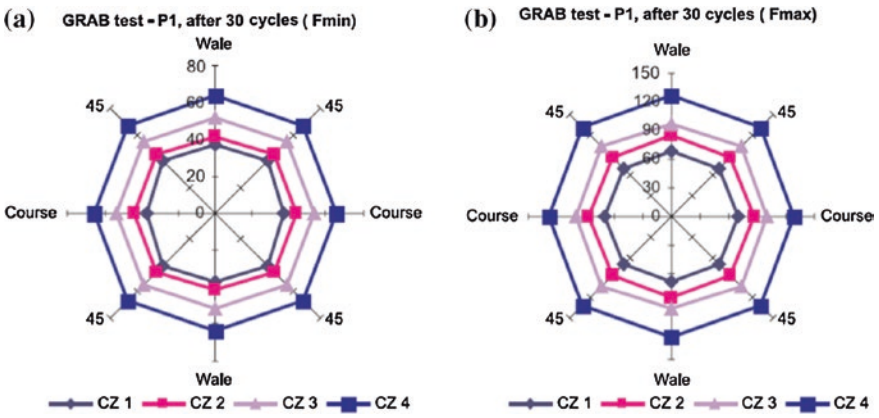

Fig. 21.4 Variation of triaxial deformation on the compression zones, patient 2 after 15 wearing–washing cycles. **a** Minimum force; **b** maximum force [18]

gradual compression features of the medical stockings used for the treatment of venous diseases. Both strip and grab tensile tests carried out on wale directions are uniaxial-like. Grab tests usually produce higher strength values than do strip tests, due to the contribution from adjacent areas to the central stressed area; consequently, for the same applied load, the elongation values obtained with the grab test are smaller than those obtained with the strip test. The experimental values obtained from earlier tests made on the wale directions of the samples (before use) exhibit the above-mentioned trend. Using the stockings before use as a reference (see Fig. 21.2a, b), the aspects of triaxial deformations represented in Figs. 21.3, 21.4, 21.5 and 21.6 suggest changes in compression level for all tested zones along the

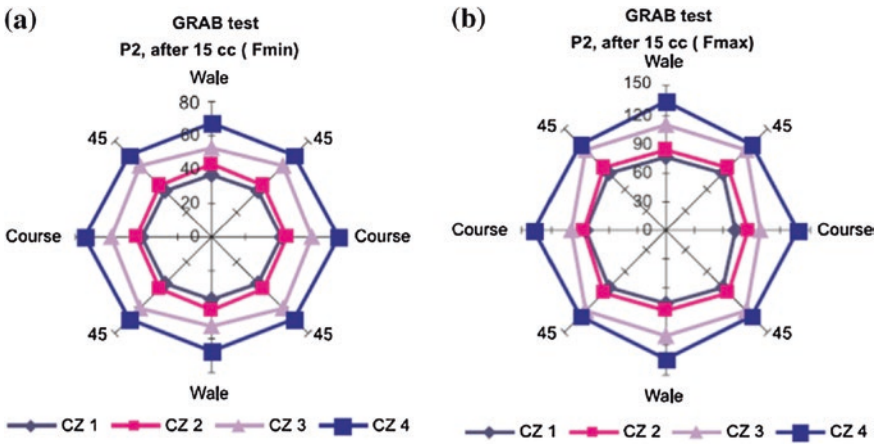

Fig. 21.5 Variation of triaxial deformation on the compression zones, patient 1 after 15 wearing–washing cycles. **a** Minimum force; **b** maximum force [18]

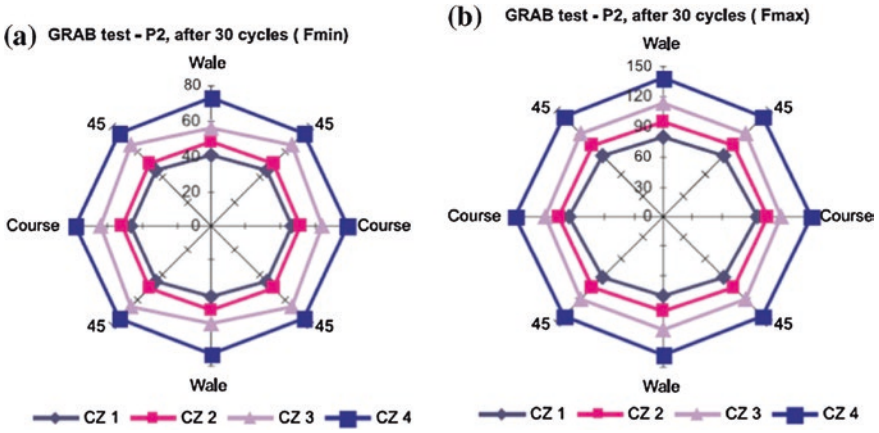

Fig. 21.6 Variation of triaxial deformation on the compression zones, patient 2 after 30 wearing–washing cycles. **a** Minimum force; **b** maximum force [18]

leg. Medical stockings having similar size, after being worn by two different patients in moderate stages of chronic venous diseases but having different limb shapes, did not exhibit changes in their compressive features that may be considered as consequences of both wearing and washing processes for different durations and stocking size fit (or lack of fit) for the patient dimensions. By wearing stocking of required size, the compressive features have been better maintained in the case of normal patients than for the sturdy shape patient (Figs. 21.5 and 21.6). In the case of sturdy patient, the smaller size of hosiery leads to a loss of compression properties with the passage of time, as shown by the increasing values of the triaxial deformation.

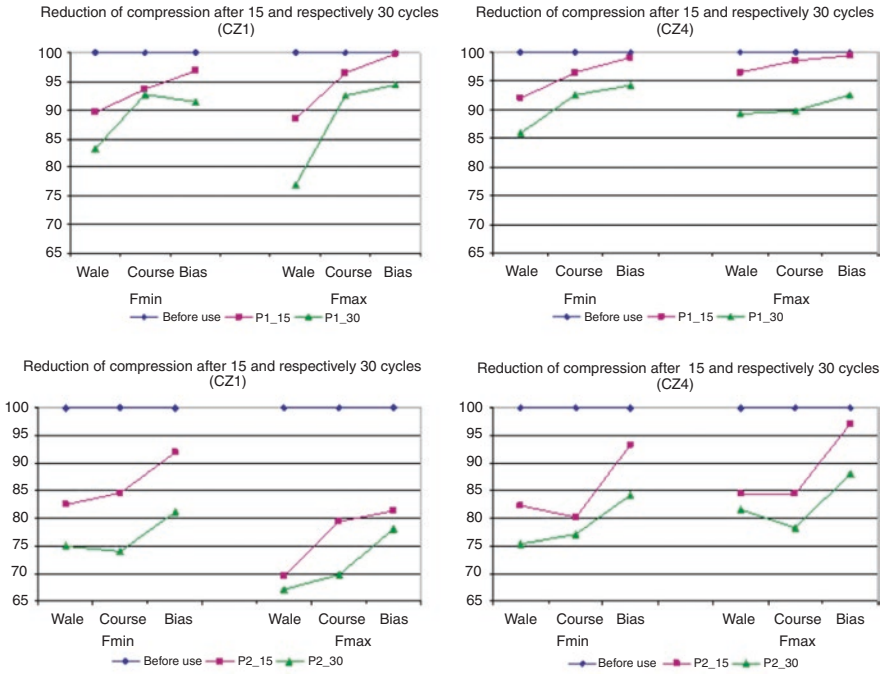

Fig. 21.7 Comparison of reduction in compression after wearing–washing cycles for two patients studied [18]

With regard to this aspect, medical monitoring revealed that compression perception was not well endured by the sturdy-shape patient at the beginning of the testing period. When the medical stocking is designed, the aim is to ensure a gradual decrease in compression starting from the value achieved at the ankle level, and this compression profile should be preserved for approximately six months; our research confirmed this requirement. The ankle value is assumed to be 100 % of the compression value for both patients, regardless of wearing time. The compression profile is represented by the percentage changes in elongation from CZ1 to CZ4, for both patients and wearing–washing times, under this level. Even though the experimental values obtained do not follow exactly the theoretical evolution of compression (100, 70, 50, and 40 %), the maintenance of well-differentiated compression areas after 30 cycles of normal wear circumstances can be clearly seen. When considering that compression variation is inversely proportional to elongation variation, the values of compression reduction expressed as percent have been represented. An illustration of comparative evolution of compression reduction after wearing–washing cycles is depicted in Fig. 21.7 for maximum (CZ1–ankle girth) and minimum (CZ4–tights at larger girth) compression zones. It is necessary to mention that wearing stockings of inappropriate size to patient's body measurements results in more accentuated reduction of compression, irrespective to the number of washing–wearing cycles.

References

1. Doherty DC, Morgan PA, Moffatt CJ (2006) Role of hosiery in lower limb lymphoedema. In: Lymphoedema framework. template for practice: compression hosiery in lymphoedema, pp 10–14. MEP Ltd, London
2. Clark M, Krimmel G (2006) Lymphoedema and the construction and classification of compression hosiery. In: Lymphoedema framework. template for practice: compression hosiery in lymphoedema, pp 2–4. MEP Ltd, London
3. Moffatt CJ (2002) Four-layer bandaging: from concept to practice. Int J Low Extrem Wounds 1(1):13–26
4. Alpagut U, Dayioglu E (2005) Importance and advantages of intermittent external pneumatic compression therapy in venous stasis ulceration. Angiology 56(1):19–23
5. Manich M, Martí M, Saurí RM, Castellar MD, Carvalho J (2006) Effect of finishing on woven fabric structure and compressional and cyclic multiaxial strain properties. Text Res J 76(1):86–93
6. Petrova A, Ashdown SP (2008) Three-dimensional body scan data analysis body size and shape dependence of ease values for pants' fit. Clothing Text Res J 26(3):227–252
7. Zhang X, Yeung KW, Li Y (2002) Numerical simulation of 3D dynamic garment pressure. Text Res J 72(3):245–252
8. ENV 12718: 2001 (draft standard). Medical compression hosiery
9. Tsujisaka T, Azuma Y, Matsumoto YI, Morooka H (2004) Comfort pressure of the top part of men's socks. Text Res J 74(7):598–602
10. Zheng J, Komatsu T, Yazaki Y, Takatera M, Inui S, Shimizu Y (2006) Evaluating shear rigidity of woven fabrics. Text Res J 76(2):145–151
11. Zheng J, Komatsu T, Takatera M, Inui S, Bao L, Shimizu Y (2008) Relationship between uniaxial and strip biaxial tensile properties of fabrics. Text Res J 78(3):224–231
12. Belcaro G, Cesarone MR, Nicolaides AN et al (2003) Prevention of venous thrombosis with elastic stockings during long-haul flights: the LONFLIT 5 JAP study. Clin Appl Thromb Hemost 9(3):197–201
13. Bassett RJ, Postle R, Pan N (1999) Experimental methods for measuring fabric mechanical properties: a review and analysis. Text Res J 69(11):866–875
14. Piroi C, Harpa R, Cristian I (2006) Regarding the durability properties of knitted fabrics with microfibre content. In: The XIth international conference ЕМФ-Sofia'06, pp 33–39. Tom III/18–20 Sept Bulgaria
15. Harpa R, Radu CD, Cristian I, Piroi C (2007) Assessment on the behavior at the fatigue tests of knitting yarns with lycra® content for elastic stocking. In: Xth international workshop SMARTEX-2007 Ivanovo, pp 176–181, Russia
16. Radu CD, Tulbure A, Agafitei G, Popescu V, Piroi C, Harpa R (2007) Knitted structures for dermatological diseases. In: Proceedings of the 5th international conference on the management of technological changes, pp 435–439. Alexandroupolis, Greece, 25–26 Aug 2007
17. Radu CD, Popescu V, Manea LR, Harpa R, Piroi C et al. (2008) Behavior of medical stockings used in chronic venous failure of leg. In: Book of abstracts: 8th AUTEX conference, p. 29. Città Studi Biella, Italy, 24–26 June 2008
18. Harpa1 R, Piroi C, Radu CD (2010) A new approach for testing medical stockings. Text Res J 80(8):683–695

Chapter 22
Tencel/Gelatin Composite Wound Dressing

22.1 Introduction

For the management of surgical wounds, dressings have been commonly used. A wide range of wound dressings have been developed to treat the different problems that happen during the process of wound healing [1, 2]. It is desirable for a wound dressing to be easily applicable and removable and cover the affected areas so as to avoid bacterial entry [3–6]. Gelatin is a protein biopolymer derived from partial hydrolysis of native collagens, the most abundant structural proteins found in animal skin, tendons, cartilage, and bones [6, 7]. Gelatin has a number of desirable properties such as good biocompatibility, low immunogenicity, plasticity, adhesiveness, promotion of cell adhesion, growth, and cost economy and hence has attracted attention of many researchers. It is hence suited for tissue engineering [8]. Anthocyanin is a natural product with polyphenolic structures that have the potential to generate hydrogen-bonded structures and nonbiodegradable collagen matrices [9–11]. It possesses good anti-oxidant properties, eliminates free radicals, reinforces blood vessel walls, protects from cardiovascular diseases, and has therefore been used in many clinical applications [12–14]. This chapter highlights the use of an innovative type of nonwoven fabric comprising a blend of gelatin and anthocyanin. This composite wound dressing has been investigated for a number of properties that include air permeability and stability of the gelatin and anthocyanin film. The wound healing capacity has also been evaluated.

N. Gokarneshan et al., *Emerging Research Trends in Medical Textiles*,
Textile Science and Clothing Technology, DOI 10.1007/978-981-287-508-2_22

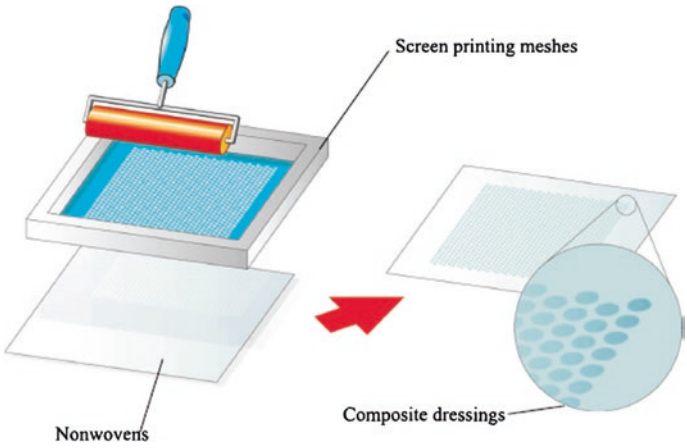

Fig. 22.1 Wound dressing preparation [15]

22.2 Preparation of the Wound Dressing

The well-stirred gelatin and GA solutions were cast onto the nonwoven fabric using the halftone technique (Fig. 22.1), and each time the volume of casting solution was 0.05 ml/cm^2. The mechanical properties of the nonwoven composite were then evaluated [15].

22.3 Measurement of Film Stability in Water

For stability studies, the weight of each film immersed in water was compared with that of the original sample [15]. To prevent inaccuracies in final film weight, all immersed samples were dried in an oven. Film stability was calculated as follows:

$$\text{Stability} = W_a/W_0 \times 100\,\%$$

where

W_a weight of sample after immersing and
W_0 weight of sample before immersing

22.4 FTIR Spectra

The FTIR spectra for the 10/0, 10/5, and 10/10 % GA films are depicted in Fig. 22.2. Considering the 10/0 % GA film for instance (wavelength between 3200 and 3400/cm), the function group (NH2) vibrated and the strength of absorbance was moderate [15].

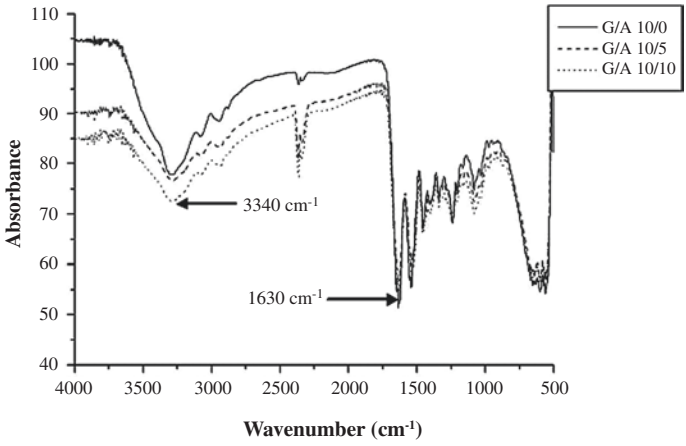

Fig. 22.2 FTIR spectra [15]

Increase in the concentration of anthocyanin under the given range of the wavelength did not yield the desired changes. The wavelength of C=O (1690–1750 cm^{-1}) was not obvious [15]. With the rise in the concentration of anthocyanin, the function group vibrated intensely. This is due to the cross-linking that tends to arise from hydrogen bonds formed between the polyphenolic structure of anthocyanin and gelatin [6], which improves the stability of GA film.

22.5 Stability of GA Film in Water

The influence of the concentration of anthocyanin on the stability of GA film in water is depicted in Fig. 22.3. On the first day, the GA film (10/0 %) got degraded fully due to the solubility of gelatin in water. The rate of degradation of the GA film reduced with the increase in concentration of anthocyanin.

Anthocyanin consists of highly hydroxylated structures capable of generating insoluble complexes with carbohydrates and proteins [8, 9], thus establishing that the anthocyanin concentration can control the degradation rate [15].

22.6 Mechanical Properties of Nonwoven Fabrics

A conducive environment is needed for wound healing to repair tissues. Tencel nonwoven had a basis weight of about 260 ± 15 g/m^2. The nonwoven has been made by opening, carding, laying, and needle punching of the Tencel fiber (Fig. 22.4). The air permeability reduces after casting GA solution onto the dressing [15]. This led to the conclusion that the GA solution blocked the dressing

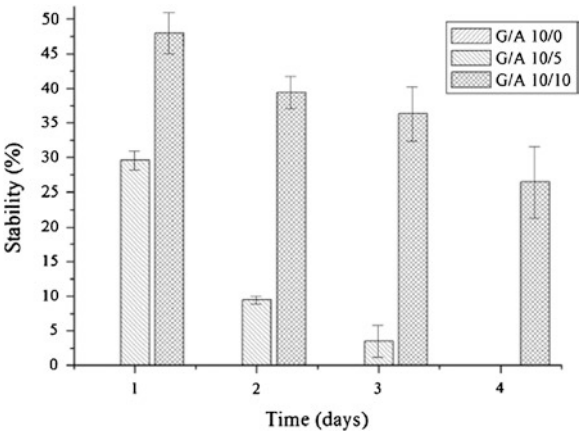

Fig. 22.3 Stability of GA film in water [15]

pores, which has resulted in the development of novel dot coating method. The investigation also compared the whole-plane coating and dot coating methods.

The tensile as well as the tear strengths of whole-plane coating have been greater than those obtained by dot coating, but the air permeability was almost nil. The dot coating method created some blank spaces. Hence, the blank spaces retained air permeability and could absorb tissue fluid.

22.7 Macroscopic Evaluation

Earlier literature has confirmed that gelatin is not cytotoxic and is crucial in wound healing [7, 10]. Four full-thickness round wounds have been made on the flank of each rat. The wound closure rate for each wound has been analyzed depending on the area covered with a commercial wound dressing as a function of time. The healing has been fast in the case of rats treated with the nonwoven GA composite dressing (Fig. 22.5). The wound covered with 10/0 % GA composite dressing festered and has been drier than other wounds. The wound has apparently inflamed [15]. The wound has been scabbed with proliferation of the epidermis on the ninth day. The scab of the wound covered with the commercial wound dressing and GA 10/5 % had peeled off due to the beginning of wound repair.

We believe that physical forces initiated by adsorption of various protein molecules from the wound surface into the GA caused the wound contractions. In contrast with the wound treated with the nonwoven GA (10/10 %) composite dressing, the wounds with the treatments healed slower.

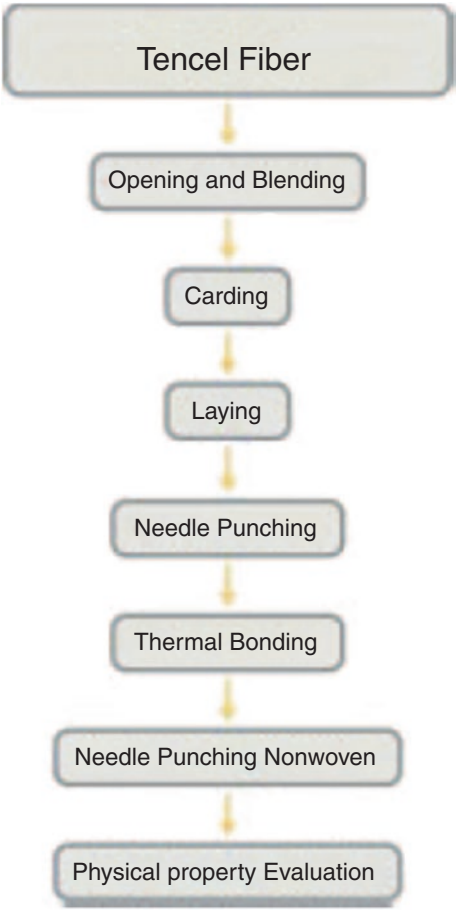

Fig. 22.4 Sequence in production of needle punching nonwoven [15]

22.8 Histological Studies

Known differences have been perceived in the wound healing of the commercial wound dressing and various concentration ratios of GA composite dressing [15]. In order to draw more inferences, the wound sites have been removed, sectioned in 5-m increments, and stained with hematoxylin and eosin reagent. On the third day, the inflamatory cells of the wound appeared and the injury could be seen upon removal of the dressing on the surface. But, infiltration of inflammatory cells and phagocytosis of the gelatin by macrophages have not been seen in the wounds treated with the nonwoven GA composite (Fig. 22.6a–d). On the sixth day,

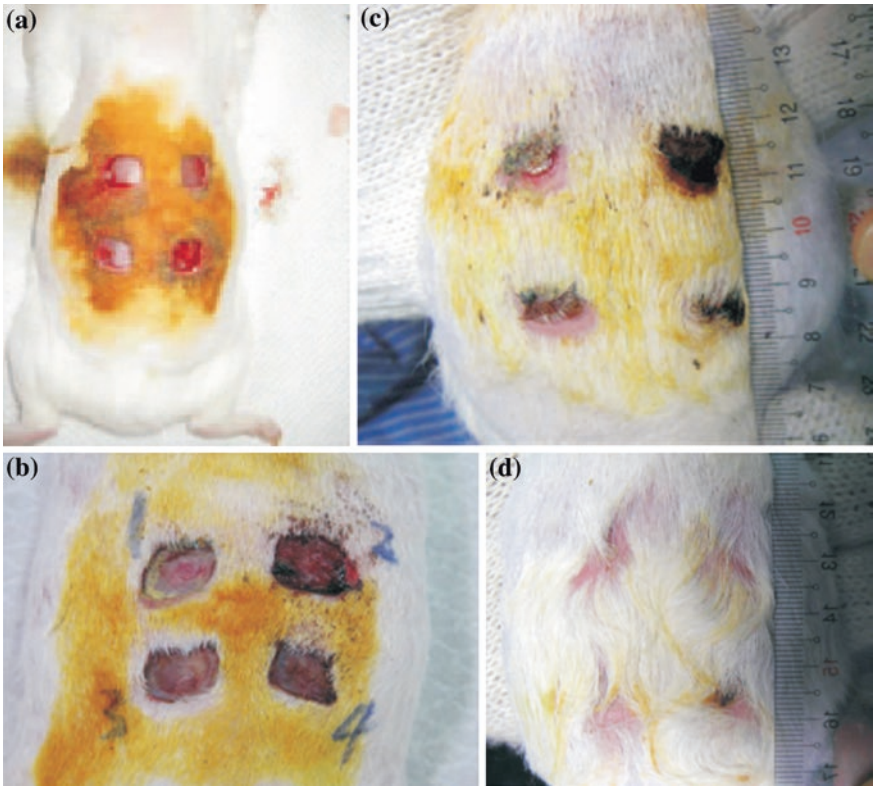

Fig. 22.5 Stages in the wound healing [15]. **a** The first day, **b** the third day, **c** the ninth day, and **d** the eighteenth day

collagen fiber, fibroblasts, and blood vessel have been produced (Fig. 22.6e–h). On the twelfth day, the proliferation of the epidermis progressed accompanied with increase of thickness (Fig. 22.6i–l). The epidermal structure of the wound with commercial wound dressing treatment was better than the sample, and the epidermis of the GA 10/5 % composite dressing did not proliferate. The replacement of the dressing wound may have been damaged, leading to slow tissue growth. The contraction of the wound has been noticed on the twenty-second day, and the GA 10/10 % composite showed improvement over the commercial wound dressing. But, the GA 10/0 % composite dressing was slow (22.6 m–p).

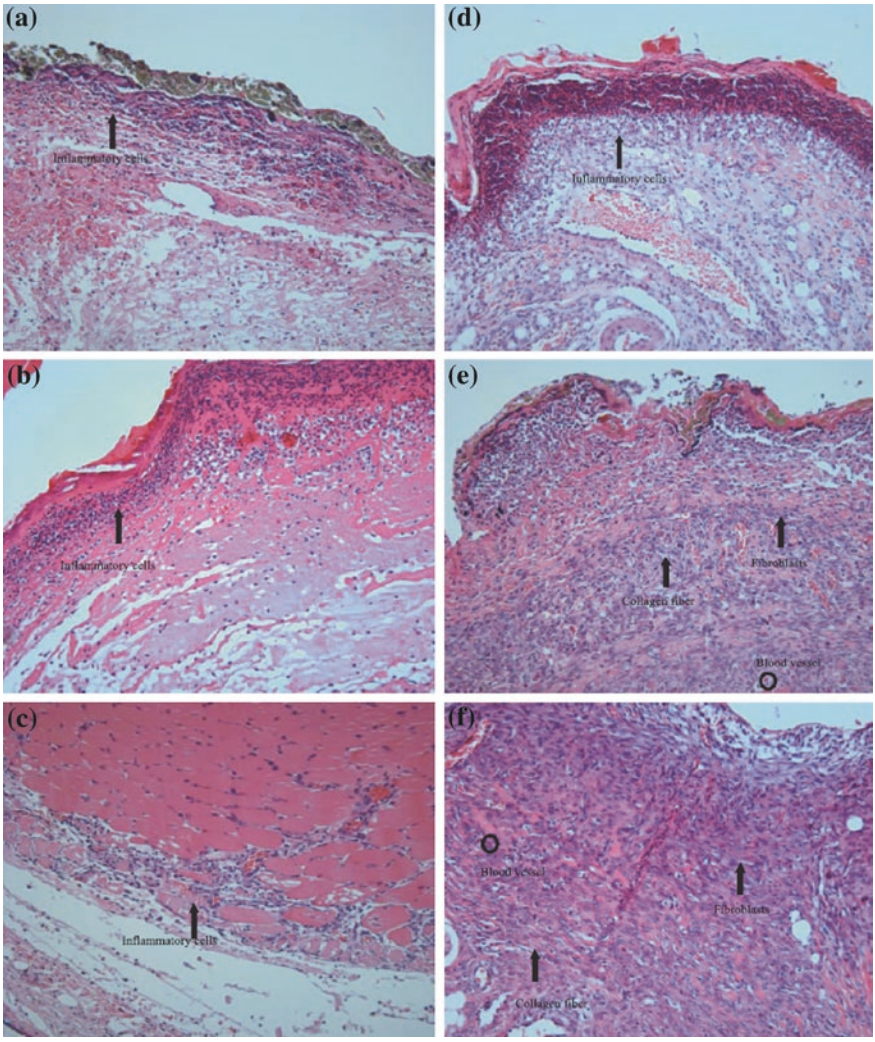

Fig. 22.6 Histological study of wound repair [15]. **a** Commercial wound dressing on day 3, **b** G/A 10/0 % composite dressing on day 3, **c** G/A 10/5 % composite dressing on day 3, **d** G/A 10/0 % composite dressing on day 3, **e** Commercial wound dressing on day 6, **f** G/A 10/0 % composite dressing on day 6, **g** G/A 10/5 % composite dressing on day 6, **h** G/A 10/0 % composite dressing on day 6, **i** Commercial wound dressing on day 12, **j** G/A 10/0 % composite dressing on day 12, **k** G/A 10/5 % composite dressing on day 12, **l** G/A 10/0 % composite dressing on day 12, **m** Commercial wound dressing on day 22, **n** G/A 10/0 % composite dressing on day 22, **o** G/A 10/5 % composite dressing on day 22, and **p** G/A 10/0 % composite dressing on day 22

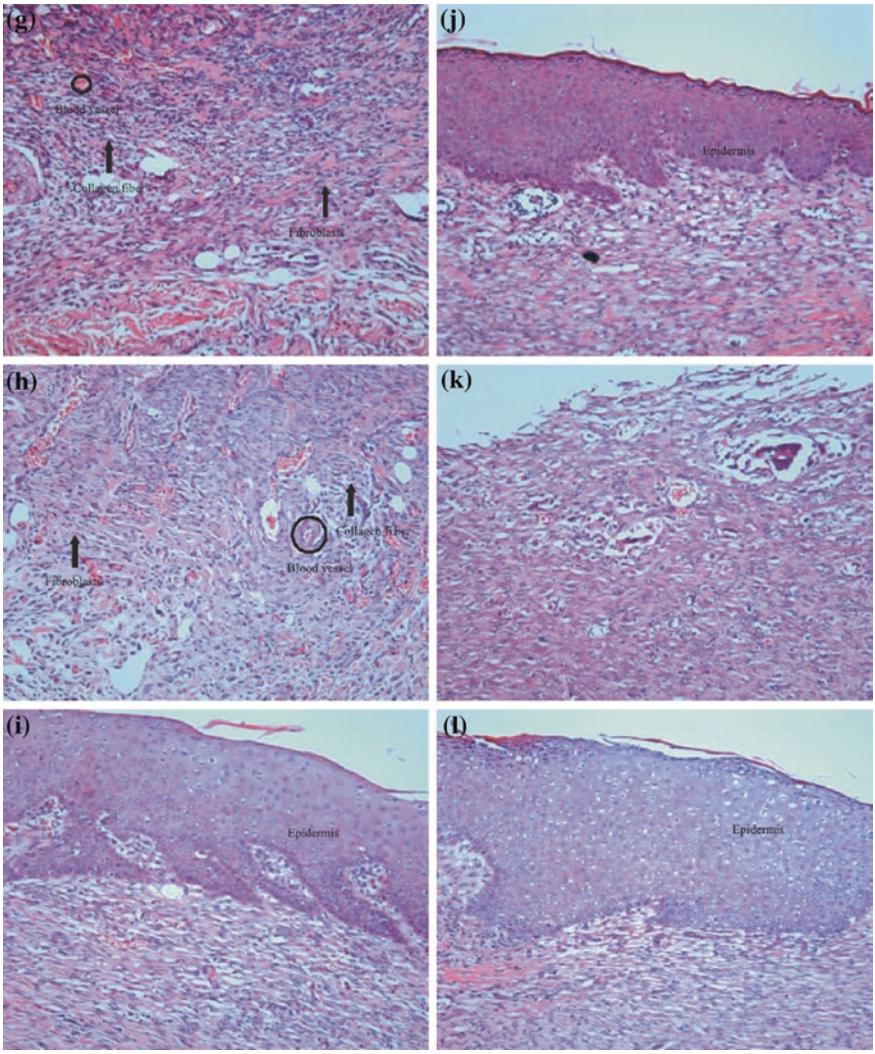

Fig. 22.6 (continued)

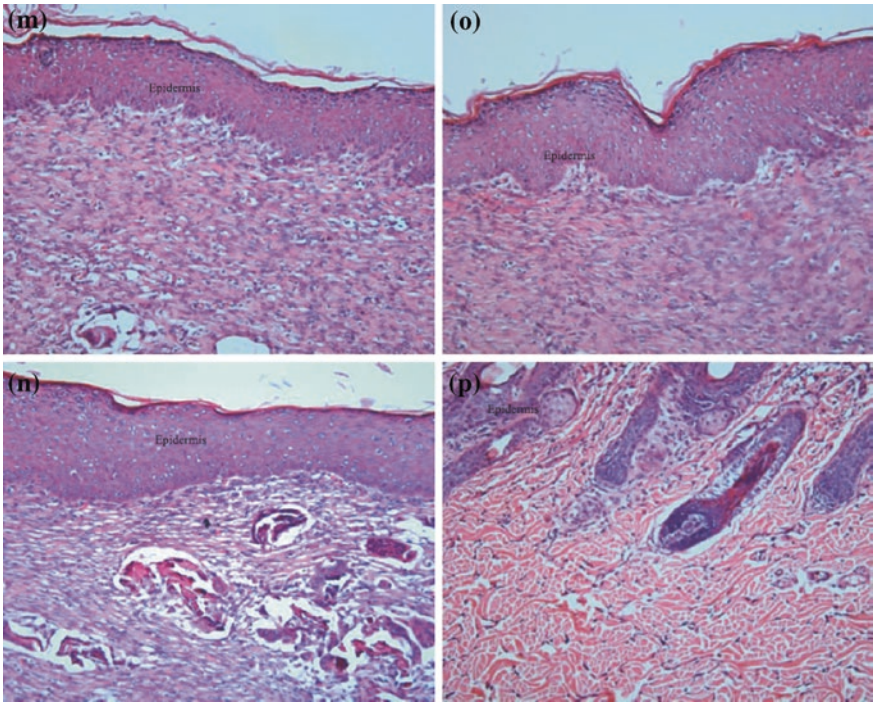

Fig. 22.6 (continued)

References

1. Attwood AI (1989) Calcium alginate dressing accelerates split skin graft donor site healing. Br J Plast Surg 42(4):373–379
2. Barnett A, Berkowitz RL, Mills R, Vistnes LM (1983) Comparison of synthetic adhesive moisture vapor permeable and fine mesh gauze dressings for split-thickness skin graft donor sites. Am J Surg 145(3):379–381
3. Chen WYJ, Bishop SM, Walker M, Rogers AA (2003) Importance of moisture balance at the wound-dressing interface. J. Wound Care 12(4):125–128
4. Winter GD (1962) Formation of the scab and the rate of epithelialization of superficial wounds in the skin of the young domestic pig. Nature 193:293–294
5. Kannon GA, Garrett AB (1995) Moist wound healing with occlusive dressings, a clinical review. Dermatol Surg 21(7):583–590
6. Balakrishnan B, Mohanty M, Umashankar PR, Jayakrishnan A (2005) Evaluation of an in situ forming hydrogel wound dressing based on oxidized alginate and gelatin. Biomaterials 26:6335–6342
7. Purna SK, Babu M (2000) Collagen based dressings—a review. Burns 26(1):54–62
8. Kim S, Nimni ME, Yang Z, Han B (2005) Chitosan/gelatin- based films crosslinked by proanthocyanidin. J Biomed Mater Res B Appl Biomater 75B(2):442–450
9. Han B, Jaurequi J, Tang BW, Nimni ME (2003) Proanthocyanidin: a natural crosslinking reagent for stabilizing collagen matrices. J Biomed Mater Res A 65A(1):118–124

10. Neumann PM, Zur B, Ehrenreich Y (1981) Gelatin-based sprayable foam as skin substitute. J Biomater Mater Res 15:9–18
11. Fukunaka Y, Iwanaga K, Morimoto K, Kakemi M, Tabata Y (2002) Controlled release of plasmid DNA from cationized gelatin hydrogels based on hydrogel degradation. J Control Release 80(1–3):333–343
12. Bridle P, Timberlake CF (1997) Anthocyanins as natural food colours—selected aspects. Food Chem 58(1–2):103–107
13. Wang HB, Nair MG, Strasburg GM, Chang YC, Booren AM, Gray JI, DeWitt LD (1999) Antioxidant and antiinflammatory activities of anthocyanins and their aglycon, cyanidin, from tart cherries. J Nat Prod 62(2):294–296
14. Blando F, Gerardi C, Nicoletti I (2004) Sour cherry (*Prunus cerasus* L) anthocyanins as ingredients for function foods. J Biomed Biotechnol 5:253–258
15. Chao-Chiung H, Ching-Wen L, and Jia-Horng L, Manufacturing process and characterization of tencel/gelatin composite dressing. Text Res J 80(4):325–333

Chapter 23
Fabric for Ulcer Prevention

23.1 Introduction

Pressure ulcer also known as 'Decubitus' ulcer is the injury caused to skin and/or underlying tissue due to pressure, or pressure coupled with shear and/or friction [1]. They are generally found in immobile patients and can take a long time to heal, and also are expensive to treat [2–4]. Pressure ulcers may be deep, originating in underlying tissue, or superficial, resulting from repeated surface friction or abrasion. Deep ulcers are caused due to lack of oxygen and nutrient supply to the skin and underlying tissue due to prolonged pressure. These ulcers result from the mass of the body pressing the skin against any hard objects such as chair, bed [5–7]. A number of pressure-relieving materials and methods are available, such as alternating pressure systems that redistribute the load or relieve the pressure at regular intervals [7, 8]. Pressure-reducing equipment, such as mattresses, cushions, and dynamic air loss systems, redistributes pressure by spreading the weight over a larger surface area [7, 9]. Superficial pressure ulcers occur due to repeated surface friction or abrasion. Shearing and friction cause skin to stretch and blood vessels to kink, resulting in impaired blood circulation in the skin. Superficial pressure ulcers are also caused by microclimate around the skin. The skin is rendered very soft and vulnerable to injury by the moisture and wetness [10]. Many investigations have been focused on the use of Australian medical sheepskin in the prevention and treatment of pressure ulcers [11, 12]. Though the findings reveal some merits, there are innumerable demerits such as itching, discomfort, excess heat. Thermal and tactile properties of textile products in direct contact with the patient's body (bed clothes and bedding) play an important role in creating a proper microclimate around the patient's body. Thermal properties are related to dissipation of metabolic heat and evaporated sweat from the skin into the environment. For patient comfort, the fabric should help maintain a thermal balance and allow the transmission of water vapor. Tactile properties of fabrics, on the other hand, are mainly established by fabric surface structure and

N. Gokarneshan et al., *Emerging Research Trends in Medical Textiles*,
Textile Science and Clothing Technology, DOI 10.1007/978-981-287-508-2_23

often expressed as feelings of softness, smoothness, itchiness, etc. [13–19]. A soft fabric with a smooth surface is desirable. This chapter focuses on the development of a functional textile product that enables to maintain appropriate microclimate around the patient's skin and provides some pressure relief for reducing or delaying the development of pressure ulcers.

23.2 Objectives and Fabric Development

The fabric has been developed with the twin objectives of achieving moisture management and pressure relief. In this regard, a face-to-face velour weaving technique was utilized to produce a spacer fabric. A spacer fabric is one that comprises of two distinctive fabric layers stitched together by a group of yarns (pile yarns). Such a structure promotes pressure relief and enables better moisture management and improved air permeability [20, 21]. Spacer fabrics can be produced either by warp knitting or weft knitting technique on a double-jersey circular knitting machine, or even on a double-insertion rapier machine. The rapier machine produces two pieces of fabric face to face in a sandwich form, and then, a reciprocating knife blade on the front of the machine separates the pieces [22]. The knife blade system has been dispensed with to obtain a spacer fabric. The spacer fabric structure has been constructed by the use of two different engineered polyester yarns that have better moisture wicking ability. One of them was made from four-channel Dacron polyester fiber (Fig. 23.1), and the other is made from microdenier polyester blended with cotton [23].

These yarns have a good ability to wick moisture away from the surface which are in contact. Earlier research revealed that ChPES yarn has better water

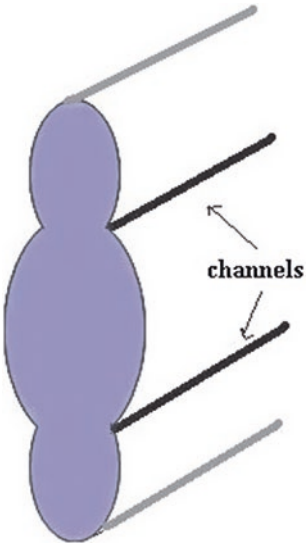

Fig. 23.1 A four-channel polyester fiber shown cross-sectionally [28]

absorbency and wicking ability. MbPES/CO yarn, on the other hand, has superior air permeability [24]. Furthermore, this yarn was found to be more compact, which in turn, was expected to lead to higher bending rigidity and less depression. Considering these findings, for the top and bottom base fabrics, ChPES yarn was chosen as warp. Top weft, which will have direct contact with skin, consisted of one of the following: ChPES, MbPES/CO, and polypropylene (PP). Also, certain special yarns having antimicrobial properties have been incorporated in the fabric structure as top weft in some fabrics. Despite these yarns being quite expensive for use in hospitals and nursing homes, based on the results of this investigation, they might be offered to patients in home care. The function of top weft yarn was to wick moisture away from the top layer of the fabric, transport it to the bottom layer, and help the dispersion of moisture to the drier areas. Bottom weft, on the other hand, consisted of one of the following yarns: ChPES, MbPES/CO, cotton (CO), and viscose (CV). The role of CO and CV was to absorb body liquids wicked away from the skin and entrap them in the bottom layer. Three types of pile yarn, comprising of channeled polyester yarn, have been made [28]. Microdenier polyester/cotton blended yarn and also polypropylene yarns have been incorporated in the pile yarns to get better stability and enhanced compression resilience in the fabric. From these combinations, 32 different spacer fabrics having 2/2 twill weave, 15 ends, and 20 picks per cm have been woven (Fig. 23.2).

Various types of yarns and pile heights have been used in the spacer fabric structures. Pile height was measured on the loom when the fabric was under tension by a ruler. The setting of the pile height on the loom has been 3.9 mm. The pile height has been enhanced to 5.0 and 6.5 mm to obtain thicker and more volumes fabrics. But, it was hard to weave the double-layered fabrics with pile height of 6.5 mm. As a result, only one sample was woven. All yarns, except polypropylene

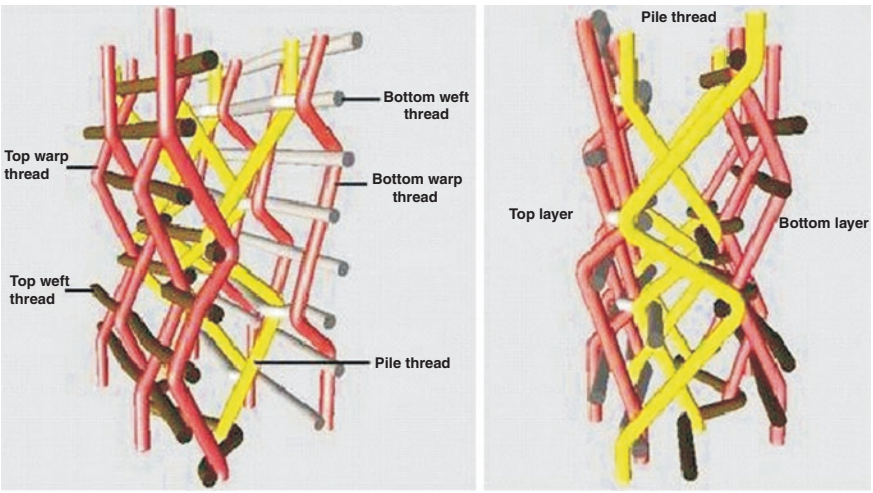

Fig. 23.2 Spacer fabric structure [28]

and Crabyon®, had a linear density of 20 × 2 tex. Crabyon®'s linear density was 10 × 4 tex, and polypropylene linear density was 300 denier. In the case of SeaCell® yarn, a SeaCell® and a MbPES/CO yarn of 20 tex were twisted together. Since the cotton yarn was bleached, greige fabrics were only subjected to a washing at 25 °C, and subsequently a moisture management agent (Cassapret® SRH A) was applied.

23.3 Thermal Properties

Figure 23.3 shows the thermal resistance values of the fabrics. Statistical evaluation has revealed that for all pile types, the greater the pile height, the better would be the thermal resistance. This effect can be observed from the samples 3-3, 6-1, and 9. As the fabrics have been woven from 100 % channeled polyester yarn, the difference between the thermal resistances values arose entirely from the pile height. This was expected since the high pile height causes more air to be captured in the structure and air has much lower thermal conductivity compared to fibers [28]. Pile type caused a significant difference in thermal resistance values as well, with pile type I having lowest and pile type II having highest value. Yarn type used as top weft and bottom weft also affected the thermal resistance values. Thermal resistance of the special test yarns (Crabyon® and SeaCell®/microdenier polyester/cotton blend yarns was lower than the rest. They were followed by polypropylene and microdenier polyester/cotton yarns. Channeled polyester yarn exhibited the best thermal resistance. In the case of the bottom weft, channeled polyester and cotton caused greater thermal resistance compared to microdenier/cotton and cotton viscose. In particular, the difference between the thermal resistance values of samples produced from channeled polyester and microdenier polyester/cotton is interesting. The channels incorporated into the fiber structure in polyester fibers seem to have substantial influence on thermal resistance. The results are in agreement with the previous investigation [24]. Figure 23.3 shows the thermal conductivity of samples. Samples with pile type I and II have substantially lower thermal conductivity than that of pile type III.

As expected, 6.5-mm pile height exhibited lesser thermal conductivity compared to 3.9- and 5.0-mm pile height. The thermal conductivity of the fabric samples with channeled polyester and cotton bottom wefts has been lesser than that of the fabric samples with microdenier polyester/cotton and cotton viscose. The entrapped air in the channeled structure of channeled polyester yarn possibly caused low thermal conductivity. Overall, cotton fiber has higher thermal conductivity compared to cotton viscose. The deviation could have arisen due to the yarn structure. Polypropylene exhibits a considerable difference in thermal conductivity among the yarns used as top weft. The fabric samples containing polypropylenes exhibited the least thermal conductivity.

This was expected since polypropylene fibers have the lowest thermal conductivity among the fibers used in this study. Moreover, the thermal conductivity of the samples with SeaCell®/microdenier polyester/cotton and Crabyon® was particularly high when a viscose bottom weft was used. This was understandable as, like viscose fibers, both SeaCell® and Crabyon® are regenerated cellulose-based fibers. Therefore, their thermal conductivity properties are expected to be identical

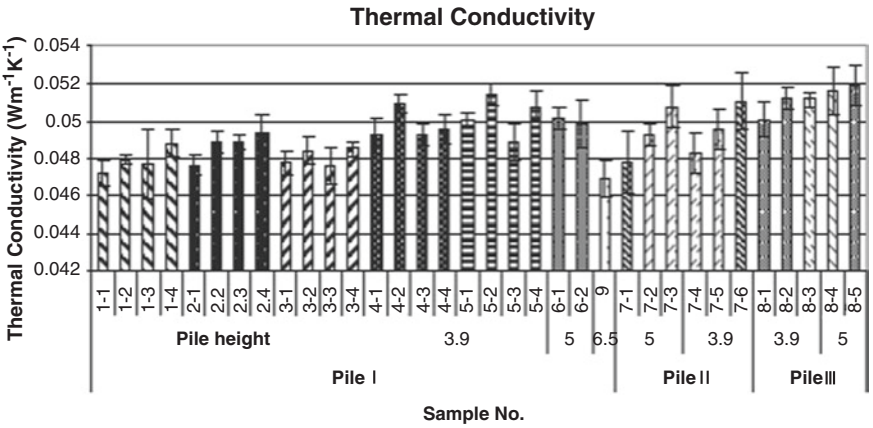

Fig. 23.3 Thermal conductivity values of fabric samples [28]

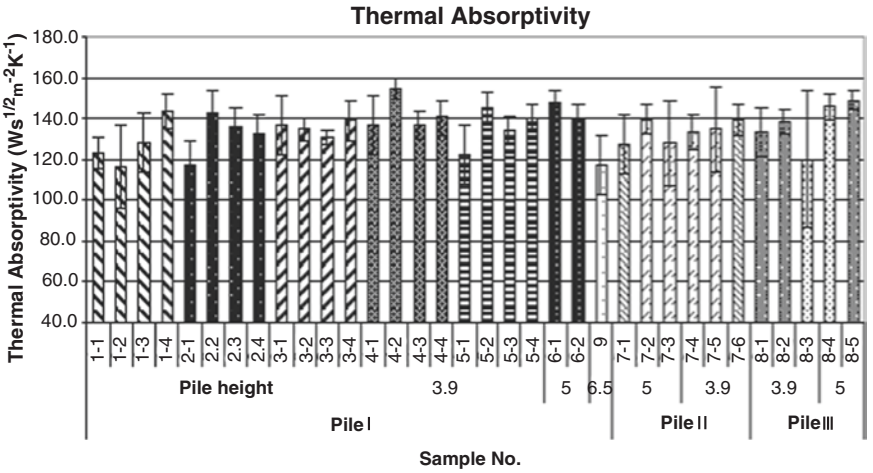

Fig. 23.4 Thermal absorptivity values of samples [28]

to viscose, which has considerably high thermal conductivity [26, 27]. Figure 23.4 shows the thermal absorptivity values of the fabric samples.

The type of pile or height of pile did not have considerable impact on thermal absorptivity as analyzed statistically. This has been acceptable, as thermal absorption is a surface property. The top weft had a considerable effect. While polypropylene weft caused the lowest thermal absorptivity value, Sea-Cell®/MbPES/CO weft caused the highest one. Effects of other yarn types on thermal absorptivity were similar. Among the yarns used as bottom weft, CO weft resulted in the lowest thermal absorptivity, which significantly differed from that of samples with ChPES and MbPES/CO bottom wefts. ChPES and MbPES/CO gave similar results. A less value of thermal absorptivity implies that the fabrics have a warmer feel, and this is preferable for the required product end use.

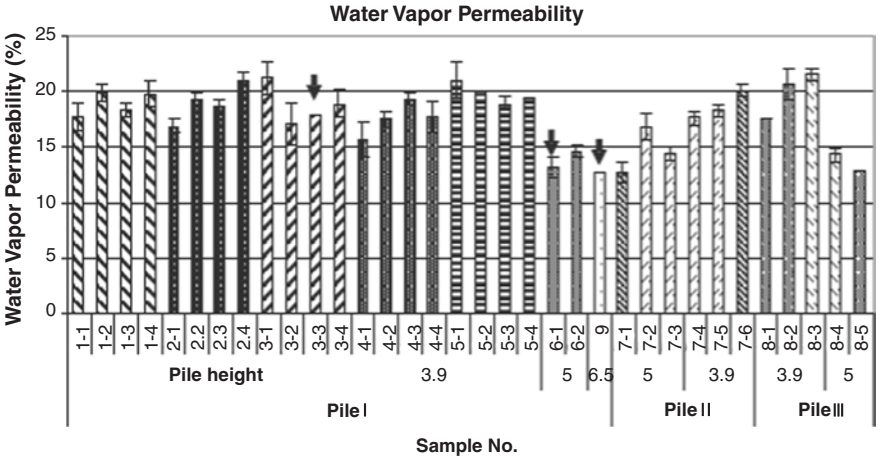

Fig. 23.5 Water vapor permeability of samples [28]

23.4 Water Vapor Permeability

The water vapor permeability of the fabrics is shown in Fig. 23.5. The water vapor permeability has not been significantly by the type of bottom weft and pile, as analyzed statistically, while the pile height had a significant influence. Referring to the figure, fabrics **3-3** (3.9 mm), **6-1** (5.0 mm) and **9** (6.5 mm) clearly indicate that the water vapor permeability reduces with increase in the pile height [28]. This can be explained by the higher amount of water vapor captured in the structure as pile height gets higher. PP and Crabyon® top wefts resulted in higher water vapor permeability. The rest of the yarns, on the other hand, caused similar values. These results showed that in the case of this particular double-layered fabric structure, water vapor permeability mainly depended on pile height. The influence of the type of weft yarn on water vapor permeability is not important.

23.5 Water Absorbency Test

23.5.1 Vertical Wicking Test

The height of fabric wicking on either direction after a duration of one hour is shown in Fig. 23.6.

Statistical results have shown that the type of pile had a considerable influence on vertical wicking properties of fabrics. Pile type I and II show better result in comparison with pile type III. The fabrics with channeled polyester weft yarns and polypropylene-added pile yarns exhibited highest wicking height in either direction.

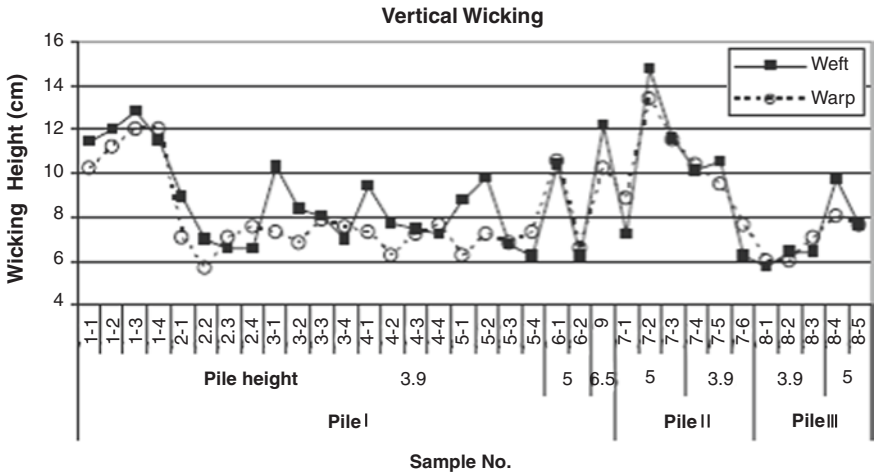

Fig. 23.6 Vertical wicking test results [28]

Polypropylene and ChPES top wefts improved the wicking height in both weft and warp directions. MbPES/CO and viscose bottom wefts, on the other hand, deteriorated the vertical wicking. Increasing pile height increased the wicking height. The capillary forces that act upon the capillary spaces in the fabric structure causes wicking [28]. Evidently, the channeled polyester fiber structure leads to fast liquid transport. Microdenier blended polyester/cotton yarn consisting of natural and synthetic fibers combined together to transfer the moisture. It appears that the synergy created by the natural and synthetic fiber composition of MbPES/CO yarn was not as effective as the channeled fiber structure in transporting liquid moisture. Pore size is a significant factor here. The water flow selects small pores during the capillary action. The channeled structure seems to create smaller pores.

23.5.2 Drop Test

The fabrics have been visually analyzed for yellow mark as shown in Fig. 23.7.

On observing the above figures, the water spread in the direction of warp in the case of the fabric having polypropylene (e.g., sample 1-3) or microdenier blend of polyester/cotton (e.g., samples 2-4 and 7-1) top weft. The transfer of water has been uniform in either fabric direction in the case of channeled polyester weft yarn (e.g., samples 3-3 and 7-2). This is due to the higher wicking ability of channeled polyester yarns [28]. Pile type or height did not seem to affect the water propagation on the fabric surface. The shape and the size of the yellow-marked area on samples with same weft yarns, and different pile type and pile height were very similar. It appears that the effect of yarn type on water spreading is dominant over

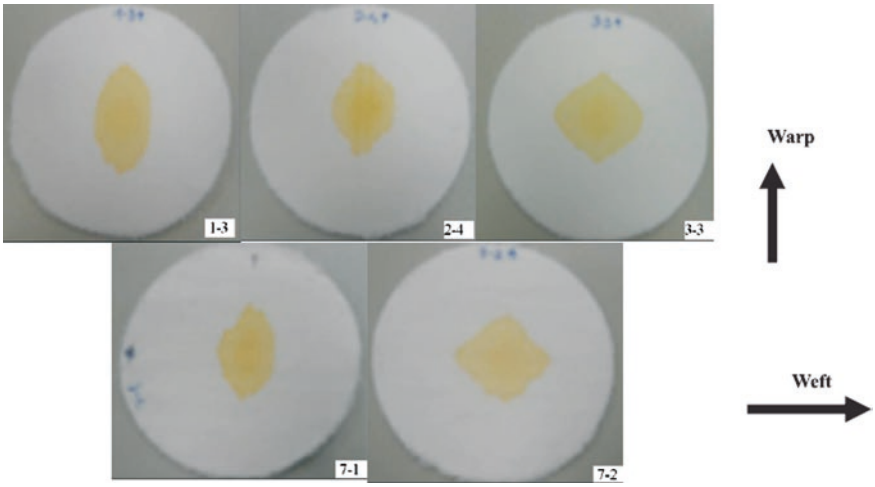

Fig. 23.7 Selected results from the drop test [28]

pile type and pile height in this particular type of fabric structure. As accurate quantitative measurements have been difficult during the test, only visual observations have been done.

23.5.3 Fabric Hand

Figures 23.8 and 23.9 depict subjective fabric hand evaluation for 19 test fabrics having viscose bottom weft.

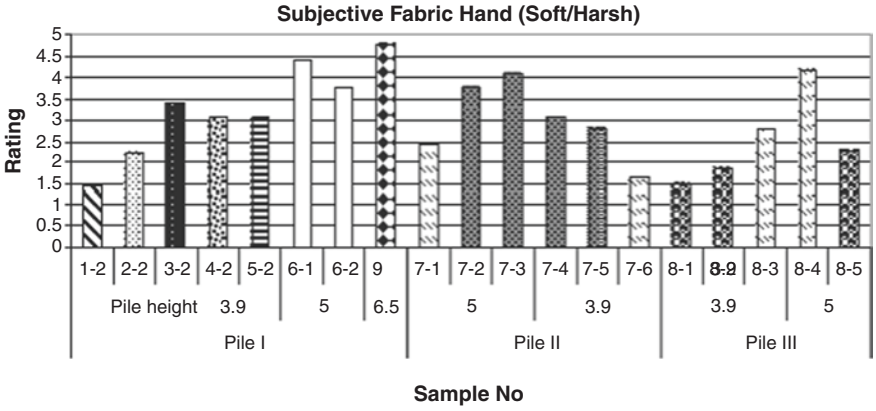

Fig. 23.8 Subjective fabric hand assessment (soft/harsh) [28]

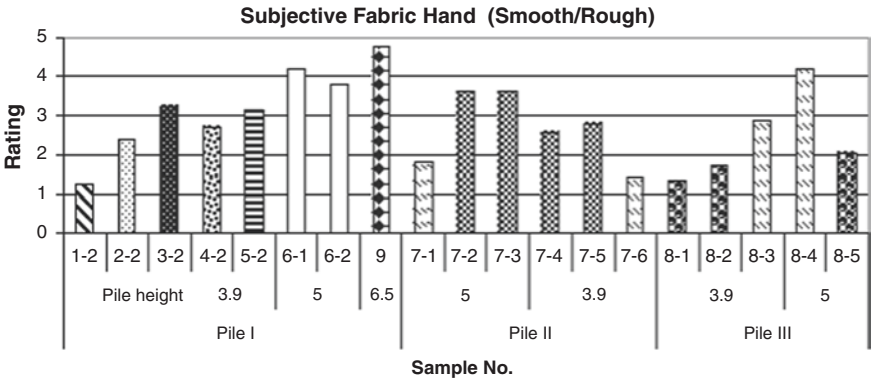

Fig. 23.9 Subjective fabric hands assessment (smooth/rough) [28]

The channeled polyester yarns exhibit a positive influence on fabric hand. However, microdenier polyester/cotton blended yarn and polypropylene yarns appeared to have a negative influence. The highest rating has been given to the fabric with the maximum pile height. Fabric hand can be defined as the total sensations experienced when a fabric is touched or manipulated by the fingers [28]. Fiber type and yarn structure plays an important role in these sensations. In this study, apart from polypropylene, all of the other yarns were made from staple fibers. Convincingly, polypropylene has been given the lowest rating. It appears that the cross-sectional shape of the channeled polyester fibers enhanced the flexibility of fiber and so also the smoothness and softness of the fabric as well.

23.5.4 Compressibility

The thickness of the fabrics has been determined under the compression loads of 75 and 1700 g/cm^2, and the compressibility percentage is calculated. The pile type and height strongly influence the compressibility of the fabrics. The polypropylene pile yarns, due to their greater stiffness, were less compressible. The compressibility of the fabrics having pile height of 5.0 mm and 6.5 mm was the same. On the other hand, the fabrics having pile height of 3.9 mm had substantially high compressibility in comparison with them [28]. Fabric thickness becomes important in compressibility of fabrics made from same fibers. Thicker fabrics are less compressible unless the structure is very bulky. Despite the fact that the double-layered fabric structure showing only a small improvement in pressure relief, it could possibly help patients feel more comfortable. Clinical trials are to be carried out to prove its effectiveness.

References

1. Hu J, Li Y, Yeung K-W, Wong ASW, Xu W (2005) Moisture management tester: a method to characterize fabric liquid moisture management properties. Textile Res J 75(1):57–62
2. Graves N, Birrell F, Whitby M (2005) Modeling the economic losses from pressure ulcers among hospitalized patients in Australia. Wound Repair Regen 13:462–467
3. Severens JL, Habraken JM, Duivenvoorden S, Frederiks CM (2002) The cost of illness of pressure ulcers in The Netherlands. Adv Skin Wound Care 15:72–77
4. Jackobs MK (1999) Cost of medical nutrition therapy in the healing of pressure ulcers. Topics Clin Nutr 14(2):41–47
5. Hobson DA (2008) Principles of pressure management. Department of Rehabilitation Science and Technology, University of Pittsburgh. http://www.wheelchairnet.org/wcn_wcu/SlideLectures. Accessed 15 Sept 2008
6. Cullum N (1995) The prevention and treatment of pressure sores. Eff Health Care Bull 2(1):1–16
7. http://www.patient.co.uk/showdoc/40002086. Accessed 15 Sept 2008
8. Bethell E (1994) Pressure sores. Alternating pressure systems are useful BMJ 309(6966):1436 (Clinical Research ed)
9. Collins F (1999) The contribution made by an armchair with integral pressure reducing cushion in the prevention of pressure sore incidence in the elderly, acutely Ill patient. J Tissue Viab 9(4):133–137
10. Pryczynska E, Lipp-Symonowicz B, Wieczorek A, Gaszynski W, Krekora K, Bittner-Czapinska E (2003) Sheet fabrics with biophysical properties as elements of joint prevention in connection with first- and second-generation pneumatic anti-bedsore mattresses. Fibres Textiles East Eur 11:50–53
11. Jolley DJ, Wright R, McGowan S, Hickey MB, Campbell DA, Sinclair RD, Montgomery KC (2004) Preventing pressure ulcers with the Australian medical sheepskin: an open-label randomised controlled trial. Med J Aust 180(7):324–327
12. McGowan S, Montgomery K, Jolley D, Wright R (2000) The role of sheepskins in preventing pressure ulcers in elderly orthopedic patients. Prim Intent 8:127–134
13. Adler MM, Walsh WK (1984) Mechanisms of transient moisture transport between fabrics. Textile Res J 54:334–343
14. Andreen JH, Gibson JW, Wetmore OL (1953) Fabric evaluations based on physiological measurements of comfort. Textile Res J 23:11–22
15. Gagge AP, Gonzalez RR (1974) Physiological and physical factors associated with warm discomfort and sedentary man. Environ Res 7:230–242
16. Goldman RF (1981) Evaluating the effect of clothing on the wearer—chapter 3. In: Cena K, Clark JA (eds) Bioengineering, thermal physiology and comfort. Elsevier Scientific Publishing Co., Amsterdam
17. Hatch KL, Woo SS, Barker RL, Radhakrishnaiah P, Markee NL, Maibach HI (1990) In vivo cutaneous and perceived comfort response to fabric part I: thermophysiological comfort determinations for three experimental knit fabrics. Textile Res J 60:405–412
18. Hollies NRS, Custer AG, Morin CJ, Howard ME (1979) A human perception analysis approach to clothing comfort. Textile Res J 49:557–564
19. Snycerski M, Frontczak-Wasiak I (2004) A functional woven fabric with controlled friction coefficients preventing bedsores. AUTEX Res J 4(3):137–142
20. http://www.fabriclink.com/dictionaries/textile. Accessed 15 Sept 2008
21. Wilkens C (1993) Raschel knitting spacer fabrics. Kettenwirkpraxis 3:E18–E20
22. Manley S (2004) The development of woven velours for the transportation market. J Textile Apparel Technol Manage 3(4):1–14
23. Katz M (1999) US Patent 5,888,914
24. Basal G, Mecit D, Duran D, Ilgaz S (2008) Bed sheets designed for improved comfort, 8th joint international conference CLOTECH'2008. Lodz, Poland

25. Hes L, Dolezal I (1989) New method and equipment for measuring thermal properties of textiles. J Textile Mach Soc Jpn 42(8):T124–T128
26. http://www.syntechfibres.com. Accessed 10 Feb 2009
27. Morton WE, Hearle JWS (1986) Physical properties of textile fibres, 3rd edn. Textile Institute Publisher, Manchester
28. Guldemet Basal1 Department of Textile Engineering, Ege University, Bornova, Izmir 35100, Turkey Sevcan Ilgaz Nil Knitting-Dyeing Company, Merter, Istanbul 34169, Turkey (2009) A functional fabric for pressure ulcer prevention. Textile Res J 79(16):1415–1426

Chapter 24
Smart Shape Memory Fabrics—Biological Aspects

24.1 Introduction

Shape memory polymers are a group of actively moving polymers that can instantly change their shapes in a predefined manner under a given set of conditions such as heat, electricity, pH value, ionic strength, light, and magnetic field [1–6]. As these polymers find medical applications owing to their combination of biocompatibility with large shape deformation and recoverability, they have attracted a great deal of scientific interest. Shape memory polymers have a wide range of tunable stiffness, tailorable switch temperatures, fast actuation, and elastic properties of the materials which are of benefit for their biomedical applications. The switch temperature can be easily adjusted by varying the soft segment and hard segment type and contents [7–9]. Earlier researches have pointed out many biomedical applications of shape memory polymers [10–12]. One example is a laser or magnetic-activated shape memory device for the mechanical removal of blood clots [13–16]. Another example is an aneurysm coil for the treatment of intracranial aneurysm in place of a platinum coil [17]. A third example is a biodegradable suture with shape memory effect [18–20]. The suture can tie itself into a perfect knot in the body after being applied to wounds. Shape memory foams are helpful for overweight patients to lose weight [21]. They could also be used to deliver drugs in the treatment of stomach and intestinal disorders [22, 23]. Shape memory polymers could also find application in orthodontics [24–26]. There are only a few biomedical applications of shape memory fabrics. This arises because of the problems associated with the synthesis of high-quality shape memory polymer for fiber spinning and the spinning technique of shape memory polymers. Recently, shape memory fibers have been developed via the wet and melt spinning techniques [27–31]. Shape memory fibers possess excellent mechanical properties and shape recovery force due to molecular orientation. They enable to create intelligent fabrics with a self-regulating structure and performance responding to surrounding temperature, in the case of apparel designs

N. Gokarneshan et al., *Emerging Research Trends in Medical Textiles*,
Textile Science and Clothing Technology, DOI 10.1007/978-981-287-508-2_24

[32, 33]. Besides, the fabrics have more capability to form 3D structures, compared with spandex and polyester due to their good shape fixity. Moreover, they possess good wearer fit and comfort, due to their good shape deformability and retention property of the fibers. They also hold promise in the biomedical material applications owing to their soft structure and permeability and are therefore more biocompatible in comparison with films or bulks. In the case of biomedical applications, it would be desirable that the shape recovery be stimulated by the temperature of the human body [34, 35]. Shape memory polyurethanes can have alterable temperatures between −50 and 100 °C, by varying soft segment and hard segment type and contents. This chapter highlights a shape memory polyurethane of the glass transition type with appropriate temperature alteration ability. Polybuthyleneadipatediol has been used as the soft segment.

24.2 Evaluation of Thermal Properties

The image of the prepared shape memory multifilament is presented in Fig. 24.1.

The glass transition temperature of the shape memory polymer has been measured by means of differential scanning calorimetry (DSC), and the curve so obtained is shown in Fig. 24.2.

The fiber so analyzed exhibits an endothermic step change at 35.90 °C, pointing the glass transition of the soft segment phase [29–31]. This temperature pertaining to the soft segment phase is used as the switch transition for the fiber to fix or unfix the shapes of the shape memory fiber below and above the thermal transition temperature. The switch temperature is almost the same as body temperature, so as to enable shape changes to be caused by human bodies. The curve shows two hard segment melting transition peaks at 121.9 and 144.0 °C. This points out that the hard segment phase has strong crystallizability [28]. In the case of shape

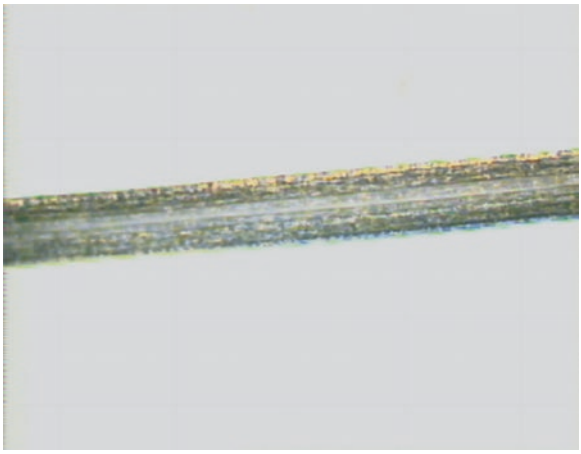

Fig. 24.1 The image of the shape memory multifilament [36]

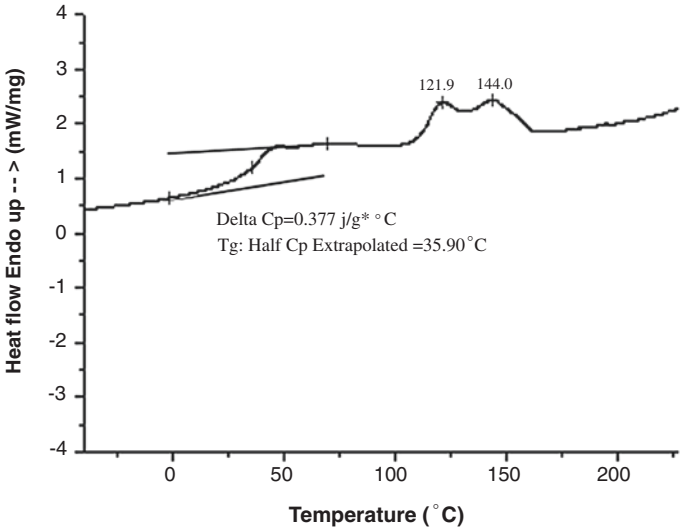

Fig. 24.2 The differential scanning calorimetric *curve* of the shape memory fiber [36]

memory polyurethanes, the shape recovery happens through the release of the stress accumulated during deformation caused by the hard segment phase [29]. Hence, it is possible to predict that the fiber can have good shape memory effects [36].

24.3 Mechanical Fiber Properties

The static strain–stress curves of shape memory fibers and films can be seen in Fig. 24.3.

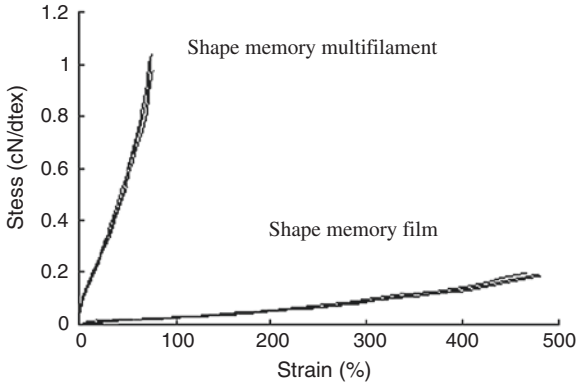

Fig. 24.3 The tensile properties of the shape memory multifilament and shape memory film [36]

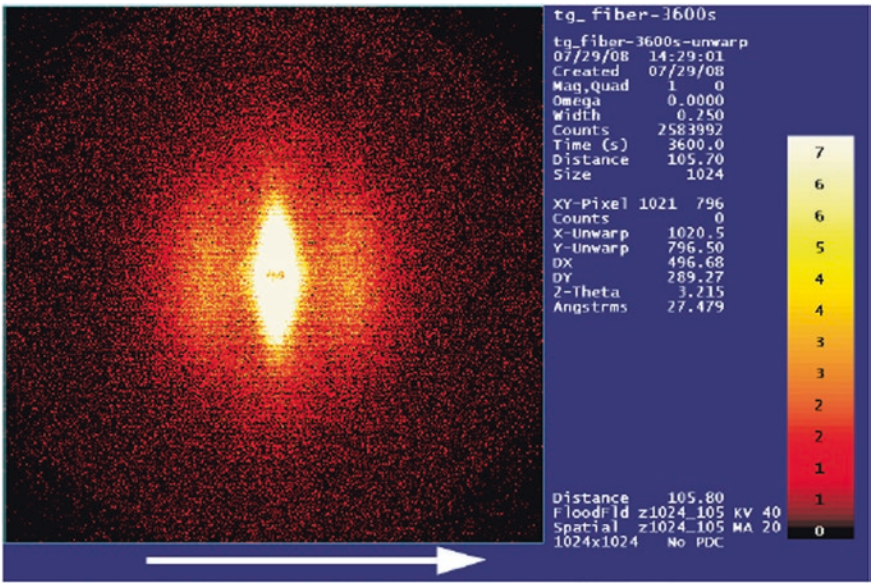

Fig. 24.4 The SAXS pattern of the shape memory fiber [36]

The average fiber tenacity is found to be 1.04 cN/dtex, and breaking elongation is 76 %. The shape memory fiber has a breaking strength around five times that of the shape memory film. These values can be attributed to the molecules' orientation in the shape memory fiber caused by the spinning process. Figure 24.4 shows the molecular orientation of the shape memory fiber by using SAXS.

The fiber axis is indicated by the arrow. The reflection from the surface of the fibers is shown as equatorial streak [36]. The complete molecular orientation of the fiber is depicted as asymmetric scattering pattern.

24.4 Shape Memory Effect of the Fiber

Figure 24.5 shows the curves depicting the thermomechanical cyclic tensile test of the shape memory fiber.

During the first phase, the shape memory fiber has a fixity ratio of more than 80 % and a recovery ratio of up to 90 %. This is indicative of good shape memory effect for the fiber prepared. The reorganization of fiber molecules, which includes molecular orientation, and crystallization or breakage of a weak place during elongation partially creates a significant difference between the first and remaining thermal phase [36]. The stress–strain behaviors become very similar after a cycle. Shape memory polymer cannot fix the temporary shape completely because of instant elastic recovery after external stress is released. Moreover, its original

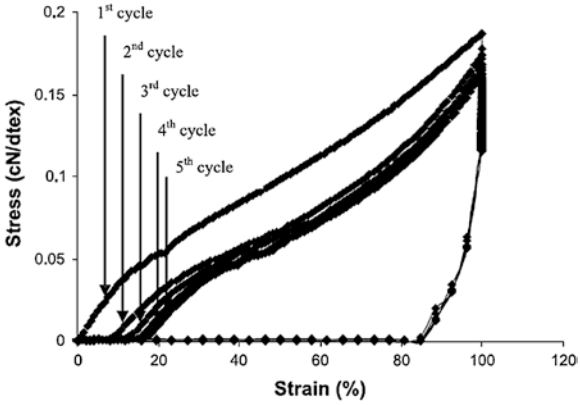

Fig. 24.5 *Curves* depicting the thermo mechanical cyclic tensile test of the shape memory fiber [36]

length is not completely recoverable owing to stress relaxation, rearrangement of molecules, and a breakage of weak point.

24.5 Shape Memory Effect of the Fabric

The shape memory characteristic of the fabric is shown in Fig. 24.6a, b.

The height of the bag speedily recovers to about 0.4 cm, after a time duration of about 2 min with rise in temperature. Figure 24.6b indicates that the bag does not recover complete flatness. This may be partially due to the molecule orientation and the broken weak point of the fiber molecules. The knit structure of the fabric is also an influencing factor. The recovery ratio could get reduced due to the friction and entanglement between fibers in the fabric. The various fabric mechanical properties and shape memory effects can be affected by alteration of fabric structures that would suit varied applications and conditions [36].

24.6 Cytotoxicity

Table 24.1 shows the biological reactivity (cellular degeneration and malformation), which has been rated on a scale of 0–4.

The responses obtained from the negative and positive controls as well as the shape memory fabric are shown in Table 24.1. The test system has been considered suitable due to the observed response, which relates to the labeled biological reactivity grade of the reference standard considered [36]. The test article met the requirements of the test if none of the cell cultures exposed to the test article exhibit greater than a mild reactivity (grade 2). The test results revealed that the shape memory fabric is cytotoxic.

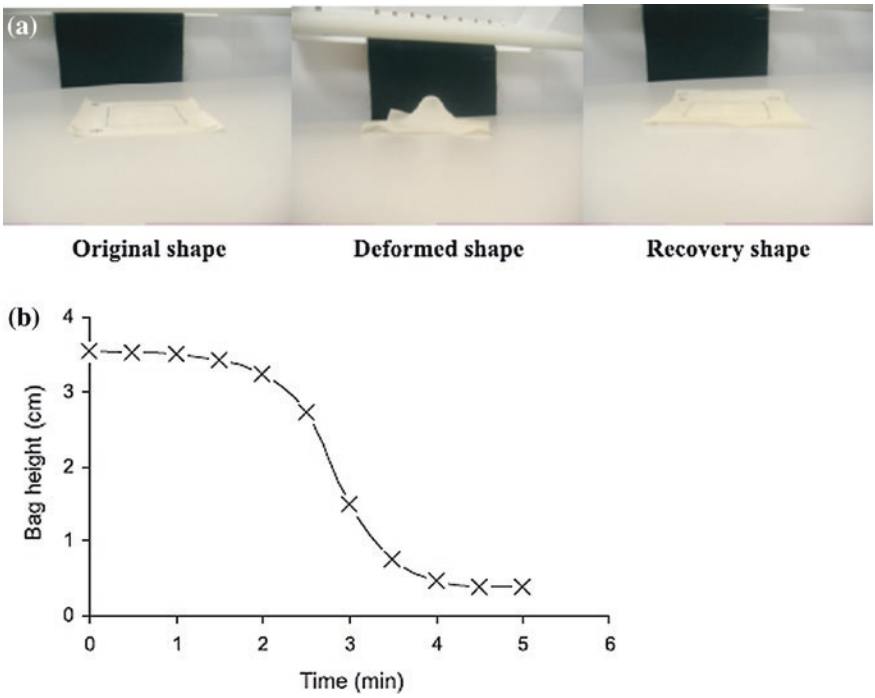

Fig. 24.6 The *curve* showing recovery of the shape memory fabric. **a** The bag shapes during the shape recovery test and **b** the variation in the height of the bag during the shape recovery as a function of time [36]

Table 24.1 Rating of biological activity [36]

Grade	Reactivity	Description of reactivity zone
0	None	No detectable zones around or under specimen
1	Slight	Some malformed or degenerated cells under specimen
2	Mild	Zone limited to area under specimen
3	Moderate	Zone extends 0.5–1.0 cm beyond specimen
4	Severe	Zone extends greater than 1.0 cm beyond specimen but does not involve entire dish

24.7 Hemolysis

The hemolysis index has been calculated as per following the equation

$$\text{Hemolysis index}\,(\%) = \frac{A_1 - A_2}{A_3 - A_2} \times 100$$

Table 24.2 Agar diffusion test results [36]

Article	Reactivity grade at 24 h
Positive control (1 cm^2 latex)	3
Positive control (1 cm^2 latex)	3
Positive control (1 cm^2 latex)	3
Negative control (physiological saline, 0.1 ml)	0
Negative control (physiological saline, 0.1 ml)	0
Negative control (physiological saline, 0.1 ml)	0
Shape memory fabric (1 cm^2)	0
Shape memory fabric (1 cm^2)	1
Shape memory fabric (1 cm^2)	1

where

A_1 is the absorption of the test group,
A_2 is the absorption of the negative control group
A_3 is the absorption of the positive control group

A mean hemolysis index from the three test samples of 5 % or less was considered to be nonhemolysis [36]. Absorption of negative control solution should not be more than 0.03; absorption of positive control solution should be 0.8 ± 0.3. The absorption data of test and control groups are presented in Table 24.2.

The free hemoglobin concentration has been measured to find out the hemolysis index of the test article extracts using the spectrophotometrical method. Under the conditions used in this study, hemolysis was not observed in the diluted rabbit blood which was in direct contact with the test article extracts. Hemolysis index of the test article was 0.35 %.

24.8 Sensitization

Table 24.3 shows the specific rating standard. The guinea pig closed patch sensitization test results of the test group (induction: 25-hilltop chamber moist with saline; challenge: 1 square inch test article using a 25-mm hilltop chamber moist with saline) are shown in Table 24.4. The guinea pig closed patch sensitization test results of the control group (dosage: 1 square inch test article using a 25-mm hilltop

Table 24.3 Hemolytic index [36]

Group	Absorption			Average	Hemolysis index (%)
Test group	0.006	0.005	0.008	0.006	
Negative control group	0.005	0.003	0.002	0.003	0.35
Positive control group	0.870	0.850	0.884	0.868	

Table 24.4 Scoring criteria for skin reactions [36]

Erythema formation		Edema formation	
No erythema	0	No edema	0
Slight erythema	1	Slight edema	1
Well-defined erythema	2	Well-defined edema	2
Moderate erythema	3	Moderate edema	3
Severe erythema to slight eschar formation	4	Severe edema	4
Total possible erythema score = 4		Total possible edema score = 4	

Table 24.5 Scoring criteria for skin reactions (rabbit) [36]

Erythema formation		Edema formation	
No erythema	0	No edema	0
Very slight erythema (barely perceptible)	1	Very slight edema (barely perceptible)	1
Well-defined erythema	2	Slight edema (edges of area well defined by definite raising)	2
Moderate to serve erythema	3	Moderate edema (area raised approximately 1 mm)	3
Severe erythema (beet redness) to slight eschar formation	4	Severe edema (area raised more than 1 mm and extending beyond area of exposure)	4
Total possible erythema score = 4		Total possible edema score = 4	

chamber moist with saline) are given in Table 24.5. Based on the test results, the shape memory fabric was not considered a sensitizer in guinea pigs [36].

24.9 Dermal Irritation

The scoring criteria for skin reactions are shown in Table 24.5. The skin irritation summary of scores for skin irritation (dose = 25 × 25 mm^2 (moist with physiological saline)) is shown in Table 24.6. All sites were intact [36]. Based on the test results, according to ISO 10993-10, the test article was not considered a dermal irritant.

Table 24.6 Summary of skin irritation

Animal (Sex)	Initial weight (kg)	Site	Score*			
			5 h	24 h	48 h	72 h
1 (M)	2.01	T**	0/0	0/0	0/0	0/0
		T	0/0	0/0	0/0	0/0
		C***	0/0	0/0	0/0	0/0
2 (F)	2.05	T	0/0	0/0	0/0	0/0
		T	0/0	0/0	0/0	0/0
		C	0/0	0/0	0/0	0/0
		C	0/0	0/0	0/0	0/0
3 (M)	2.09	T	0/0	0/0	0/0	0/0
		T	0/0	0/0	0/0	0/0
		C	0/0	0/0	0/0	0/0
		C	0/0	0/0	0/0	0/0

*Scores—Erythema edema
**T—Test article site
***C—Control site

References

1. Gutowska A, Bae YH, Jacobs H, Feijen J, Kim SW (1994) Thermosensitive interpenetrating polymer network: synthesis, characterisation, and macromolecular release. Macromolecules 27:4167–4175
2. Asaka K, Oguro K (2000) Bending of polyelectrolyte membrane platinum composites by electric stimuli. J Electroanal Chem 480:186–198
3. Feil H, Bae YH, Feijen T, Kim SW (1992) Mutual influence of pH and temperature on the swelling of ionizable and thermosensitive hydrogels. Macromolecules 25:5228–30
4. Siegal RA, Firestone BA (1988) pH-dependent equilibrium swelling properties of hydrophobic polyelectrolyte copolymer gels. Macromolecules 21:3254–3259
5. Jiang HY, Kelch S, Lendlein A (2006) Polymers move in response to light. Adv Mater 18:1471–1475
6. Makhosaxana XP, Filipcsei G, Zrınyi M (2000) Preparation and responsive properties of magnetically soft poly(N-isopropylacrylamide) gels. Macromolecules 33:1716–1719
7. Volk BL, Lagoudas DC, Chen YC (2008) Thermomechanical characterization of the nonlinear, rate dependent response of shape memory polymers. In: Proceedings of SPIE—the international society for optical engineering, vol 6929, Behavior and mechanics of multifunctional and composite materials 2008, San Diego, CA, USA, p 69291B
8. Tobushi H, Hayashi S, Hoshio K, Miwa N (2006) Influence of strain-holding conditions on shape recovery and secondary-shape forming in polyurethane-shape memory polymer. Smart Mater Struct 15:1033–1038
9. Hu JL, Ji FL, Wong YW (2005) Dependency of the shape memory properties of a polyurethane upon thermomechanical cyclic conditions. Polym Int 54:600–605
10. Langer R, Tirrell DA (2004) Designing materials for biology and medicine. Nature 428:487–492
11. Laroche FEFG, Fiset M, Mantovani D (2002) Shape memory materials for biomedical applications. Adv Eng Mater 4:91–104
12. Sharp AA, Panchawagh HV, Ortega A, Artale R, Richardson-Burns S, Finch DS, Gall K, Mahajan RL, Restrepo D (2006) Toward a self-deploying shape memory polymer neuronal electrode. J Neural Eng 3:L23–L30

13. Maitland DJ, Metzger MF, Schumann D, Lee A, Wilson TS (2002) Photothermal properties of shape memory polymer micro-actuators for treating stroke. Lasers Surg Med 30:1–11
14. Small W IV, Wilson TS, Benett WJ, Loge JM, Maitland DJ (2005) Laser-activated shape memory polymer intravascular thrombectomy device. Opt Express 13:8204–8213
15. Small W IV, Metzger MF, Wilson TS, Maitland DJ (2005) Laser-activated shape memory polymer microactuator for thrombus removal following ischemic stroke: preliminary in vitro analysis. IEEE J Sel Topics Quantum Electron 11:892–901
16. Schmidt AM (2006) Electromagnetic activation of shape memory polymer networks containing magnetic nanoparticles. Macromol Rapid Commun 27:1168–1172
17. Hampikian JM, Heaton BC, Tong FC, Zhang Z, Wong CP (2006) Mechanical and radiographic properties of a shape memory polymer composite for intracranial aneurysm coils. Mater Sci Eng C 26:1373–1379
18. Smart surgery future materials (through textile technology index) (2004) (News in Bref). (Brief Article), 1:33–34
19. Lendlein A, Langer R (2002) Biodegradable. Elastic Shape- Memory Polymers for Potential Biomedical Applications, Science 96:1673–1676
20. Langer RS, Lendlein A (2003) Biodegradable shape memory polymeric sutures. World Patent WO 2003088818:A2
21. Marco D, Eckhouse S (2000) Biodegradable self-inflating intragastric implants for curbing appetite, US Patent 20070156248, USA
22. Huang WM, Lee CW, Teo HP (2006) Thermomechanical behavior of a polyurethane shape memory polymer foam. J Intel Mat Syst Struct 17:753–760
23. Wache HM, Tartakowska DJ, Hentrich A, Wagner MH (2004) Development of a polymer stent with shape memory effect as a drug delivery system. J Mater Sci Mater Med 14:109–112
24. Yasuo S (1998) Shape-memory, biodegradable and absorbable material, US Patent, 19980189973
25. Mather PT, Liu C, Burstone CJ (2005) Shape memory polymer orthodontic appliances, and methods of making and using the same, european patent EP1844097. World Patent 2006071520:2006
26. Liu C, Mather PT, Burstone C (2006) In: Proceedings of the annual technical conference—society of plastics engineers, 64th, society of plastics engineers, Brookfield, CT, USA, pp 1356–1360
27. Zhu Y, Hu JL, Yeung LY, Lu J, Meng QH, Chen SJ, Yeung KW (2007) Effect of steaming on shape memory polyurethane fibers with various hard segment contents. Smart Mater Struct 16:969–981
28. Zhu Y, Hu JL, Yeung LY, Liu Y, Ji FL, Yeung KW (2006) Development of shape memory polyurethane fiber with complete shape recoverability. Smart Mater Struct 15:1385–1394
29. Meng QH, Hu JL, Zhu Y, Lu J, Liu Y (2007) Morphology, phase separation, thermal and mechanical property differences of shape memory fibres prepared by different spinning methods. Smart Mater Struct 16:1192–1197
30. Ji FL, Zhu Y, Hu JL, Liu Y, Yeung LY, Ye GD (2006) Smart polymer fibers with shape memory effect. Smart Mater Struct 15:1547–1554
31. Meng QH, Hu JL (2008) Study on poly(ε-caprolactone)-based shape memory copolymer fiber prepared by bulk polymerization and melt spinning. Polym Adv Technol 19:131–136
32. Tang SLP, Stylios GK (2006) An overview of smart technologies for clothing design and engineering. Int J Clothing Sci Technol 18:108–128
33. Liu Y, Chung A, Hu JL, Lu J (2007) Shape memory behavior of SMPU knitted fabric. J Zhejiang Univ Sci A 8:830–834
34. Tao XM (2001) Smart fibres, fabrics and clothing, vol 3. Woodhead Publishing Limited, Cambridge
35. Mattila HR (2006) Intelligent Textiles and Clothing, vol 3. Woodhead Publishing Limited, Cambridge
36. Meng Qinghao, Jinlian Hu, Zhu Yong (2009) Jing Lu and Baohua Liu biological evaluations of a smart shape memory fabric. Text Res J 79(16):1522–1533

Chapter 25
Chitosan-based Viscose Material in Gynecological Treatment

25.1 Introduction

During the recent years, cellulosic fibers have been used in the development of medical textile products, as proved by the literature available [1–8]. Owing to their active surface area, strength, and molecular structure, cellulosic fibers exhibit enormous possibilities in the design of bioactive, biocompatible, and advanced materials [9]. One such area of application could be cellulose tampons which are used by women and have biodegradable and antimicrobial properties. It protects from physiological and pathological vaginal discharge, which could otherwise increase the vaginal pH beyond the desirable limit of 3.6–4.5 [10]. An increase in pH may cause a reduction in the natural defense of the vagina. This suggests conduciveness for development of bacteria [11] and hence prone to infection of bladder [12]. A number of techniques and formulations have been evolved in order to manage the problem of increased pH value of the vagina, than the normal [13]. But these have been unsatisfactory from the practical point of view considering the usage and acceptability. Therefore, the development of materials for prevention and treatment of gynecological infections still represent a significant challenge. Chitosan is the next most abundant polysaccharide found on earth, in comparison with cellulose. It is a biopolymer that is polycationic and covers a broad spectrum of medical properties activity, such as antibacterial, antifungal, and hemostatic properties [14–18]. Chitosan possesses many desirable characteristics, with regard to vaginal infections

(a) It is effective against yeast *Candida albicans*, which is the etiological agent causing vaginal candidiasis most frequently [19]
(b) It is effective against *Staphylococcus aureus*, which is the etiological agent causing toxic shock syndrome most frequently [20]

N. Gokarneshan et al., *Emerging Research Trends in Medical Textiles*,
Textile Science and Clothing Technology, DOI 10.1007/978-981-287-508-2_25

(c) It is effective in pharmaceutical applications as a drug delivery system, such as in the case of treatment for ovarian cancer [21], and
(d) As it has no harmful effect, it can be safely used during pregnancy, since it helps to maintain a healthy vaginal environment conducive for avoiding premature childbirth [22].

Hence, chitosan is highly suitable for adsorption onto cellulose fibers and thereby impart antimicrobial activity. This chapter highlights the functionalization of viscose cellulose using chitosan. The objective is to assess the potential use of such a material for the development of new tampons, which apart from maintaining/creating the desired physiological pH value, would also possess antibacterial and antimycotic properties. The tampons do not exhibit negative effects, such as inflammation risks, and infections from yeasts, and on repeated use, help to sustain the required moisture in the vagina.

25.2 Technical Aspects of Tampons

Table 25.1 shows the mass of the tampons, absorbency, and vertical pressure stability. The results are the mean values of five separate measurements. The mass of the tampons increased slightly with the spraying of chitosan–lactic acid and chitosan–acetic acid. However, the increase is almost within standard deviations of the measurements. The chitosan–lactic acid formulation shows a higher increase in absorbency ranging between 16 and 26 %, when compared with the chitosan–acetic acid formulation(14 and 0 %), without considering the drying techniques [23]. Both acetic and lactic acid are highly hygroscopic; acetic acid melts at about 16 °C and lactic acid at 53 °C, and hence, the increased absorbency for functionalized, air-dried tampons was expected. The lower values of absorbency for both samples was due to the drying in the air chamber; for the sample treated by chitosan–lactic acid formulation by around 10 %, meanwhile the chitosan–acetic acid sample dried in air had a lower absorbency than the one dried in the chamber. The capacity of absorption did not exhibit change when compared with the reference sample as observed with the formulation of chitosan–acetic acid dried in air. The reason for this is that acetic acid is liquid at room temperature, so one would expect it to evaporate more easily than lactic acid during drying. Hence, the hygroscopicity of functionalized

Table 25.1 Technical factors of untreated tampons and tampons containing 1 % chitosan [23]

Notation	Mass of tampon	Absorbency	Vertical pressure stability
A	3.2 ± 0.3	11.2 ± 0.1	32.0 ± 1.5
B	3.5 ± 0.1	13.0 ± 0.2	44.0 ± 1.2
C	3.7 ± 0.4	14.2 ± 0.3	49.0 ± 1.8
D	3.5 ± 0.2	12.8 ± 0.2	37.0 ± 0.9
E	3.3 ± 0.1	11.2 ± 0.05	32.0 ± 1.4

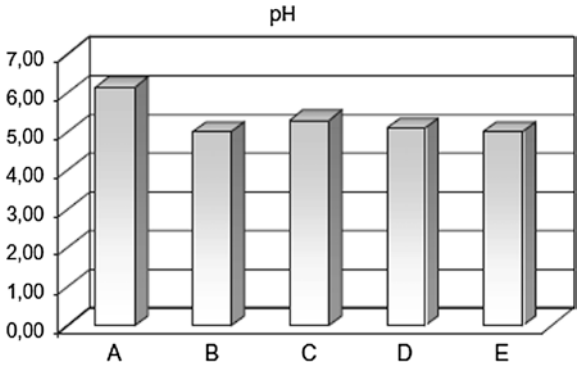

Fig. 25.1 pH of tampons' aqueous extract [23]

dry tampons possibly decreases due to the acid evaporation. This was more pronounced in the case of chitosan–acetic acid tampons (sample D). The formulation of chitosan–lactic acid combined with air-drying gave the highest increase in absorbency. Treatment with chitosan/lactic acid (samples B and C) considerably increased the tampon vertical pressure stability (from 32, to 44 and 49 N, respectively, higher). After treatment with chitosan–acetic acid, the tampon vertical pressure stability was approximately at the same level as for the referenced tampon. This can again result from the evaporation of acetic acid. Another possibility is intermolecular interactions between cellulose and chitosan/lactic acid. The hydroxyl groups in chitosan lactates can form hydrogen bonds with the hydroxyl groups of cellulose leading to improvement in mechanical properties (higher stiffness), such as improved stability of the final material. One of the most important parameters of the tampon is the pH of its aqueous extract. Earlier research has pointed out that lactic (US patents 2005/0124799, 6656913, and 7056891), citric, and acetic acid incorporated into natural fiber strips are released from their surfaces and adjust the pH to a physiological acidic value. The pH values of the distilled water extract after immersion of the tampons are presented in Fig. 25.1. The findings reveal that treatment with chitosan–lactic acid or chitosan–acetic acid effectively reduces the pH value of water in contact with the tampons. This indicates a potential ability to maintain the pH value at the optimal physiological pH value in the vagina. The technical factors measured for the functionalized tampons fall within the limits of product standards, as defined within this special field, and in accordance with the European Pharmacopy.

25.3 Adsorption of Chitosan

25.3.1 Amino Group Amount

The critical molecular properties which control the antimicrobial activity of chitosan are the quantity and location of amino groups. The amino groups of chitosan are protonated and permit the growth inhibition of different bacteria

(Gram-negative and Gram-positive) under acidic medium. The antibacterial activity of chitosan has been explained by two mechanisms, which stress upon the necessity of the amount of active amino groups [23]. In one mechanism, the polycationic nature of chitosan interferes with the bacterial metabolism by stacking on the cell's surface. The other mechanism is the binding of chitosan with deoxyribonucleic acid (DNA) to inhibit messenger ribonucleic acid (mRNA) synthesis. Hence, it is necessary to measure the number of functional groups that influence the antimicrobial property of the material. The amounts of amino groups in different samples (tampons) determined by conductometric titration and conventional Kjeldahl analysis are shown in Table 25.2. The coefficient of variation (CV) of the amount of amino groups determined by conduct metric titration was less than 2 % for all samples. Both techniques confirm that amino groups were introduced into the viscose material by spraying with chitosan. The amino groups increased with higher chitosan concentration and have been independent of the method of drying the tampons.

Initial research has revealed (see Table 25.2) that viscose fibers treated by 0.5 % chitosan solution in lactic acid and dried in an air chamber contain 20 % less amino groups than the same fibers treated by 0.8 % of chitosan solution. An increase in the concentration of chitosan in solution to 1 % caused increase in the fiber amino group content to about 40 % in sample B in comparison with the same sample impregnated by 0.8 % chitosan solution and even more than 80 % when this sample was impregnated by 0.5 % chitosan solution. More amino groups were detected on viscose material functionalized with chitosan dissolved in acetic acid solution (around 2 mmol/kg fiber higher than for lactic acid). It seems justifiable that the conformation of the chitosan was more expanded in the lactic acid than in the acetic acid solutions. Lactic acid is the stronger acid (lactic acid p*Ka* 3.86 at 25 °C; acetic acid p*Ka* 4.76 at 25 °C), and thus, less lactic acid than acetic acid is needed to reach pH 3.6. Further, the ionic strength was lower at pH 3.6; the chitosan was more expanded and thus formed a thinner layer on the fiber surface when adsorbed. Therefore, less chitosan adsorbed from lactic than from acetic acid solutions. The results from Kjeldahl analysis (total nitrogen content in percentage) indicate similar trends as those obtained by conductometric titration.

Table 25.2 Amino groups in untreated viscose fibers and also fibers with 1 % chitosan [23]

Notation	Conductometric titration (NH_2) (mmol/kg fibers)	Kjeldahl method total nitrogen content (N_2) (%)
A	0.5	0
B	14.80	15
C	14.18	13
D	16.12	20
E	16.52	21
B (0.5 % chitosan solution)	8.21	
B (0.8 % chitosan solution)	10.55	

25.3.2 *In Vitro Growth Inhibition of Various Microorganisms by Chitosan-Treated Tampons*

The antimicrobial properties of the samples have been tested. They have been measured within two weeks of sample preparation. The antimicrobial characteristics have been tested for control samples sprayed with acetic and lactic acids only. The results show that these acids alone did not provide the tampons with antimicrobial properties. Inhibition of microorganisms was in both cases less than 67 %. The antimicrobial activity against the microorganisms of tampons air-dried and treated by chitosan–lactic acid solution increased with increasing amount of amino groups in the fibers. Among all samples, the best results were obtained with tampons sprayed by 1 % chitosan in lactic acid and dried in the air chamber (tampon B). These were active against all microorganisms and inhibited growth of all of them, except *S. aureus* and *Escherichia coli* by 100 %. The inhibition has been 75 % in the case of *S. aureus* and 27 % in the case of *E. coli*, which was very slightly or not at all inhibited by other tampons. Investigation has not been possible at higher concentrations of chitosan since the solution viscosities were too high to permit spraying. In the case of lactic acid, the decrease has been greater than with case of acetic acid. The lactic acid appears to contribute better to the in vitro growth inhibition of different microorganisms as compared with acetic acid. But, both control samples have been considered ineffective as antimicrobial material. With tampon C, the same formulation was used (chitosan–lactic acid) as in tampon B, but drying was performed in an open-air atmosphere. The antimicrobial activity of tampon C was also good; all tested microorganisms were reduced, but not to the same extent as with tampon B (see Table 25.3).

The antibacterial activity of tampons D and E was substantially lower and they even stimulated growth of the fungi [*C. albicans* (–20 %) and *Candida glabrata* (−88 %)]. Obviously, the combination chitosan–lactic acid formulation is more appropriate for reduction of microorganisms than chitosan–acetic acid. Comparison of lactic and acetic acids shows that acetic acid is a much milder antibacterial organic agent. Air-dried tampons were apparently somehow contaminated by exposure to the air atmosphere, which stimulated the growth of microorganisms or even caused microbiological or chemical degradation of the chitosan. The moisture content of air-dried tampons was actually still 37–40 % (determined by halogen dryer). Hence, microbiological contamination of them during storage can be expected. It has been shown that any decrease in the molecular weight of chitosan increases antimicrobial activity, but this increase is limited to certain molecular weights only, 26 below which activity declines. Tampon E stimulated growth of fungi and showed no antimicrobial activity against *S. aureus* or *E. coli*. Sample D, prepared with identical formulation (chitosanacetic acid) as tampon E, exhibited much better results. It would appear that the phenomenon could be attributed to the drying procedure which resulted in the drying of the tampon within a few hours. The growth of the microbes has been limited in this case. On the hand, the tampons dried in air were wet and exposed to the air for more than

Table 25.3 Antimicrobial properties of the untreated and treated viscose tampons [23]

Notation	Negative control	*Staphylococcus aureus* (%)	*E. coli* (%)	*Streptococcus agalactiae* (%)	*Candida albicans* (%)	*Candida glabrata* (%)
A	Sterile	17	0	70	28	0
B	Sterile	79	27	100	100	100
C	Sterile	7	13	100	45	100
D	Sterile	0	0	36	17	3
E	Sterile	0	0	65	−20	−88
Control samples lactic acid, air-dried	Sterile	40	30	25	67	50
Control samples acetic acid, air-dried	Sterile	8	2	3	33	44
B (0.5 %) chitosan solution	Sterile	70	0	100	0	98
B (0.8 %) chitosan solution	Sterile	73	0	100	65	98

30 h e prior to drying. The investigation confirms that both lactic and acetic acid can be used to render the fiber samples capable of adjusting pH to physiological level, and also that only chitosan enables antimicrobial activity of the viscose material, whether when sprayed by chitosan–lactic acid or chitosan–acetic acid.

25.4 Suitability of Chitosan-Acid Treated Tampons for Gynecological Use

The tampons developed during this research proved better than existing ones, which only maintain the physiological pH value. Viscose fibers coated by chitosan dissolved in acetic or lactic acids both inhibit the growth of microorganisms and adjust the pH [23]. The optimum level of antimicrobial activity has been reached when a chitosan–lactic acid mixture was used in combination with drying in the air chamber. The growth of the various microorganisms tested has been inhibited. The antibacterial activity of sample B has been evaluated for various types of microorganisms and ranged between 79 and 100 %, except for Gram-negative *E. coli*, which was reduced by only 27 %. When theoretically considered, the use of these tampons can reduce the possibility of repeated vaginal infections caused by yeasts, particularly, *C. glabrata*, which is very resistant to clinical treatment. During antibiotic treatment, women often experience vaginal discharge, mostly caused by *C. albicans*. Hence, the preventive use of tampons would be assured in these patients. The use of such tampons could prove beneficial for pregnant women, as (in vitro) trials have confirmed resistance of the tampons against *Streptococcus agalactiae* bacteria, which pose serious problems for pregnant women and their infants.

References

1. Edward JV, Buschle-Diller G, Goheen SC (2006) Modified fibres with medical and specialty applications. Springer, Berlin
2. Browning BL (1967) Methods of wood chemistry. Interscience Publisher, New York
3. Kaputskii FN, Gert EV, Torgashov VI, Zubets OV (2006) Combination of oxidative and hydrolytic functions of nitric acid in production of enterosorbents based on carboxylated microcrystalline cellulose. Fibre Chem 37:417–504
4. Kotel'nikova NE, Wegener G, Paakkari T, Serimaa R, Demidov VN, Serebriakov AS et al (2003) Silver intercalation into cellulose matrix. An X-ray scattering, solid state 13C NMR, IR, X-ray photoelectron, and Raman study. Russ J Gen Chem 73:418–426
5. Czaja W, Krystynowicz A, Bielecki S, Brown RM (2006) Microbial cellulose—the natural power to heal wounds. J Biomater 27:145–151
6. Hoenich N (2006) Cellulose for medical applications: past, present, and future. BioResources 1:270–280
7. Ravi Kumar MNV (2000) A review of chitin and chitosan applications. React Funct Polym 46:1–27

8. Lim SH, Hudson SM (2004) Synthesis and antimicrobial activity of a water-soluble chitosan derivative with a fiber-reactive group. Carbohydr Res 339:313–319
9. Bliss SJ, Manning SD, Tallman P, Baker CJ, Pearlman MD, Marrs CF et al (2002) Group B. Streptococcus colonization in male and non-pregnant female university students: a cross-sectional prevalence study. Clin Infect Dis 34:184–190
10. Boskey ER, Telsch KM, Whaley KJ, Moench TR, Cone RA (1999) Acid production by vaginal flora in vitro is consistent with the rate and extent of vaginal acidification. Infect Immun 67:5170–5175
11. Tomas MS, Bru E, Nader-Macias ME (2003) Comparison of the growth and hydrogen peroxide production by vaginal probiotic lactobacilli under different culture conditions. Am J Obstet Gynecol 188:35–44
12. Perrotta C, Aznar M, Mejia R, Albert X, Ng CW (2008) Oestrogens for preventing recurrent urinary tract infection in postmenopausal women. Cochrane Database Syst Rev 16:CD005131
13. Eriksson K, Carlsson B, Forsum U, Larsson PG (2005) A double-blind treatment study of bacterial vaginosis with normal vaginal lactobacilli after an open treatment with vaginal clindamycin ovules. Acta Derm Venereol 85:42–46
14. Chung YS, Lee KK, Kim JW (1998) Durable press and antimicrobial finishing of cotton fabrics with a citric acid and chitosan treatment. Text Res J 68:722–755
15. Liu J, Wang Q, Wang A (2007) Synthesis and characterization of chitosan-g-poly (acrylic acid)/sodium humate superabsorbent. Carbohydr Polym 70:166–173
16. Zitao Z, Cheng L, Jinmin J, Yanliu H, Donghui C (2003) Antibacterial properties of cotton fabrics treated with chitosan. Text Res J 73:1103–1106
17. Urreaga M, de la Orden MU (2006) Chemical interactions and yellowing in chitosan-treated cellulose. Eur Polym J 42:2606–2616
18. Yang Q, Dou F, Borun L, Shen Q (2005) Studies of cross linking reaction on chitosan fiber with glyoxal. Carbohydr Polym 59:205–210
19. Calamari S, Bojanich A, Barembaum S, Azcurra A, Virga C, Dorronsoro S (2004) High molecular weight chitosan and sodium alginate effect on secretory acid proteinase of *Candida albicans*. Rev Iberoam Micol 21:206–208
20. Yang TC, Chou CC, Li CF (2005) Antibacterial activity of N-alkylated disaccharide chitosan derivatives. Int J Food Microbiol 97:237–245
21. Berrada M, Serreqi A, Dabbarh F, Owusu A, Gupta A, Lenhert S (2005) A novel non toxic camptothecin formulation for cancer therapy. Biomaterials 26:2115–2120
22. Hirnle L, Heimrath J, Woyton J, Klosek A, Hirnle G, Malolepsza-Jarmolowska K (2001) Application of 2 % clindamycin cream in the treatment of bacterial vaginosis and valuation of methylcellulose gel containing the complex of Chitosan F and PVP k-90 with lactic acid as carrier for intravaginally adhbited medicines in the cases of pregnancies with the symptoms of preterm delivery. Ginekol Pol 72:1096–1100
23. Fras Zemljic L, Sauperl O, But I, Zabret A, Lusicky M (2011) Viscose material functionalized by chitosan as a potential treatment in gynecology Lidija. Text Res J 81(11):1183–1190

Chapter 26
Polymer Braided Tubular Structures for Medical Applications

26.1 Introduction

Tubular structures are generally manufactured by the braiding technique. They find multivaried applications, such as medical textiles, composites, sporting goods, and mechanical and civil engineering parts. The braided structures used in medical application are known as stents, which are used in the cylindrical surfaces of the body. They are made of either plastic or metal materials. They are self-expanding and implantable and are used to repair blood vessels affected by disease [1]. The geometrical relationships between the variables in the case of metal stent have been established [2]. Even though the metal stents are biocompatible, the ratio of self-expansion to the initial diameter is very limited. Therefore, polymeric materials may be preferred, which also have good long-term stability inside the body. The properties of materials used directly affect the behavior of the braided tubular fabrics. The feasibility of producing an ideal tubular braiding structure from polymeric materials suitable in medical applications has been investigated. Polyester has been found suitable owing to its biocompatibility and long-term stability [3]. Despite the fact that braiding is a conventional technique, little literature is available on it [4, 5]. Though braided fabrics have limited applications in traditional textiles compared to woven and knitted structures, it enjoys wider applications in technical and industrial applications, particularly textile composites and aircraft parts. The mechanical properties and basic model of the braided fabric structures have been well researched. In one of the works, a mechanical model of the braided fabrics has been provided by means of a repeated unit cell. A geometrical definition of a unit cell has been developed and the model has been used to predict the mechanical behavior of the braided fabrics [4]. In yet another interesting work, the crimp effects and the calculation of braid geometry have been studied [5], wherein the effects of the mandrel diameter on the geometry of the model have not been included. A subsequent work investigated the effects of mandrel diameter in fabric

N. Gokarneshan et al., *Emerging Research Trends in Medical Textiles*,
Textile Science and Clothing Technology, DOI 10.1007/978-981-287-508-2_26

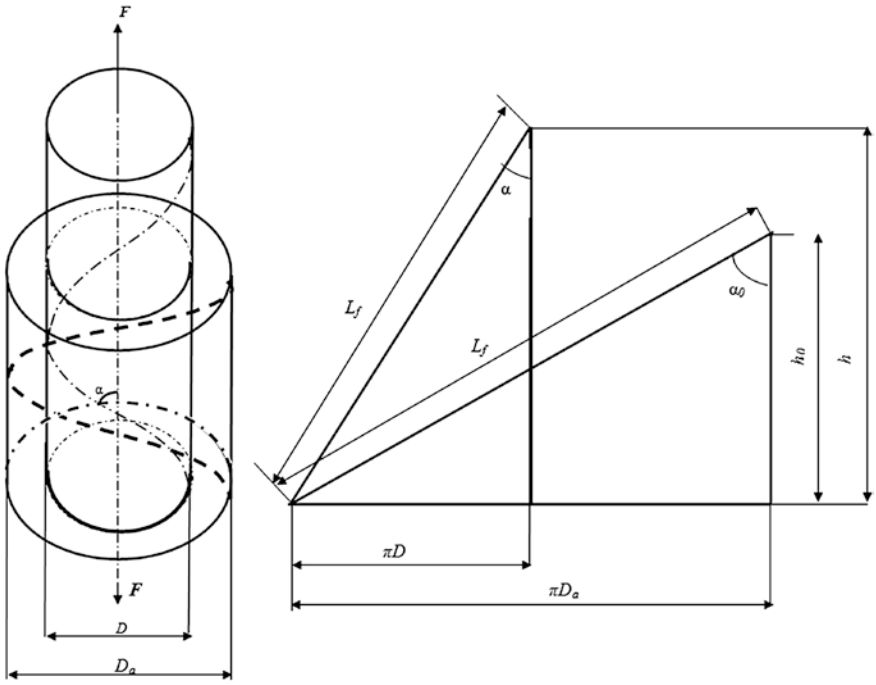

Fig. 26.1 Braided tube geometry before and after axial load application [8]

braiding [6]. The maximum crimp is found to be at a braiding angle of 45°, at which the helical angle is at its maximum level [7]. The geometry of braided fabric is characterized by many variables, including yarn bending stiffness. In this chapter, the radial force of the braided tube is considered in relation to the diameter of the monofilament yarns. The relationships between the braid angle, helical length, braid diameter, and elastic force have been developed. In order to be used as stents, braided tubular stents should have a high elastic radial force. Upon application of axial tensile force/radial compressive force, the stent extends in axial direction and its diameter gets reduced as shown in Figs. 26.1 and 26.2. On withdrawing the applied force, an axial tensile force acts opposite to the initial tensile force balances the force, accompanied radial expansion of the stent.

26.2 Geometry of Braided Stent

Due attention has to be given in the design of stent, so as to achieve satisfactory performance from a tubular-graded structure [8]. Hence, the analysis of the tubular braided geometric structures becomes essential. The expansion of the tubular structure generates outward radial forces. The diameter of the mandrel and the yarn are related to the initial average and external tube diameter (Fig. 26.3):

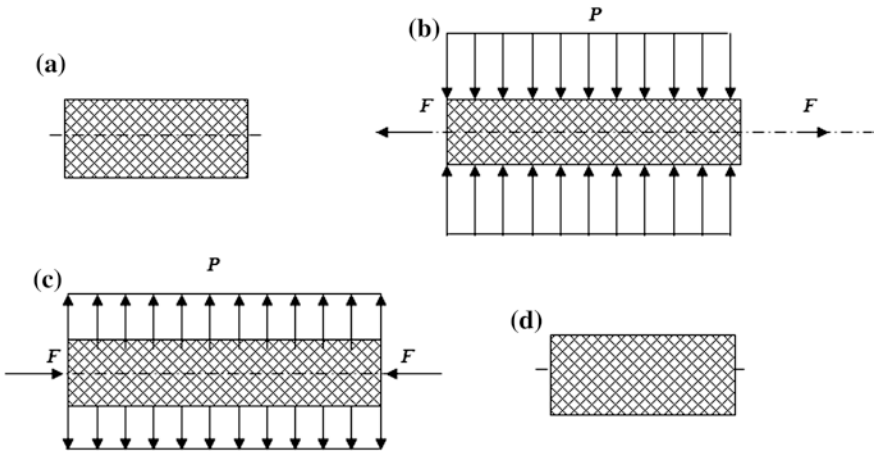

Fig. 26.2 Changes in stent structure under influence of forces [8]. **a** Initial condition—forces balanced. **b** F axial force and P axial extension, radial contraction. **c** Removal of axial force. **d** Force balance restabilized

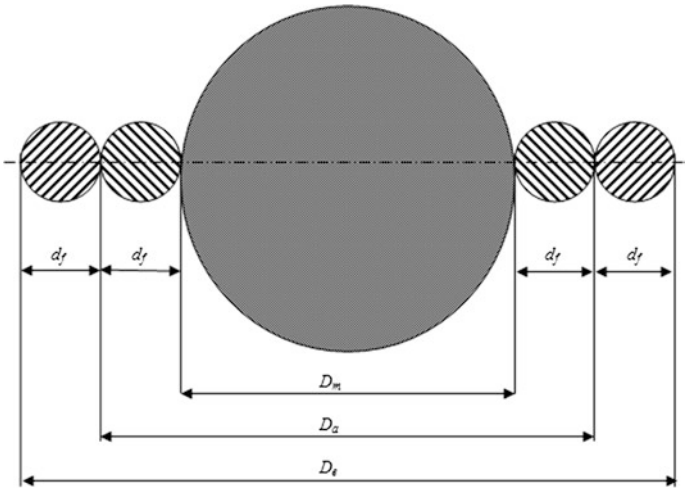

Fig. 26.3 Mandrel and yarns shown cross-sectionally [8]

$$D_a = D_m + 2d_f = D_e - 2d_f$$

where D_a is the average stent diameter, D_m is the mandrel diameter, D_e is the maximum external diameter representing the outer border of the stent, and d_f is the filament diameter. The initial length of a filament twist can be obtained as

$$h_o = \frac{\pi D_a}{\tan \alpha_0}$$

where α_o is the initial braid angle. Then, the number of coils, n_c, in the braided tube is obtained as

$$n_c = \frac{h_s}{h_o}$$

where h_s is the total length of the braided stent. The length of one filament per turn, L_f, which is defined as 'coil length,' is equal to

$$L_f = \frac{\pi D_a}{\sin \alpha_o}$$

where D and α are the new stent diameter and braid angle, respectively. When subjected to an axial load, F, the length of the braided tube increases as its diameter reduces. Coil length does not change before and after applying load F. This assumption is applicable provided there is no extension in the filament length under the force applied. Hence, the new stent diameter is

$$D = D_a \frac{\sin \alpha}{\sin \alpha_o}$$

The extension of the stent length, Δh, is calculated as

$$\Delta h = \frac{\pi D_a (\cos \alpha - \cos \alpha_o)}{\sin \alpha_o}$$

and the length of one twist after applying the load becomes

$$h = h_o + \Delta h$$

The total stent length after application of the force, F, is

$$H_s = n_c (h + \Delta h)$$

The total filament length, L_t, employed in the stent can be calculated as

$$L_t = n_c n_f L_f$$

where n_f is the number of filaments. The braided tube surface area is πDL. Although the enclosed area of the structure is normally defined as the product of total filament length and filament diameter, the cover is reduced by the area of each intersection. The shape of the intersection takes a diamond form, and the area of this intersection is

$$A_i = \frac{d 2_f}{\sin 2\alpha}$$

The calculation for number of intersections, N_i, in a given braided tube is made by dividing the stent into transverse slices such that each slice contains $n_f/2$ intersections. From above equation, the total area of the intersection becomes.

$$A_{total} = \frac{N_i d_f 2}{\sin(2\alpha)}$$

26.3 Mechanical Properties of the Braided Tube

A braided tubular structure could be visualized as an open coiled helical spring having freely rotating ends [8]. In this case, the following equation was derived to determine the axial load, F, on a braided tube [2, 9, 10]:

$$F = 2n_{\mathrm{f}}\left[\frac{GI_{\mathrm{p}}\sin\alpha}{C_3}\left(\frac{2\cos\alpha}{C_3} - C_1\right) - \frac{EI}{\tan\alpha C_3}\left(\frac{2\sin\alpha}{C_3} - C_2\right)\right]$$

$$C_1 = \frac{\cos(2\alpha_o)}{D_\alpha}, \quad C_2 = \frac{2\sin^2(\alpha_{\mathrm{o}})}{D_\alpha}, \quad \text{and} \quad C_3 = \frac{D_\alpha}{\sin(\alpha_o)}$$

where C_1, C_2, and C_3 are constants depending on the initial average braided diameter, D_{a}, and braid angle, α_{o}.

I and I_{p} are the moment and polar moment of inertia of the fiber, respectively.

G is the modulus of rigidity and E is the modulus of elasticity of braided tubes.

The bending rigidity of fibers is influenced by radial load of the braided tube. When a load, F, is applied to a braided tube, the fabric diameter reduces, while its length increases. A specific amount of energy dW should be applied to the braided tube in order to stretch the length of a braided tube by an incremental value, dh. The same amount of dimensional rearrangement occurs with a radial pressure, P, at a diameter change, dD. The integrals of both longitudinal and radial change yield the amount of energy required for the dimensional changes. This situation can be simply demonstrated as

$$\mathrm{d}W = \int_{L_{\mathrm{o}}}^{L} F\mathrm{d}h$$

$$\mathrm{d}W = \int_{D_\alpha}^{D} P\mathrm{d}h$$

The deflection, dh, is the result of the radial pressure, P, applied to an idealized wall of the braided fabric tube. When an axial tensile or a radial compressive force acts on the braided tube, the length of the tube increases as the value of the tensile force or radial pressure increases. The diameter reduces as the braiding angle, α, reduces. The four cases are depicted Fig. 26.2 as given below:

- first case: during the initial condition, the braided tube is stable, and the total force acting on the tube is nil.
- second case: the tensile force, F, or radial pressure, P, acts on the structure. The diameter of the structure reduces and the length increases under the influence of the forces.
- third case: the structure tends to regain its original position, owing to the stored energy during release of the braided tube.
- forth case: it is a final stage in which the diameter increases with the decrease in length till restabilizes as in the preliminary state. For a braided fabric compressed by a radial amount of dD/2, from above equations may be rewritten as

$$\mathrm{d}W = \frac{P\pi DL\mathrm{d}D}{2}$$

Then, the radial pressure, P, is given by

$$P = -\frac{2Fn_{\mathrm{c}}}{DL}\tan\alpha$$

The radial stiffness of the structure affects the radial force. The radial stiffness is determined by a number of parameters that include the number of filaments used in the braided tube, the tube diameter, and the braid angle. The value of the radial stiffness is influenced by the modulus of the fiber.

26.4 Description of Materials Used

Two different diameters of polyester monofilament yarns were used to make tubular braided structures. The properties of the monofilament yarns have been evaluated. The tubular braided structures were produced by using 16- and 32-head braiding machines. It was necessary to use a cylindrical core, called a 'mandrel,' during manufacturing of the braided tubular samples. There were four different mandrel diameters used in this work. The mechanical and geometrical properties of the braided tubes produced have been measured. It was assumed that the braid tube retains constant volume when subjected to a load; therefore, the value of the rigidity modulus is only one-third of its modulus because the Poisson's ratio is 0.5 for constant volume deformation.

Due to the high stiffness of the polyester filament yarns, it was necessary to apply heat-set to the samples produced. The heat-setting operations are mainly used to remove the internal stresses in the fabric and obtain a more stable and predictable geometrical structure. Three different heat-setting temperatures and heat-setting times were used in the experiment with a laboratory-type oven that was able to heat the specimens up to 450 °C. The heat-setting temperatures were set to 175, 200, and 225 °C and the heat-setting time was 10, 20, and 30 min for each temperature level. In total, three replicates were produced for each level of combinations. Figure 26.4 shows some tubular braided structures that were manufactured in this study.

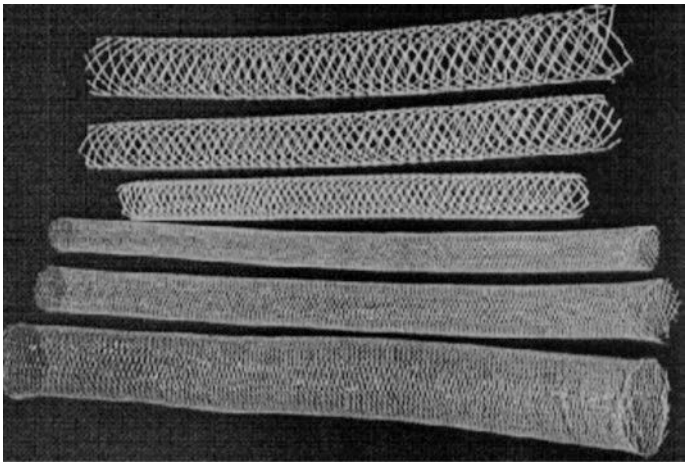

Fig. 26.4 Experimentally produced braided tubular structures [8]

26.5 Results of Findings

The axial tensile force is plotted as a function of the filament extension for diameters of 0.3 and 0.9 mm (Fig. 26.5).

The axial tensile force increases with the length of the stent [8]. At longer stent length, the curves get steeper since greater force is required to overcome the structural resistance to extension. In other words, the longitudinal stiffness of the stent increases as the stent is stretched further. The experimental values match well with

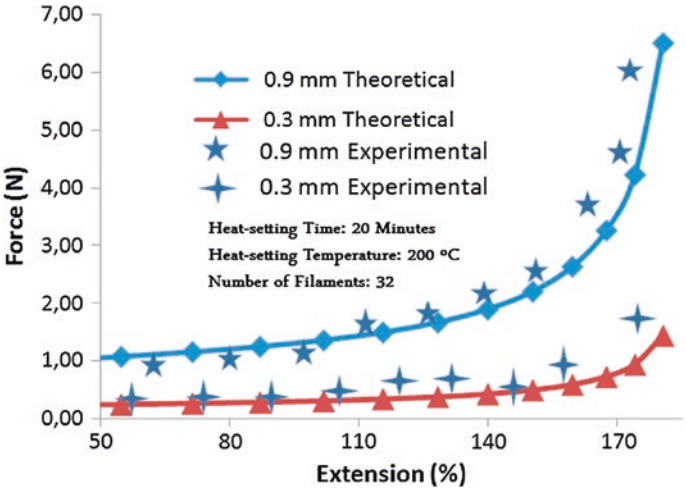

Fig. 26.5 *Curves* depicting axial tensile force and stent length extension [8]

the theoretically predicted values. The extent of the radial pressure exerted by the stent as a function of stent diameter is shown in Fig. 26.6.

The radial pressure increases with decrease in stent diameter. The agreement between experimental and theoretical data is also satisfactory for the radial pressure, as in the axial tensile force. Considering that the stent volume remains fixed, an increase in the length of the stent reduces the diameter of the stent. The cover factor of a stent becomes crucial for providing a good support to the walls of the vein. Braided structures are most open type of structures compared to other types of fabric structures. The experimental and theoretical percentage of fabric cover as a function of the stent diameter is shown in Fig. 26.7.

As can be seen from the Fig. 26.8, there is a point in each curve where the area covered by the yarns is at the minimum level. This level corresponds to the case where the yarns on the braided fabric intersect each other at or close to 90°. As the braid angle deviates from 90°, the stent diameter increases or decreases,

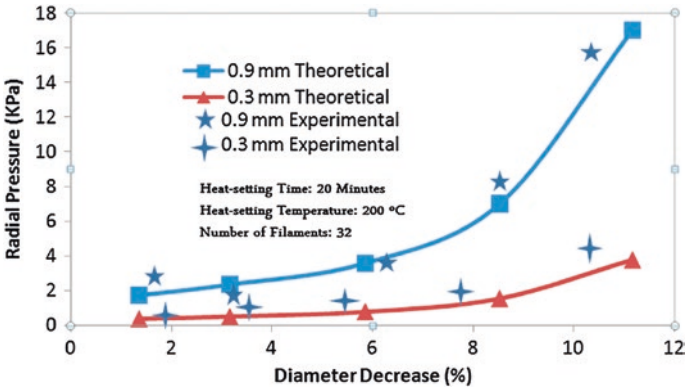

Fig. 26.6 *Curves* depicting radial pressure and changes in stent diameter [8]

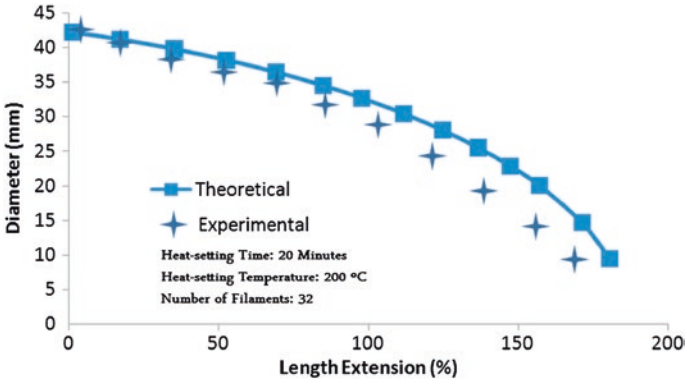

Fig. 26.7 *Curve* depicting change in stent diameter with elongation [8]

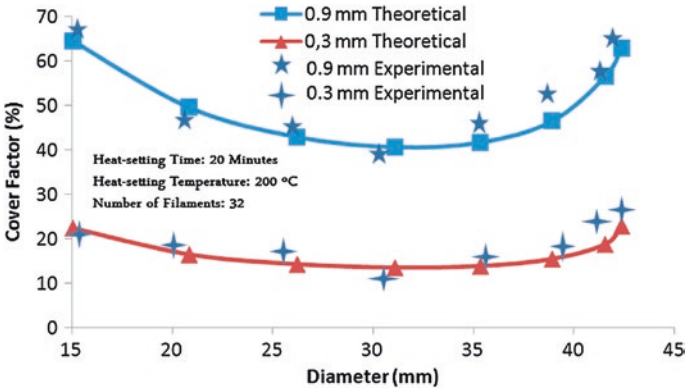

Fig. 26.8 *Curves* showing influence of stent diameter on cover factor [8]

depending on the loading conditions. The extremes of these two cases are called 'jamming' conditions, wherein the cover factor is at a maximum. Higher fabric covers are achieved at greater filament diameters.

The results show that the radial pressure and tensile force depend on the diameter of the braided tube and the number of filaments used in that fabric. The axial load and the radial pressure increase as the number of filaments increase in a braided tube. The tensile force increases sharply from the diameter 22.3 to 33.4 mm. However, this increase is very small, from 33.4 to 42.9 mm, due to the fact that the percentage of diameter increase is smaller. In order to analyze the mean differences of the tensile and the compression force of the tubular braided structures, ANOVA tests were conducted. The ANOVA analysis of the tensile strength and the compression tests have been done. The heat-setting temperature and heat-setting time did not show a significant effect on the tensile or compression force in the ranges that were used. The reason heat-setting did not make a big difference in the braided tubular structures in the present work could be because the heat-setting levels were above the critical temperatures. The tubular structures are openend loose structures; therefore, the fabric cover factor is very low. As a result, the structures respond to the tensile and compressive forces by undergoing a purely geometrical deformation rather than showing a ructural or material resistance. Since the structure of the tubular braided tubes is very open, the heat-setting effects could be insignificant. Another reason for the indifference in heat-setting effects could be the testing range. During both tensile and compression test, the structures were never loaded to the extent where the maximum geometrical deformation reached the point where the stent started to show structural and material resistance. However, heat-setting increased the handling of the stents during testing of the samples. The experimental design was intended as a split-plotformat. The effects of time, heat-setting time, number of filaments, and diameter of the braided tube were analyzed. All factors were fixed. In the tensile and compression tests, there were three replicates for each level of testing combinations.

To calculate F-null values, residual analysis [11] was used. The SAS statistical package program was used to analyze the data observed from the heat-setting experiment. The number of filaments present and the diameter of the tube showed a significant effect at the 1 % confidence interval for both the tensile and the compressive forces. Analysis of variance showed that the diameter of the braided tube and the number of the filaments used in the tube had significant effects for both compressive and tensile forces. The heat-setting temperature was significant for the tensile force, but it did not have any effect on the compression force. Since the main effect of temperature was insignificant, two-way interactions including the temperature were also insignificant. The rest of the two-way interactions showed a significant effect. Three-way interactions did not show a significant effect with the exception of time, number of filaments, and diameter for the tensile force, as expected due to the diameter and the number of the filaments involved.

References

1. Schmitt PJ (1992) A radially self-expanding implantable intraluminal device. US patent no: PCT/US93/08649
2. Jedwab MR, Clerc CO (1992) A study of the geometrical and mechanical properties of a self-expanding metallic stent-theory and experiment. J Appl Biomat 4:77
3. Paris E, King MW, Guidoin RG, Delermo J, Deng X, Douville Y (1994) Innovations and deviations in therapeutic vascular devices: polymeric biomaterials. Marcel Dekker Inc., New York
4. Ko FK, Pastore CM, Head AA (1976) Handbook of industrial braiding. Atkins & Pearce, Covington, KY
5. Goff JM (1976) The geometry of tubular braided structures. Masters thesis, Georgia Institute of Technology, Atlanta, GA
6. Du GW, Popper P (1990) Process model of circular braiding. In: Processing of polymers and polymeric composites, ASME, vol 19, p 119
7. Zhang Q, Beale D, Adanur S, Broughton RM, Walker RP (1997) Geometrical analysis of two-dimensional braided fabric structure. J Text Inst 88:41
8. Yuksekkaya ME, Adanur S (2009) Analysis of polymeric braided tubular structures intended for medical applications. Text Res J 79(2):99–109
9. Dieter GE (1976) Mechanical metallurgy, 2nd edn. McGraw-Hill, Tokyo
10. Wahl AM (1963) Mechanical spring, 2nd edn. McGraw-Hill, New York
11. Montgomery DC (2005) Design and analysis of experiments, 6th edn. Wiley, New York

Chapter 27
Influence of Fabric Parameters on the Durability of Textile Heart Valve Prosthesis

27.1 Introduction

Percutaneous vascular surgery has made noteworthy progress during the past two decades [1, 2]. With the recent advent of the stent graft implantation, this noninvasive holds a good promise in heart valve replacement [3]. This chapter focuses on the investigation of the long-term fatigue behavior of polyester fabrics woven with different yarns and construction parameters so as to assess its suitability for heart valve replacement. During surgery, a heart valve undergoes flexural and tensile stress. A fabric having lower flexural resistance can be expected to have a longer working life. Textile materials possess high tensile strength and high flexibility. The flexibility renders them to be suitable for apparels. The fibers in yarns and yarns in fabric slip when subject to flexing. Polyester fiber has been commonly used in cardiac implants, owing to its biocompatibility and resistance to degradation on contact with body fluids [4, 5]. In vitro analysis has revealed that polyester fabric behaves in a dynamic manner [6–8]. When an assembly is bent, the resistance to bending will be governed by the combined bending rigidity of the individual elements and the frictional forces between the elements that resist slippage between them [9–11]. Very little content is available in the literature pertaining to the role of friction of cohesion between the elements of an assembly [12–14]. The inter-filament cohesion is considered to be crucial in the case of textile heart valve development, wherein extensive cyclic flexing should happen. The leaflet material of the valve is subjected to flexural and tensile stress during each valve cycle. The tension force active on the valve leaflet is borne by the filaments and exerts forces between yarns and also between filaments, owing to the cohesion of the fabric structure. The radial forces create friction forces at the contact points. During the flexure of the leaf let, these friction forces will consequently need to be overcome before the required flexing will occur. The energy associated with that movement will be dissipated at the contact zone where the phenomenon occurs. The cyclic

N. Gokarneshan et al., *Emerging Research Trends in Medical Textiles*,
Textile Science and Clothing Technology, DOI 10.1007/978-981-287-508-2_27

flexing tends to damage the surface it contacts, since it results in energy increase that gets dissipated. The continued cycling of textile heart valve prosthesis at the rate of heart pulse could result in filament damage or rupture, despite having a low fabric stiffness. A detailed assessment of these effects will help to predict a material's durability when used as a heart valve. The effects of yarn and fabric construction on the long-term cyclic bending of fabrics has been investigated so as to assess which particular fabric construction parameters would provide the suitable for the application.

27.2 Measurement of Fabric Stiffness Before Cycling

The effect of fabric construction and yarn parameters on the initial bending stiffness has been evaluated by measuring the bending stiffness of the fabrics at loom state and after giving the necessary finishing treatments as well [15]. The obtained values also served as a control for subsequent performances after cycling. Figure 27.1 shows the findings wherein the absolute average value of measured stiffness is given. Five fabrics of the same construction were tested and their values averaged so as to get reliable results. The bars reflect the magnitude of the standard deviation. Also shown in this figure are the values of the stiffness ratio KB. These results show that there are some significant differences in values of both B_{exp} and KB among the fabrics tested. The stiffness values have been measured as well as calculated.

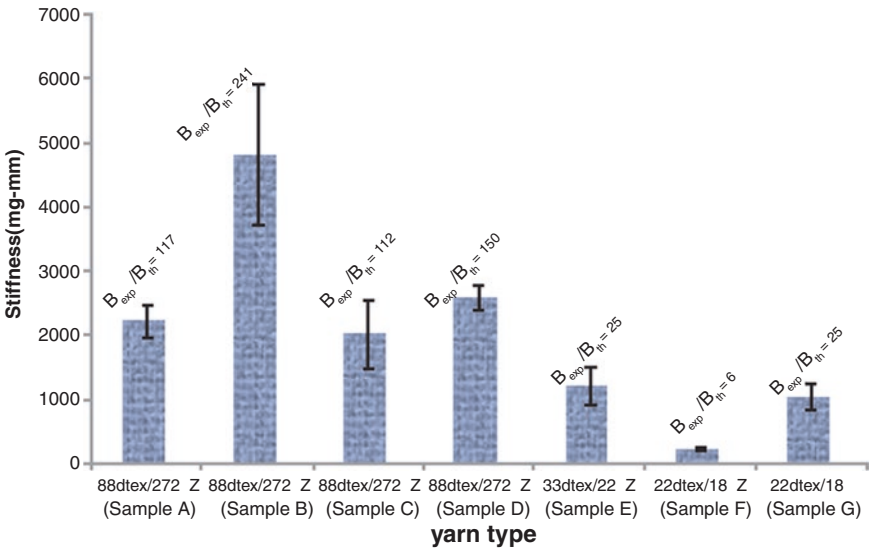

Fig. 27.1 Initial bending stiffness [15]

27.3 Effect of Fabric Set on Initial Stiffness

Comparing the various fabrics, which have the same yarn but different fabric set, it can be observed that altering the structure of the fabric changes the stiffness properties. When changing warp set (samples B and D), an increase in the number of ends by about 17 % causes a corresponding increase in Bth; however, B_{exp} increases by about 60 %. The higher bending rigidity caused due to increased thread count and increased adhesion between threads contributes to the higher bending rigidity of the fabric [15]. The greater the number of yarns within a fixed fabric width causes greater contacts between filaments of the warp yarn. The bending stiffness of the fabrics increases with more filament contacts, creating greater forces of adhesion. Similar phenomenon can be observed on comparing other fabrics (A and C in Table). The difference in that case is, however, much less, probably due to a lower pick density than considered in the previous pair. Thus, the frictions effects in both warp and weft directions are combined. The increase in pick density also caused an increase in fabric stiffness, which can be visualized on comparing fabrics A and B or C and D. The increase is attributed to the greater number of contacts between the yarns, and hence, this leads to increase in the yarn-to-yarn friction. Upon analyzing the KB values, for the same Bth value, for each pair, the ratio value increases greatly with pick density.

27.4 Effect of Yarn-Specific Surface Area on Initial Stiffness

Making a comparison between a microdenier filament yarn fabric and a coarse denier filament yarn fabric (fabrics C and E), both of the same overall tightness (same Russel's factor), the microdenier filament structure E is characterized by a higher measured stiffness value. This is in contrast to the fact that the theoretical stiffness of the microdenier filament yarn fabric is lower (Bth = 17 mg mm) than that of the coarse denier filament yarn fabric (Bth = 60 mg mm). Accordingly, the relatively higher measured value and the much higher KB value in the former is due to higher yarn-specific surface and higher surface contacts between filaments [15].

27.5 Effect of Yarn Count on Initial Stiffness

By comparing fabric E with F, characterized by about the same specific surface area (around 4.8 cm^2/m) but different count, it can be seen that the higher count led to higher stiffness [15]. It can be attributed to the greater moment of inertia associated with the coarser yarn.

27.6 Effect of Yarn Twist on Initial Stiffness

Fabrics F and G are identical except the yarns in F are twisted and those in G are flat. Hence, *B*th values are identical. The findings indicate that the B_{exp} and KB values are much greater for the flat or nontwisted yarn [15]. Thus, flat yarns create a structure with higher tightness for similar warp and weft densities. The test results affirm that many yarn and fabric construction parameters influence a fabric's measured or actual stiffness value. The filaments in a yarn and yarns in a fabric have varying degrees of contacts, depending on material and construction factors, and they lead to different amounts of internal friction that influences stiffness.

27.7 Effect of Cyclic Loading on Properties and Material

Five samples of a particular fabric have been tested to assess sample to sample variability. The fabrics have been tested together at 5 Hz cycling rate for around five million cycles. Change in properties was determined for evaluation of short-term response and long-term response of the fabrics. The tests did not exceed 5 million cycles since it has been noted that for all fabrics tested, the construction was well conditioned and the properties were well stabilized with little or no further change in bending stiffness values within this range of cycling. The change in stiffness with cycling tends to remain unaltered, irrespective of the fabric parameters. A typical result found is given in Fig. 27.2, which shows the behavior noted in the microdenier 88/272 fabric sample (sample B) in which the phenomenon observed is typical of all samples. The changes in the fabric stiffness could be

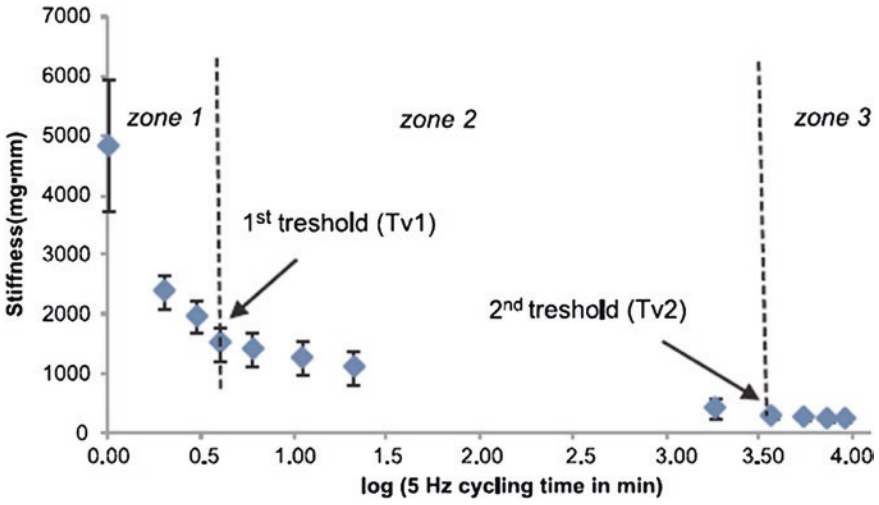

Fig. 27.2 Change of bending stiffness with time [15]

divided into three zones [15]. The first zone is characterized by an abrupt decrease in bending stiffness, spanning over only about 900 cycles (corresponding to a 15-min period in vivo). The change happens irrespective of fabric parameters. The second stage involves a much slower change (the reduction rate is below 10 %/minute), and the third is much slower (the reduction rate is less than 0.1 %/minute). This stiffness modification pattern can be considered as a generally expected rearrangement process in fabric.

27.8 The Fabric Rearrangement Process

Pictorial views of the fabric construction as taken from a microscope (magnified three times) so as to get a better understanding of the fabric rearrangement process before and after cycling (Fig. 27.3). As could be seen, the yarns that appeared previously compact became loose after the cycling process [15]. There has been an average increase of 10 % in warp yarn width (from initial state to first threshold value).

The explanation could be provided as follows. The fabric strips are subjected to a combination of flexure and tension stress during cycling Fig. 27.4. The warp yarns are held under tension by clamps, whereas the weft yarns are untensioned. Fabric structure under flexing stress tends naturally to reorganize in order to reach a minimum deformation energy state, like in any physical phenomenon. One way for filaments away from the neutral axis in warp yarns to reduce tension is for them to move toward the neutral axis. The yarn tends to flatten subsequently. Thus, the change that happens is irreversible owing to the friction at the crossover points. This results in an increase in yarn width, as can be seen in Fig. 27.3.

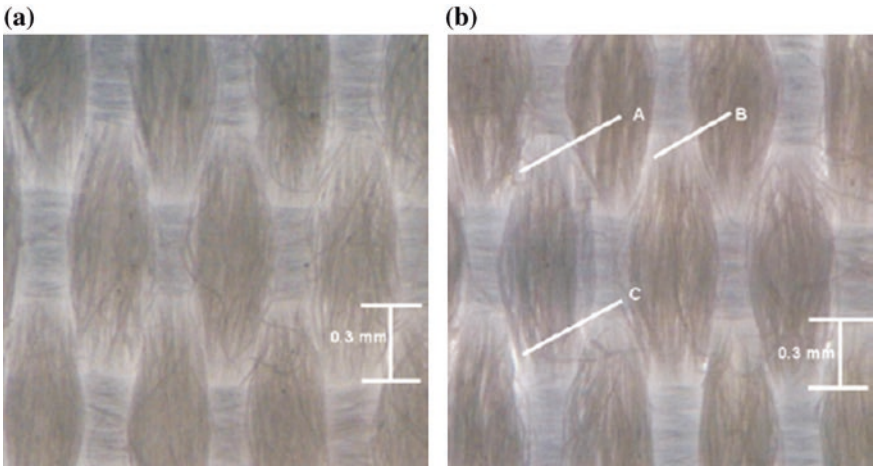

Fig. 27.3 Micrographs obtained from fabrics observed (pertaining to sample B) [15]. **a** Before cycling. **b** After cycling

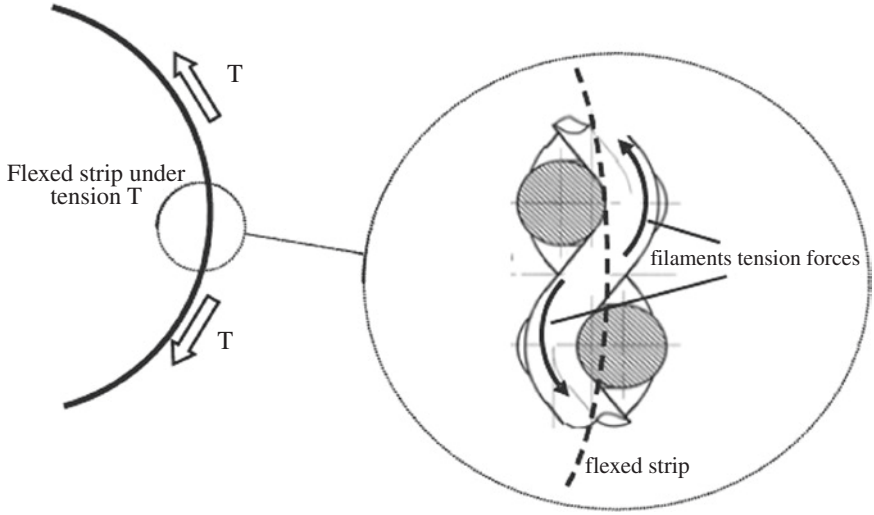

Fig. 27.4 Fabric strip subjected to tension [15]

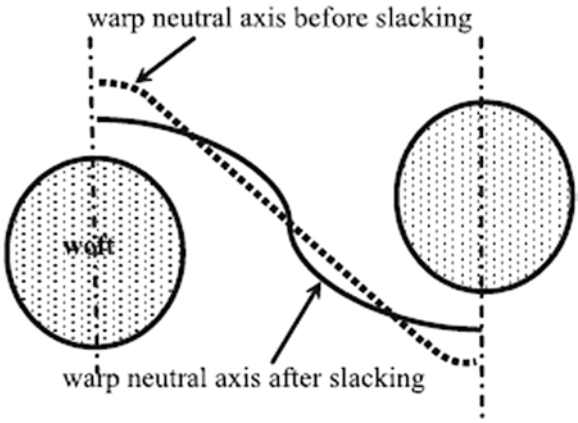

Fig. 27.5 Slackening of yarn neutral axis [15]

When the ends of the warp yarn are clamped, the movement of the neutral axis of the warp ends closer to fabric plane will lead to a decrease in crimp and hence results in an increase in slack between two picks (Fig. 27.5).

The warp yarn gets more slackened subsequently, resulting in some open space in the fabric structure as reflected at points A, B, and C in Fig. 27.3. Such an alteration of yarn structure is unchangeable and gets initiated at the first cycle and completed rapidly, that is, in the first zone, resulting in a stabilized relaxed state of fabric. The rearrangement creates a fall in the radial forces within the filaments in yarn and results in reduced internal friction and hence in fabric stiffness. The observations made suggest bending resulted in reduced yarn density [12].

The fabric dimensions and hence the fabric count remain unchanged. Accordingly, the rearrangement occurred only at the level of the warp yarn; the overall fabric construction was not affected by the rearrangement mechanism. Since weft yarn did not undergo changes, either in crimping or in yarn cross section, the fabric thickness measured was not different after cycling. Owing to the method we used in calculating porosity, its value also did not change. The rearrangement led only to the repositioning of the polyester filaments in a volume of porous material that remained constant. The differences in results among different fabric samples can now be examined. This is done on the basis of the following criteria: (1) the difference in the first threshold values (Tv1); (2) the difference in the second threshold values (Tv2); (3) the relaxation slope value as noted in zone 1; and (4) the stiffness ratio KB reached when the conditioning is fully completed at Tv2. In order to use a linear scale, however, only part of zone 2 could be displayed. The total time window represented is 20 min at 5 Hz cycling corresponding to approximately 1.5 h under physiological conditions. As the point representing Tv2 is outside the timescale represented, the values of bending stiffness and KB, and the number of cycles (millions) corresponding this point are noted separately in the figures.

27.9 Influence of Fabric Set on the Rearrangement Process

Figures 27.6 and 27.7 show the stiffness evolution curves for fabrics A, B, and D of the fabric containing microdenier 88 dtex/272 yarn but having different construction sets. The increase in pick density value (for the same number of

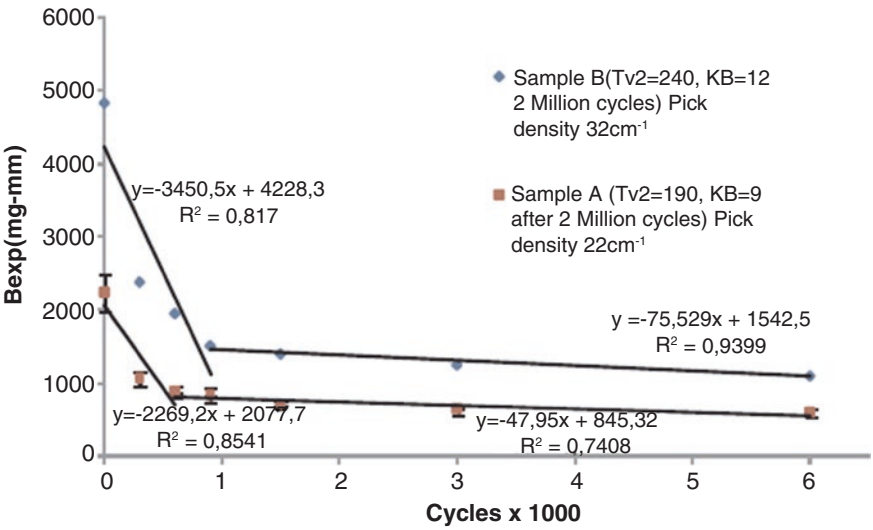

Fig. 27.6 Stiffness and pick density [15]

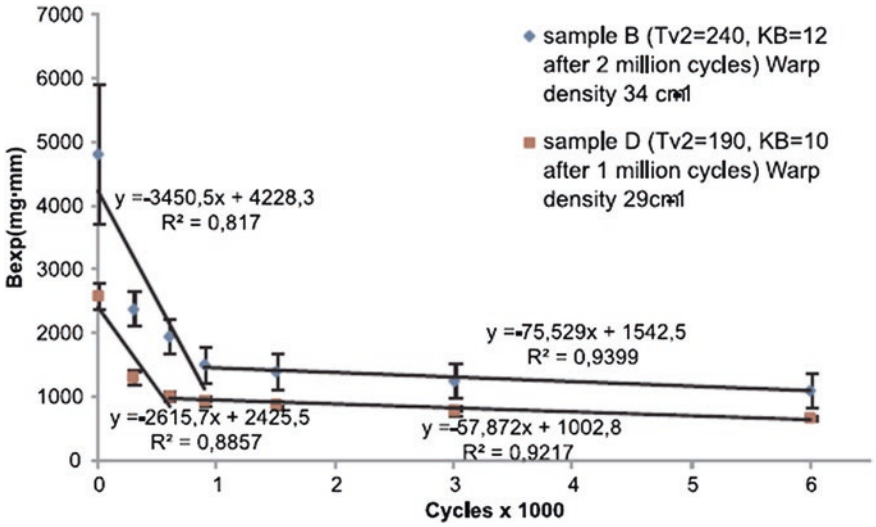

Fig. 27.7 Stiffness and warp density [15]

ends) affected the rearrangement process (Fig. 27.6). The most outstanding differences we see are in the values corresponding to Tv1 and Tv2: the first stiffness threshold value Tv1 of the higher pick density (32 cm^{-1}) fabric, relative to lower (22 cm^{-1}), is higher (1520 vs. 878 mg mm) and takes longer to reach (after 4 min, instead of 3 min). The second stiffness threshold value Tv2, which is reached after 2 million cycles for both sets, is also greater for the tighter fabric, that is, it is about 30 % higher. The difference in the value of KB is due to higher residual forces of cohesion in the denser fabric, under the condition that calculated stiffness (elastic) is the similar for both fabrics. One may assume that continued cycling beyond Tv2 will convert these cohesion forces into dissipated energy due to friction and eventually lead to a rupture of filaments. Hence, based on the above results, it can be expected that the rupture will take place relatively sooner in the tighter fabric. Results in Fig. 27.7 show that decrease in the warp density leads to a decrease in the Tv1 stiffness value as well as in the time corresponding this value. Tv2 value is also less (35 %) and reached relatively earlier (1 million vs. 2 million cycles) for the less tight fabric. The results obtained also imply the importance of friction in influencing bending stiffness, as observed with the results in the previous pair. The increase in density of warp contributed only 17 % increase in *B*th value but 26 % increase in final B_{exp}, clearly due to an increase in friction because of the increase in contacts.

27.10 Influence of Yarn-Specific Surface Area on the Rearrangement Process

It has been considered necessary to assess whether, for a fabric with the same Russel's factor, it is better to work with a microdenier filament yarn fabric with increased specific surface area or with a coarse denier filament yarn fabric with lower surface area. Hence, the results of fabrics C (microdenier filament yarn fabric) and E (regular denier filament yarn fabric) have been compared, both with the tightness values around 100 (Fig. 27.8). It can observed overall that in all fabrics, including this pair, the magnitude of Tv1 increases with higher initial or control B_{exp} value, and longer it takes to reach this first relaxed or threshold value. A unique result noted with the coarse denier filament yarn sample (E) is that this material has nearly reached its final threshold value Tv2 at the point that Tv1 is reached. It shows a rapid relaxation involving energy dissipation in the structure. Conversely, fabric made from the microdenier filament yarn (C), having higher initial stiffness (B_{exp}), takes longer duration to attain its first threshold value (Tv1) and then continued to relax and attain its second final threshold value after 1 million cycles, which is half the value of the fabric with coarse denier filament yarn. In other words, the line relating to the fine denier filament yarn sample crossed that of the coarse denier filament yarn sample and ended up at a significantly lower position relative to the coarse denier filament yarn sample. The bending stiffness becomes important at this point, to estimate the bending stiffness due to internal

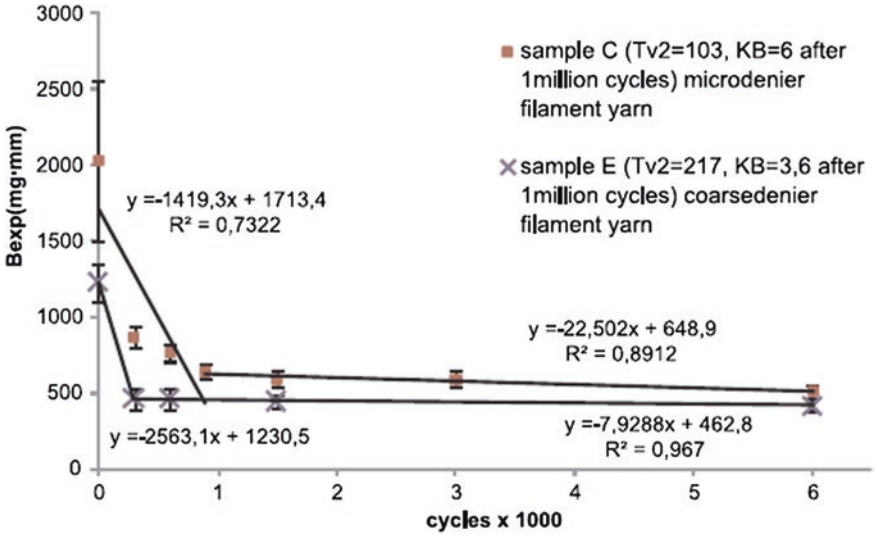

Fig. 27.8 Effect of specific surface area [15]

friction (*B* friction) in the case of both materials. This stiffness is related to the elastic (theoretical, *B* elastic) and total stiffness. Using the data obtained, the stiffness value due to internal friction can be given at the three points in the stiffness-cycle curve. The results evidently point out that the microdenier filament yarn, owing to internal friction has been subjected to faster and greater structural rearrangement, resulting in lower final stiffness in comparison with the coarse denier filament yarn, and this is considered to be crucial. When the final friction stiffness values are divided by the number of filaments involved in the 5 mm width of the two structures (7888 for microdenier and 1320 for coarse), assuming that the friction energy dissipated is equally spread on all filaments, it can be concluded that the coarse filament would undergo a dissipation energy 10 times higher in each cycle than would the microdenier filament. Considering that the coarse denier filament is about 5 times greater in cross-sectional area in comparison with the fine denier filament (107 vs. 23 μm^2), the coarse denier filament material would abrade and degrade faster than the fine denier filament material. It can thus be established that the microdenier filament yarn lasts longer in the dynamic flexing application.

27.11 Influence of Yarn Twist on the Rearrangement Process

The results of two fabrics of 22 dtex/18 fil, with and without twist, have been analyzed to determine the role of twist. The two fabrics had identical set. These fabrics have low Russel's factor of 70 due to low pick density, which enabled to separate the influence of twisting from the influence of fabric tightness. Both the fabrics attain their first threshold values almost at the same time (300 cycles). However, the twisted yarn fabric has been subjected to very little initial rapid relaxation. This fabric is already very close, even before cycling, to the final conditioned structure. The low friction effects within the structure can be substantiated by the Russel's factor of 70 [15]. The micrographs of the twisted (Fig. 27.9) and the flat (Fig. 27.10) yarn fabrics show that the structure of the twisted is more open and has greater distance between the yarns than is the case with the structure of the flat yarn fabrics. The second threshold value of the twisted yarn fabric is close to its elastic value (KB = 2). Conversely, the flat yarn fabric has a first threshold value of stiffness about four times that of the twisted yarn and has higher relaxation slopes in phases 1 and 2. The end (second threshold) value of this material is also higher with a KB = 7. Figure 27.10 shows the micrograph indicating that the flat yarn structure ends up being tighter (with yarns closer to each other), even with same fabric set and strip width. The flat yarn sample is accordingly characterized by higher inter-yarn friction. Hence, the influence of lateral inter-yarn friction is higher in these materials resulting in greater stiffness (Fig. 27.11).

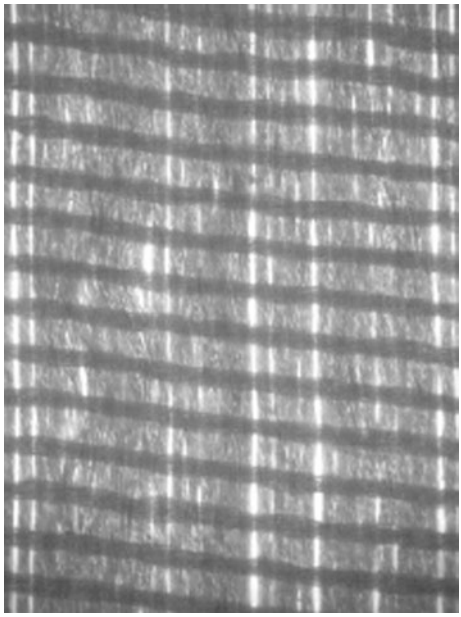

Fig. 27.9 Fabric F (*twisted*) [15]

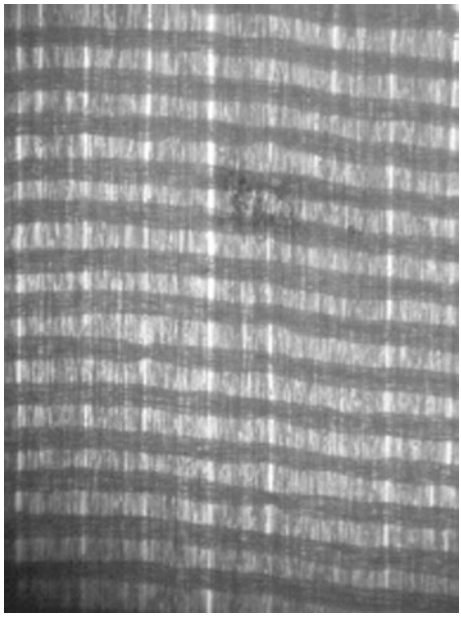

Fig. 27.10 Fabric G (*flat*)

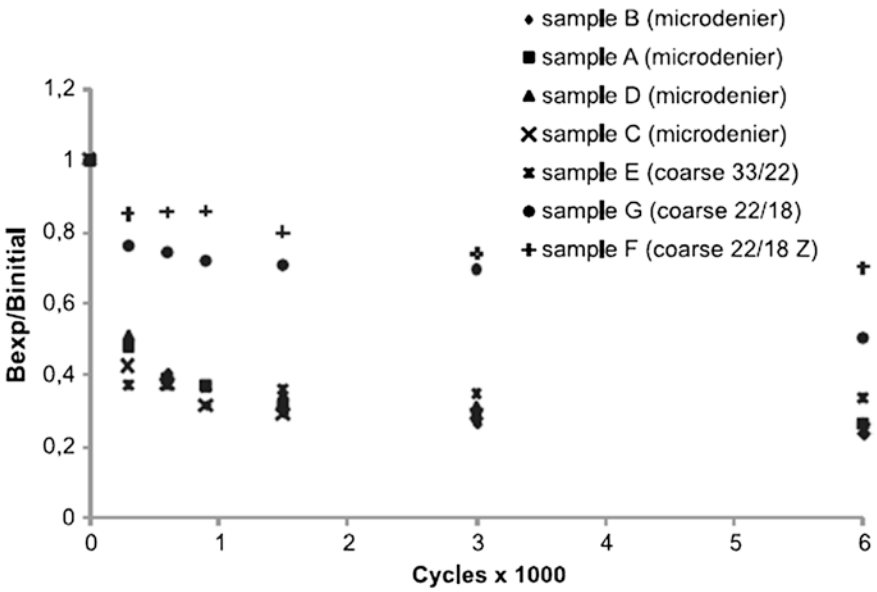

Fig. 27.11 Loss of stiffness as a fraction of initial stiffness [15]

27.12 Relative Changes in Structures with Cycling

When B_{exp} is plotted as a fraction of the initial value against the number of cycles, it is possible to observe that all fabrics undergo rearrangement in structures and become more flexible and the change varies from fabric to fabric [15]. All fabrics have undergone a reduction in stiffness to a smaller or greater degree due to cyclical flexing. The reduction has been high, to the extent of 70 %, except for the fabrics with low-count coarse denier filament yarn (with and without twist).

References

1. Sigwart U, Puel J, Mirkovitch V, Joffre F, Kappenberger L (1987) Intravascular stents to prevent occlusion and restenosis after transluminal angioplasty. N Engl J Med 316:701–706
2. Henry M, Klonaris C, Amor M, Henry I, Tzetanov K (2005) State of art: which stent for which lesion in peripheral interventions? Textile Heart Inst J 27(2):119–126
3. Cribier A, Eltchaninoff H, Bash A, Borenstein N, Tron C, Bauer F, Derumeaux G, Anselme F, Laborde F, Leon MB (2002) Percutaneous transcatheter implantation of an aortic valve prosthesis for calcific aortic stenosis: first human case description. Circulation 106:3006–3008
4. Van Damme H, Deprez M. Creemers E, Limet R (2005) Intrinsic structural failure of polyester (Dacron) vascular grafts. A general review. Acta Chir Belg 105:249–255
5. Von Recum A, Jane E (1998) Handbook of Biomaterials evaluation: scientific, technical, and clinical. CRC Press, Boca Raton, pp 89–96

6. Heim F, Durand B, Kretz JG, Chakfe N (2003) Method for producing an aortic or mitral heart valve prosthesis and resulting aortic or mitral heart valve, WO 03/090645
7. Heim F, Durand B, Chakfe N (2008) Textile heart valve prosthesis: manufacturing process and first in vitro performances. Textile Res J 78(12):1124–1131
8. Heim F, Durand B, Chakfe N (2006) Textile heart valve prosthesis: influence of the fabric parameters on its hydrodynamic performances in vitro. Res J Textile Apparel 58:75–86
9. Backer S (1952) Mechanics of bent yarn. Textile Res J 22:668
10. Grosberg P (1966) The mechanical properties of woven fabrics, part II: the bending of woven fabric. Textile Res J 36:205
11. Platt MM, Klein WG, Hamburger WJ (1958) Mechanics and elastic performances of textile materials: part XIV. Textile Res J 28:611
12. Skelton J (1974) Frictional effects in fibrous assemblies. Textile Res J 44:716
13. Skelton J (1974) Frictional damping in multicomponent assemblies. Textile Res J 44:716
14. Owen JD, Livesey RG (1964) Cloth stiffness and hysteresis in bending. J Textile Inst 55:516
15. Heim F, Bhupendar Gupta S (2009) Textile heart valve prosthesis: the effect of fabric construction on long term durability. Textile Res J 79(11):1001–1013